



UNIVERSITY OF  
BIRMINGHAM

# **Wideband and Reconfigurable Antennas for Emerging Wireless Networks**

by

**Elham Ebrahimi**

A Thesis submitted to  
The University of Birmingham  
For the degree of  
Doctor of Philosophy (PhD)

School of Electronic, Electrical and  
Computer Engineering  
College of Engineering and Physical  
Sciences  
The University of Birmingham  
September 2011

UNIVERSITY OF  
BIRMINGHAM

**University of Birmingham Research Archive**

**e-theses repository**

This unpublished thesis/dissertation is copyright of the author and/or third parties. The intellectual property rights of the author or third parties in respect of this work are as defined by The Copyright Designs and Patents Act 1988 or as modified by any successor legislation.

Any use made of information contained in this thesis/dissertation must be in accordance with that legislation and must be properly acknowledged. Further distribution or reproduction in any format is prohibited without the permission of the copyright holder.



# **Abstract**

The growing demand for development and deployment of new wireless services has influenced the hardware design procedure including antennas and radio frequency (RF) front end, particularly in portable devices. Hence, novel solutions that are multiband, multimode, low profile, low cost and easy to integrate into the feature-rich compact devices are required.

The research described in this thesis concerns integrating wideband and narrowband functionality and therefore adding to the versatility of the antenna systems in various wireless scenarios. The integration concept is based on sharing some sections of one antenna between several other antennas. This approach may be useful in designing multimode wireless terminals while keeping the required antenna footprint small. Based on this concept a demonstrator antenna is designed and verified. The power coupling between the two modes is studied and several solutions are presented.

To demonstrate the versatility of this concept, the possibility of frequency reconfiguration is explored for narrowband mode using matching circuits with fixed elements. Wideband and reconfigurable narrowband functionality may potentially be of advantageous in emerging wireless communication systems such as software defined radio and cognitive radio for wideband sensing and reconfigurable narrowband communication procedure.

Furthermore, the antenna integration within a device platform is studied. A technique is proposed to mitigate the unwanted effects of printed circuit board on the printed wideband antenna characteristics. As a result the radiation pattern, gain and group delay are stabilised across the band.



# List of Publications

## Patent

- P. S. Hall and **E. Ebrahimi**, "Combined Wideband and Narrowband Antenna for Cognitive Radio Applications," UK patent application GB0816755.3.

## Journal

- **E. Ebrahimi**, O. Litschke, R. Baggen, P. S. Hall, "Device integrated printed UWB antenna," to be submitted to IET Proc. Antennas and Propagation.
- **E. Ebrahimi**, J. Kelly and P. S. Hall, "Integrated wide-narrowband antenna for multi-standard radio," IEEE Trans. Antennas and Propagation, vol. 59, no. 7, pp. 2628-2635, July 2011.
- **E. Ebrahimi**, O. Litschke, R. Baggen, P. S. Hall, "Isolation enhancement of planar disc antenna and ground plane in UWB applications," Electronics Letters, vol. 46, no. 23, pp. 1539 – 1541, Nov. 2010.
- **E. Ebrahimi** and P. S. Hall, "Integrated wide-narrowband antenna for multiband applications," Microwave and Optical Technology Letters, vol. 52, no. 2, pp. 425-430, Feb. 2010.

## Conference papers

- **E. Ebrahimi**, O. Litschke, R. Baggen, P. S. Hall, "Pattern control of UWB printed antenna on large ground plane," accepted for EuCAP 2011.
- **E. Ebrahimi**, O. Litschke, R. Baggen, and P. S. Hall, "Integration of planar UWB antennas in real life systems," LAPC 2010, Loughborough, UK, Nov 2010.
- D. Jasteh, **E. Ebrahimi**, P. S. Hall, and P. Gardner "Feed network for antenna decoupling," in Proc. LAPC 2009, Loughborough, UK, Nov 2009.
- **E. Ebrahimi**, J. Kelly, and P. S. Hall, "A reconfigurable narrowband antenna integrated with wideband monopole for cognitive radio applications," in Proc. APS 2009, USA.
- P. S. Hall, P. Gardner, J. Kelly, **E. Ebrahimi**, M. R. Hamid, F. Ghanem, F. J. Herraiz-Martinez and D. Segovia-Vargas, "Reconfigurable Antenna Challenges for Future Radio Systems," in Proc. EuCAP 09, Berlin, Germany, Mar. 2009.
- **E. Ebrahimi** and P. S. Hall, "A dual port wide-narrowband antenna for cognitive radio," in Proc. EuCAP 09, Berlin, Germany, Mar. 2009.
- P. S. Hall, P. Gardner, J. Kelly, **E. Ebrahimi**, M. R. Hamid, and F. Ghanem, "Antenna challenges in cognitive radio," (invited paper) in Proc. ISAP 08, Taiwan, Oct. 2008.
- J. Kelly, **E. Ebrahimi**, P. S. Hall, P. Gardner, and F. Ghanem, "Combined wideband and narrowband antennas for cognitive radio applications," in The IET seminar on Cognitive Radio and Software Defined Radios: Technologies and techniques, London, UK, Sep. 2008.
- P. Gardner, M. R. Hamid, P. S. Hall, J. Kelly, F. Ghanem, and **E. Ebrahimi**, "Reconfigurable antennas for cognitive radio: requirements and potential design

approaches," in The IET seminar on Wideband, multiband antennas and arrays for defence or civil applications, London, UK, Mar. 2008.

# Acknowledgement

First and foremost, I would like to thank my supervisor Professor Peter S. Hall, whose support, assurance and continued belief in my ability has contributed enormously to the existence of this thesis. I would also like to thank Dr Peter Gardner for his contributions in numerous discussions, and Dr Costas Constantinou whose comments were always gratefully received.

I am truly indebted and thankful to Mr. Alan Yates for his patience and passion for teaching me all the tips and tricks for fabricating and measuring the antennas.

I wish to express my sincere gratitude to Dr Matthias Geissler at IMST GmbH, Germany, and his team: Dr Marta Martinez, Rens Baggen, Oliver Litschke, Dr Jurgen Kunisch, Bahram Sanadgol and Marta Arias Campo who made the third year of my studies, the unforgettable and unique experience of my life.

To the members of the Applied Antenna and Electromagnetic Laboratory, past and present, I owe sincere and earnest thankfulness; to Dr James Kelly, Dr Lida Akhoondzadeh Asl, Dr Yuriy Nechayev, Dr Farid Ghanem, Dr Mohammad Rijal Hamid, Donya Jasteh, Sampson Hu for their help and friendship.

I am hugely grateful to my family for their generous support throughout my PhD, and indeed the whole of my life. Their wisdom, kindness and excellent advice have made me who I am today and I hope that I have made them proud. Thanks Dad for believing in me and thanks Mom for your infinite love. Thanks to my sister, Elmira and my brother Omid, for all the fun and laughter they bring to my life.

Above all I must thank Kianoush. You are everything I could ask for and more. Thank you so much for putting up with the stress and strain of the last year or so. I could not have done it without you. I love you with all my heart, thank you so much for everything. You truly are amazing.

# List of Contents

|                                     |     |
|-------------------------------------|-----|
| Abstract.....                       | i   |
| List of Publications .....          | ii  |
| Acknowledgement .....               | iv  |
| List of Contents.....               | v   |
| List of Figures.....                | x   |
| List of Tables .....                | xix |
| List of Abbreviations .....         | xx  |
| Chapter 1 Introduction.....         | 1   |
| 1.1 Background.....                 | 1   |
| 1.2 Motivation and Objectives ..... | 2   |
| 1.3 Layout of Thesis .....          | 4   |
| References.....                     | 6   |
| Chapter 2 Antenna Theory .....      | 7   |
| 2.1 Introduction.....               | 7   |
| 2.2 Hertzian Dipole.....            | 8   |
| 2.3 General Antenna Parameters..... | 10  |
| 2.3.1 Antenna Impedance .....       | 10  |
| 2.3.2 Impedance Matching.....       | 11  |
| 2.3.3 Reflection Coefficient.....   | 11  |
| 2.3.4 Antenna Bandwidth .....       | 12  |
| 2.3.5 Radiation Pattern.....        | 13  |

|           |  |    |
|-----------|--|----|
| 2.3.6     | Directivity, Gain and Efficiency .....                         | 14 |
| 2.4       | UWB Antenna Characterization .....                             | 15 |
| 2.4.1     | Frequency Domain Signal Link .....                             | 15 |
| 2.4.2     | Time Domain Signal Link.....                                   | 17 |
| 2.4.3     | UWB Parameters .....   | 18 |
| 2.4.4     | Antenna Elements .....   | 21 |
| 2.5       | Summary .....  | 30 |
|           | References.....  | 31 |
| Chapter 3 | Antenna Design Challenges for Emerging Wireless Services ..... | 35 |
| 3.1       | Introduction.....  | 35 |
| 3.2       | Ultra Wideband Technology.....                                 | 36 |
| 3.2.1     | UWB Benefits.....  | 38 |
| 3.2.2     | UWB Applications.....  | 39 |
| 3.3       | Cognitive Radio .....  | 39 |
| 3.3.1     | Spectrum Sensing and Allocation .....                          | 43 |
| 3.3.2     | Ultra Wideband Cognitive Radio.....                            | 44 |
| 3.4       | Antenna Requirements for Multi Standard Radio.....             | 45 |
| 3.4.1     | Wideband Antennas .....  | 45 |
| 3.4.2     | Multiband Antennas.....  | 50 |
| 3.5       | Reconfigurable Radio .....                                     | 66 |
| 3.6       | Summary .....  | 70 |
|           | References.....  | 70 |
| Chapter 4 | Integrated Wideband-Narrowband Antenna .....                   | 80 |

|           |   |     |
|-----------|---|-----|
| 4.1       | Introduction.....   | 80  |
| 4.2       | Integration Concept.....  | 81  |
| 4.3       | Antenna Geometry and Design.....                                | 82  |
| 4.3.1     | Wideband Antenna- Circular Disc Monopole Antenna .....          | 82  |
| 4.3.2     | Narrowband Antenna .....  | 86  |
| 4.3.3     | Integrated Antenna-Circular Disc Monopole and PIFA Design ..... | 86  |
| 4.3.4     | Wideband Antenna - Hour Glass Monopole Antenna Design .....     | 89  |
| 4.3.5     | Integrated Antenna-Hour Glass Monopole Antenna and PIFA .....   | 90  |
| 4.4       | Parametric Analysis .....                                       | 99  |
| 4.4.1     | Wideband Antenna Parameters .....                               | 100 |
| 4.4.2     | Narrowband Antenna Parameters .....                             | 103 |
| 4.4.3     | Integration Parameters .....                                    | 105 |
| 4.5       | Discussion.....   | 109 |
| 4.6       | Summary .....   | 112 |
|           | References.....   | 112 |
| Chapter 5 | Port Isolation.....   | 114 |
| 5.1       | Introduction.....   | 114 |
| 5.2       | Field Coupling in the Wideband-Narrowband Antenna .....         | 115 |
| 5.3       | Isolation Enhanced Wideband-Narrowband Antenna.....             | 117 |
| 5.3.1     | Configuration A .....   | 118 |
| 5.3.2     | Configuration B .....   | 120 |
| 5.3.3     | Configuration C .....   | 122 |
| 5.4       | External Decoupling Feed Network .....                          | 124 |

|           |   |     |
|-----------|---|-----|
| 5.4.1     | Decoupling Network Design Theory .....                              | 124 |
| 5.4.2     | Decoupling Network for Integrated Wideband-Narrowband Antenna ..... | 129 |
| 5.5       | Concluding Remarks and Summary .....                                | 136 |
|           | References.....   | 138 |
| Chapter 6 | Reconfigurable Wideband-Narrowband Antenna.....                     | 139 |
| 6.1       | Introduction.....   | 139 |
| 6.2       | Impedance Matching Circuit Design .....                             | 141 |
| 6.2.1     | The L Network.....  | 141 |
| 6.2.2     | The $\Pi$ Network .....   | 142 |
| 6.2.3     | Tuned Integrated Wideband-Narrowband Antenna .....                  | 144 |
| 6.3       | Discussion.....   | 150 |
| 6.4       | Summary.....  | 151 |
|           | References.....   | 152 |
| Chapter 7 | Device Integrated Printed UWB Antenna.....                          | 153 |
| 7.1       | Introduction.....   | 153 |
| 7.2       | Antenna Design.....   | 163 |
| 7.2.1     | The Isolated Antenna .....  | 163 |
| 7.2.2     | Antenna Integration with the PCB.....                               | 164 |
| 7.3       | Analysis .....  | 170 |
| 7.3.1     | Surface Currents.....   | 170 |
| 7.3.2     | Impedance Matching.....   | 170 |
| 7.3.3     | Radiation Pattern.....  | 171 |
| 7.3.4     | Gain.....   | 172 |

|            |  |     |
|------------|--|-----|
| 7.3.5      | Field Coupling to the PCB .....                            | 175 |
| 7.3.6      | Group Delay .....  | 177 |
| 7.3.7      | Time Signals .....   | 177 |
| 7.4        | Experimental Verification.....                             | 180 |
| 7.5        | Summary .....  | 189 |
|            | References.....  | 189 |
| Chapter 8  | Conclusions and Future Work.....                           | 194 |
| 8.1        | Conclusions.....   | 194 |
| 8.2        | Future Work.....   | 199 |
| Appendix A | Simulation Software.....                                   | 201 |
| A.1        | Computer Simulation Technology (CST) †.....                | 201 |
| A.2        | Empire XCcel †.....  | 204 |
| A.2.1      | The Yee algorithm .....                                    | 205 |
| Appendix B | Antenna Measurement Techniques .....                       | 209 |
| B.1        | Background to Antenna Measurement.....                     | 209 |
| B.2        | Antenna Test Range .....                                   | 209 |
| B.3        | Antenna Range Instrumentation †.....                       | 209 |
| B.4        | Typical Applications of Antenna Range Instrumentation..... | 211 |
| B.4.1      | Near-Field Range .....                                     | 211 |
| B.4.2      | Indoor Far-Field Range .....                               | 211 |
| B.5        | Special Precautions for Measurements .....                 | 212 |
| Appendix C | Component Datasheets.....                                  | 215 |
| Appendix D | Substrate Datasheet.....                                   | 236 |



# List of Figures

|  |    |
|--|----|
| Fig. 1.1 Challenges in wireless technology. The highlighted boxes are discussed in this dissertation. ....   | 6  |
| Fig. 2.1 Antenna as a transition device .....  | 8  |
| Fig. 2.2 Coordinate system for Hertzian dipole. ....   | 8  |
| Fig. 2.3 Equivalent circuit of an antenna .....  | 11 |
| Fig. 2.4 UWB system link level characterization in frequency domain. ....  | 16 |
| Fig. 2.5 UWB system link level characterization in time domain. ....   | 18 |
| Fig. 2.6 Group delay measurement system set-up. Two main orientations are face to face and side by side.....   | 20 |
| Fig. 2.7 Dipole antenna with (a) balanced feeding (b) unbalanced feeding (c) balun. ....   | 22 |
| Fig. 2.8 Geometry of a monopole antenna. The ground plane acts as an electric mirror, hence, a monopole with length $l/2$ is equivalent to a dipole with length $l$ . .... | 24 |
| Fig. 2.9 Monopole antenna variations.....  | 24 |
| Fig. 2.10 Planar inverted F antenna (PIFA) .....   | 25 |
| Fig. 2.11 Various shapes of the patch antenna ¶.....   | 26 |
| Fig. 2.12 Variants on patch antenna feed arrangements ¶ .....  | 26 |
| Fig. 2.13 Geometry of a typical square microstrip patch antenna. ....  | 26 |
| Fig. 2.14 Geometry of a centre fed thick dipole. ....  | 27 |
| Fig. 2.15 Geometry of conical antennas. Increasing the volume of the poles increases the bandwidth.....  | 28 |
| Fig. 2.16 Vertical planar monopole antennas with various shapes (a) square, (b) trapezoid, (c) triangular, (d) circle, (e) ellipse.....                                    | 28 |

|  |    |
|--|----|
| Fig. 2.17 Vertical planar monopole antennas with improved characteristics. (a) square monopole with notches, (b) square monopole with bevels, (c) shorted square monopole with bevels, (d) square monopole with fork-shape feeding, (e) cross square monopole. ....  | 29 |
| Fig. 2.18 Typical configurations of printed UWB antennas. (a) microstrip fed bevelled square monopole, (b) CPW fed circular disc monopole, (c) printed circular dipole antenna, (d) slot antenna, (e) elliptic monopole with elliptic ground plane.....  | 29 |
| Fig. 2.19 Geometry of common frequency independent antennas.....   | 30 |
| Fig. 3.1 UWB supports large relative and absolute bandwidth compared to narrowband and wideband communication. ....  | 37 |
| Fig. 3.2 The cognition cycle in cognitive radio network. ....  | 41 |
| Fig. 3.3 Dynamic spectrum access model.....  | 42 |
| Fig. 3.4 Hierarchical access model (a) spectrum underlay, (b) spectrum overlay. ....   | 43 |
| Fig. 3.5 Cognitive radio architecture with parallel sensing and communications. ....   | 44 |
| Fig. 3.6 Cognitive radio architecture with combined sensing and communications.....  | 44 |
| Fig. 3.7 Various shapes of the radiators for CPW fed UWB monopoles.....  | 48 |
| Fig. 3.8 Various modified ground plane for UWB monopoles, (a) have notches, slots and slits, (b) bevels, (c) cut outs and bevels at the feed point. ....   | 49 |
| Fig. 3.9 Various feeding structures for UWB monopoles, (a) asymmetrically feeding, (b) multiple feeding points. ....   | 49 |
| Fig. 3.10 Schematic of UWB antenna operation principle † .....   | 49 |
| Fig. 3.11 Examples of dual band inverted F and L antennas. (a) A double inverted-L antenna for dual-band operation, (b) An inverted-L antenna with a parasitic inverted-L (PIL) element for bandwidth enhancement, (c) An inverted-FL antenna for dual-band operation, (d) An inverted-FL antenna with a parasitic inverted-L element for bandwidth enhancement..... | 51 |
| Fig. 3.12 Some dual band top patches for PIFA. Dual band is achieved by creating two resonant paths on the patch by cutting slots and slits † .....  | 51 |
| Fig. 3.13 Multiband antenna design technique using additional resonating path (Note that this diagram is a symbolic representation of the technique).....  | 52 |

|  |    |
|--|----|
| Fig. 3.14 Multiband antenna design technique using filtering structures (Note that this diagram is a symbolic representation of the technique).....  | 52 |
| Fig. 3.15 A band notched antenna using a wide slot antenna and an interdigital hairpin resonator filtering structure .....   | 54 |
| Fig. 3.16 Dual band antenna based on band notching a wideband antenna .....  | 54 |
| Fig. 3.17 Several examples of various band rejection techniques using, (a) U shaped slot † (b) L shaped slot (spurline) † (c) split ring resonator † (d) parasitic element . ....  | 55 |
| Fig. 3.18 Multiband antenna design technique using multiple element. (Note that this diagram is a symbolic representation of the technique).....   | 56 |
| Fig. 3.19 Schematic diagrams of multiband antennas based on multiple antenna approach, (a) dual port PILA and PIFA † (b) dual port slot antenna † (c) monopole and disc cone antenna , (d) reconfigurable monopole and PIFA . .... | 57 |
| Fig. 3.20 15 different two-antenna configurations on a finite ground plane. The matchsticks symbolize the PIFAs, and the dot on the matchstick denotes the location of the shorting pin †  | 58 |
| Fig. 3.21 Schematic diagram of the 2.4-GHz planar polarization-diversity antenna with a polarization-selection p-i-n diode circuit. ....   | 60 |
| Fig. 3.22 Schematic diagram of the three port orthogonal dipole antenna with integrated baluns for polarization diversity. ....  | 60 |
| Fig. 3.23 Schematic diagram of the four port orthogonal slot antenna with a cross slot inserted in between elements for port isolation and bandwidth enhancement † .....   | 60 |
| Fig. 3.24 Left: Two-port antenna without coupling cancellation. Right: Cancellation of path A by a second path B † .....   | 61 |
| Fig. 3.25 Schematic diagram of MIMO antennas with slits in the ground plane.....   | 62 |
| Fig. 3.26 Schematic diagram of the MIMO antennas with stub. ....   | 63 |
| Fig. 3.27 Schematic diagram of the PIFAs with (a) split ring resonator (b) parasitic decoupling element † (c) suspended transmission line. ....  | 64 |
| Fig. 3.28 Schematic diagram of the antenna with combination of decoupling techniques.....  | 64 |
| Fig. 3.29 The function blocks of the decoupling structure . ....   | 65 |

|   |    |
|---|----|
| Fig. 3.30 Schematic diagram of the LTE antenna with a branchline decoupling feed network  | 65 |
| Fig. 3.31 Schematic of the reconfigurable antennas.   | 69 |
| Fig. 4.1 Coplanar waveguide configuration   | 83 |
| Fig. 4.2 The geometry of the CPW fed circular disc monopole antenna.  | 84 |
| Fig. 4.3 Simulated reflection coefficient of circular disc monopole antenna shown in Fig. 4.2.  | 85 |
| Fig. 4.4 H-field distribution at (a) 3GHz and (b) 17 GHz.   | 85 |
| Fig. 4.5 The geometry of a PIFA.  | 86 |
| Fig. 4.6 The geometry of the integrated circular disc monopole and PIFA.  | 87 |
| Fig. 4.7 The simulated reflection coefficients of narrowband PIFA and circular disc wideband antennas shown in Fig. 4.6.                              | 88 |
| Fig. 4.8 The simulated transmission coefficient of the integrated disc monopole and PIFA shown in Fig. 4.6.   | 89 |
| Fig. 4.9 The geometry of the CPW fed hour glass monopole antenna.   | 90 |
| Fig. 4.10 Simulated and measured reflection coefficient of hour glass monopole antenna shown in Fig. 4.9.   | 90 |
| Fig. 4.11 The geometry of the integrated hour glass wideband antenna and PIFA.  | 92 |
| Fig. 4.12 Simulated and measured reflection coefficient of the hour glass wideband antenna shown in Fig. 4.11.  | 93 |
| Fig. 4.13 Simulated and measured reflection coefficient of the narrowband PIFA shown in Fig. 4.11.  | 93 |
| Fig. 4.14 Simulated and measured transmission coefficient of the integrated hour glass monopole and PIFA shown in Fig. 4.11.                          | 93 |
| Fig. 4.15 Simulated and measured radiation pattern of the wideband antenna shown in Fig. 4.11 at 4.4 GHz. (a) <i>xy</i> -plane, (b) <i>zy</i> -plane. | 95 |
| Fig. 4.16 Simulated and measured radiation pattern of the wideband antenna shown in Fig. 4.11 at 10 GHz. (a) <i>xy</i> -plane, (b) <i>zy</i> -plane.  | 95 |

|  |     |
|--|-----|
| Fig. 4.17 Simulated and measured radiation patterns of the narrowband antenna shown in Fig. 4.11 at 5.15GHz (a) $xy$ -plane, (b) $zx$ -plane. ....             | 95  |
| Fig. 4.18 Simulated input impedance of the wideband antenna shown in Fig. 4.11. ....   | 96  |
| Fig. 4.19 Simulated input impedance of the narrowband antenna shown in Fig. 4.11. ....   | 96  |
| Fig. 4.20 Current distributions when the wideband antenna is excited and the narrowband antenna is terminated to a $50\Omega$ load.(a) 4.4GHz, (b) 10GHz. .... | 97  |
| Fig. 4.21 Current distributions when the narrowband antenna is excited and the wideband antenna is terminated to a $50\Omega$ load.(a) 4.4GHz, (b) 10GHz. .... | 98  |
| Fig. 4.22 Simulated 3D radiation pattern of wideband antenna shown in Fig. 4.11. (a) 4.4GHz, (b) 10GHz. ....   | 99  |
| Fig. 4.23 Simulated 3D radiation pattern of narrowband antenna shown in Fig. 4.11 at 5.15GHz. ....   | 99  |
| Fig. 4.24 Simulated reflection coefficient curves for different $W_g$ (a) wideband antenna, (b) narrowband antenna. ....                                       | 101 |
| Fig. 4.25 Simulated reflection coefficient curves for different $L_g$ (a) wideband antenna, (b) narrowband antenna. ....                                       | 103 |
| Fig. 4.26 Simulated reflection coefficient curves for different $L_p$ (a) wideband antenna, (b) narrowband antenna. ....                                       | 105 |
| Fig. 4.27 Simulated reflection coefficient curves for different $W_p$ . ....   | 106 |
| Fig. 4.28 Simulated reflection coefficient curves for different $d$ ....   | 107 |
| Fig. 4.29 Simulated reflection coefficient curves for different $h$ (a) wideband antenna, (b) narrowband antenna. ....   | 108 |
| Fig. 4.30 Integrated slot antenna and monopole. ....   | 109 |
| Fig. 4.31 Two port monopole antenna. ....  | 110 |
| Fig. 4.32 Two port wideband and rotating narrowband antenna $\uparrow$ . ....  | 110 |
| Fig. 4.33 Two port UWB MIMO antenna. ....  | 110 |

|   |     |
|---|-----|
| Fig. 5.1 The schematic of the antenna with highlighted microstrip to tapered slot transition.   | 115 |
| Fig. 5.2 Simulated current distribution at 5.15GHz. (a) top view (b) bottom view.   | 115 |
| Fig. 5.3 Simulated transmission coefficient curves for different d.   | 116 |
| Fig. 5.4 Geometry of configuration A, (a) top view, (b) bottom view.  | 118 |
| Fig. 5.5 Simulated and measured S parameter of configuration A antenna. (a) Transmission coefficient, (b) wideband antenna reflection coefficient, (c) narrowband antenna reflection coefficient. | 119 |
| Fig. 5.6 Geometry of configuration B, (a) top view, (b) bottom view.  | 120 |
| Fig. 5.7 Simulated and measured S parameter of configuration B antenna. (a) Transmission coefficient, (b) wideband antenna reflection coefficient, (c) narrowband antenna reflection coefficient. | 121 |
| Fig. 5.8 Geometry of configuration C, (a) top view, (b) bottom view.  | 122 |
| Fig. 5.9 Simulated and measured S parameter of configuration C antenna. (a) Transmission coefficient, (b) wideband antenna reflection coefficient, (c) narrowband antenna reflection coefficient. | 123 |
| Fig. 5.10 Block diagram of the antenna with the decoupling network.   | 124 |
| Fig. 5.11 Block diagram of the antenna with the decoupling network and compensating transmission lines.   | 127 |
| Fig. 5.12 Decoupling network design steps.  | 129 |
| Fig. 5.13 S parameters of the integrated wideband-narrowband antenna.   | 130 |
| Fig. 5.14 Calculated $\phi_2 - \phi_1$ .  | 130 |
| Fig. 5.15 Calculated $\theta'$ .  | 130 |
| Fig. 5.16 Calculated scattering parameter with and without network for the whole 3-11GHz band.  | 131 |
| Fig. 5.17 Port matching variation after adding the network (a) wideband antenna (b) narrowband antenna.   | 133 |

|  |     |
|--|-----|
| Fig. 5.18 The geometry of the 180° hybrid. ....  | 134 |
| Fig. 5.19 Simulated 180° hybrid coupler S parameter. ....  | 135 |
| Fig. 5.20 Simulated S parameters of the antenna and decoupling network. ....   | 136 |
| Fig. 5.21 Measured transmission coefficient for all three configurations and the reference antenna. ....   | 137 |
| Fig. 6.1 Circuit diagrams L-section matching network, (a) normal (b) reversed. ....  | 141 |
| Fig. 6.2 Three-element matching network (a) $\Pi$ network (b) T network. ....  | 143 |
| Fig. 6.3 Equivalent L network for a $\Pi$ network. ....  | 143 |
| Fig. 6.4 The topology of the antenna with an integrated matching circuit. ....   | 145 |
| Fig. 6.5 Tuning circuit diagram for 4GHz. ....   | 146 |
| Fig. 6.6 Simulated and measured reflection coefficient of the antenna with a 4 GHz matching circuit. ....  | 146 |
| Fig. 6.7 Tuning circuit diagram for 8GHz. ....   | 148 |
| Fig. 6.8 Simulated and measured reflection coefficient of the antenna with a 8 GHz matching circuit. ....  | 148 |
| Fig. 6.9 Tuning circuit diagram for 10GHz. ....  | 149 |
| Fig. 6.10 Simulated and measured reflection coefficient of the antenna with a 10 GHz matching circuit. ....  | 149 |
| Fig. 7.1 (a) The Nike+ iPod sport set (b) a PIFA antenna on the sensor component (c) chip antenna on the receiver. ....  | 154 |
| Fig. 7.2 (a) Four sector Vivaldi antenna, (b) isolated antenna radiation pattern, (c) the four sector Vivaldi antenna mounted on a television camera (d) integrated antenna radiation patterns. .... | 156 |
| Fig. 7.3 UWB mono-cone antenna integrated into a DVD player and the calculated radiation pattern at 7GHz. ....   | 157 |
| Fig. 7.4 Internal 2.4 GHz UWB antenna for wireless dongle applications. ....   | 157 |
| Fig. 7.5 Reported solutions for ground plane surface current in UWB antennas. (a) Ferrite choke (b) ground plane slots (c) asymmetric feeding and radiator. ....                                     | 159 |

|   |     |
|---|-----|
| Fig. 7.6 (a) edge current RF choke (b) coaxial cable RF choke (c) RF chokes on horn antenna (d) RF choke on handset antenna (e) RF choke on handset antenna                                     | 161 |
| Fig. 7.7 The geometry of the isolated antenna.  | 164 |
| Fig. 7.8 The 3D view of the integrated antenna.   | 164 |
| Fig. 7.9 The geometry of the antenna integrated with PCB. (The dotted rectangles represent areas of conventional CPW and conductor-backed CPW)  | 166 |
| Fig. 7.10 Schematic of conductor-backed CPW on a dielectric substrate of a finite thickness   | 166 |
| Fig. 7.11 The CPW to microstrip transition feeding. Electric field at each cross-section along the transition, (a) microstrip, (b) CBCPW, (c) CPW.  | 167 |
| Fig. 7.12 Surface current distribution on the ground plane of the integrated antenna at 7.25 GHz.   | 168 |
| Fig. 7.13 Modeling the integrated antenna with an asymmetrically-fed dipole.  | 168 |
| Fig. 7.14 The geometry of the antenna integrated with PCB with RF chokes.   | 169 |
| Fig. 7.15 Surface current distribution on the PCB for integrated antenna with RF chokes at 7.25GHz.   | 170 |
| Fig. 7.16 Simulated reflection coefficients of the isolated antenna and integrated antenna with and without RF chokes.  | 171 |
| Fig. 7.17 Simulated antenna gain patterns in H and E planes, (a) 6 GHz, (b) 7.25 GHz, (c) 8.5 GHz.  | 173 |
| Fig. 7.18 The antenna gain pattern in xy-plane. RF chokes improve and stabilize the radiation pattern in H- plane in all frequencies.   | 174 |
| Fig. 7.19 Simulated (a) reflection coefficient (b) radiation patterns of the integrated antenna for different lengths of the PCB. The stable results show that the PCB radiation is controlled. | 175 |
| Fig. 7.20 Simulated (a) reflection coefficient (b) radiation patterns of the integrated antenna for different widths of the PCB. The stable results show that the PCB radiation is controlled.  | 176 |



|   |     |
|---|-----|
| Fig. 7.21 The antenna group delay in $xy$ -plane, (a) isolated antenna, (b) integrated antenna without RF chokes, (c) integrated antenna with RF chokes.....  | 179 |
| Fig. 7.22 The time signals (a) excitation pulse (b) received signal at $\theta=90^\circ$ , $\varphi=0^\circ$ . Integration results in smaller received signal level and stronger ringing effect. .... | 180 |
| Fig. 7.23 Final prototype board cross-section.....  | 181 |
| Fig. 7.24 Final antenna prototype and the feedline cross section. ....  | 182 |
| Fig. 7.25 Photos of the final prototype. ....   | 184 |
| Fig. 7.26 Antenna reflection coefficient in time domain. ....   | 185 |
| Fig. 7.27 The ungated and gated measured reflection coefficient. ....   | 186 |
| Fig. 7.28 Simulated and measured reflection coefficient.....  | 187 |
| Fig. 7.29 The measured efficiency and peak gain.....  | 187 |
| Fig. 7.30 The simulated and measured radiation patterns at 8.5GHz, (a) 6 GHz, (b) 7.25 GHz, (c) 8.5 GHz. ....   | 188 |
| Fig. 8.1 Summary of the areas covered and the main achievements in this dissertation. ....  | 199 |

## List of Tables

|  |     |
|--|-----|
| Table 3.1 FCC emission power limit for various UWB applications in each operating band . | 37  |
| Table 6.1 Element values for the normal L network at 4GHz. ....                          | 146 |
| Table 6.2 Calculated element values for the high pass $\Pi$ network at 8GHz. ....        | 148 |
| Table 6.3 Calculated element values for the reversed high pass L network at 10GHz. ....  | 149 |
| Table 6.4 Efficiency and gain of various narrowband antennas. ....                       | 150 |
| Table 7.1 3D gain variations for the three cases. ....                                   | 172 |
| Table 7.2 Group delay variation comparison for the two scenarios. ....                   | 177 |

## List of Abbreviations

|                |   |
|----------------|---|
| <b>CBCPW</b>   | Conductor <b>B</b> acked <b>Co</b> Planar <b>W</b> aveguide                 |
| <b>CPW</b>     | <b>Co</b> Planar <b>W</b> aveguide  |
| <b>CR</b>      | Cognitive <b>R</b> adio   |
| <b>DGS</b>     | <b>D</b> efected <b>G</b> round <b>S</b> tructure                           |
| <b>DVB-H</b>   | <b>D</b> igital <b>V</b> ideo <b>B</b> roadcasting- <b>H</b> igh definition |
| <b>EBG</b>     | <b>E</b> lectromagnetic <b>B</b> and <b>G</b> ap                            |
| <b>EM</b>      | <b>E</b> lectro <b>M</b> agnetic  |
| <b>EMC</b>     | <b>E</b> lectromagnetic <b>C</b> ompatibility                               |
| <b>FCC</b>     | <b>F</b> ederal <b>C</b> ommunication <b>C</b> ommission                    |
| <b>FDTD</b>    | <b>F</b> inite <b>D</b> ifference <b>T</b> ime <b>D</b> omain               |
| <b>FIT</b>     | <b>F</b> inite <b>I</b> ntegration <b>T</b> echnique                        |
| <b>GPS</b>     | <b>G</b> lobal <b>P</b> ositioning <b>S</b> ystem                           |
| <b>GSM</b>     | <b>G</b> lobal <b>S</b> ystem for <b>M</b> obile <b>C</b> ommunication      |
| <b>HF</b>      | <b>H</b> igh <b>F</b> requency  |
| <b>ID</b>      | <b>I</b> ndustrial <b>D</b> esign   |
| <b>IMT2000</b> | <b>I</b> nternational <b>M</b> obile <b>T</b> elecommunications-2000        |
| <b>IR</b>      | <b>I</b> mpulse <b>R</b> adio   |
| <b>ISM</b>     | <b>I</b> ndustrial <b>S</b> cientific <b>M</b> edical                       |

|              |  |
|--------------|--|
| <b>LTE</b>   | <b>Long Term Evolution</b>                             |
| <b>MEMS</b>  | <b>MicroElectroMechnaical System</b>                   |
| <b>MIC</b>   | <b>Microwave Integrated Circuit</b>                    |
| <b>MIMO</b>  | <b>Multiple Input Multiple Output</b>                  |
| <b>OFDM</b>  | <b>Orthogonal Frequency Division Multiplexing</b>      |
| <b>OSA</b>   | <b>Opportunistic Spectrum Access</b>                   |
| <b>PCB</b>   | <b>Printed Circuit Board</b>                           |
| <b>PCS</b>   | <b>Personal Communication Service</b>                  |
| <b>PIFA</b>  | <b>Planar Inverted F Antenna</b>                       |
| <b>PILA</b>  | <b>Planar Inverted L Antenna</b>                       |
| <b>RF</b>    | <b>Radio Frequency</b>                                 |
| <b>SDR</b>   | <b>Software Defined Radio</b>                          |
| <b>SMA</b>   | <b>Sub Miniature version A</b>                         |
| <b>U-NII</b> | <b>Unlicensed National Information Infrastructure</b>  |
| <b>USB</b>   | <b>Universal Serial Bus</b>                            |
| <b>UWB</b>   | <b>Ultra WideBand</b>                                  |
| <b>VHF</b>   | <b>Very High Frequency</b>                             |
| <b>WiMAX</b> | <b>Worldwide Interoperability for Microwave Access</b> |
| <b>WLAN</b>  | <b>Wireless Local Area Network</b>                     |

# **Chapter 1      Introduction**

## **1.1      Background**

The large (more than 25cm long) and heavy (about two Kilograms) Motorola DynaTAC 8000X analogue mobile phone in 1983 was just a beginning to probably one of the most successful inventions in the history. Since then, mobile phones have evolved immensely both in design and function; the bulky devices that were once used exclusively for making and receiving voice calls are currently light and compact and used to send and receive emails, take pictures, play music, game, FM radio and TV. Moreover, easy access to internet for the internet-obsessed societies opens a world of opportunities to every user and yet, this is just the beginning.

It is the demand and appetite for innovations which is driving the overall rapid growth of wireless technology and literally changing people's lives in all sorts of useful ways. Telecommunication industry is not the only market that benefits from the advances in wireless technology; the healthcare, medical diagnosis, treatment and monitoring systems, automotive production and industrial remote monitoring systems have also considerably gained from improvement of the wireless systems. There is a vast opportunity for wearable and logistic applications in security systems and these are just a few applications among many

others. What is really interesting is the fact that it appears that there will be further developments in due course that will challenge the understanding of wireless technology.

## **1.2 Motivation and Objectives**

The impacts of advances in wireless technology deployment are the primary motivations for this research.

Wireless communication systems have evolved substantially over the last two decades. Along with the explosive growth in the number of wireless communication users and applications, the number of wireless standards has been growing and is expected to continue in future, as the demand for various types of wireless services is increasing. Consequently, the regulatory agencies, scientists, engineers and wireless product manufacturers are all facing some tough challenges in realizing efficient wireless communication systems (i.e. networks and terminals). The escalating number of emerging services and standards is reflected in two aspects: 1) spectrum crowding and 2) hardware design complications.

As more and more devices go wireless, spectrum regulatory bodies will confront spectral crowding and coexistence of wireless services with different bandwidth requirements [1]. In general there are four approaches for managing the spectrum access [2].

1) *Licensed spectrum for exclusive usage*, in which the licensee has exclusive usage rights for a specific spectrum.

2) *Licensed spectrum for shared usage*, which restricts the licensed spectrum for shared usage to a specific technology. An example of this approach could be the spectrum used for public safety services.

3) *Unlicensed spectrum*, where the spectrum is available to all radio systems operating according to the regulated standards. The industrial, scientific and medical (ISM) 2.4 GHz band and the unlicensed national information infrastructure (U-NII) 5–6 GHz bands are examples of unlicensed or license exempt spectrum.

4) *Open spectrum*, in which everyone is allowed to access any range of the spectrum without any restriction. However, in order to maintain the quality of service and avoid interference and complexity a minimum set of rules should be respected in this approach.

With the licensed spectrum approach, spectrum resources could often be wasted. For instance, in some cases the spectrum allocated to a communication system is more than what is required. Therefore, only part of the allocated spectrum is used by that specific service and other portions of the spectrum become unused. Similarly, if a service with allocated spectrum is not commercially successful, the licensed spectrum might remain unused. Hence, large parts of the spectrum are currently used inefficiently. Paradoxically, 90-95% of the licensed radio spectrum is not in use at any location at any given time especially that the current radio regulatory regime is too complex to handle the increasingly dynamic nature of emerging wireless applications [2]. Added to the facts that the number of wireless services collocated in a limited range of frequency and also the demand for additional spectrum for higher data rate is growing fast, the regulatory bodies are motivated to employ new strategies in order to resolve the spectrum scarcity in some bands and inefficient use of spectrum in other bands.

Aiming at relaxing the spectrum crowding, in 2002 the Federal Communication Commission (FCC) authorized the unlicensed use of ultra wideband (UWB) technology. Since then, the UWB technology has received significant attention from industry and academia. However, as more parties and technologies utilize unlicensed spectrum, it is becoming more crowded and consequently less available to all. This again necessitates the availability of more spectrum, or more efficient ways to access the spectrum. Cognitive radio (CR) is the key enabling technology which provides the capacity to share the wireless channel with the licensed and unlicensed users in an opportunistic way. Moreover, it can be envisaged that combining UWB and cognitive radio might be promising for resolving the spectrum scarcity and crowding in near future.

As pointed out earlier, the growing demand for development and deployment of new technologies and services has also influenced the hardware design procedure including antennas and radio frequency (RF) front end, particularly in portable devices. To support

multiple services (each with a different RF frequency, bandwidth, modulation etc.) such devices require antenna and RF circuitry with specific characteristics. In order to be fitted into the modern, light and compact terminals, the antennas need to be small and low profile as well as being able to support as many services as possible. Predictably, compact multiband and wideband antennas are necessary for such feature-rich devices.

On the other hand, emerging wireless networks such as CR also impose new requirements on the antenna. Networks with dynamic access to the spectrum might require wideband spectrum sensing running in the background while the system is functioning in its conventional mode of operation. If necessary, the sensing block then feeds back to the communication block for the essential reconfigurations. Realization of such networks involves designing antenna and RF solutions with specific characteristics such as frequency, pattern or polarization reconfigurability.

In the modern compact terminals the antenna is in close proximity of other components such as the printed circuit board (PCB) (populated with all the RF and electronic components), battery and display. Hence, the electromagnetic interaction between the antenna and the other parts should be controlled to avoid any possible degradation of antenna radiation characteristics.

The main objectives for this research are as follow:

- to develop antenna solution for dynamic spectrum access,
- to model and develop antenna concept for compact portable devices in emerging multi standard radios,
- to integrate small antennas into a compact device.

## **1.3 Layout of Thesis**

The thesis is organized as follows. Chapter 2 is dedicated to a brief review of antenna design parameters and elements. UWB antenna elements together with the parameters for characterizing them are reviewed since a large portion of this research focuses on this class of antennas.



Chapter 3 reviews the current and future spectrum management approaches. Due to their higher efficiency the focus is on open and flexible spectrum access techniques. Therefore, their requirements and challenges imposed on designing antennas are explored. In the second part the antenna requirements for multimode terminals are studied and some of the previous works are reviewed.

An antenna solution for multi standard radios is introduced in Chapter 4. A novel concept for efficiently using the space allocated for the antenna is detailed. A two port hybrid wideband-narrowband antenna is introduced as a demonstrator for the proposed concept. The antenna operation principle, design procedure, simulated and measured results are presented in Chapter 4.

The problem of mutual coupling between the ports of the proposed hybrid antenna is addressed in Chapter 5 where two decoupling techniques are introduced, verified and compared.

Chapter 6 introduces another feature of the proposed antenna solution. In addition to a fixed wideband and narrowband functionality, it is also possible to tune the narrowband antenna across a wide range of frequencies. This feature might be promising for operation in networks with dynamic access to the spectrum. The antenna with several matching circuits is examined and verified.

Chapter 7 investigates the practical challenges in designing and integrating small printed UWB antennas into the device platform. The design procedure of a printed planar disc monopole for integration into a large PCB is explored in this chapter. The main goal in the proposed approach is to de-embed the effect of the PCB in order to reasonably maintain radiation characteristics of the antenna in isolation. The antenna together with the PCB is manufactured and measured and simulated results are compared.

Finally Chapter 8 draws conclusion to the work. The primary objectives are reviewed and the significant achievements are highlighted. Furthermore, this chapter presents the challenges which are still remained and worthwhile to investigate as future research topics.

Fig. 1.1 illustrates the issues addressed in this thesis in summary.

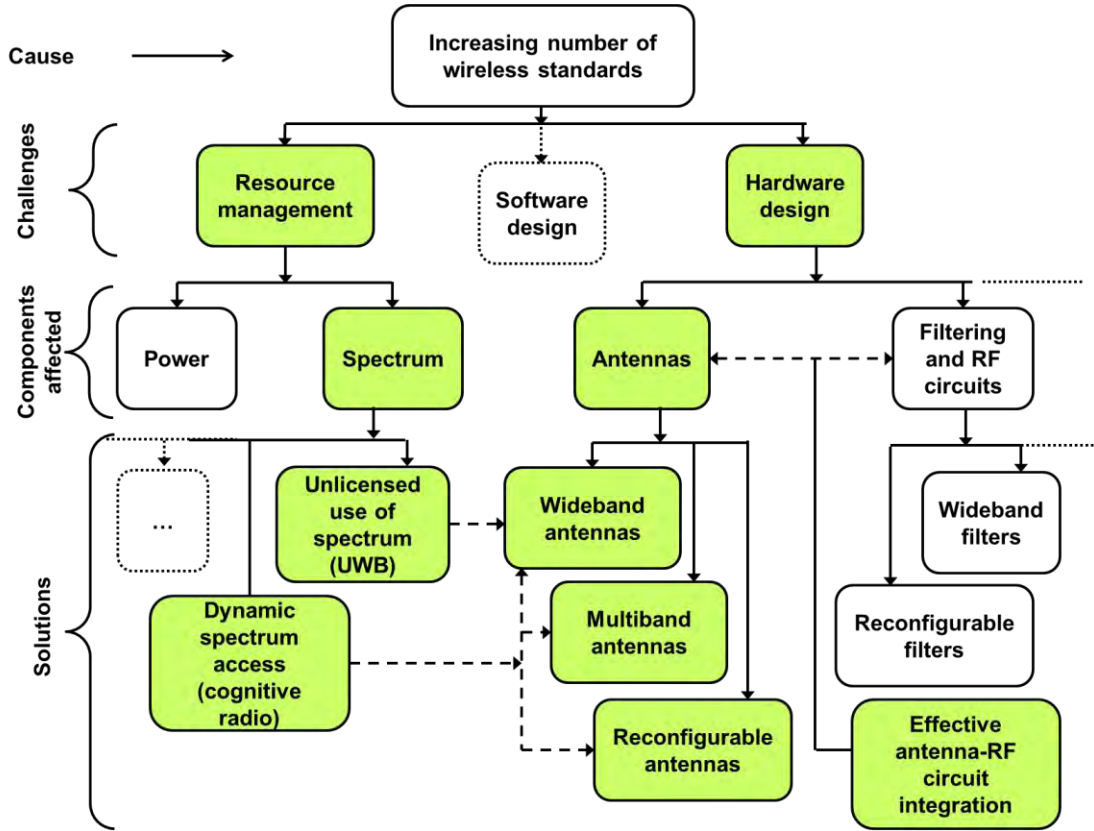


Fig. 1.1 Challenges in wireless technology. The highlighted boxes are discussed in this dissertation.

## References

- [1] H. Arslan, Z. N. Chen and M.-G. Di Benedetto, *Ultra Wideband Wireless Communication*, JohnWiley & Sons, ISBN 0-471-71521-2, New Jersey, United States of America, 2006.
- [2] L. Berlemann and S. Mangold, *Cognitive Radio and Dynamic Spectrum Access*, JohnWiley & Sons, ISBN 978-0-470-51167-1, West Sussex, United Kingdom, 2009.

## **Chapter 2      Antenna Theory**

### **2.1      Introduction**

An *antenna* is defined by the IEEE Standard Definitions [1] as “a means for radiating or receiving radio waves”. It transforms the electric energy to electromagnetic energy and vice versa. In other words the antenna enables the transition of energy between a guiding device, such as coaxial line or a waveguide to free-space as shown in Fig. 2.1[2]. In a radio link the antenna is the final block on the transmission side and is the first block on the receiving side. Thus, the antenna is a fundamental and essential component of all wireless communication systems.

As the most fundamental antenna element, the Hertzian dipole is elaborated in this chapter. It will then be used to define the common antenna parameters and terminology. Antennas can be classified into numerous groups according to their radiation principle, physical structure, manufacturing technology and/or radiation characteristics. However, only some antenna elements which have been commonly used in small wireless devices will be reviewed here. In order to complement the next chapters the antenna definitions and parameters relevant to wideband and UWB systems will also be reviewed and the evolution of the UWB antennas from simple forms to current types will be described.

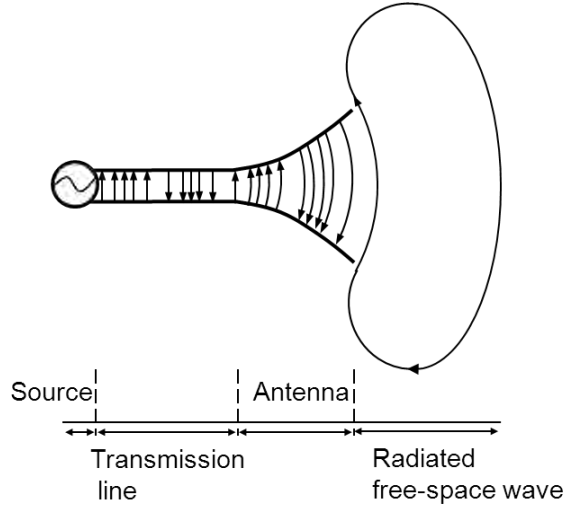


Fig. 2.1 Antenna as a transition device [2].

## 2.2 Hertzian Dipole

A wire of infinitesimal length  $dl$  ( $dl \ll \lambda$ ) is known as a Hertzian dipole. The wire is very thin and its radius  $a$  is much smaller than the wavelength. It is the fundamental antenna element since any finite-length antenna can be modelled as an infinite number of Hertzian dipoles. As shown in Fig. 2.2 the dipole is positioned symmetrically at the origin of the coordinate system and excited by a current  $I(t)$  along the  $z$ -axis. Since the antenna is very short, the dipole is equivalent to a constant current source  $I_0 dl$ .

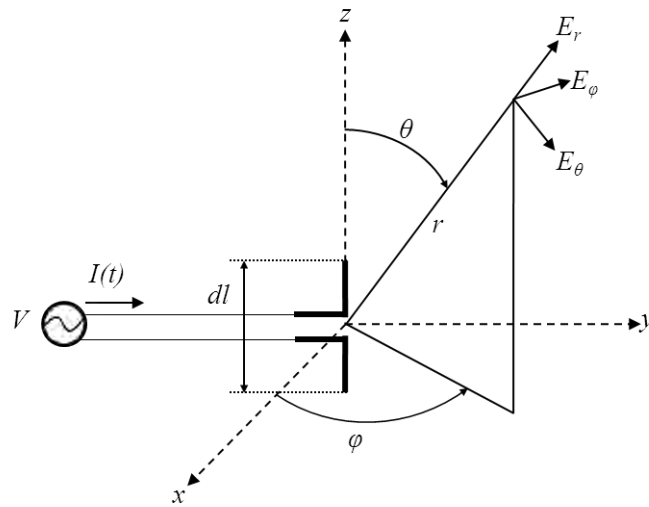


Fig. 2.2 Coordinate system for Hertzian dipole.

To obtain the radiated electromagnetic fields, it is required to solve Maxwell's equations [2]. First the vector potential  $\vec{A}$  needs to be calculated by (2.1). It is important to note that throughout this thesis all calculations are done for the waves propagating in free space.

$$\vec{A} = \frac{\mu_0 I_0 dl}{4\pi r} e^{-jkr} \vec{z} \quad (2.1)$$

It is then transformed to spherical coordinates with

$$A_r = A_z \cos \theta = \frac{\mu_0 I_0 dl}{4\pi r} e^{-jkr} \cos \theta \quad (2.2)$$

$$A_\theta = A_z \sin \theta = \frac{\mu_0 I_0 dl}{4\pi r} e^{-jkr} \sin \theta$$

$$A_\phi = 0.$$

The relation between  $\vec{A}$ ,  $\vec{H}$  and  $\vec{E}$  can be defined by Maxwell's equation:

$$\nabla \times \vec{E} = -j\omega\mu\vec{H} \quad (2.3)$$

$$\vec{H} = \frac{1}{\mu} \nabla \times \vec{A}$$

Following this procedure the  $E$ - and  $H$ -field can be found with (2.4).

$$H_r = H_\theta = 0 \quad (2.4)$$

$$H_\phi = j \frac{\mu_0 I_0 dl \sin \theta}{4\pi r} \left[ 1 + \frac{1}{jkr} \right] e^{-jkr}$$

$$E_r = \eta \frac{\mu_0 I_0 dl \sin \theta}{2\pi r^2} \left[ 1 + \frac{1}{jkr} \right] e^{-jkr}$$

$$E_\theta = j\eta \frac{\mu_0 I_0 dl \sin \theta}{4\pi r} \left[ 1 + \frac{1}{jkr} - \frac{1}{(kr)^2} \right] e^{-jkr}$$

$$E_\phi = 0$$

where  $k = \frac{2\pi}{\lambda}$  is the wave number and  $\eta = \sqrt{\mu/\epsilon}$  is the intrinsic impedance in  $\Omega$ .

The fields can be simplified by defining three sub-regions around the antenna; reactive region, radiating near-field and far-field region. The far-field region is characterized by  $kr \gg 1$  in which the fields can be simplified to (2.5).

$$H_\phi \approx j \frac{\mu_0 I_0 dl \sin \theta}{4\pi r} e^{-jkr} \quad (2.5)$$

$$E_\theta \approx j \eta \frac{\mu_0 I_0 dl \sin \theta}{4\pi r} e^{-jkr}$$

$$E_\phi \approx E_r = H_r = H_\theta = 0$$

In this region the angular field distribution is essentially independent of the distance from the antenna. The field components are perpendicular to each other and transverse to the direction of propagation.

## 2.3 General Antenna Parameters

### 2.3.1 Antenna Impedance

The antenna impedance,  $Z_a$ , is defined as the ratio of the voltage at the feeding point of the antenna  $V(0)$  to the resulting current flowing in the antenna  $I$  as shown in (2.6).

$$Z_a = \frac{V(0)}{I} \quad (2.6)$$

$$Z_a = R_a + jX_a$$

where  $X_a$  is the antenna reactance and  $R_a = R_r + R_l$  is the antenna resistance,  $R_r$  is the radiation resistance and  $R_l$  is the Ohmic loss occurring in the antenna. The equivalent circuit for an antenna system is depicted in Fig. 2.3.

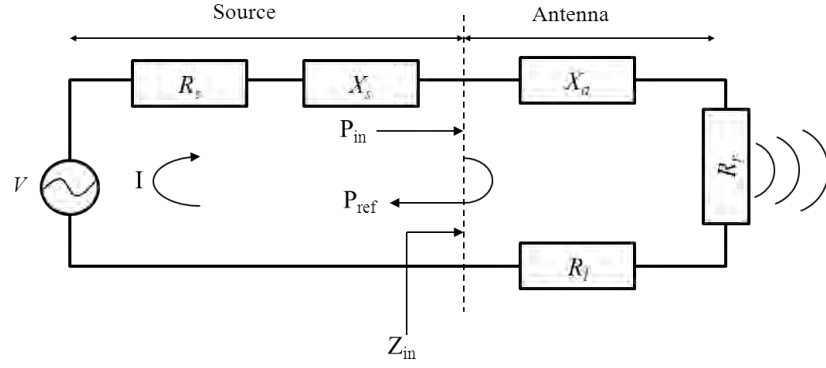


Fig. 2.3 Equivalent circuit of an antenna

### 2.3.2 Impedance Matching

In order to deliver the maximum power from the source to the antenna the antenna impedance should be matched to the generator impedance. This means that the conditions in (2.7) should be satisfied.

$$R_s = R_a \quad (2.7)$$

$$X_s = -X_a$$

### 2.3.3 Reflection Coefficient

Reflection coefficient is a measure of effectiveness of power delivered to a load such as an antenna. If the power incident on the antenna is  $P_{in}$  and the reflected power from the antenna to the source is  $P_{ref}$ , the degree of mismatch between the reflected and incident power is given with (2.8).

$$\text{Reflection coefficient} = -10 \log_{10} \left( \frac{P_{in}}{P_{ref}} \right) (dB) \quad (2.8)$$

### 2.3.4 Antenna Bandwidth

Antenna bandwidth is defined as “the range of frequencies within which the performance of the antenna, with respect to some characteristic, conforms to a specified standard” [1]. It can be determined either as *absolute bandwidth* or a *fractional bandwidth*. Taking  $f_l$  and  $f_h$  as the lower and higher ends of the bandwidth the absolute bandwidth is simply defined as the difference of the two ends ( $f_h - f_l$ ). It is within this range that the antenna characteristics such as input impedance, pattern, beamwidth or gain are within the acceptable values specified by the standard. The fractional bandwidth is expressed as the percentage of the frequency difference over the centre frequency as shown in (2.9).

$$\text{Fractional bandwidth (\%)} = 2 \frac{f_h - f_l}{f_h + f_l} \times 100 \quad (2.9)$$

An antenna is classified as *narrowband* if the fractional bandwidth is below 1% otherwise it is wideband [3]. A UWB antenna, according to the FCC, is an antenna with a bandwidth exceeding 500 MHz. In 2002, the FCC also authorized the unlicensed usage of the 3.1- 10.6 GHz for UWB applications [4]. The European regulation sets the 6-8.5 GHz as the UWB band [5].

Generally in wireless communications, the impedance bandwidth is defined as the range of frequencies over which the antenna reflection coefficient is less than -10 dB. However for most wireless, device-integrated small antennas such as digital video broadcasting- high definition (DVB-H) antennas, due to the limitations the standard is relaxed and the reflection coefficient of -6 dB and even lower may be acceptable [6]. It is important to note that the reflection coefficient is a measure of reflected power at the antenna port. Therefore, low reflection coefficient shows that most of the incident power is not reflected to the port. However, it does not show if the power is radiated or dissipated as loss. Thus, the reflection coefficient is not sufficient for characterizing the antenna and other parameters such as efficiency should also be taken into consideration.



### 2.3.5 Radiation Pattern

According to IEEE standard definition the antenna radiation pattern is “a mathematical function or a graphical representation of the radiation properties of the antenna as a function of space coordinates. In most cases, the radiation pattern is determined in the far-field region and is represented as a function of the directional coordinates”. The two- or three-dimensional spatial distribution of radiated energy in the coordinate shown in Fig. 2.2 is of most concern. The three-dimensional pattern can be constructed using multiple two-dimensional patterns. In practice, few plots of pattern at certain  $\varphi$  and  $\theta$  values are used to derive the required information.

For a linearly polarized antenna, performance is often described in terms of its principal  $E$ - and  $H$ -plane patterns. The  $E$ -plane is defined as “the plane containing the electric field vector and the direction of maximum radiation,” and the  $H$ -plane as “the plane containing the magnetic-field vector and the direction of maximum radiation” [1].

The antenna radiation pattern can be described using three main radiation patterns. A hypothetical lossless antenna having equal radiation in all directions provides an *isotropic pattern* [1]. Such radiator is not physically realizable; however, it is often taken as a reference for expressing the directive properties of actual antennas. A *directional pattern* is provided by an antenna which radiates or receives electromagnetic waves more effectively in some directions than in others. In case that the pattern is essentially non-directional in a given plane and directional in any orthogonal plane then the pattern is called *omni-directional*. An omni-directional pattern is then a special type of a directional pattern.

Polarization of an antenna in a given direction is defined as “the polarisation of the wave transmitted (radiated) by the antenna.” Polarization of a radiated wave is defined as “that property of an electromagnetic wave describing the time-varying direction and relative magnitude of the electric-field vector; specifically, the figure traced as a function of time by the extremity of the vector at a fixed location in space, and the sense in which it is traced, as observed along the direction of propagation.” Polarization then is the curve traced by the end

point of the arrow (vector) representing the instantaneous electric field. The field must be observed along the direction of propagation.

Polarisation may be classified as linear, circular, or elliptical. If the vector that describes the electric field at a point in space as a function of time is always directed along a line, the field is said to be linearly polarized. In general, however, the figure that the electric field traces is an ellipse, and the field is said to be elliptically polarized. Linear and circular polarizations are special cases of elliptical, and they can be obtained when the ellipse becomes a straight line or a circle, respectively. The figure of the electric field is traced in a clockwise (CW) or counter clockwise (CCW) sense. The ratio of orthogonal components of the radiating field is known as axial ratio.

It is important to note that other than the antenna impedance bandwidth, the antenna bandwidth can be defined for other parameters such as polarization or axial ratio.

### **2.3.6 Directivity, Gain and Efficiency**

The ratio of the radiation intensity  $U$  in a given direction from the antenna to the radiation intensity of an isotropic antenna  $U_0$  is known as the directivity  $D$  of an antenna [1].

In mathematical form, it can be written as (2.10)

$$D = \frac{U}{U_0} = \frac{U}{(P_{rad}/4\pi)} \quad (2.10)$$

where  $P_{rad}$  is the total radiated power. If the direction is not specified, the direction of maximum intensity is used to describe the antenna directivity.

Another useful parameter for describing the antenna radiation characteristics is antenna gain  $G$ . Its definition is closely related to the directivity. Unlike directivity which only describes the directional properties of the antenna, the antenna gain is a measure that takes into account the radiation efficiency  $e_{rad}$  as well as the directivity.

Using the equivalent circuit of the antenna in (2.6) the radiation efficiency of the antenna is the ratio of power delivered to the radiation resistance  $R_r$  to the power delivered to

the total antenna resistance, that is  $R_a = R_r + R_l$ . So, the radiation efficiency can be written as (2.11) and the antenna gain can then be calculated using (2.12).

$$e_{rad} = \frac{\frac{1}{2} R_r |I|^2}{\frac{1}{2} R_r |I|^2 + \frac{1}{2} R_l |I|^2} = \frac{R_r}{R_r + R_l} \quad (2.11)$$

$$G = e_{rad} D. \quad (2.12)$$

## 2.4 UWB Antenna Characterization

Narrowband antenna characteristics are typically described in frequency domain. Such characteristics are normally assumed to be constant over the narrow bandwidth. For UWB systems, the frequency-dependent characteristics of the antennas together with the frequency-dependent behaviour of the channel have to be considered. UWB systems are often realized in impulse-based technology, and therefore the time-domain properties have to be considered as well [4]. Hence there is a demand for both a frequency domain representation and a time domain representation of the system description.

### 2.4.1 Frequency Domain Signal Link

The following parameters are required to express the frequency domain link:

- amplitude of transmit signal  $U_{Tx}(f)$  in [V],
- amplitude of receive signal  $U_{Rx}(f)$  in [V],
- radiated field strength at distance  $r$   $E_{Tx}(f, r, \theta_{Tx}, \phi_{Tx})$  in [V/m],
- transfer function of the transmit antenna  $G_{Tx}(f, r, \theta_{Tx}, \phi_{Tx})$  in [m],
- transfer function of the receive antenna  $G_{Rx}(f, r, \theta_{Tx}, \phi_{Tx})$  in [m],
- characteristic transmit antenna impedance  $Z_{C,Tx}(f)$  in [ $\Omega$ ],
- characteristic receive antenna impedance  $Z_{C,Rx}(f)$  in [ $\Omega$ ],
- distance between Tx-Rx antennas  $r_{TxRx}$  in [m].

The transmitting antenna transfer functions  $G_{Tx}(f, r, \theta_{Tx}, \varphi_{Tx})$  relates the transmit signal to the radiated field strength for an antenna in the transmit mode (see (2.13)). The antenna transfer functions represent a two dimensional vector with two orthogonal polarization components  $G_{co}$  (co-polar) and  $G_x$  (cross-polar). The channel transfer function for free space is defined in (2.13), where  $c_0$  is the speed of light in free space. For rich scattering environments, e.g., indoor, the influence of the channel can be described by a frequency-dependent channel transfer matrix calculated by, for example, ray-tracing techniques.

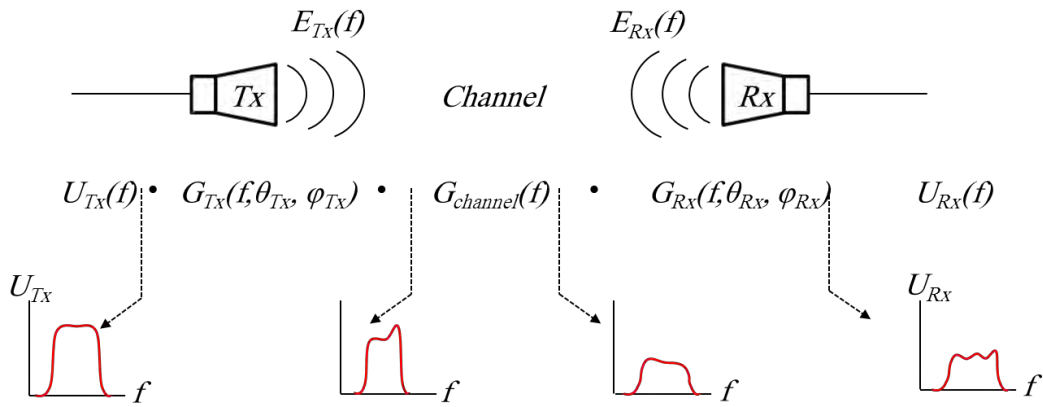


Fig. 2.4 UWB system link level characterization in frequency domain.

$$\frac{E_{Tx}(f, r)}{\sqrt{Z_0}} = G_{channel}(f, r_{TxRx}) G_{Tx}(f, \theta_{Tx}, \varphi_{Tx}) \frac{U_{Tx}(f)}{\sqrt{Z_{C,Tx}}} \quad (2.13)$$

$$G_{channel}(f, r_{TxRx}) = \frac{e^{-j\omega r_{TxRx}/c_0}}{2\sqrt{\pi} r_{TxRx} c_0}. \quad (2.14)$$

The total description of a free space UWB propagation link is given by (2.15).

$$\frac{U_{Rx}(f)}{\sqrt{Z_{C,Rx}}} = G_{Rx}(f, \theta_{Rx}, \varphi_{Rx}) \frac{e^{-j\omega r_{TxRx}/c_0}}{2\sqrt{\pi} r_{TxRx} c_0} G_{Tx}(f, \theta_{Tx}, \varphi_{Tx}) \frac{U_{Tx}(f)}{\sqrt{Z_{C,Tx}}}. \quad (2.15)$$

With these parameters, the Tx-Rx link is illustrated in Fig. 2.4, including the channel. The small graphs symbolize the typical influence of the link contributions. Both transmit and receive transfer functions are related to each other by Lorentz theorem of reciprocity. An

expression that takes into account the UWB properties of the system has been derived in [7] and shown in (2.16).

$$j\omega G_{Rx}(f, \theta_{Rx}, \varphi_{Rx}) \sim G_{Tx}(f, \theta_{Tx}, \varphi_{Tx}) \quad (2.16)$$

In the typical system shown in Fig. 2.4 the system transfer function  $H_{sys}$  is defined as in (2.17).

$$\begin{aligned} G_{sys} &= \frac{U_{Rx}(f)}{U_{Tx}(f)} \\ &= G_{Rx}(f, \theta_{Rx}, \varphi_{Rx}) \frac{e^{-j\omega r_{TxRx}/c_0}}{2\sqrt{\pi} r_{TxRx} c_0} G_{Tx}(f, \theta_{Tx}, \varphi_{Tx}) \frac{\sqrt{Z_{C,Rx}}}{\sqrt{Z_{C,Tx}}}. \end{aligned} \quad (2.17)$$

### 2.4.2 Time Domain Signal Link

In UWB systems the antenna may be excited with an impulse. The elements of the UWB time domain link characterization are:

- amplitude of transmit signal  $u_{Tx}(t)$  in [V],
- amplitude of receive signal  $u_{Rx}(t)$  in [V],
- impulse response of the transmit antenna  $g_{Tx}(t, \theta_{Tx}, \varphi_{Tx})$  in [m/ns],
- impulse response of the receive antenna  $g_{Rx}(t, \theta_{Rx}, \varphi_{Rx})$  in [m/ns],
- radiated field strength  $e_{Tx}(t, r, \theta_{Tx}, \varphi_{Tx})$  in [V/m].

In the time domain, the antenna transient response  $g(t, \theta, \varphi)$  becomes more adequate for the description of impulse systems. The transient response is dependent on time, but also on the angles of departure  $(\theta_{Tx}, \varphi_{Tx})$ , respectively, angles of arrival  $(\theta_{Rx}, \varphi_{Rx})$ , and polarization [8]. Consequently, the antennas do not radiate the same pulse in all directions. This may cause severe problems in communications. Therefore, in characterizing a UWB system it is important to consider the contribution of the antenna angular behaviour.

The Tx-Rx link in time domain is illustrated in Fig. 2.5. The small graphs symbolize the typical influence of the link contributions. The received signal can be related to the

transmitted signal as given in (2.18). The multiplication in frequency domain (see (2.13)) is substituted by convolution operation (\*) in time domain. In a line of sight free-space propagation channel the channel transient response is calculated by (2.19).

$$\frac{u_{Rx}(t)}{\sqrt{Z_{C,Rx}}} = g_{Rx}(t, \theta_{Rx}, \varphi_{Rx}) * g_{channel} * g_{Tx}(t, \theta_{Tx}, \varphi_{Rx}) * \frac{u_{Tx}(t)}{\sqrt{Z_{C,Tx}}} \quad (2.18)$$

$$g_{channel}(t, r_{TxRx}) = \frac{1}{2\sqrt{\pi}r_{TxRx}c_0} \delta\left(t - \frac{r_{TxRx}}{c_0}\right). \quad (2.19)$$

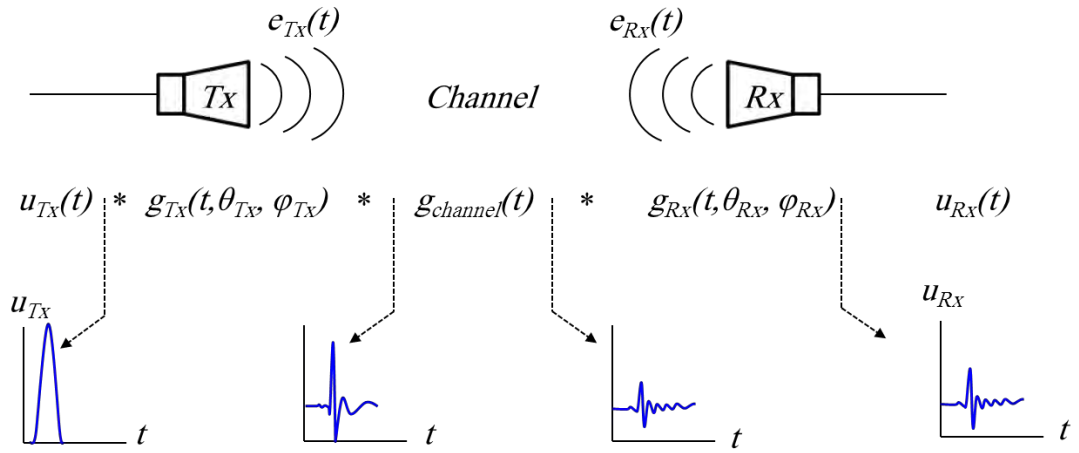


Fig. 2.5 UWB system link level characterization in time domain.

The relation between the transient responses for transmit and receive mode in time domain can be written as (2.20).

$$\frac{\partial u_{Rx}(t)}{\partial t} \sim u_{Tx}(t). \quad (2.20)$$

### 2.4.3 UWB Parameters

Depending on the application of the UWB antenna the relevant parameters from the time or frequency domains can be selected. The Fourier transform is used to switch from the frequency domain to the time domain. The following are important parameters of UWB antennas.

- *Peak value of the impulse response*  $P(\theta, \varphi)$  is the maximal value of the strongest peak of the antenna transient response.
- *Pulse width* is a measure for describing the broadening of the radiated impulse. This value should not exceed a few hundred picoseconds in order to ensure high data rates in communication.
- *Ringing* is an undesired effect in UWB antenna. The energy storage or multiple reflections in the antenna result in oscillation of the radiated pulse after the main peak. This energy is of no use and lowers the peak value. The duration of ringing  $\tau_r$ , is expressed as the time until the pulse amplitude has fallen from the peak value below a certain lower limit  $\alpha$ . The ringing is expressed in *ns* and should be small, i.e. less than a few pulse width.
- *Group delay*  $\tau_g(\omega)$  quantitatively evaluates the dispersive performance of the antenna. It is defined in frequency domain as given in (2.21).

$$\tau_g(\omega) = -\frac{d\psi(\omega)}{d\omega} = -\frac{d\psi(f)}{2\pi df} \quad (2.21)$$

where  $\psi(f)$  is the phase component of the system transfer function  $G_{sys}$ . A constant group delay implies a non-distorted structure with a linear phase variation versus frequency. The non-linear phase indicates the resonant character of the device, which implicates the ability of the structure to store the energy. It results in ringing and oscillations of the antenna impulse response  $g(t)$  [9]. A measure for the constancy of the group delay is the deviation from the mean group delay. Non-resonant structures such as Vivaldi antenna provide slowly oscillating group delay over the whole frequency band. On the other hand frequency independent structures such as a log-periodic antenna show strong and sharp oscillations over the whole frequency band. This is caused by frequency dependant phase centre movement. In practice to investigate the system performance two similar antennas (Tx and Rx) are positioned in their far-field region (see Fig. 2.6). The system transfer function would be then measured for two orientations of the antennas, namely face to face and side by side.

In case the group delay in other directions are required, it can be calculated by measuring the antenna transfer function in the required direction or plane. The system transfer function can then be calculated using (2.16) and (2.17).

- *Fidelity* of an antenna is a measure of how accurately the received voltage available at the antenna terminal reproduces the behaviour of the transient field incident upon the antenna, or for the transmitting case how accurately the time integral of the transmitted field reproduces the behaviour of the voltage applied to the antenna terminals. It should be clear that the antenna fidelity is waveform specific; that is, an antenna may provide a high-fidelity reproduction for some waveforms and be unable to provide equivalent fidelity for many other waveforms [10].

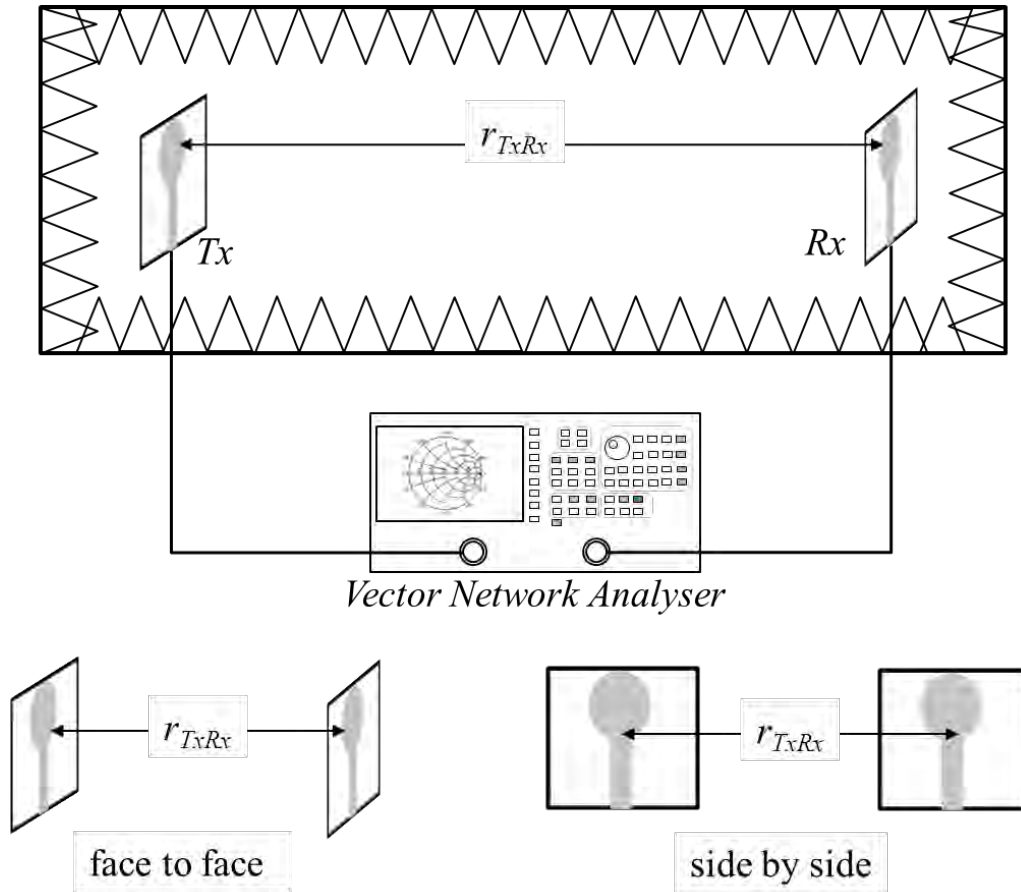


Fig. 2.6 Group delay measurement system set-up. Two main orientations are face to face and side by side.



## 2.4.4 Antenna Elements

### 2.4.4.1 Finite Length Dipole

Earlier in this chapter the electromagnetic (EM) fields from a Hertzian dipole were calculated. A dipole with finite length  $l$  can be analysed as a superimposition of infinite number of Hertzian dipoles. That allows us to integrate the Hertzian dipole far-field EM fields over the dipole length. Finite length dipoles are of practical interest, an example of which is depicted in Fig. 2.7a. If the antenna is fed by a sinusoidal voltage source, the current distribution on the dipole is approximately proportional to its maximum value  $I_{max}$ . Assuming the far-field component of the Hertzian dipole is  $dE_\theta$  then the far-field components of a finite length dipole is given by (2.22).

$$E_\theta = \int_{-\frac{l}{2}}^{\frac{l}{2}} dE_\theta \quad (2.22)$$

$$E_\theta \cong j\eta \frac{I_{max} e^{-jkr}}{2\pi r} \left[ \frac{\cos\left(\frac{kl}{2} \cos \theta\right) - \cos\left(\frac{kl}{2}\right)}{\sin \theta} \right]$$

$$H_\phi = \frac{E_\theta}{\eta}$$

Using (2.22) it is possible to calculate the fields for a dipole with a certain length. For instance a half-wavelength dipole shows a radiation resistance of  $R_r=75\Omega$  and directivity  $D=1.64$ . It has an omni-directional radiation pattern in azimuth plane ( $xy$ -plane in Fig. 2.2) and in the elevation plane it has a figure of eight shape pattern with one main lobe. However, by increasing the dipole length multiple lobes would be developed in the radiation pattern. This implies that the power radiated along the main lobe decreases once multi lobes develop, which is detrimental in most wireless applications. Such variation in radiation patterns also indicates the change that occurs with frequency, since the radiation characteristics depend on the ratio between the physical length  $L$  and the wavelength  $\lambda$ .

When a dipole is fed by a two-wire balanced (symmetrical) transmission line, the feeding current in a half-cycle of one wire is of the same magnitude but  $180^\circ$  out-of-phase from that in the corresponding half-cycle of the other wire. If in addition the spacing between the two wires is very small ( $s \ll \lambda$ ), the fields radiated by the current of each wire are essentially cancelled by those of the other. The net result is an almost ideal (and desired) non radiating transmission line. This feeding arrangement is known as balanced feeding [2]. A coaxial cable on the other hand is inherently unbalanced. The inner and outer conductors of the coax are not coupled to the antenna in the same way; therefore, they provide an unbalance. The unbalance is caused by a net current which flows to ground on the outside part of the outer conductor. Hence, the cable radiates and affects the radiation patterns. This phenomenon is shown in Fig. 2.7b.

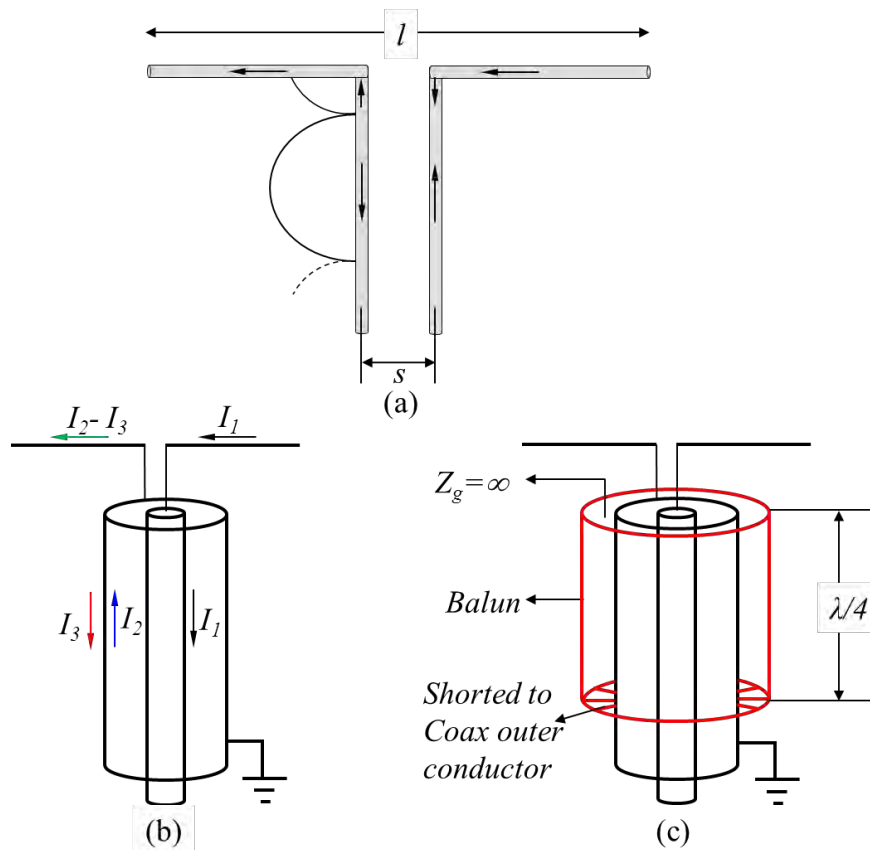


Fig. 2.7 Dipole antenna with (a) balanced feeding (b) unbalanced feeding (c) balun.

The current  $I_3$  which flows on the outside of the outer conductor is determined by the impedance  $Z_g$  seen from the outer shield to the ground. If  $Z_g$  can be made very large,  $I_3$  can be reduced significantly. Devices that can be used to balance inherently unbalanced systems, by cancelling or choking the outside current, are known as *baluns* (*balance to unbalance*). One type of a balun is that shown in Fig. 2.7c, known as a *bazooka* balun. It is a shorted  $\lambda/4$  long metal sleeve which encapsulates the coaxial line. Using this technique the impedance between the outer coaxial shield and ground can be made very large and  $I_3$  can be reduced significantly. Electrically the input impedance at the open end of this  $\lambda/4$  shorted transmission line, which is equivalent to  $Z_g$ , will be very large (ideally infinity). Therefore, the unwanted current  $I_3$  will be choked, if not completely eliminated, and the system will be nearly balanced.

#### **2.4.4.2 Monopole**

When one arm of the dipole is replaced with a large ground plane the new arrangement is a monopole antenna (see Fig. 2.8). If the ground plane is large enough the monopole radiation matches the dipole radiation behaviour, since the ground plane acts as electric mirror and creates the other half. A monopole antenna is inherently unbalanced. Hence, it is suitable to be connected directly to the centre conductor of a coaxial cable and grounded to the outer shield.

Comparing to the dipole, just half of the power is radiated above the ground and hence the radiation resistance of a monopole is half and directivity is double that of a dipole.

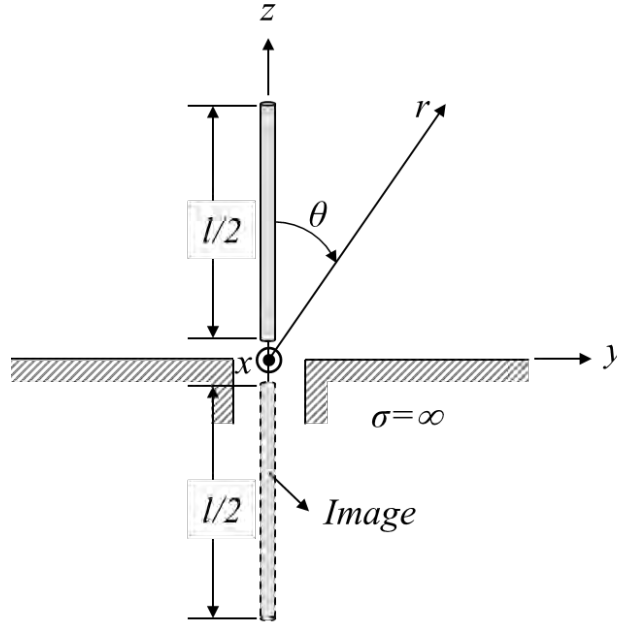


Fig. 2.8 Geometry of a monopole antenna. The ground plane acts as an electric mirror, hence, a monopole with length  $l/2$  is equivalent to a dipole with length  $l$ .

#### 2.4.4.3 Planar Inverted F Antenna

Fig. 2.9 shows the two variations of monopole antenna. A monopole bent to reduce the height is an inverted L antenna (ILA). As a consequent this antenna has a very low radiation resistance and a high capacitive reactance. Therefore, the radiation efficiency is low and matching requires a high inductive load. Inverted F antenna (IFA) is an enhanced version of ILA. By implementing a parallel shorting pin between the feeding point and the ground plane the inductive component of the impedance can be improved. Benefiting from profile features ILA and IFA have been widely used in wireless communication.

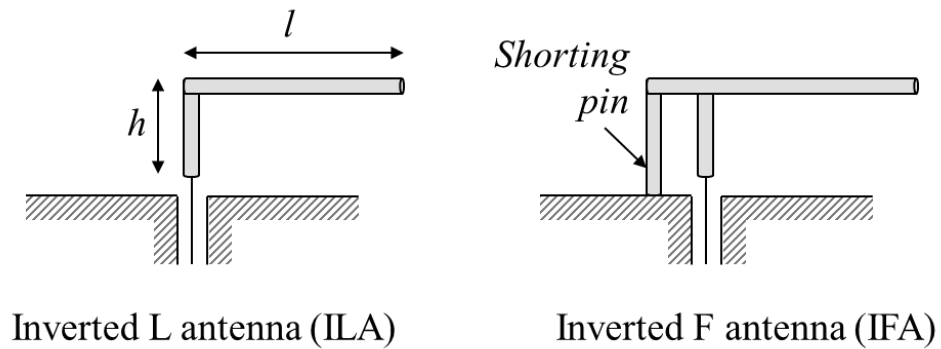


Fig. 2.9 Monopole antenna variations.

An IFA has an inherently low impedance bandwidth, typically 2%. By replacing the top horizontal arm with a planar element parallel to the ground plane as depicted in Fig. 2.10, it is possible to increase the bandwidth. In addition to their good radiation characteristics, PIFAs are also very versatile. By adjusting the position and shape of the feeding and shorting plate it is possible to improve certain radiation characteristics such as bandwidth [11]-[15]. It is possible to design multiband or wideband PIFAs by introducing extra shorting plates or slots and slits at proper positions on the top plate or ground plane [17]-[19]. Therefore, they are very popular in internal handset antennas.

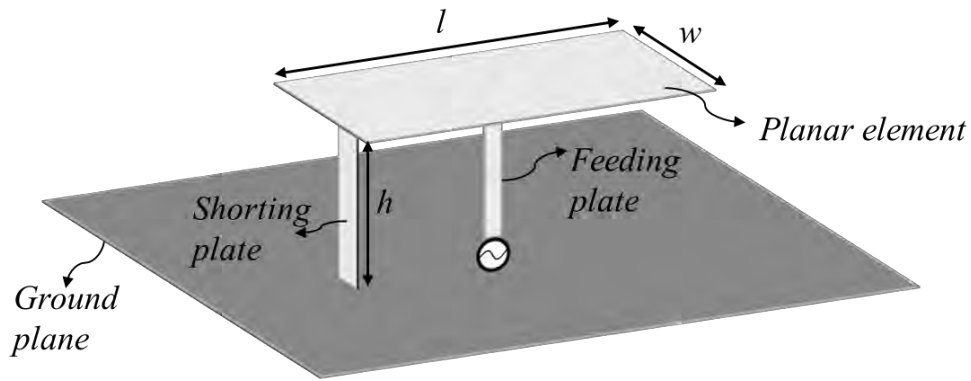


Fig. 2.10 Planar inverted F antenna (PIFA)

#### **2.4.4.4 Printed Antennas**

Antennas can also be made using printed circuit techniques. Various shapes and structures can be *etched* on a single- or double-sided copper-clad dielectric. Different classes of antennas can be manufactured using this method. Due to their many advantages patch antennas are very popular. They are low profile, conformable to different surfaces. A tremendous amount of work has been done on microstrip antennas over the past 25 years. The principal shapes of patch antenna and possible variants on them are shown in Fig. 2.11a and b, respectively. The main feeding techniques of a patch antenna are depicted in Fig. 2.12. Combining different patch shapes and feeding arrangement would increase the multiplicity of possible microstrip patch antenna designs. Fig. 2.13 shows an example of a very well-known microstrip square patch antenna [20]. It radiates in the  $x$  direction. By adjusting the patch

length  $l$  it is possible to tune the resonance frequency. Variations in  $w$  mainly change the radiation resistance. Microstrip antennas are relatively narrowband.

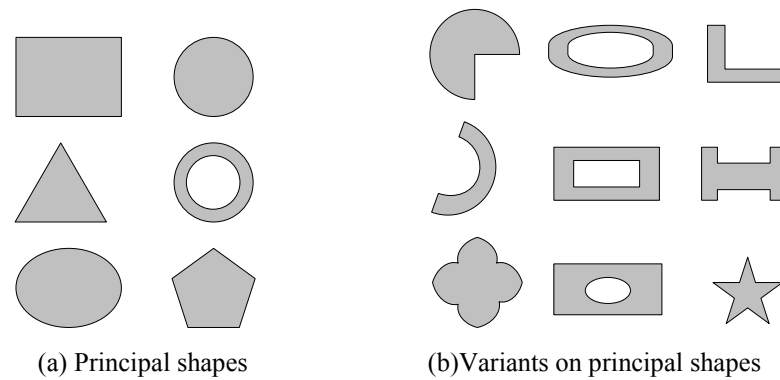


Fig. 2.11 Various shapes of the patch antenna [20].

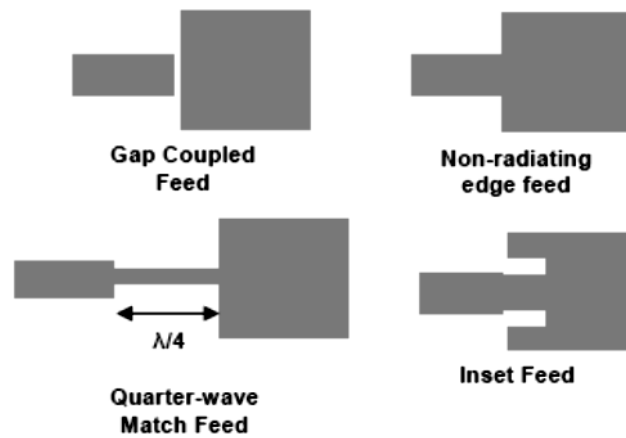


Fig. 2.12 Variants on patch antenna feed arrangements [20].

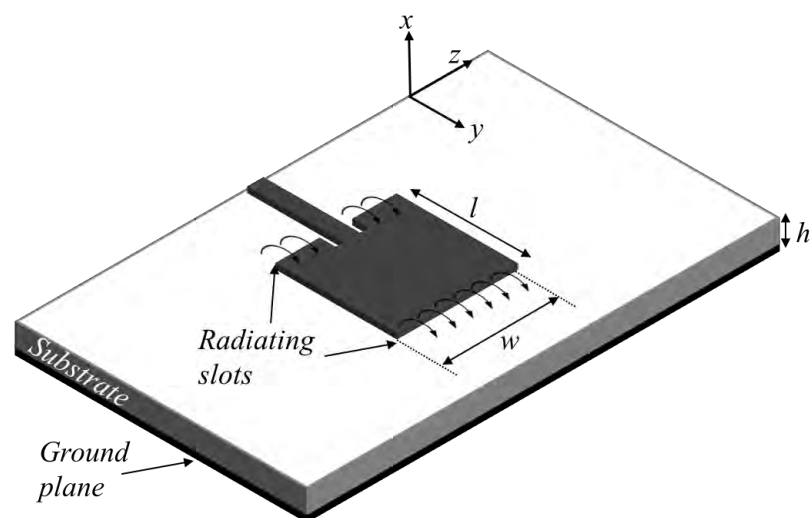


Fig. 2.13 Geometry of a typical square microstrip patch antenna.

#### 2.4.4.5 Wideband Antennas

##### *Dipoles and Monopoles*

Resonant antennas such as finite length thin wire dipoles and monopoles do not provide good radiation characteristics over a wide range of frequencies. However, due to their simplicity and good radiation characteristics, there have been attempts to improve the bandwidth.

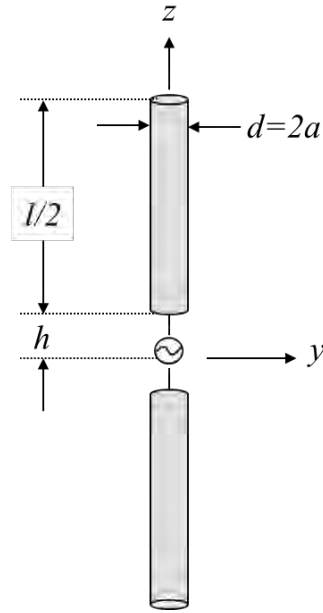


Fig. 2.14 Geometry of a centre fed thick dipole.

The impedance bandwidth of a dipole is mainly a function of its wire radius-to-length ratio or  $d/l$  (see Fig. 2.14) [2]. By calculating the input impedance of a thick dipole it can be confirmed that for a given length wire its impedance variations become less sensitive as the  $d/l$  ratio increases. Thus, more broadband characteristics can be obtained by increasing the volume of the dipole with a fixed length. This observation also follows the Chu-Harrington theory on the antenna bandwidth and its volume [21], [22].

Similarly it is also possible to increase the volume and therefore the bandwidth by replacing the wire element with a volumetric structure. As an example the conical antenna is demonstrated in Fig. 2.15. The conical or rotationally symmetric monopoles are bulky and not suitable for some applications.

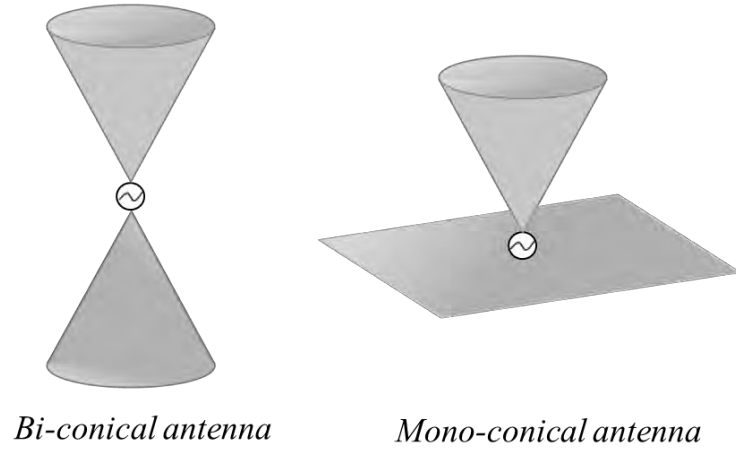


Fig. 2.15 Geometry of conical antennas. Increasing the volume of the poles increases the bandwidth.

Alternatively, planar elements have been used to replace the wire elements of the monopoles to broaden the impedance bandwidth and keep the size acceptable [23]-[24]. Several examples are depicted in Fig. 2.16 . To further improve the bandwidth numerous techniques have been proposed such as notching or bevelling the bottom edge of the plate [25], [26], multiple point feeding [28] or shorting the plate [26]. There have also been configurations with orthogonal plates to improve the radiation pattern stability [29]. Simple demonstrations of such configurations are shown in Fig. 2.17 .

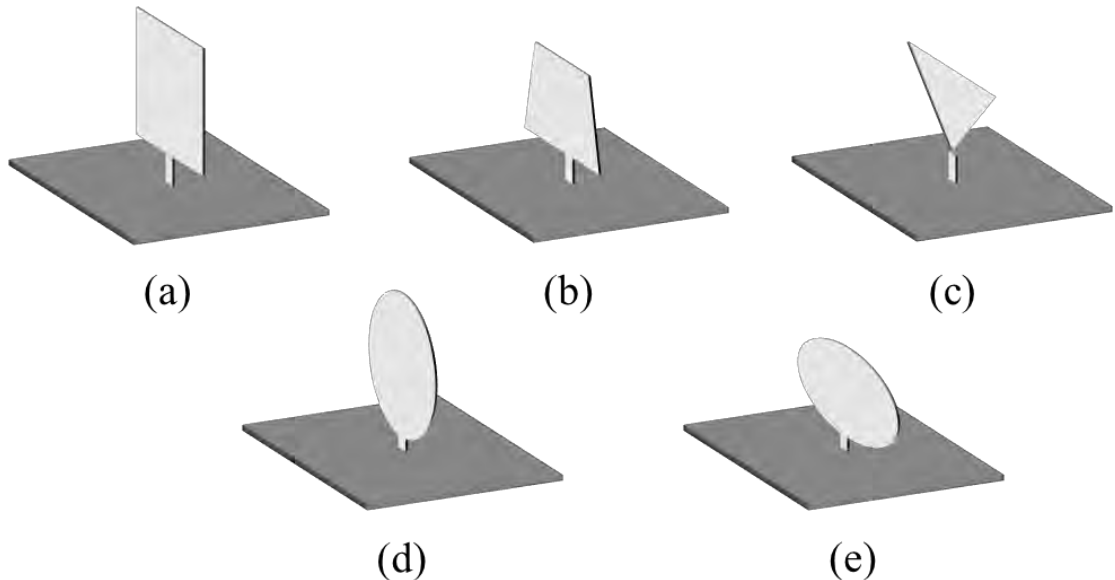


Fig. 2.16 Vertical planar monopole antennas with various shapes (a) square, (b) trapezoid, (c) triangular, (d) circle, (e) ellipse.



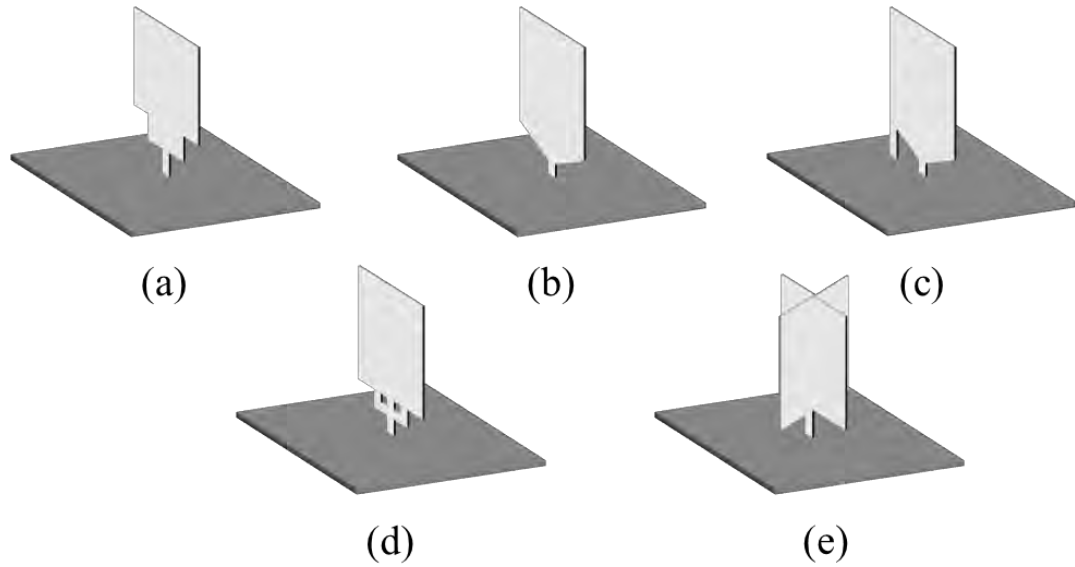


Fig. 2.17 Vertical planar monopole antennas with improved characteristics. (a) square monopole with notches, (b) square monopole with bevels, (c) shorted square monopole with bevels, (d) square monopole with fork-shape feeding, (e) cross square monopole.

In order to design more practical antennas for small and compact wireless devices, the printed versions of above mentioned monopoles were developed [24], [30]-[32]. Some typical designs are shown in Fig. 2.18 . Similar to vertical monopoles various patch shapes can be used in such antennas. Feeding mechanism can be microstrip, coplanar waveguide (CPW), aperture or capacitive coupling.

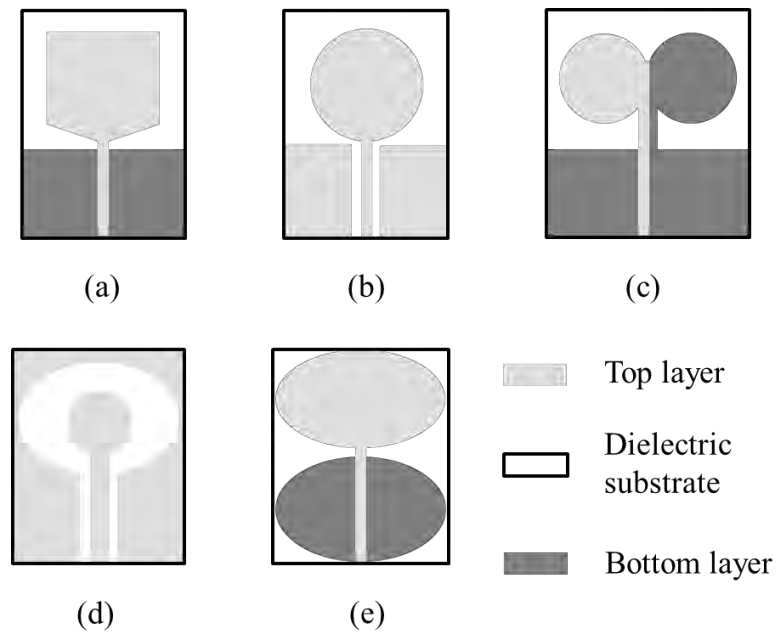
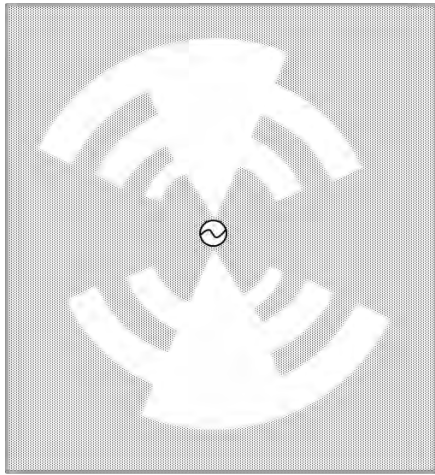


Fig. 2.18 Typical configurations of printed UWB antennas. (a) microstrip fed bevelled square

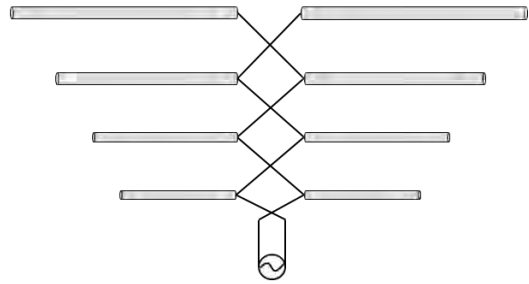
monopole, (b) CPW fed circular disc monopole, (c) printed circular dipole antenna, (d) slot antenna, (e) elliptic monopole with elliptic ground plane.

### ***Frequency Independent Antennas***

Frequency independent antennas also show stable performance over a wide range of frequencies. They have a self-scaling structure which is described by angles [2]. Typical design are the self-complementary log-periodic structures, such as planar log-periodic slot antennas, bidirectional log-periodic antennas, log-periodic dipole arrays, two/four-arm log spiral antennas, and conical log-spiral antennas [33]. Some examples are shown in Fig. 2.19. Although such antennas are wideband, they are not suitable for the impulse based communication link. The multi resonant nature of such configurations results in a non-stable phase centre versus frequency- this would distort the received pulse.



A planar log-periodic slot antenna



A log-periodic dipole array

Fig. 2.19 Geometry of common frequency independent antennas.

## **2.5 Summary**

Antennas are essential parts of a radio link. The main antenna characteristics were reviewed in this chapter. A radio link was defined in both frequency and time domain. Specifically, in an impulse based system, the UWB antenna has to satisfy certain

requirements. In the frequency domain the antenna requires to have a wide bandwidth, stable radiation pattern and group delay. Pulse widening and strong ringing effects are not desirable in UWB time domain characterization. Some commonly used antenna elements were also introduced in this chapter. Among them, wideband printed monopoles and PIFA form the base of antenna designs in next chapters.

## References

- [1] IEEE standard definitions on Antenna and propagation, *IEEE Trans. Antennas Propag.*, vol. AP-17, no. 3, May 1969; Vol. AP-22, No. 1, Jan. 1974; and vol. AP-31, no. 6, Part II, Nov. 1983.
- [2] C. A. Balanis, *Antenna Theory Analysis and Design*, by John Wiley & Sons, INC, 2005.
- [3] B. Allen, M. Dohler, E. Okon, W. Malik, A. Brown and D. Edwards, *Ultra Wideband Antennas and Propagation for Communications, Radar and Imaging*, John Wiley and Sons, Ltd, 2007.
- [4] FCC, Revision of Part 15 of the commission's rules regarding ultra wideband transmission systems, ET Docket 98-153, FCC 02-48, Feb. 14, 2002.
- [5] The Commission of the European Communities, "Commission decision on allowing the use of the radio spectrum for equipment using ultra-wideband technology in a harmonised manner in the Community", *Official Journal of the European Union*, 21 Feb. 2007.
- [6] D. Sanchez-Hernandez, *Multiband Integrated Antennas for 4G Terminals*, Artech House, INC, 2008.
- [7] J. Kunisch and J. Pamp, "UWB radio channel modelling considerations," in *Proc. ICEAA '03*, Turin, Sep. 2000.
- [8] W. Wiesbeck, G. Adamiuk and C. Sturm, "Basic properties and design principle of UWB antennas", *Proceedings of the IEEE*, vol. 97, no. 2, 372-385, 2009.

- [9] D.-H. Kwon, "Effect of antenna gain and group delay variations on pulse-preserving capabilities of ultra wideband antennas," *IEEE Trans. Antennas Propag.*, vol. 54, pp. 2208–2215, Aug. 2006.
- [10] O. E. Allen, D. A. Hill, and A. R. Ondrejka, "Time-domain antenna characterizations," *IEEE Trans Electromagnetic Compatibility*, vol. 35, no. 3, Aug. 1993.
- [11] R. Feick, H. Carrasco, M. Olmos and H. D. Hristov, "PIFA Input Bandwidth Enhancement by Changing Feed Plate Silhouette," *Electron Lett.*, vol. 40, no. 15, pp. 921–922, July 1004.
- [12] F. S. Chang, and K. L. Wong, "A Broadband Probe-Fed Planar Patch Antenna with a Short Probe Pin and a Conducting Cylinder Transition," *Microw. Opt. Technol. Lett.*, vol. 31, no. 4, pp. 282–284, Nov. 2001.
- [13] Z. N. Chen, and M. Y. W. Chia, "A Feeding Scheme for Enhancing the Impedance Bandwidth of a Suspended Plate Antenna," *Microw. Opt. Technol. Lett.*, vol. 38, no. 1, pp. 21–25, July 2003.
- [14] J. -H. Jung, H. Choo, and I. Park, "Small Broadband Disc-Loaded Monopole Antenna with Probe Feed and Folded Stripline," *Electron Lett.*, vol. 41, no. 14, pp. 788–789, July 2005.
- [15] H.T. Chattha, Y. Huang and Y. Lu, "PIFA bandwidth enhancement by changing the widths of feed and shorting plate," *IEEE Antennas Wireless Propag. Lett.*, vol. 8, pp.637 – 640, 2009.
- [16] A. Khoshniat, H. S. Mopidevi and B. A. Cetiner, "Broadband capacitively fed tapered type PIFA with modified ground plane," *Electron Lett.*, vol. 46 , no. 7, pp. 474 – 475, 2010.
- [17] L. Kwang-Jae, L. Taek-Kyung and J.W. Lee "Bandwidth enhanced planar inverted-F antenna with modified ground structure," in *Proc. Asia-Pacific Microwave Conference, 2007. APMC 2007*, 2007.

- [18] A. Cabedo, J. Anguera, C. Picher, M. Ribo and C. Puente, "Multiband handset antenna combining a PIFA, slots, and ground plane modes," *IEEE Antennas Propag. Trans.*, vol. 57, no. 9, pp. 2526 – 2533, 2009.
- [19] R. Hossa, A. Byndas and M.E. Bialkowski, "Improvement of compact terminal antenna performance by incorporating open-end slots in ground plane," *IEEE Microw. Wireless Components Lett.*, vol. 14, no. 6, pp. 283 – 285, 2004.
- [20] J.R. James, P. S. Hall, *Handbook of microstrip antenna*, 1989, Peter Peregrinus Ltd.
- [21] L. J. Chu, "Physical limitations of omnidirectional antennas," *Journal Appl. Phys.*, vol. 19, pp. 1163-1175, Dec.1948.
- [22] R. F. Harrington, "Effect of antenna size on gain, bandwidth and efficiency," *Journal Res. Nat. Bur. Stand.*, vol. 64D, pp. 1-12, Jan.-Feb. 1960.
- [23] N. P. Agrawall, G. Kumar and K. P. Ray, "Wide-band planar monopole antennas," *IEEE Trans. Antennas Propag.*, vol. 46, no. 2, pp. 294-295, Feb. 1998.
- [24] Z. N. Chen, M. J. Ammann, X. Qing; X. H. Wu, T. S. P. See and A. Cat, "Planar antennas," *IEEE Microwave Mag.*, vol. 7, no 6, pp. 63-73, 2006.
- [25] S.-W. Su, K.-L. Wong and C.-L. Tang, "Ultra-wideband square planar monopole antenna for IEEE 802.16a operation in the 2–11-GHz band," *Microw. Opt. Technol. Lett.*, vol. 42, no 6, pp. 463–466, September 2004.
- [26] M.J. Ammann and Z.N. Chen, "A wideband shorted planar monopole with bevel," *IEEE Trans. Antennas Propag.*, vol. 51, pp. 901–903, 2003.
- [27] E. Lee, P.S. Hall and P. Gardner, "Compact wideband planar monopole antenna," *Electron Lett.*, vol. 35, pp. 2157–2158, 1999.
- [28] K.-L. Wong, C.-H. Wu and S.-W. Su, "Ultra wide-band square planar metal-plate monopole antenna with a trident-shaped feeding strips," *IEEE Trans. Antennas Propag.*, vol. 53, no. 4, pp. 1262 – 1269, 2005.

- [29] M. J. Ammann, "Improved pattern stability for monopole antennas with ultra wideband impedance characteristics," in *Proc. IEEE Antennas Propag. Society Int. Symp.*, vol. 1, pp. 818–821, June 2003.
- [30] J. Liang, L. Guo, C. C. Chiau, X. Chen and C. G. Parini, "Study of CPW-fed circular disc monopole antenna for ultra wideband applications", *IEE Proc. Microw., Antennas Propag.*, vol. 152, no. 6, pp. 520-526, Dec 2005.
- [31] J. Liang, C Chiau, X. Chen and C.G. Parini, "Study of a Printed Circular Disc Monopole Antenna for UWB Systems," *IEEE Trans. Antennas Propag.*, vol. 53, no. 11, pp. 3500-3504, Nov. 2005.
- [32] Z. N. Chen, T. S. P. See and X. Qing, "Small printed ultra wideband antenna with reduced ground plane effect," *IEEE Trans. Antennas Propag.*, vol. 55, no. 2, pp. 383-388, 2007.
- [33] P.E. Mayes, "Frequency-independent antennas and broad-band derivatives thereof," *Proceedings of the IEEE*, vol. 80, pp. 103–112, 1992.

## **Chapter 3    Antenna    Design    Challenges    for Emerging Wireless Services**

### **3.1        Introduction**

Coexistence of several wireless standards in a limited bandwidth, increasing demand for high data rate applications, and rising traffic are some of the drivers for new spectrum management techniques. The introduction of UWB technology which allows unlicensed use of a specific band with limited transmitted power was one step towards relaxing the spectrum usage regulations. Due to the wide bandwidth and lower transmission power, UWB technology provides unique features for many applications. These benefits and applications are reviewed in 3.2.

Although the UWB systems are being deployed in many situations, mobile operating bands are still over-crowded while other bands such as TV or satellite are under-utilized. Cognitive radio is the key solution for improving the spectrum usage efficiency. The definition and working principles of CR are explained in 3.3. Along with the intelligent, software controlled sub-systems CR requires special hardware arrangement for sensing and searching the spectrum and communication which are discussed in 3.3.1. CR needs to work within the existing systems with different carrier frequencies and bandwidth requirements which means wideband and multiband antennas are still required in CR networks. Therefore, a brief review is carried out in sections 3.4 and 3.5 on the available wideband and multiband

antenna design techniques. Optimal performance in CR networks and users is linked with the ability to change the communication parameters. In terms of hardware requirements, reconfigurable antennas become essential. Hence, section 3.5 goes through the available frequency reconfiguration techniques mainly for small and printed antennas. Then the recently proposed antenna solutions specifically for CR are also introduced. It is important to note that there is an extensive literature available on the above mentioned topics; however, the best effort has been made to select and present part of the literature which is in the same direction of the whole thesis.

## **3.2 Ultra Wideband Technology**

Considering the regulated access to the spectrum and the limited bandwidth availability, responding to the demand for higher capacity and data rates requires innovative technologies that can coexist with devices operating at various frequency bands. UWB communication which is an underlay (or sometimes referred as shared unlicensed) system, coexists with licensed and unlicensed narrowband systems. According to the FCC rulings, UWB is defined as any wireless scheme that occupies either a fractional bandwidth greater than 20% or more than 500 MHz of absolute bandwidth. The FCC has also permitted the UWB radio transmissions in the unlicensed frequency band from 3.1 GHz to 10.6 GHz. The European Communication Commission has also published the regulations for the 6-8.5GHz band for UWB applications [1]. The coexistence of UWB system with other technologies is on condition that a strict transmission power regulation, shown in Table 3.1, is followed. A UWB signal occupies extremely large bandwidth (i.e. more than 500MHz) where the radio frequency (RF) energy is spread over an enormous spectrum which is wider than any licensed narrowband wireless system and invisible to them due to the low power emission (see Fig. 3.1).



Table 3.1 FCC emission power limit for various UWB applications in each operating band

|               |                 |         | Operation Band (GHz) |                    |                   |                   |                    |                    |
|---------------|-----------------|---------|----------------------|--------------------|-------------------|-------------------|--------------------|--------------------|
|               |                 |         | 0.96<br>to<br>1.61   | 1.61<br>to<br>1.99 | 1.99<br>to<br>3.1 | 3.1<br>to<br>10.6 | 10.6<br>to<br>22.0 | 22.0<br>to<br>29.0 |
| EIRP<br>(dBm) | Communications  | Indoor  | -75.3                | -53.3              | -51.3             | -41.3             | -51.3              | -51.3              |
|               |                 | Outdoor | -75.3                | -63.3              | -61.3             | -41.3             | -61.3              | -61.3              |
|               | Imaging         |         | -53.3                | -51.3              | -41.3             | -41.3             | -41.3              | -51.3              |
|               | Vehicular radar |         | -75.3                | -63.3              | -63.3             | -63.3             | -41.3              | -41.3              |

In spite of the low power transmission, UWB offers attractive solutions in many wireless communication areas, including wireless personal area networks, wireless telemetry and telemedicine, and wireless sensors networks. With its wide bandwidth, UWB has a potential to offer a capacity much higher than the current narrowband systems for short-range applications.

A possible technique for implementing UWB is impulse radio (IR), which is based on transmitting extremely short (in the order of nanoseconds) and low power pulses. Other implementations, such as direct sequence spreading, are also popularly used with impulse radio-based implementations. Impulse radio is advantageous in that it eliminates the need for up- and down-conversion and allows low- complexity transceivers [2]. It also enables various types of modulation to be employed, including on–off keying, pulse-amplitude-modulation, pulse-position-modulation, phase-shift-keying, as well as different receiver types such as the energy detector, rake, and transmitted reference receivers.

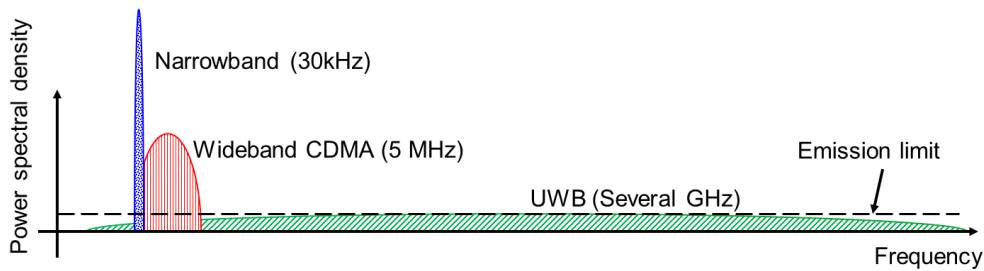


Fig. 3.1 UWB supports large relative and absolute bandwidth compared to narrowband and wideband communication.

Another strong candidate for UWB is multicarrier modulation, which can be realized using orthogonal frequency division multiplexing (OFDM). OFDM has become a very popular technology due to its special features such as robustness against multipath interference, ability to allow frequency diversity with the use of efficient forward error correction coding, capability of capturing the multipath energy efficiently, and ability to provide high bandwidth efficiency through the use of sub-band adaptive modulation and coding techniques. OFDM can overcome many problems that arise with high bit rate communication, the most serious of which is time dispersion. In OFDM, the data-bearing symbol stream is split into several lower rate streams, and these sub-streams are transmitted on different carriers. Since this increases the symbol period by the number of non-overlapping carriers (sub-carriers), multipath echoes affect only a small portion of neighbouring symbols. Remaining inter-symbol interference can be removed by cyclically extending the OFDM symbol [2].

### **3.2.1 UWB Benefits**

UWB (both impulse radio and multicarrier) also offers great flexibility of spectrum usage. This system is characterized in fact by a variety of parameters that can enable the design of adaptive transceivers and that can be used for optimizing system performance as a function of the required data rate, range, power, quality of service, and user preference. UWB technology provides high data rates over very short range. The data rate can, however, be traded-off for extension in range. Similarly, data rate and range can be traded-off for power, especially for low data rate and short range applications. Most importantly, the same device can be designed to provide service for multiple applications with a variety of requirements without the need for additional hardware [2].

The high temporal resolution of UWB signals results in low fading margins, implying robustness against multipath. Since UWB signals span a very wide frequency range they show relatively low material penetration losses, giving rise to better link margins [2].

Excellent time resolution is another key benefit of UWB signals for ranging applications. Due to the extremely short duration of transmitted pulses, sub decimetre ranging is possible. In IR-UWB systems, no up/down-conversion is required at the transceivers, with the potential benefit of reducing the cost and size of the devices. Other benefits of UWB include low power transmission and robustness against eavesdropping (since UWB signals look like noise) [2]. On the other hand, it is important to note that UWB receivers are a little bit difficult to build, due to the need to synchronise the TX and RX.

### **3.2.2 UWB Applications**

UWB has several applications all the way from wireless communications to radar imaging, and vehicular radar. The ultra wide bandwidth and hence the wide variety of material penetration capabilities allows UWB to be used for radar imaging systems, including ground penetration radars, through-wall radar imaging, surveillance systems, and medical imaging. Images within or behind obstructed objects can be obtained with a high resolution using UWB [2].

Similarly, the excellent time resolution and accurate ranging capability of UWB can be used for vehicular radar systems for collision avoidance, guided parking, etc. Positioning location and relative positioning capabilities of UWB systems are other great applications that have received significant attention. Last but not least is the wireless communication application, which is arguably the reason why UWB became part of the wireless world, including wireless home networking, high-density use in office buildings and business cores, UWB wireless printer, keyboard, wireless speakers, wireless universal serial bus (USB), high-speed wireless personal area networks, wireless body area networks, wireless sensors networks, wireless telemetry, and telemedicine [2].

## **3.3 Cognitive Radio**

As mentioned in the introduction the fourth approach for spectrum management is the evolution towards dynamic and open access spectrum which requires some level of

intelligence in the networks and is not achievable by pure hardware-based radios. In the early 1990s Joseph Mitola introduced the idea of combining the hardware and software; software defined radio (SDR) [3]. These radios typically have a RF front end with a software-controlled tuner. Baseband signals are passed into an analogue-to-digital converter. The quantized baseband is then demodulated in a reconfigurable device such as a field-programmable gate array, digital signal processor, or personal computer. The reconfigurability of the modulation scheme makes it a software-defined radio. In his 2000 dissertation, Mitola took the SDR concept one step further, coining the term cognitive radio [4]. CRs are essentially SDRs with artificial intelligence, capable of sensing and reacting to their environment.

A CR system employs technology that allows the system to obtain knowledge of its own operational and geographical environment, established policies and its internal state; to dynamically and autonomously adjust its operational parameters and protocols according to its obtained knowledge in order to achieve predefined objectives; and to learn from the results obtained [5].

In terms of spectrum use the above definition can be translated as below:

CR system employs technology that allows the system to obtain knowledge about the spectrum usage in its surrounding environment, to dynamically and autonomously adjust the transmission channel (carrier frequency and bandwidth) according to the current spectrum usage and requirements and learn from the results obtained by focusing on the most promising channels. This procedure is demonstrated in Fig. 3.2.

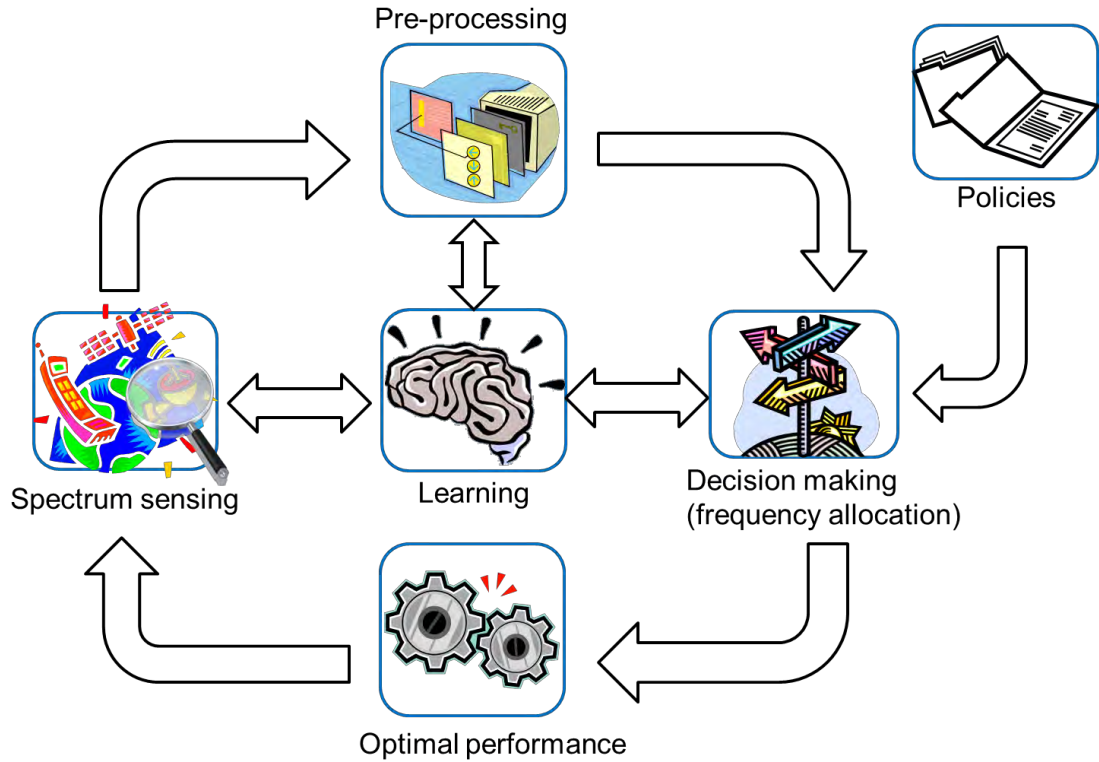


Fig. 3.2 The cognition cycle in cognitive radio network.

The approaches to dynamically manage the access to the spectrum can be categorized to three main groups: the dynamic exclusive use model, the open sharing model, and the hierarchical access model [6]. This classification is illustrated in Fig. 3.3

Similar to the current spectrum regulation policy, in the dynamic exclusive use model, specific bands are allocated to services for exclusive use. However, to improve the spectrum efficiency some level of flexibility is introduced. Two approaches go under this category: spectrum property rights and dynamic spectrum allocation. In the first approach, the spectrum property rights, the licensees are allowed to sell and trade spectrum and to freely choose technology.

On the other hand in the second approach, spatial and temporal traffic statistics of different services are exploited to improve the spectrum usage efficiency.

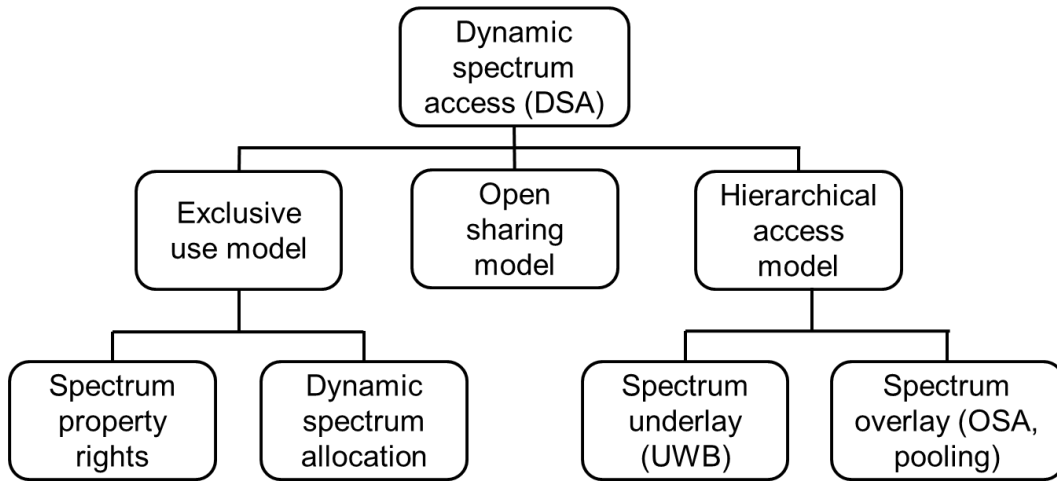


Fig. 3.3 Dynamic spectrum access model.

The open sharing model is mainly based on the huge commercial success of wireless services operating in the ISM band, in which all users have equal opportunities to access the spectrum. A hierarchical access model is based on the hierarchical priority of primary users over secondary users. In this model, the spectrum allocated to the primary users is available to the secondary users until they do not interfere with the primary users' transmission. The two approaches proposed for spectrum sharing in this model are spectrum underlay and spectrum overlay (also known as opportunistic spectrum access or OSA). In the spectrum underlay approach the secondary users are allowed to transmit with low transmit power as if they are invisible to the primary users. On the other hand in spectrum overlay the secondary users are allowed to use the licensed bands in case they are not used by the primary users at the time. Therefore, in order to avoid primary users this technique is based on identifying and exploiting the spectrum holes (spectrum white space) defined in space, time and frequency. In comparison, the underlay approach does not rely on detection and exploitation of spectrum holes due to the low power transmission. Whereas, with the added cost and complexity for detecting spectrum white space in the overlay approach, the secondary users can transmit with higher power and therefore can be used for medium or high range applications as well. Both approaches are shown in Fig. 3.4 [7].

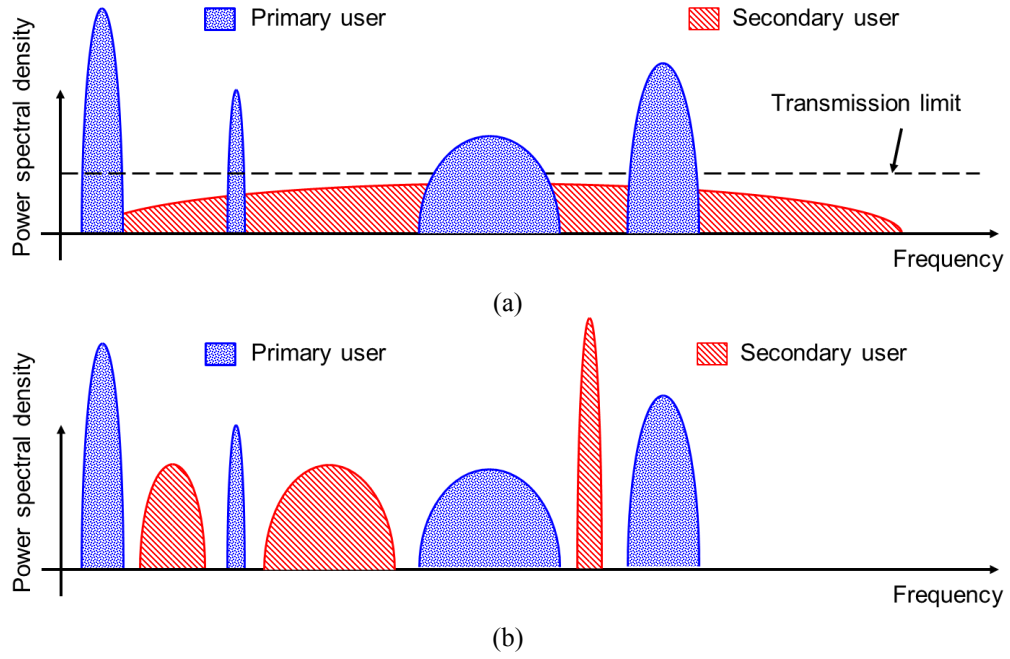


Fig. 3.4 Hierarchical access model (a) spectrum underlay, (b) spectrum overlay.

### 3.3.1 Spectrum Sensing and Allocation

In order to identify the spectrum holes in OSA model, CR systems need to scan the spectrum and spot the vacant or idle parts of the spectrum which is known as *spectrum sensing*. Based on the information CR knows about its own internal state and surrounding environment, it then determines the optimum frequency band and subsequently starts the *communication*. This procedure is referred to as communication. Two main approaches for spectrum sensing and communication are as follow:

- A. The continuous spectrum sensing is carried out in a process in parallel to the communication link as shown in Fig. 3.5.
- B. A single channel is used for both spectrum sensing and communication as shown in Fig. 3.6.

A two antenna system is proposed for approach (A) [8]. One antenna is wideband and omni-directional, feeding a receiver capable of both coarse and fine spectrum sensing over a broad bandwidth. The second antenna is directional and feeds a frequency agile front end that can be tuned to the selected band. A single wideband antenna feeding both spectrum sensing module and the frequency agile front end can also be a solution for approach (A) [9].

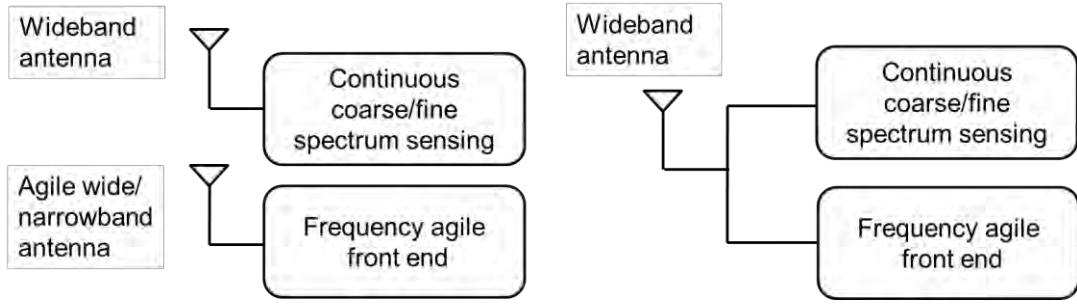


Fig. 3.5 Cognitive radio architecture with parallel sensing and communications.

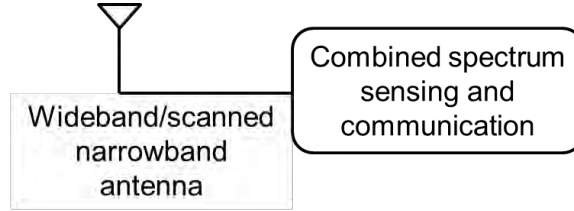


Fig. 3.6 Cognitive radio architecture with combined sensing and communications

In approach (B), spectrum sensing and radio reconfiguration are performed when the communication link quality falls below defined thresholds. In [10], two thresholds are used. Link quality falling below the first threshold triggers spectrum sensing, so that a better system configuration can be identified that will meet the link quality requirements. When the quality degrades below a second lower threshold, the system is reconfigured.

Considering the system requirements discussed above a potential antenna solution for CR might be an antenna with multiple functionalities. The potential system might include an antenna with wideband frequency response and omni-directional radiation pattern for spectrum sensing together with reconfigurable narrowband functionality. Narrowband functionality can be achieved by supplementary filtering in the RF stage; however, this might add to the complexity of the RF front end circuitry. Filtering and reconfiguration can be included into the antenna in order to reduce the complexity of the filtering circuits in RF stage.

### 3.3.2 Ultra Wideband Cognitive Radio

Considering that UWB technology is based on the underlay spectrum access, it can be beneficial to CR systems based on underlay spectrum sharing approach. Moreover, since the



UWB signal power is below noise level it is very hard to be detected therefore it provides highly secure communication.

If the regulations are revised, then the UWB can also be used for overlay spectrum sharing where it transmits with higher power in case the target spectrum is free. Then it is also possible to use it for combined underlay and overlay. This feature can be very helpful in some scenarios. For instance, if UWB is in overlay mode, and the call drops and it is not possible to continue, it switches to underlay mode and maintains the communication even with lower quality. Pulse shaping and therefore spectrum shaping is one of the UWB features which can be valuable in environments with rapid changes. For instance, an IR-UWB system can respond to a decrease in available bandwidth by switching to a different wider pulse shape, and can do the opposite if there is more bandwidth to use. Therefore, the introduction of cognitive features along with opportunistic spectrum usage will further enhance current spectrum efficiency.

### **3.4 Antenna Requirements for Multi Standard Radio**

The increasing numbers of new wireless services have resulted in growing demand for wireless devices in different applications. More and more applications and services are added into the wireless devices. The antennas in such devices should support all the required frequency bands which indicates that the antennas need to be either wideband or multiband. Various techniques have been practiced and presented in the literature to design antenna solutions for multi standard radios. Some of the main approaches are reviewed in the next sections.

#### **3.4.1 Wideband Antennas**

Several types of wideband antennas were reviewed in Chapter 2. Specifically this section looks over the printed wideband antennas. It is due to their low profile, light weight and low manufacturing costs that printed antennas are very common in small wireless devices. It is also easy to completely integrate a microstrip patch antenna on a PCB with other

planar circuitries. In addition to their attractive physical and manufacturing advantages, microstrip antennas are very versatile in terms of impedance, resonant frequency, radiation pattern, polarization and operating mode, by choice of shape and feeding arrangement. Many techniques, such as adding shorting pins, varactor diodes, loading and slotting the patch, or introducing parasitic elements, can be applied to the antenna to enhance specific radiation characteristics [11]-[14].

Microstrip patch antennas in their basic forms are considered as narrowband antenna (typically between 1% and 10%). This essentially limits the application of this type of antenna. For this reason, much effort has been devoted to the development of broadband techniques. The techniques can be categorized to two main groups: impedance matching techniques and multiple resonances introduction. By incorporating a broadband impedance matching technique between the antenna and the feeder, good matching over a broad frequency range can be attained. The matching network can be a quarter-wavelength impedance transformer, tuning stubs, active components and many more combinations [14]. Alternatively, if closely distributed resonances are well excited simultaneously, the bandwidth can be enhanced. The simple configuration based on this approach would be to use multiple parasitic elements to add extra resonant path and therefore increase the bandwidth [15].

#### ***3.4.1.1 Ultra Wideband Antennas***

UWB communication demands ultra wide bandwidth which basic patch antennas cannot support. It was pointed out in Chapter 2 that monopole antennas can be modified to provide wide bandwidth. Printed monopoles are the planar versions of the wire monopoles. Similar to wire antennas, printed UWB monopoles are composed of two major parts, namely the radiator and the ground plane. In order to achieve the desired impedance matching variations can be made to the radiator as depicted in Fig. 3.7. It can be a polygon being fed either from one of straight edges (Fig. 3.7a) or from one of the corners (Fig. 3.7b). In order to enhance the performance of the antenna, the radiator may have a smooth bottom (Fig. 3.7c), bevels or notches (Fig. 3.7d), different cut outs (Fig. 3.7e), added stubs or parasitic elements

(Fig. 3.7f), or combinations and derivations of all the mentioned options for good matching. The radiation in such antennas is not only dependant on the size and shape of the radiator. Investigations show that the ground plane also contributes to the radiation. Therefore, the shape and dimensions of the ground need to be optimized to accomplish good UWB radiation. In view of that there could be various modifications in the ground plane as shown Fig. 3.8. The ground plane may have notches, slots and slits (Fig. 3.8a), bevels (Fig. 3.8b) and cut outs and bevels at the feed point (Fig. 3.8c) [15]-[24].

In printed monopole antennas, the feeding configuration has considerable effect on the impedance matching. Several feeding arrangements are illustrated in Fig. 3.9. In comparison with microstrip designs coplanar waveguide (CPW)-fed UWB antennas are better candidates due to their simple configuration, manufacturing advantages, repeatability, and low cost. The radiator can be fed asymmetrically, or be connected to the ground plane via a shorting pin as shown in Fig. 3.9a. In order to control the current distribution on the radiator, it can be fed through multiple points either by having multiple feed lines or having a fork shaped feed line as it is depicted in Fig. 3.9b. These are just few examples of planar feeding and many other types of feeding are possible as well. The impedance matching is optimized by the shaping of the radiator and controlling the height of the feeding gap and the size and shape of the ground plane [15]-[17].

Although various shapes and types of feeding have been examined in the literature, most of the antennas in this class operate based on one principle that is overlapping of closely distributed several resonance modes. Investigations show that the first resonance is determined by the overall height of the radiator, which implies that at lower end of the frequency band the antenna operates in an oscillating mode i.e. standing wave mode. At the high frequency end, the slot formed by the lower edge of the radiator and the top edge of the ground plane supports the travelling wave. In the middle of the band, the antenna operated in a hybrid mode of standing and travelling waves. The principle of the antenna operation across the whole spectrum is illustrated in Fig. 3.10 [16].

Since the targeted application for the antennas studied and proposed in this thesis is small wireless consumer products, the focus is on omni-directional antennas and therefore directional solutions such as Vivaldi or log periodic antennas are not reviewed in this chapter.

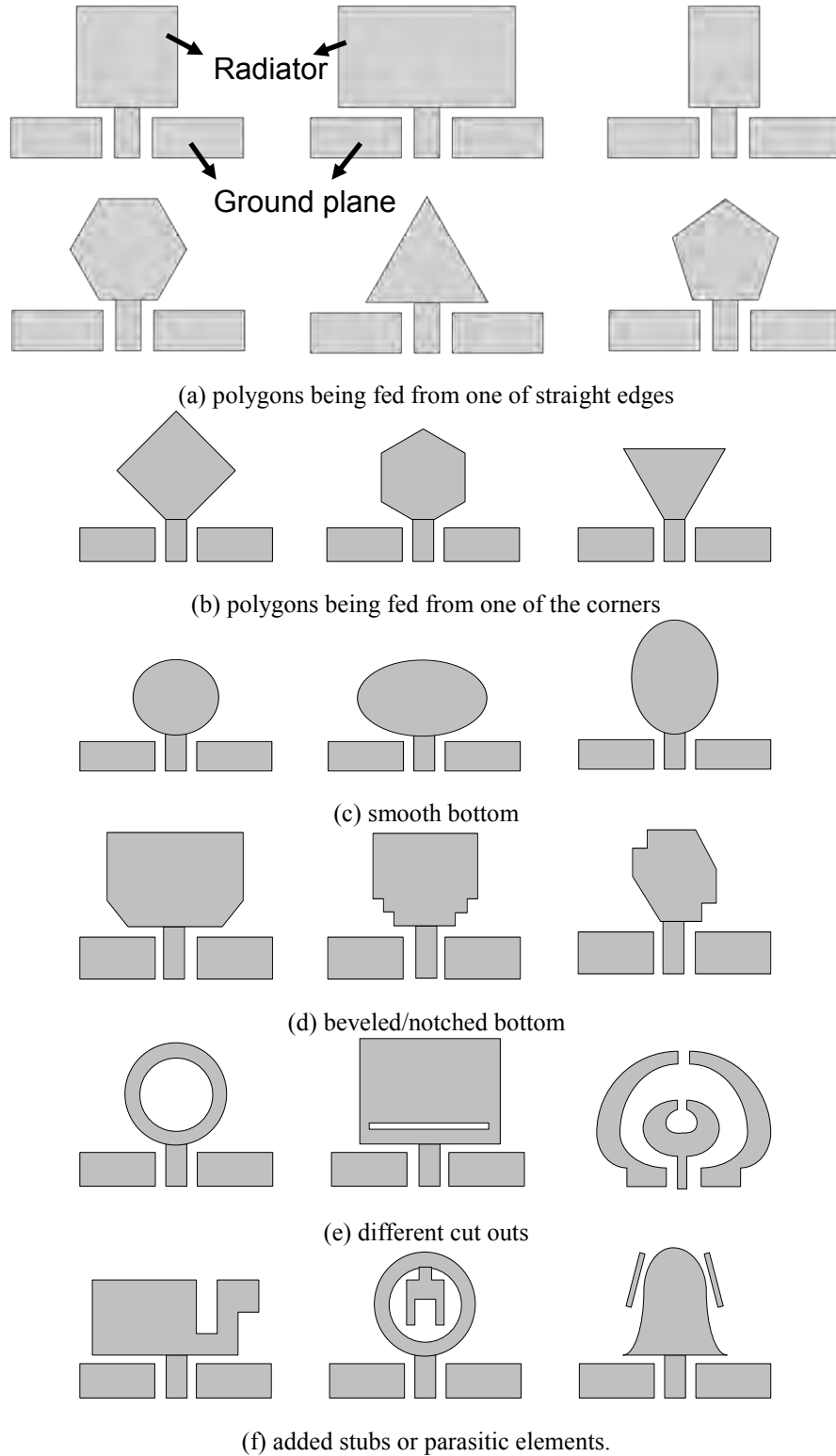


Fig. 3.7 Various shapes of the radiators for CPW fed UWB monopoles.

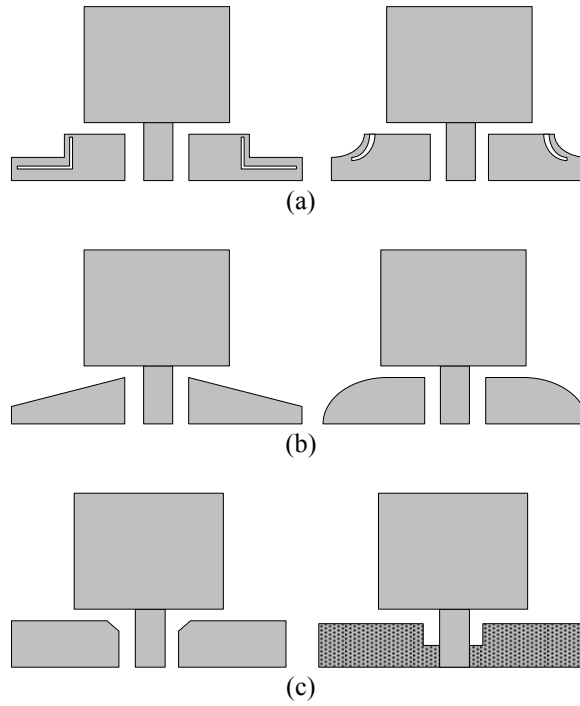


Fig. 3.8 Various modified ground plane for UWB monopoles, (a) have notches, slots and slits, (b) bevels, (c) cut outs and bevels at the feed point.

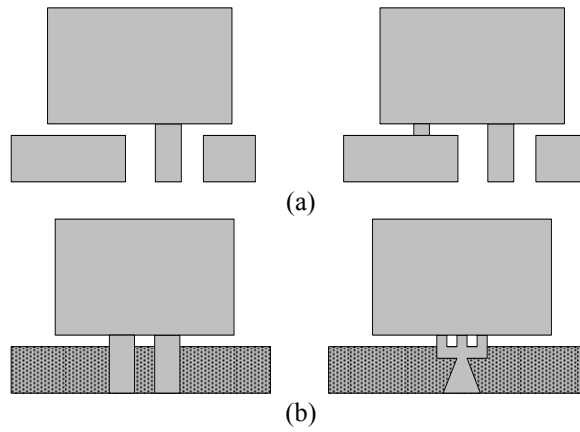


Fig. 3.9 Various feeding structures for UWB monopoles, (a) asymmetrically feeding, (b) multiple feeding points.

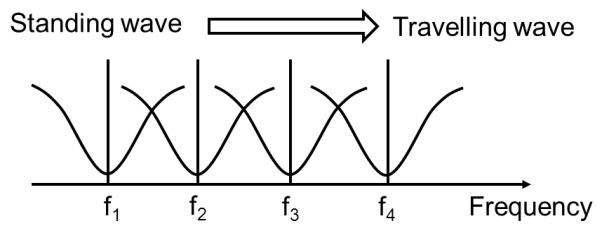


Fig. 3.10 Schematic of UWB antenna operation principle [16].

### **3.4.2 Multiband Antennas**

Another antenna solution for feature-rich devices is the compact multiband antenna which has received considerable amount of attention [25]-[48]. During the past years the traditional external monopole antenna (whip antenna) has evolved to internal antennas in handsets. The requirement for multiband operation began with the widespread use of GSM in two frequency bands. In Europe, two widely separated bands, band III (Tx: 1710–1755 MHz, Rx: 2110–2155 MHz) and band VIII (Tx: 880–915 MHz, Rx: 925–960 MHz), were the first to be used. This introduced a need to design an antenna with a single feed that could operate in two relatively narrow bands, with one band centred at a frequency that is approximately twice that of the other. Due to their low profile nature (planar) inverted F antennas (PIFAs) and (planar) inverted L antennas (PILAs) have been widely utilized in various devices.

Although the classic PIFA or PILA are not wideband, depending on the application and manufacturing technology, several methods are suggested to develop wideband or multiband (P)IFAs and (P)ILAs [25]-[47] (see Fig. 3.11). Approaches such as replacing the shorting wire by a shorting strip [25], adding parasitic radiators coupled to the driven element [26]-[31], modifying the feeding structure [32]-[34], cutting slot(s) or slit(s) from the radiator or ground plane [35]-[39], loading the radiators with resistive, capacitive, inductive or dielectric material [40]-[45] or a combination of the above mentioned techniques [46], [47] were followed in practice to improve the bandwidth.

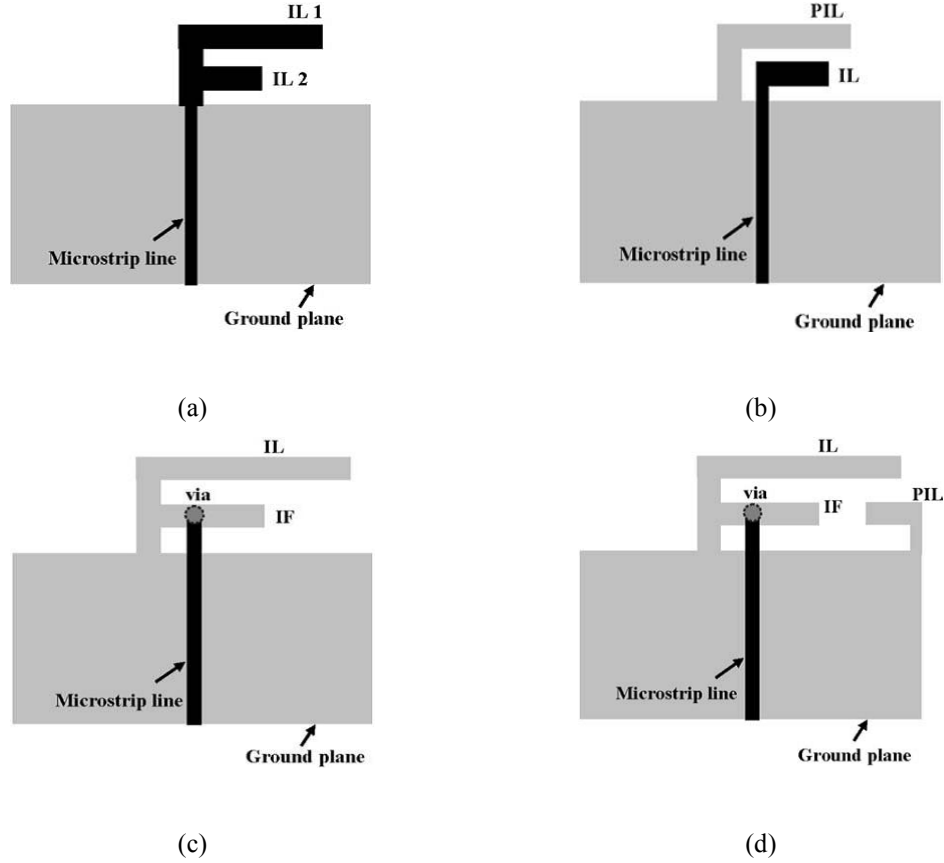


Fig. 3.11 Examples of dual band inverted F and L antennas. (a) A double inverted-L antenna for dual-band operation, (b) An inverted-L antenna with a parasitic inverted-L (PIL) element for bandwidth enhancement, (c) An inverted-FL antenna for dual-band operation, (d) An inverted-FL antenna with a parasitic inverted-L element for bandwidth enhancement.

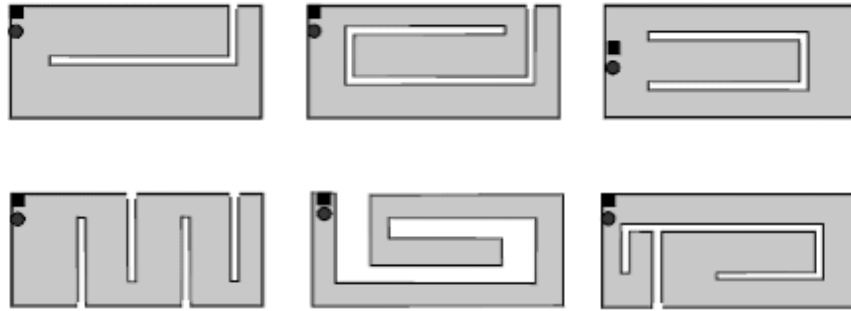


Fig. 3.12 Some dual band top patches for PIFA. Dual band is achieved by creating two resonant paths on the patch by cutting slots and slits [48].

Cutting slots or slits out of the PIFA radiator results in a meandered radiator (see Fig. 3.12). Meandering effectively elongates the surface current path on the antenna and adds to the number of operating modes while maintaining the dimensions compact. Using this technique it is possible to design antennas with multiple resonant paths, and hence, by closely

distributing or overlapping the resonances multiband or broadband performance can be achieved. This technique is summarized symbolically in Fig. 3.13. By adding extra resonating paths ( $L_2$  and  $L_3$ ), a single antenna can then be responsive to multiple narrow bands of interest ( $f_1$ ,  $f_2$  and  $f_3$ ). Although very popular in handset antenna design, elongating or adding extra resonant path is not applicable to non-resonating antennas such as printed UWB monopole antennas.

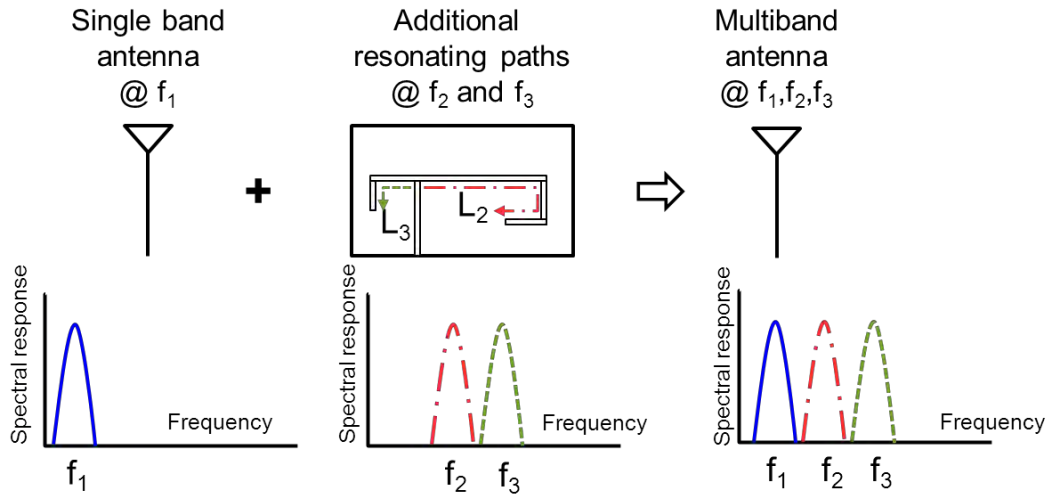


Fig. 3.13 Multiband antenna design technique using additional resonating path (Note that this diagram is a symbolic representation of the technique).

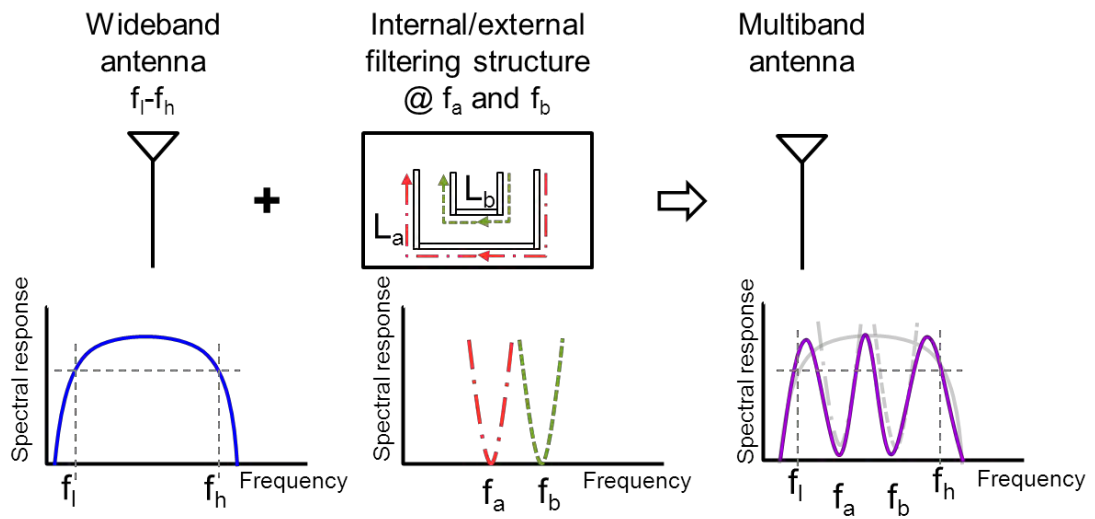


Fig. 3.14 Multiband antenna design technique using filtering structures (Note that this diagram is a symbolic representation of the technique).



Another technique for accomplishing multiband functionality is to use the combination of a wideband antenna and a filtering structure as shown symbolically in Fig. 3.14. The filtering can be done after the antenna by means of transmission line (see Fig. 3.15 ) or lumped element filters [49]-[51]. The transmission line structures at microwave frequencies require large space which might not be available in some applications. Even if lumped element filters were used, they need to be connected to the antenna through transmission line which may add to the cost and complexity of the system. On the other hand, it is possible to integrate the filtering operation into a wideband antenna. This will result in a multiband antenna. The possibility to provide this function in the antenna can significantly relax the requirements imposed upon the filtering electronics within the wireless device. Moreover, the resulting bands in this technique are not necessarily narrowband. In fact it depends on the bandwidth of the original antenna and the filtering technique incorporated. As is shown in Fig. 3.16, a dual band operation (2.4 and 5.2 GHz band) was accomplished by cutting a notch from the radiating patch of a CPW fed monopole in [52]. Various filtering techniques have been reported in the literature [53]-[62]. Probably, the most common method to introduce band notch in the frequency response of a wideband antenna is to etch slots on the radiators or feeding structures, such as U-shaped slots [53], [54], L-shaped slots [55], and H-shaped slots [56]. Adding a parasitic strip [57], [58] near the radiation elements or the ground planes is another way to create stop bands. In addition, loading resonators to the feeding line is also a good way to realize band-notched characteristics. Several types of resonators such as split ring resonators [59], complementary split ring resonators [60], coplanar waveguide resonant cells [61], and half-mode substrate integrated waveguide cavities [62], were proposed for the band notched UWB antennas. The schematic of some of these examples are shown in Fig. 3.17.

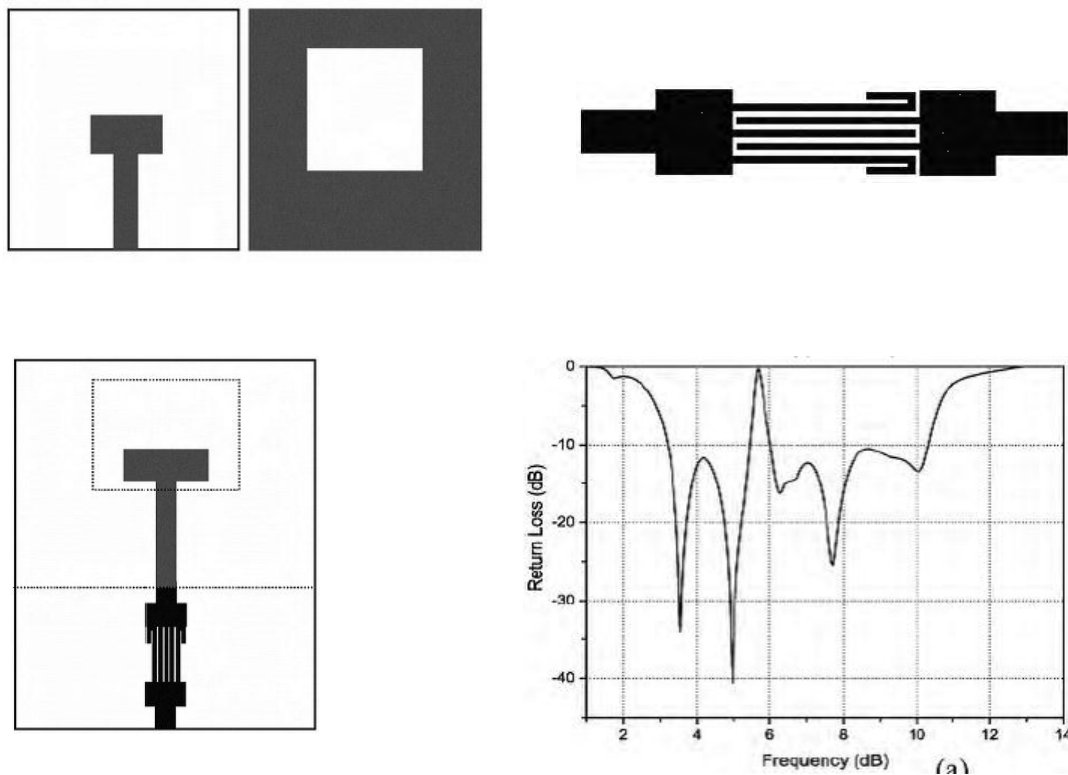


Fig. 3.15 A band notched antenna using a wide slot antenna and an interdigital hairpin resonator filtering structure [51].

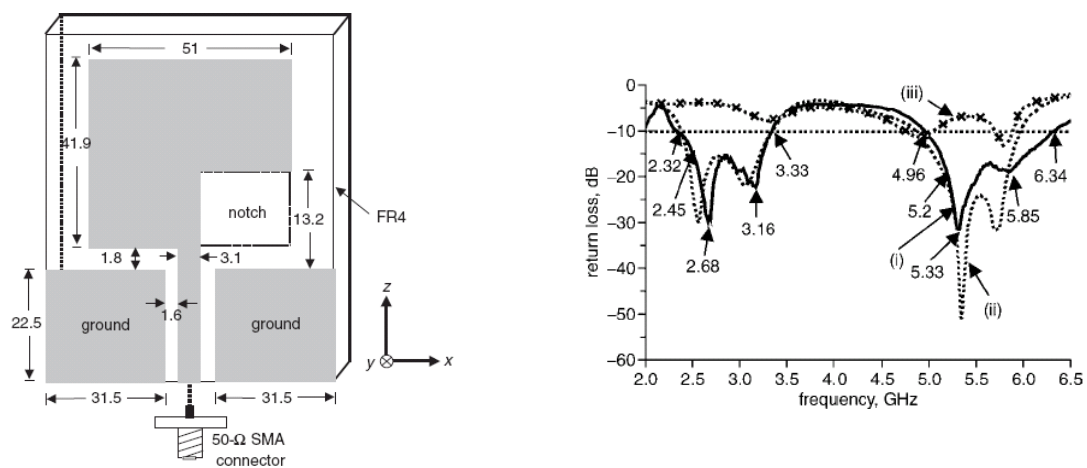


Fig. 3.16 Dual band antenna based on band notching a wideband antenna [52].

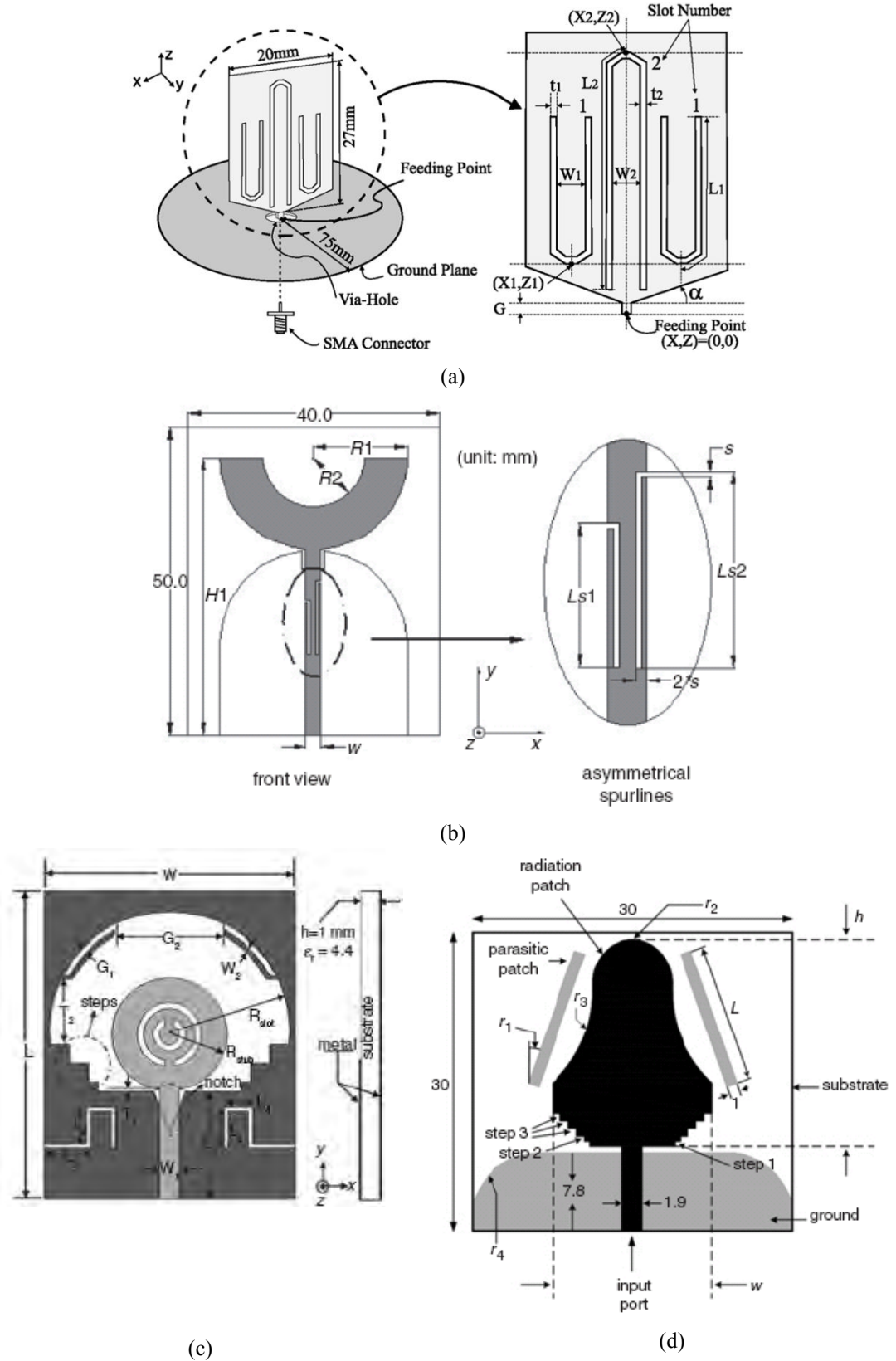


Fig. 3.17 Several examples of various band rejection techniques using, (a) U shaped slot [54], (b) L shaped slot (spurline) [55], (c) split ring resonator [56], (d) parasitic element [57].

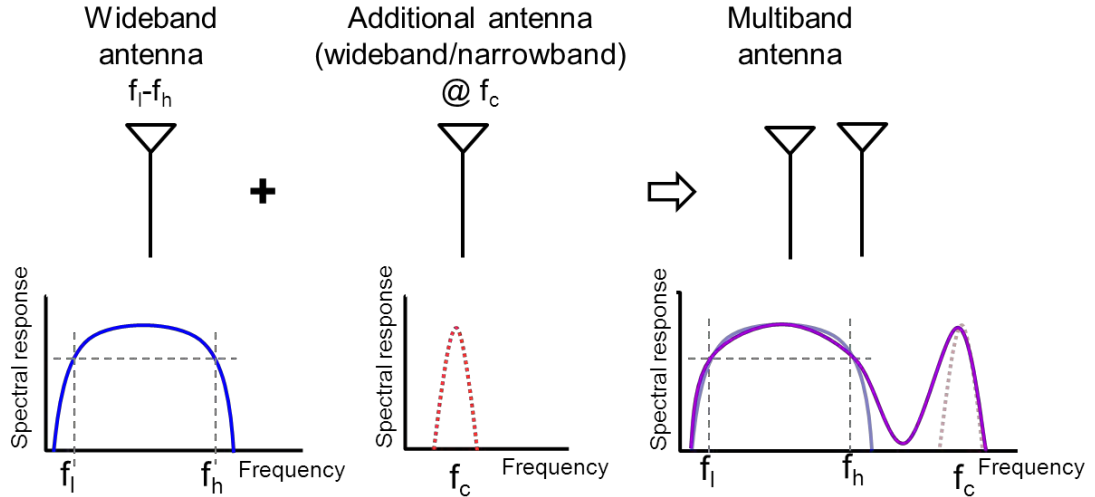


Fig. 3.18 Multiband antenna design technique using multiple element. (Note that this diagram is a symbolic representation of the technique).

### 3.4.2.1 Multi Element Antennas

An alternative approach to design antennas suitable for multi standard radio applications is to employ several antennas (see Fig. 3.18). In its simplest case that multiple antennas are placed next to each other, this technique might not seem very promising for compact devices. However, together with an efficient integration concept this technique can prove valuable.

A dual port antenna for operation at international mobile telecommunications-2000 (IMT-2000), global positioning system (GPS) and wireless local area network (WLAN) bands was proposed in [63]. As shown in Fig. 3.19a it consists of two radiating elements; PIFA with folded branches for GPS and WLAN band, and a PILA for IMT-2000 band. The two antennas were printed next to each other on the top layer of the substrate. The approach might be effective when there is less limitation on antenna space requirements. Furthermore, the close proximity of the ports might result in mutual coupling between the ports. A more efficient approach was presented in [64], where two slot antennas were combined together (see Fig. 3.19b). The outer slot antenna operates at 2.37 to 2.55GHz (lower part of 802.11a/b/g) and the inner slot operates at 3.5 GHz worldwide interoperability for microwave access (WiMAX)

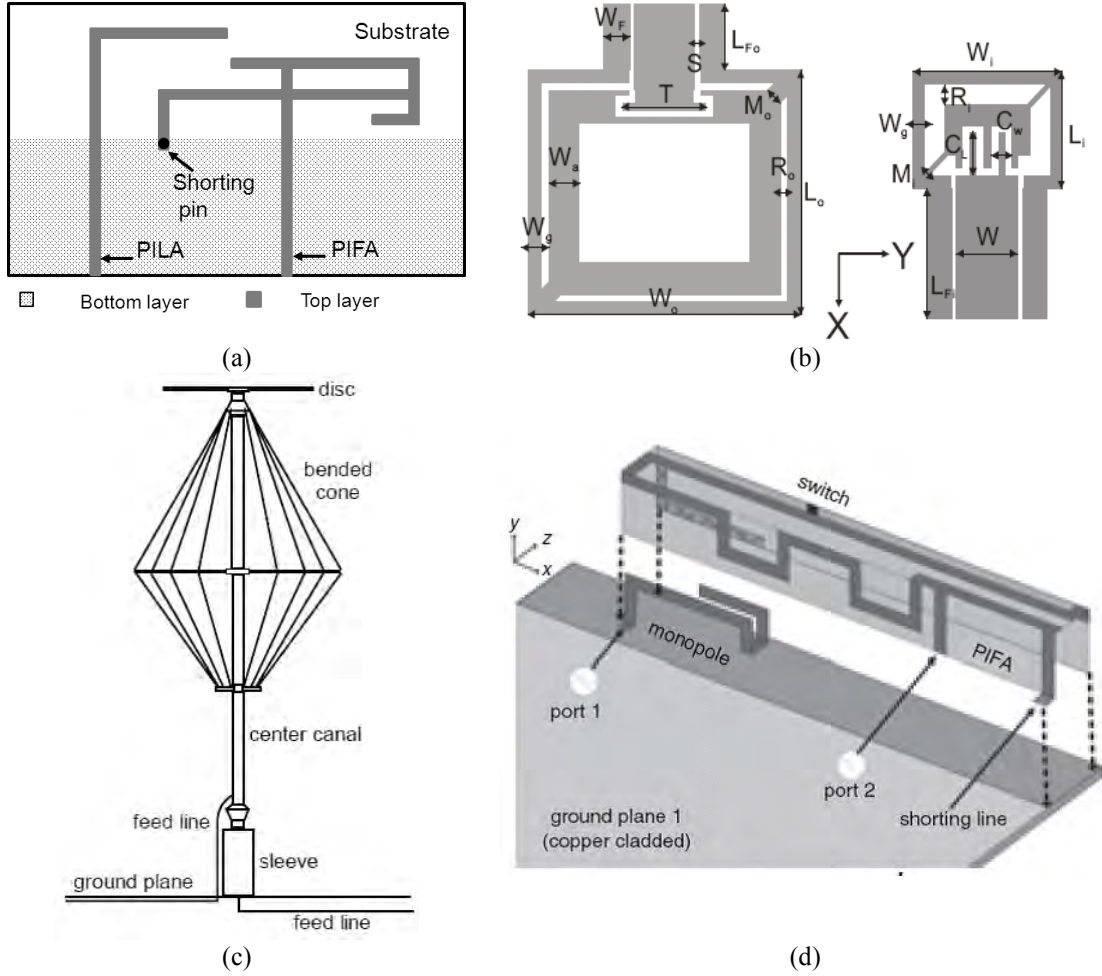


Fig. 3.19 Schematic diagrams of multiband antennas based on multiple antenna approach, (a) dual port PILA and PIFA [63], (b) dual port slot antenna [64], (c) monopole and disc cone antenna [65], (d) reconfigurable monopole and PIFA [66].

and 5.125 to 6GHz (higher part of 802.11a/b/g) bands. Low port mutual coupling was achieved by the specific configuration of the ports. This approach is not only limited to wireless radio applications. In [65] a dual feed broadband antenna is introduced which is suitable for high frequency (HF) and very/ultra high frequency (V/UHF) communication or electromagnetic compatibility (EMC) applications. The antenna was composed of a monopole and a disc-cone antenna. Two coaxial cables were used for feeding. The first cable is inserted in the centre canal (Fig. 3.19c) and connected to the disc-cone structure and near the sleeve it is bent and fixed under the ground plane. The second one fed the monopole with the aid of the sleeve (Fig. 3.19c). This technique is also very popular for designing reconfigurable antennas, where each element can be tuned independently [66]-[67]. For instance in [66] a PIFA is combined with a monopole within space taken by the PIFA, and a switch is used in the PIFA

for frequency reconfiguration, as shown in Fig. 3.20d. With the switch on and off this antenna covers long term evolution (LTE), global system of mobile communication (GSM) 900, personal communications service (PCS) 1900, m-WiMAX (3.6GHz) and WLAN 802.11a. A two port coupling element chassis antenna was proposed in [67]. Two sets of matching circuit were allocated to each antenna to achieve wide reconfiguration. Overall, each technique has its own benefits and drawbacks. Depending on the application and requirements a suitable technique should be adopted. In the next section the techniques to overcome the port coupling in multi element antenna systems are reviewed.

### 3.4.2.2 Port Isolation

In multi standard radio systems with simultaneously operating antennas, excellent isolation between antenna ports is a requirement. In the case that operating frequency bands are sufficiently widely separated, embedded or external filtering structures can be used to provide the required isolation. On the other hand, there are applications where bands have to be closely spaced or even have to occupy the same band such as multiple input multiple output system (MIMO), where in principle the demanded isolation cannot be achieved with microwave filters or where isolation provided by filters is not sufficient. Various port decoupling techniques have been reported in the literature [69]-[86].

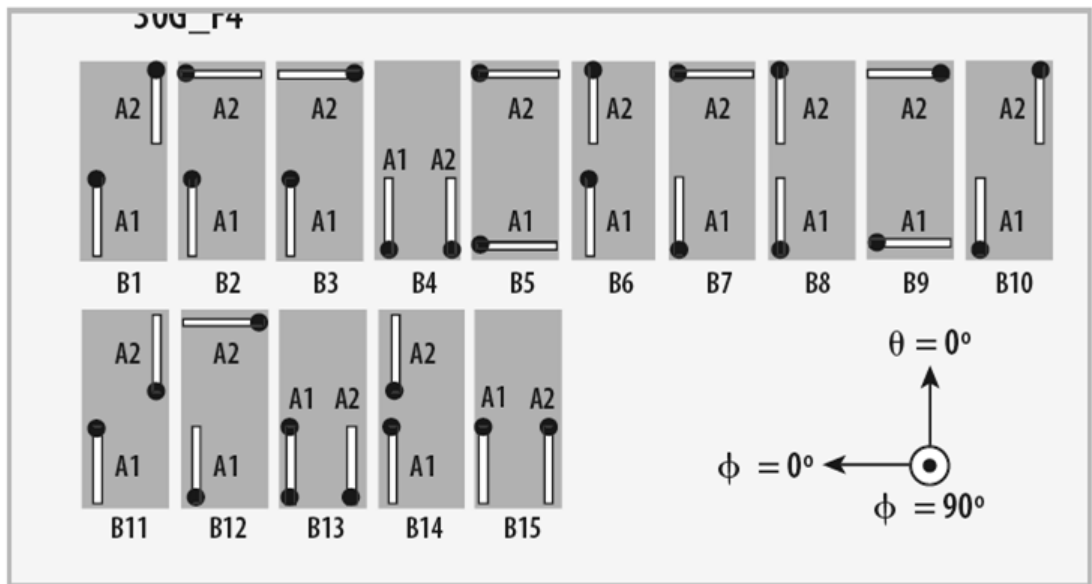


Fig. 3.20 15 different two-antenna configurations on a finite ground plane. The matchsticks symbolize the PIFAs, and the dot on the matchstick denotes the location of the shorting pin [70].

High antenna port isolation is well-known to be available from widely spaced antennas. Good isolation can be achieved by separating antennas by much more than half a wavelength. However, not always half a wavelength is available on the device especially at low frequencies. To achieve maximum separation for instance in a typical mobile phone or laptop the antennas are distributed around the periphery of the device.

When multiple antennas are collocated on a single device, some factors such as the antenna positions relative to each other and to the ground influence the radiation. Moreover, in applications such as mobile phones, the ground plane or device chassis is considered as part of the antenna and therefore contributes to the radiation. Hence, it is important to find the appropriate configuration of antennas which can satisfy all the system requirements. In [70] Jakobsen et al. related the antenna mutual orientations and locations to the mutual coupling between two identical antennas on an infinite ground plane. They investigated 15 symmetrical as well as asymmetrical coupling scenarios using two identical PIFAs located close to each other on the finite ground plane as shown in Fig. 3.20. They concluded that in MIMO application in addition to low mutual coupling, the bandwidth should also be maintained to achieve good MIMO performance. Therefore, taking into account bandwidth and mutual coupling configuration B4 has the best performance although it is not the case with the largest spacing.

In some applications, due to the constraint of the spacing of the antenna elements, polarization diversity is preferred. It has even been suggested by Andrews et al. [71] that, with three orthogonal components of the electric field and three of the magnetic field, it is possible to obtain six independent channels at a single point. In other word, the relative orientation and position of the antennas can improve the port isolations. In [72] two orthogonal polarization-diversity printed dipole antennas are presented (see Fig. 3.21). A three-port antenna consisting of three mutually perpendicular dipole antennas as shown in Fig. 3.22, has been suggested by [73]. The mutual couplings between the antenna elements in such configuration are less than 18 dB. A four port slot antenna was proposed in [74]. Each antenna element is designed on each side of the square shaped board. In order to further

improve the mutual coupling a cross slot is inserted in between the antenna elements (shown in Fig. 3.23). The slot can on one hand reduce some of the mutual coupling through separating the common shared small ground plane and on the other it helps maintaining the bandwidth.

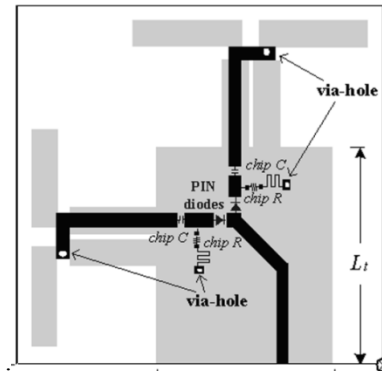


Fig. 3.21 Schematic diagram of the 2.4-GHz planar polarization-diversity antenna with a polarization-selection p-i-n diode circuit [72].

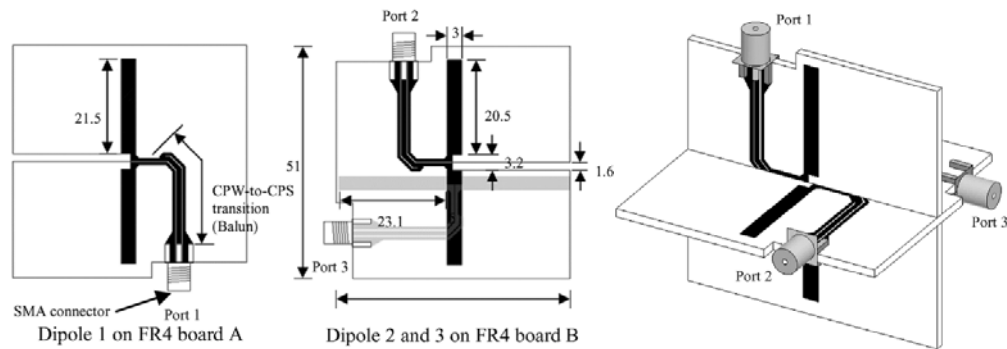


Fig. 3.22 Schematic diagram of the three port orthogonal dipole antenna with integrated baluns for polarization diversity [73].

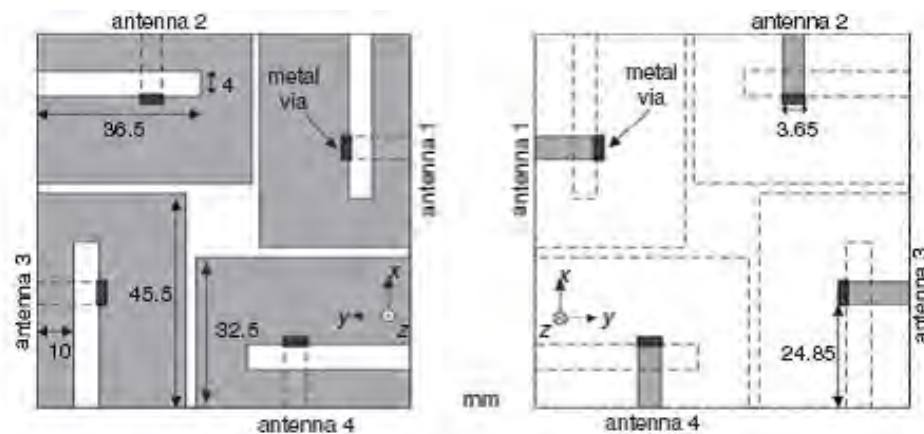


Fig. 3.23 Schematic diagram of the four port orthogonal slot antenna with a cross slot inserted in between elements for port isolation and bandwidth enhancement [74].



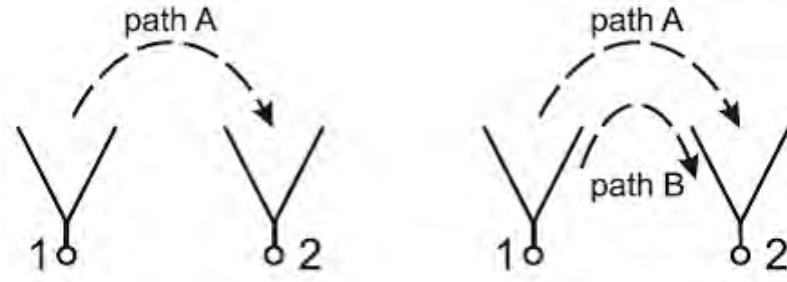


Fig. 3.24 Left: Two-port antenna without coupling cancellation. Right: Cancellation of path A by a second path B [75].

In fact, isolation between the antenna ports can be enhanced by employing cancellation techniques [75]. These techniques require a modification of the antenna structure such that in addition to the already existing “propagation path A” (Fig. 3.24, left) a second path B is created (Fig. 3.24, right) whose parameters can be adjusted to cancel the unwanted transmission via path A. The cancellation path can be formed through various techniques [76]-[84].

A well-known practice is the introduction of resonant defects such as slots, slits and stubs on the ground plane between the antennas [76]-[79]. In [76] two PIFAs are placed on the top and bottom of the mobile chassis to achieve the largest spacing possible (see Fig. 3.25a). Furthermore, two coupled quarter-wavelength slits are inserted into the ground plane between the antennas. The slits introduce resonances and insert transmission zero in the coupling path between the PIFAs. This reduces the coupling without significantly disturbing antenna performance. This technique is also examined in [77] for printed PIFAs (see Fig. 3.25b) achieving  $S_{21}$  less than -25dB. Fig. 3.25c shows another attempt for reducing port coupling between two PIFAs studied in [78]. They achieved coupling better than 15dB across the band. A printed WLAN MIMO antenna with reduced coupling is presented in [79]. A T-stub section is added to the ground plane as shown in Fig. 3.26a and about 50% improvement comparing to the conventional case is achieved. To support a wider bandwidth for UWB MIMO a multiple branch structure (see Fig. 3.26b) can be replaced with the T-stub [80]. In this work,  $S_{21}$  less than -10dB is maintained for the UWB band. Lihao et al [81] included a split ring resonator on the common ground between the antennas as shown in Fig. 3.27a to limit the port coupling.

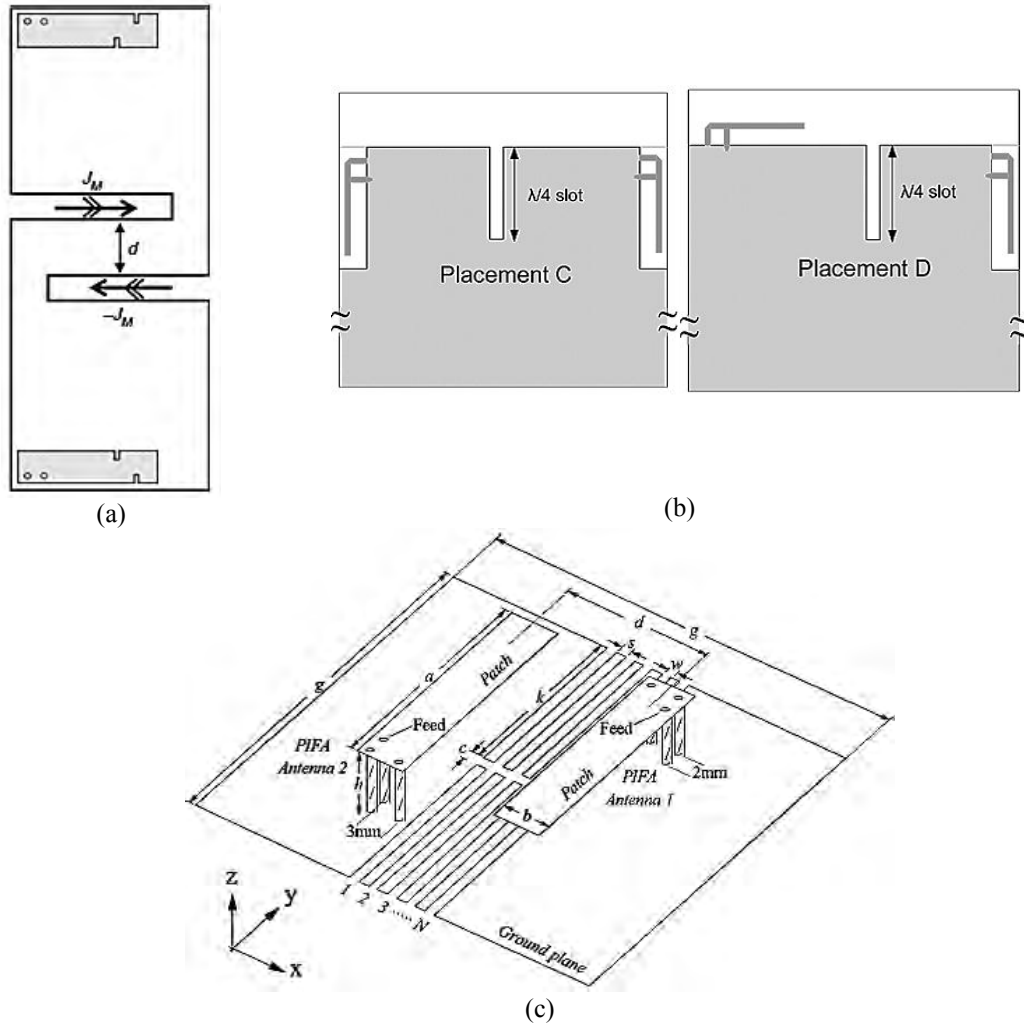


Fig. 3.25 Schematic diagram of MIMO antennas with slits in the ground plane, (a) [76], (b) [77], (c) [78].

Furthermore, the cancellation technique is practiced in [82] by inserting a parasitic structure between the dipoles shown in Fig. 3.27b. In principle this method introduces one more coupling path and this coupling path creates another coupled current with pre-determined magnitude and phase in order to cancel out the original coupling. Using this technique, measured  $S_{21}$  better than -30dB for the band of interest at 2.45GHz has been achieved. In [83] a suspended transmission line is inserted between the PIFAs shorting and/or feeding points as the cancellation paths (see Fig. 3.27c). When the shorting strips face each other and linked via the bridging suspended transmission line, the transmission coefficient is stable and better than -20dB across the 0.8-2.6GHz band. This concept is combined with other techniques such as optimum antenna orientation and position in [84]. As shown in Fig. 3.28

two folded monopoles are printed orthogonally to achieve pattern and polarisation diversity at the same time. High port isolation is obtained by adding a connecting line to the face of the feedline. The connecting line linking the two antennas is used to cancel the reactive coupling between these antennas.

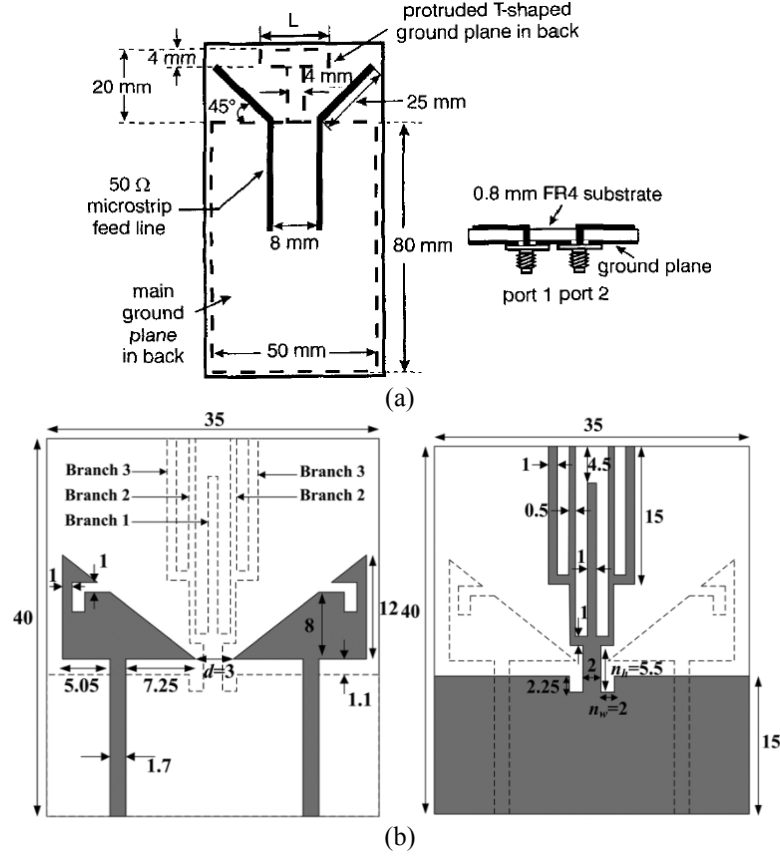


Fig. 3.26 Schematic diagram of the MIMO antennas with stub (a) [78], (b) [78].

The isolation between the closely spaced antennas can also be improved by means of external microwave feed networks [85], [86]. In [85] a four-port decoupling network is proposed, with two output ports connected to the antennas, for reducing the coupling between the two resultant new input ports. Each input port is in turn connected to a matching network for improving the input impedance. Fig. 3.29 shows the function blocks of the decoupling structure. The decoupling network consists of two transmission lines in order to transform the complex trans-admittance to a purely imaginary one. A shunt reactive component is then attached in between the transmission lines ends to cancel the resultant imaginary trans-admittance. Finally, a simple lumped-element circuit is added to each port for input

impedance matching. This method is examined on two printed monopoles for operation at 2.4GHz. The transmission coefficient without the network is more than -5dB which reduces to -35dB when the technique is applied.

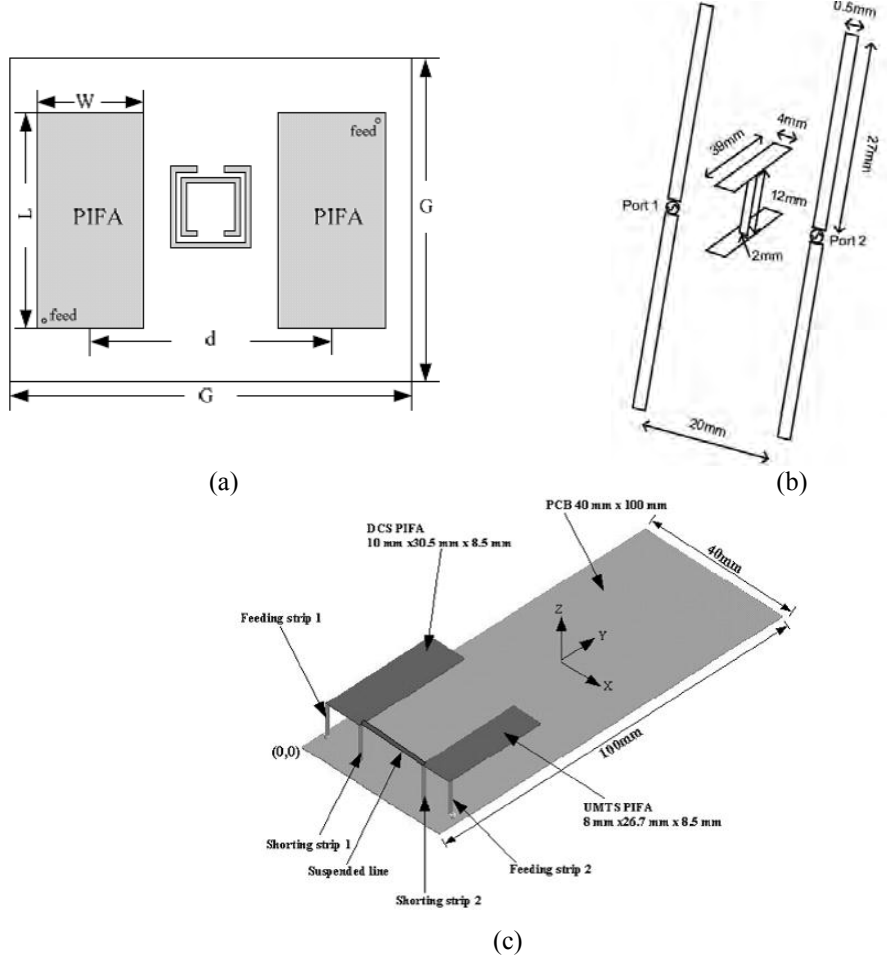


Fig. 3.27 Schematic diagram of the PIFAs with (a) split ring resonator [81] (b) parasitic decoupling element [82] (c) suspended transmission line [83].

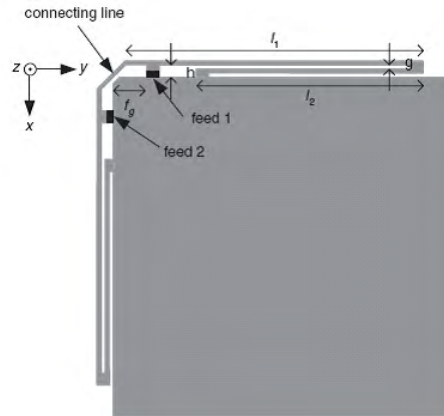


Fig. 3.28 Schematic diagram of the antenna with combination of decoupling techniques [84].

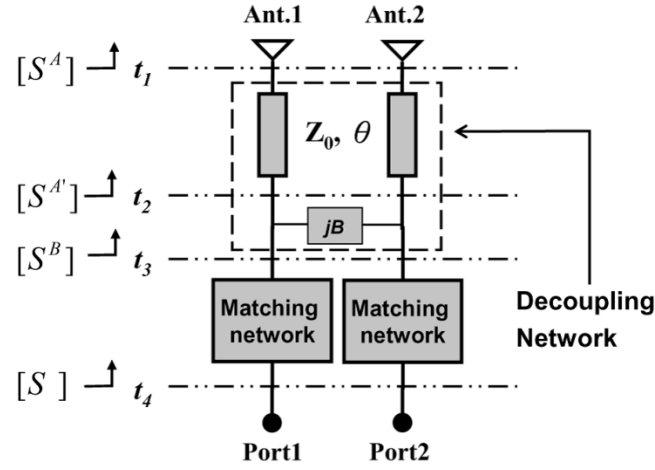


Fig. 3.29 The function blocks of the decoupling structure proposed in [85].

To compensate the size of the microwave networks, particularly at low frequencies, a lumped element feed network is proposed in [86]. An LC-based branchline hybrid coupler has been integrated with the long term evolution (LTE) antenna array as shown in Fig. 3.30. The branchline hybrid coupler is designed at 710 MHz using the passive inductors and capacitors. Each quarter wavelength transmission line section of the branch line coupler has been replaced with its equivalent pi-network consisting of a series inductor and two parallel capacitors. Fig. 3.30 shows the configuration of the branchline coupler. Multi element antenna solutions offer extra degrees of freedom which can be beneficial to future radio applications. These features are reviewed in the next section.

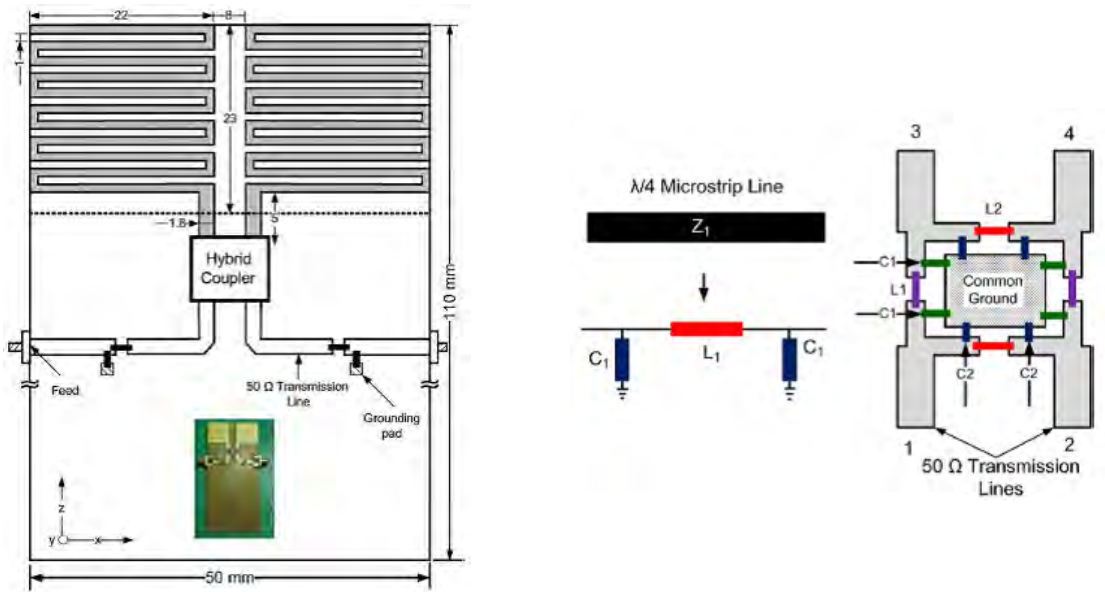


Fig. 3.30 Schematic diagram of the LTE antenna with a branchline decoupling feed network [86].

### **3.5 Reconfigurable Radio**

The user-device interactions, rich multipath environment, increasing number of users and services pose unpredictable and/or harsh electromagnetic environments for antennas in portable devices. This suggests that more robust antenna solutions are required for future devices. Antenna reconfigurability in such a situation could provide numerous advantages. For instance, the ability to tune the antenna's operating frequency could be utilized to change operating bands, filter out interfering signals, or tune the antenna to account for a new environment. If the antenna's radiation pattern could be changed, it could be redirected towards the access point and use less power for transmission, resulting in a significant savings in battery power [87].

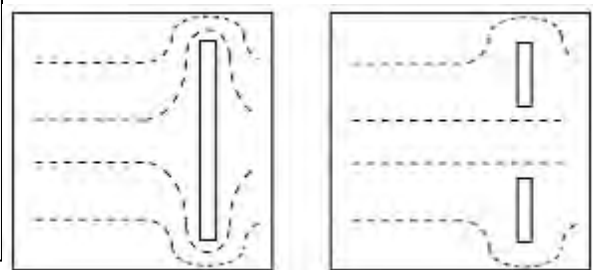
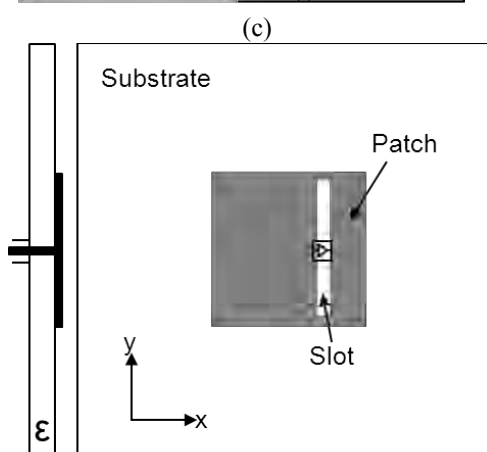
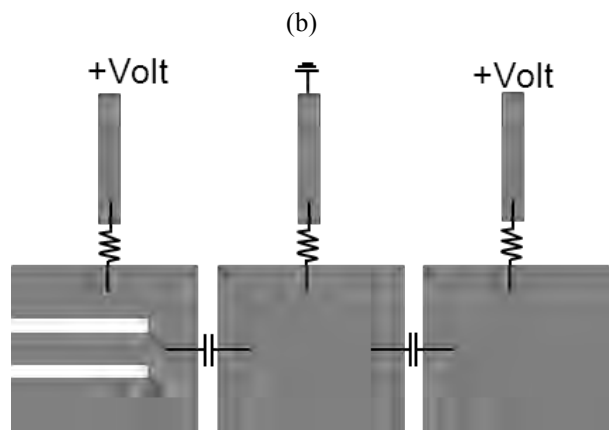
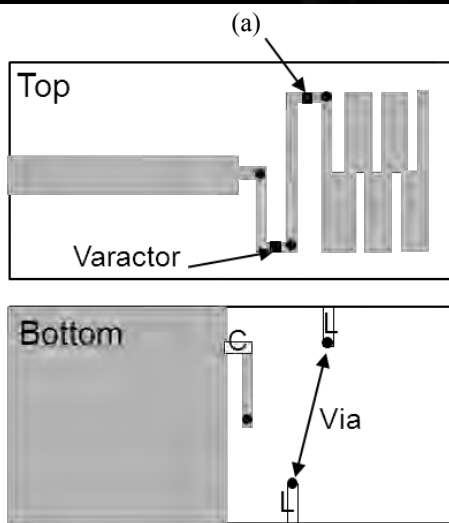
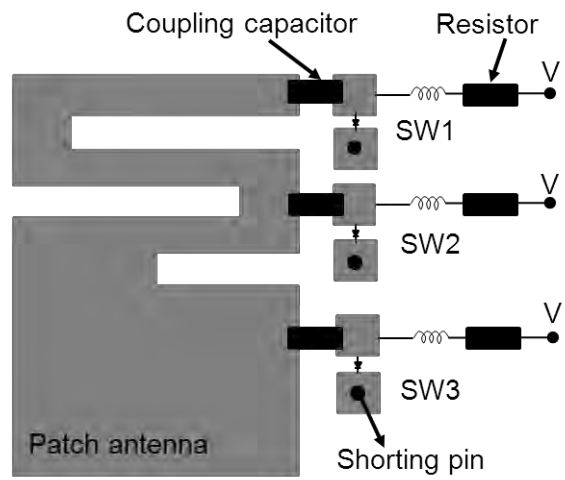
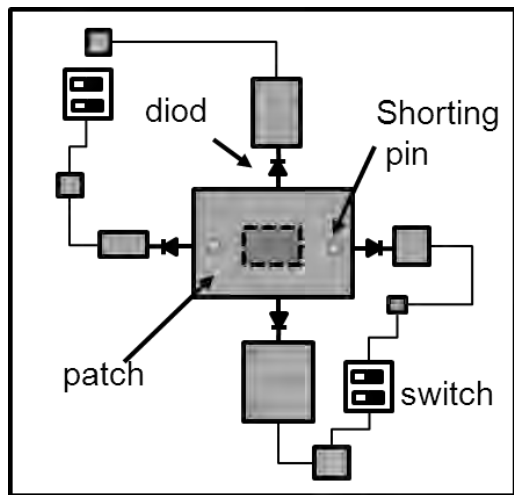
An alternative approach towards the unpredictable and time variant environment, instead of increasing the sensitivity of the system components (such as antennas), is to react to the change and switch to a more optimum operating state. This is basically what CR is foreseen to do. Therefore, CR requires reconfigurable systems to complete the cognition cycle for enhanced performance. The reconfigurability can be added to different components of the system. However, reconfigurable antennas relax the complexity of the RF circuits. The literature on reconfigurable antennas is quite extensive. For this reason specifically some of the frequency-reconfigurable patch and PIFAs are reviewed to provide required background information for the next chapters [88]-[95].

Frequency reconfigurability in resonant antennas is mainly achieved by varying the effective length of the structure. Recently, a reconfigurable monopolar patch antenna was presented in [88]. Four open stubs are attached to the rectangular patch through four pin diodes, and hence eight different patch sizes and consequently eight operating frequencies are achieved. PIN diodes are used in a slotted rectangular patch loaded by a number of posts close to the patch edge [89] to tune the antenna from 620 to 1150MHz. A pin and a varactor diode are incorporated into a meander type monopole [90]. The pin diode is used for frequency switching (macro-tuning) between 2 GHz band and 5 GHz band. In addition, the varactor is

used for frequency tuning (micro-tuning) within wireless service bands (2.3–2.48 GHz and 5.15–5.35 GHz) to produce constant antenna gain.

The antenna can also be tuned by changing the path of radiating currents and yet maintaining the active footprint of the antenna. This approach was analysed in [91] by etching a slot in a conventional microstrip patch. The slot is perpendicular to the direction of the first resonance current path. The current path on the patch changes depending on the bias voltage of a PIN diode which is positioned in the centre of the slot. Similarly a fragmented patch antenna with three gaps in which varactors diodes are accommodated was suggested in [92]. Reconfigurable multiband performance can be achieved by this technique.

Another technique is to tune a specific band by means of external impedance matching circuits. In [93] an external re-matching circuit was used to switch a 0.748 to 0.912 GHz antenna to operate over a 1.84 to 2.185 GHz band. A reconfigurable tuning network was suggested in [94] to tune a coupling element cell phone antenna across a very wide range band (100MHz -2GHz). In [95], a variable capacitor and an inductor are placed at the antenna feeding of a microstrip patch to achieve tuning possibility from 2.6 to 3.35 GHz. The schematic of the above mentioned antennas are shown in Fig. 3.31.



(e)



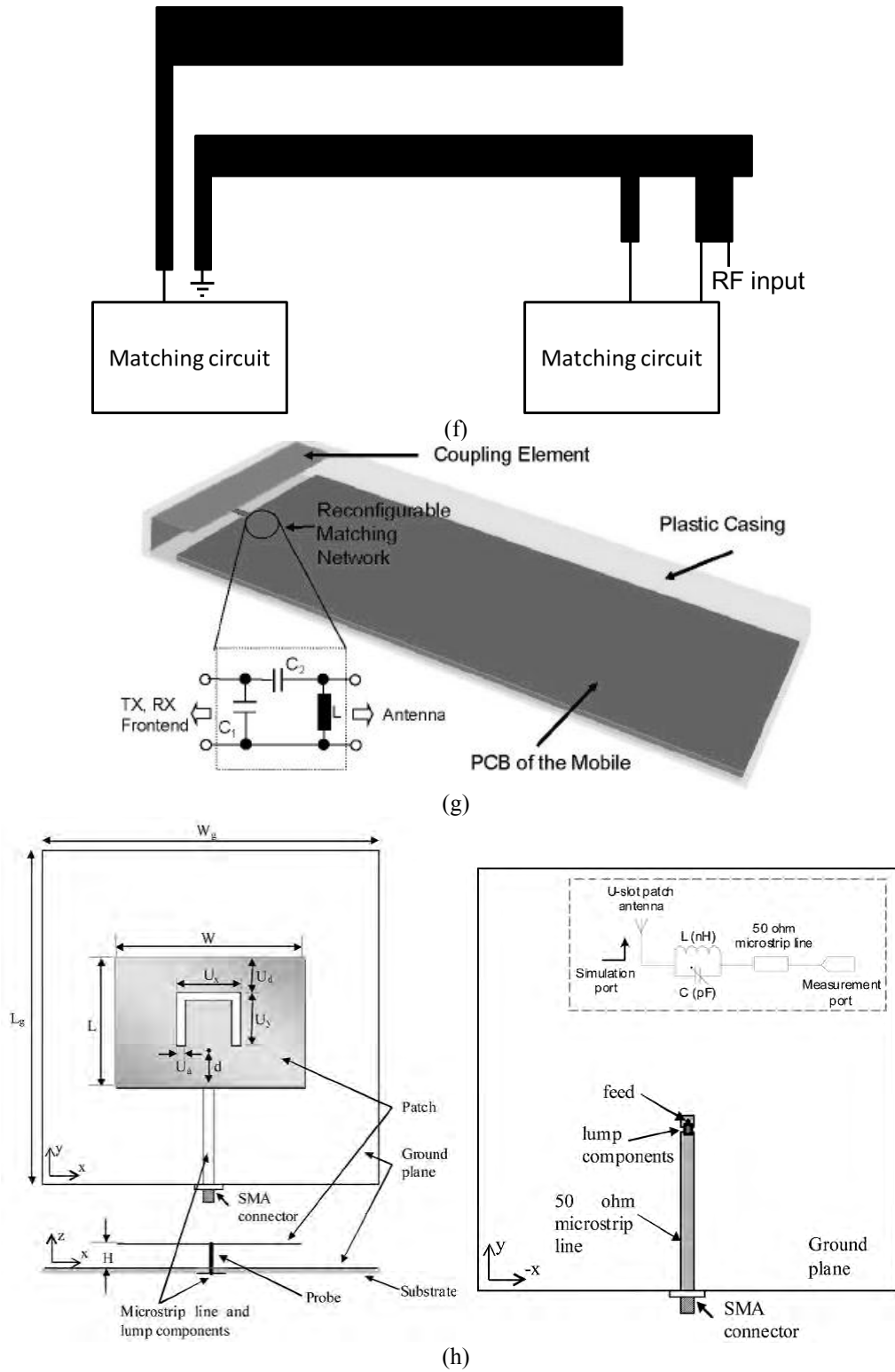


Fig. 3.31 Schematic of the reconfigurable antennas, (a) [88], (b) [89], (c) [90], (d) [91], (e) [92], (f) [93], (g) [94], (h) [95].

### 3.6 Summary

The impacts of increasing number of wireless services and demand for higher data rate on spectrum management and hardware arrangement were elaborated in this chapter. The required background on involving topics including spectrum management approaches, UWB, CR technology and antenna design approaches and challenges for designing wideband, multiband and reconfigurable antennas were briefly reviewed in this chapter.

### References

- [1] Commission of the European Communities, “Commission decision of 21/II/2007 on allowing the use of the radio spectrum for equipment using ultra-wideband technology in a harmonised manner in the community,” Brussels, February 21, 2007.
- [2] H. Arslan, Z. N. Chen and M.-G. Di Benedetto, *Ultra Wideband Wireless Communication*, JohnWiley & Sons, ISBN 0-471-71521-2, New Jersey, United States of America, 2006.
- [3] Mitola, J. The software radio architecture. *IEEE Communications Magazine*, 1995.
- [4] Mitola, J. Cognitive radio: *An integrated agent architecture for software defined radio*. Ph.D. Dissertation, KTH, 2000.
- [5] Report ITU-R SM.2152 Definitions of Software Defined Radio (SDR) and Cognitive Radio System (CRS). 2009.
- [6] L. Berlemann and S. Mangold, *Cognitive Radio and Dynamic Spectrum Access*, JohnWiley & Sons, ISBN 978-0-470-51167-1, West Sussex, United Kingdom, 2009.
- [7] Q. Zhao and B. M. Sadler, “A survey of dynamic spectrum access,” *IEEE Signal Process. Mag.*, vol. 24, no. 3, pp. 79–89, May 2007.
- [8] Y. Hur, J. Park, W. Woo, K. Lim, C.-H. Lee, H.S. Kim and J. Laskar, “A wideband analog multi-resolution spectrum sensing (MRSS) technique for cognitive radio (CR)

- systems”, *Proceedings. IEEE International Symposium on Circuits and Systems*, 21-24 May 2006.
- [9] J. Laskar, R. Mukhopadhyay, Y. Hur, C.-H. Lee and K.;Lim, “Reconfigurable RFICs and modules for cognitive radio”, *Topical Meeting on Silicon Monolithic Integrated Circuits in RF Systems*,. 18-20 Jan. 2006
- [10] H. Harada, “A Software Defined Cognitive Radio Prototype,” *IEEE 18th International Symposium on Personal, Indoor and Mobile Radio Communications*, 2007. 3-7 Sept. 2007.
- [11] I. J. Bahl and P. Bhartia, *Microstrip Antennas*. Dedham, MA: Artech House, 1980.
- [12] J. R. James, P. S. Hall and C. Wood, *Microstrip Antennas: Theory and Design*. London: Peter Peregrinus (IEE), 1981.
- [13] K. C. Gupta and A. Benalla, *Microstrip Antenna Design*. Norwood, MA: Artech House, 1988.
- [14] J. R. James and P. S. Hall, *Handbook of Microstrip Antennas*. London: Peter Peregrinus (IEE), 1988.
- [15] Z. N. Chen and M. Y.W. Chia, *Broadband Planar Antennas: Design and Applications*, John Wiley & Sons Ltd, ISBN-13: 978-0-470-87174-4, West Sussex, England, 2006.
- [16] B. Allen, M. Dohler, E. E. Okon, W. Q. Malik, A. K. Brown and D. J. Edwards, *Ultra-Wideband Antennas and Propagation for Communications, Radar and Imaging*, John Wiley & Sons Ltd, ISBN-13 978-0-470-03255-8, West Sussex, England, 2007.
- [17] Z. N. Chen, *Antennas for Portable Devices*, John Wiley & Sons Ltd, ISBN 978-0-470-03073-8, West Sussex, England, 2007.
- [18] C. J. Liang, C.C. Chiau, X. Chen and C. G. Parini, “Study of a printed circular disc monopole antenna for UWB systems,” *IEEE Trans. Antennas Propagat.*, vol. 53, pp. 3500–3504, Nov. 2005.

- [19] J. Liang, L. Guo, C.C. Chiau, X. Chen and C.G. Parini, "Study of CPW-fed circular discmonopole antenna for ultra wideband applications," in *Proc. IEE Microw. Antennas Propagat*, vol. 152, pp.520-526, Dec. 2005.
- [20] S. W. Su, J.H. Chou and K. L. Wong, "Internal ultrawideband monopole antenna for wireless USB dongle applications," *IEEE Trans. Antennas Propagat.*, vol. 55, no. 4, pp. 1180–1183, Apr. 2007.
- [21] K.Bahadori and Y. R. Samii, "A miniaturized elliptic-card UWB antenna with WLAN band rejection for wireless communications," *IEEE Trans. Antennas Propagat.*, vol. 55, no. 11, pp. 3326–3332, Nov. 2007.
- [22] J Jung, W. Choi, and J. Choi, "A SmallWideband Microstrip-fed Monopole Antenna," *IEEE Microwave and Wireless Components Letters*, vol. 15, no. 10, pp. 703-705, October 2005.
- [23] M. Ojaroudi, Sh. Yazdanifard, N. Ojaroudi, and M. Naser-Moghaddasi, "Small Square Monopole Antenna With Enhanced Bandwidth by Using Inverted T-Shaped Slot and Conductor-Backed Plane," *IEEE Trans. Antennas Propag.*, vol. 59, no. 2, pp. 670-674, February 2011.
- [24] M.A. Antoniadis and G.V. Eleftheriades, "A Compact Multiband Monopole Antenna With a Defected Ground Plane," *IEEE Antennas Wireless Propag. Lett.*, vol. 7, pp. 652-655, 2008.
- [25] H.T. Chattha, Y. Huang and Y. Lu, "PIFA bandwidth enhancement by changing the widths of feed and shorting plate," *IEEE Antennas Wireless Propag. Lett.*, vol. 8, pp.637 – 640, 2009.
- [26] L. L. Rauth, J. S. McLean, K. B. Dorner, J. R. Casey and G. E. Crook, "Broadband low-profile antenna for portable data terminal," *IEEE Int. Symp. Antennas Propag.*, vol. 1, pp. 438–441, June 1997.
- [27] H. Nakano, N. Ikeda, Y. Wu, R. Suzuki, H. Mimaki and J. Yamauchi, "Realization of dual-frequency and wide-band VSWR performances using normal-mode helical and inverted-F antennas," *IEEE Trans. Antennas Propag.*, vol. 46, no. 6, pp. 788–793, 1998.

- [28] P. Song, P. S. Hall, H. Ghafouri-Shiraz and D. Wake, ‘Triple-band planar inverted-F antenna,’ *IEEE Int. Symp. Antennas Propag.*, vol. 2, pp. 908-911, 1999.
- [29] T. Okuno and K. Hirasawa, “A semicircular planar inverted-F antenna with a parasitic element,” *8<sup>th</sup> International Conference on Communication Systems*, vol. 2, pp. 1170–1173, November 2002.
- [30] R. L. Li, G. DeJean, M. M. Tentzeris and J. Laskar, “Development and analysis of a folded shorted-patch antenna with reduced size,” *IEEE Trans. Antennas Propag.*, vol. 52, no. 2, pp. 555–562, 2004.
- [31] K. Oh and K. Hirasawa, “A dual-band inverted-L-folded antenna with a parasitic wire,” *IEEE Int. Symp. Antennas Propag.*, vol. 3, pp. 3131–3134, June 2004.
- [32] Z. N. Chen and M. Y. W. Chia, “Broadband planar inverted-L antennas,” *IEE Proceedings: Microw., Antennas Propag.*, vol. 148, no. 5, pp. 339–342, 2001.
- [33] A. Kishk, K. F. Lee, W. C. Mok and K. M. Luk, “A wide-band small size microstrip antenna proximately coupled to a hook-shaped probe,” *IEEE Trans. Antennas Propag.*, vol. 52, no. 1, pp. 59–65, 2004.
- [34] R. Feick, H. Carrasco, M. Olmos and H. D. Hristov, “PIFA input bandwidth enhancement by changing feed-plate silhouette,” *Electron. Lett.*, vol. 40, no. 15, pp. 921–922, 2004.
- [35] P. Salonen, M. Keskilammi and M. Kivikoski, “Single-feed dual-band planar inverted-F antenna with U-shaped slot,” *IEEE Trans. Antennas Propag.*, vol. 48, no. 8, pp. 1262–1264, 2000.
- [36] Z. N. Chen and M. Y. W. Chia, “Broadband probe-fed notched plate antenna,” *Electron. Lett.*, vol. 36, no. 7, pp. 599–600, 2000.
- [37] Z. N. Chen, “Impedance characteristics of a probe-fed L-shaped plate antenna,” *Radio Science*, vol. 36, no. 6, pp. 1377–1384, 2001.
- [38] D. Nashaat, H. A. Elsadek and H. Ghali, “Dual-band reduced-size PIFA antenna with U-slot for Bluetooth and WLAN applications,” *IEEE Int. Symp. Antennas Propag.*, vol. 2, pp. 962–965, June 2003.

- [39] K. Ogawa, T. Uwano and M. Takahshi, "Shoulder-mounted planar antenna for mobile radio applications," *IEEE Trans. Vehicular Technol.*, vol. 49, no. 3, pp. 1041–1044, 2000.
- [40] C. R. Rowell and R. D. Murch, "A capacitively loaded PIFA for compact mobile telephone handsets," *IEEE Trans. Antennas Propag.*, vol. 45, no. 5, pp. 837–842, 1997.
- [41] C. R. Rowell and R. D. Murch, "A compact PIFA suitable for dual-frequency 900/1800-MHz operation," *IEEE Trans. Antennas Propag.*, vol. 46, no. 4, pp. 596–598, 1998.
- [42] T. Lo and Y. Hwang, "Bandwidth enhancement of PIFA loaded with very high permittivity material using FDTD," *IEEE Int. Symp. Antennas Propag.*, vol. 2, pp. 798–801, June 1998.
- [43] Z. N. Chen, K. Hirasawa, K. W. Leung and K. M. Luk, "A new inverted-F antenna with a ring dielectric resonator," *IEEE Trans. Vehicular Technol.*, vol. 48, no. 4, pp. 1029–1032, 1999.
- [44] G. A. Ellis and S. Liw, "Active planar inverted-F antennas for wireless applications," *IEEE Trans. Antennas Propag.*, vol. 51, no. 10, pp. 2899–2906, 2003.
- [45] G. Lui and R. D. Murch, "Compact dual-frequency PIFA designs using LC resonators," *IEEE Trans. Antennas Propag.*, vol. 49, no. 7, pp. 1016–1019, 2001.
- [46] K. L. Virga and Y. Rahmat-Samii, "Low-profile enhanced-bandwidth PIFA antennas for wireless communications packaging," *IEEE Trans. Antennas Propag.*, vol. 45, no. 10, pp. 1879–1888, 1997.
- [47] P. Ciaisi, R. Staraj, G. Kossiavas and C. Luxey, "Compact internal multiband antenna for mobile phone and WLAN standards," *IEEE Microw. Wireless Components Lett.*, vol. 14, no. 4, pp. 148–150, 2004.
- [48] K. L. Wong, *Planar antennas for wireless communications*, Wiley Series in Microwave and Optical Engineering.

- [49] J. Yoon, D. Kim, C. Park, "Implementation of UWB antenna with bandpass filter using microstrip-to-CPW transition matching," *Asia Pacific Microwave Conference*, 2009.
- [50] K. U-Yen, E.J. Wollack, T. Doiron, J. Papapolymerou and J. Laskar, "The design of a compact, wide spurious-free bandwidth bandpass filter using stepped impedance resonators," *In Proc. European Microwave Conf.*, Paris, France, Oct. 2005.
- [51] M. Djaiz, A. Habib, M. Nedil, and T. A. Denidni, "Design of UWB filter -antenna with notched band at 5.8ghz," *3rd IEEE International Symposium on Microwave, Antenna, Propagation and EMC Technologies for Wireless Communications*, 2009.
- [52] W.-C. Liu and C.-M. Wu, "Broadband dual-frequency CPW-fed planar monopole antenna with rectangular notch," *Electron. Lett.*, vol. 40, no. 11, pp. 642-643, 2004.
- [53] Y. J. Cho, K. H. Kim, D. H. Choi, S. S. Lee, and S. O. Park, "A miniature UWB planar monopole antenna with 5-GHz band-rejection filter and the time-domain characteristics," *IEEE Trans. Antennas Propag.*, vol. 54, no. 5, pp. 1453–1460, May 2006.
- [54] W. S. Lee, D. Z. Kim, K. J. Kim, and J. W. Yu, "Wideband planar monopole antennas with dual band-notched characteristics," *IEEE Trans. Microw. Theory Tech.*, vol. 54, no. 6, pp. 2800–2806, Jun. 2006.
- [55] Y. H. Zhao, J. P. Xu, and K. Yin, "Dual band-notched ultra-wideband microstrip antenna using asymmetrical spurlines," *Electron. Lett.*, vol. 44, no. 18, pp. 1051–1052, Aug. 2008.
- [56] J. Y. Deng, Y. Z. Yin, S. G. Zhou, and Q. Z. Liu, "Compact ultrawideband antenna with tri-band notched characteristic," *Electron. Lett.*, vol. 44, no. 21, pp. 1231–1233, Oct. 2008.
- [57] K. H. Kim, Y. J. Cho, S. H. Hwang, and S. O. Park, "Band-notched UWB planar monopole antenna with two parasitic patches," *Electron. Lett.*, vol. 41, no. 14, pp. 783–785, Jul. 2005.

- [58] K. H. Kim and S. O. Park, "Analysis of the small band-rejected antenna with the parasitic strip for UWB," *IEEE Trans. Antennas Propag.*, vol. 54, no. 6, pp. 1688–1692, Jun. 2006.
- [59] Y. Zhang, W. Hong, C. Yu, Z. Q. Kuai, Y. D. Dong, and J. Y. Zhou, "Planar ultra wideband antennas with multiple notched bands based on etched slots on the patch and/or split ring resonators on the feed line," *IEEE Trans. Antennas Propag.*, vol. 56, no. 9, pp. 3063–3068, Sep. 2008.
- [60] T. N. Chang and M. C. Wu, "Band-notched design for UWB antennas," *IEEE Antennas Wireless Propag. Lett.*, vol. 7, pp. 636–640, 2008.
- [61] S. W. Qu, J. L. Li, and Q. Xue, "A band-notched ultrawideband printed monopole antenna," *IEEE Antennas Wireless Propag. Lett.*, vol. 5, no. 1, pp. 495–498, Dec. 2006.
- [62] Y. D. Dong, W. Hong, Z. Q. Kuai, C. Yu, Y. Zhang, J. Y. Zhou, and J. X. Chen, "Development of ultra wideband antenna with multiple band notched characteristics using half mode substrate integrated waveguide cavity technology," *IEEE Trans. Antennas Propag.*, vol. 56, no. 9, pp. 2894–2902, Sep. 2008.
- [63] J. I. Kim, Y. J. Chong, and J. I. Choi, "Printed multiband terminal antenna for multiple wireless services," *12<sup>th</sup> International Conference on Antennas and Propagation*, 2003.
- [64] C. Y. Mo and J. C. Cheng, "A novel tri-band dual-port coplanar waveguide-fed slot loop antenna for WLAN and WiMAX applications," *6<sup>th</sup> Asia-Pacific Microwave Conference*, 2008.
- [65] Zong Xian-zheng; Nie Zai-ping and Yang Xue-heng, "Novel Dual Feed Broadband Antennas with a Combined Shape," *4<sup>th</sup> Asia-Pacific Conference on Environmental Electromagnetics*, 2006.
- [66] J. Cho, C.W. Jung and K. Kim, "Frequency-reconfigurable two-port antenna for mobile phone operating over multiple service bands," *Electronics Letters*, vol. 45, no. 20, pp. 1009 – 1011, 2009.



- [67] Z.H. Hu, C.T.P. Song, J. Kelly, P.S. Hall and P. Gardner, "Wide tuneable dual-band reconfigurable antenna," *Electronics Letters*, vol. 45, no. 22, 2009.
- [68] P. Bahramzy and M. Sager, "Dual-feed ultra-compact reconfigurable handset antenna for penta-band operation," *IEEE Antennas and Propagation Society International Symposium (APSURSI)*, 2010.
- [69] H. Wong, K.-L. Lau and K.-M. Luk, "Design of dual-polarized l-probe patch antenna arrays with high isolation," *IEEE Trans. Antennas Propag.*, vol. 52, no. 1, 2004.
- [70] K. B. Jakobsen and J. Thaysen, "Checking capacity for MIMO configurations," <http://www.mwrf.com/Articles/Index.cfm?ArticleID=15797&pg=1> , June 2007
- [71] M. R. Andrews, P. P. Mitra, and R. de Carvalho, "Tripling the capacity of wireless communications using electromagnetic polarization," *Nature*, vol. 409, no. 6818, pp. 316–318, Jan. 2001.
- [72] H. R. Chuang and L. C. Kuo, "3-D FDTD design analysis of a 2.4 GHz polarization-diversity printed dipole antenna with integrated balun and polarization-switching circuit for WLAN and wireless communication applications," *IEEE Trans. Microw. Theory Tech.*, vol. 51, no. 2, pp. 374–381, Feb. 2003.
- [73] C.-Y. Chiu, J.-B. Yan and R. D. Murch, "Compact three-port orthogonally polarized MIMO antennas," *IEEE Antennas Wireless Propag. Lett.*, vol. 6, pp. 619–622, 2007.
- [74] S. Zhang, P. Zetterberg, S. He, "Printed MIMO antenna system of four closely-spaced elements with large bandwidth and high isolation," *Electron. Lett.* vol. 46 , no. 15, pp. 1052 – 1053, 2010.
- [75] D. Esser, B. Solan and H. Chaloupka, "Improved antenna isolation in transmit/receive applications," German Microwave Conference - GeMiC 2006.
- [76] T. Kokkinos, E. Liakou, A.P. Feresidis, "Decoupling antenna elements of PIFA arrays on handheld devices," *Electron. Lett.*, vol. 44, no. 25, pp. 1442-1444, 2008.

- [77] M. Karaboikis, C. Soras, G. Tsachtsiris and V. Makios, "Compact dual-printed inverted-f antenna diversity systems for portable wireless devices," *IEEE Antennas Wireless Propagat. Lett.*, vol. 3, pp. 9-14, 2004.
- [78] C. Y. Chiu, C. H. Cheng, R. D. Murch, and C. R. Rowell, "Reduction of mutual coupling between closely-packed antenna elements," *IEEE Trans. Antennas Propag.*, vol. 55, no. 6, pp. 1732–1738, Jun. 2007.
- [79] T.Y. Wu, S.T. Fang, and K.L. Wong, "Printed diversity monopole antenna for WLAN operation," *Electron. Lett.*, 2002, 38, (25), pp. 1625–1626
- [80] Z. Shuai, Y. Zhinong, X. Jiang and H. Sailing, "Ultrawideband MIMO/diversity antennas with a tree-like structure to enhance wideband isolation," *IEEE Antennas Wireless Propag. Lett.*, vol. 8, pp. 1279 – 1282, 2009.
- [81] H. Lihao, Z. Huiling H. Zhang, C. Quanming, "Reduction of mutual coupling between closely-packed antenna elements with split ring resonator (SRR)," *International Conference on Microwave and Millimeter Wave Technology (ICMMT)*, 2010.
- [82] A.C.K. Mak, C.R. Rowell, R.D. Murch, "Isolation enhancement between two closely packed antennas," *IEEE Trans. Antennas Propag.*, vol. 56 , no. 11, pp. 3411 – 3419, 2008.
- [83] A. Diallo, C. Luxey, P.L. Thuc, R. Staraj, and G. Kossiavas, "Study and reduction of the mutual coupling between two mobile phone PIFAs operating in the DCS 1800 and UMTS bands," *IEEE Trans. Antennas Propag.*, vol. 54, no. 11, pp. 3063–3073, Nov. 2006.
- [84] S. Park, C. Jung, "Compact MIMO antenna with high isolation performance," *Electron. Lett.* vol. 46, no. 6, pp. 390-391, 2010.
- [85] S.-C. Chen; Y.-S. Wang; S.-J. Chung, "A decoupling technique for increasing the port isolation between two strongly coupled antennas," *IEEE Trans. Antennas Propag.*, vol. 56, no. 12, pp. 3650-3658, 2008.

- [86] R.A. Bhatti, Soongyu Yi, Seong-Ook Park, "Compact antenna array with port decoupling for LTE-standardized mobile phones," *IEEE Antennas Wireless Propag. Lett.*, vol. 8, pp. 1430-1433, 2009.
- [87] J. T. Bernhard, *Reconfigurable Antennas*, Morgan and Claypool, ISBN 9781598290271, 2007.
- [88] T. Y. Han and C. T. Huang, "Reconfigurable monopolar patch antenna," *Electronics Letters*, vol. 46, Feb 4 2010.
- [89] A.-F. Sheta and S. F. Mahmoud, "A widely tuneable compact patch antenna," *IEEE Trans. Antennas Propag.*, vol. 55, pp. 3300-3309, Nov 2007.
- [90] C. W. Jung, Y. J. Kim, Y. E. Kim, and F. De Flaviis, "Macro-micro frequency tuning antenna for reconfigurable wireless communication systems," *Electronics Letters*, vol. 43, pp. 201-202, Feb 15 2007.
- [91] Yang, F., and Rahmat-Samii, Y., "Patch antenna with switchable slot (PASS): Dual frequency operation," *Microwave Optical Technology Lett.*, vol. 31, pp. 165–168, Nov. 2001.
- [92] S. Baylis, S. Aguilar and T. Weller, "Wide bandwidth varactor-tuned patch antenna," *Electronics Letters*, vol. 45, July 30 2010.
- [93] K. R. Boyle and P. G. Steeneken, "A five-band reconfigurable PIFA for mobile phones," *IEEE Trans. Antennas Propag.*, vol. 55, pp. 3300-3309, Nov 2007.
- [94] D. Manteuffel, M. Arnold, "Considerations for reconfigurable multi-standard antennas for mobile terminals," *International Workshop on Antenna Technology: Small Antennas and Novel Metamaterials*, 2008.
- [95] S. L. S. Yang, A. A. Kishk, and K. F. Lee, "Frequency reconfigurable U-slot microstrip patch antenna," *IEEE Antennas Wireless Propag. Lett.*, vol. 7, pp. 127-129, 2008.

## **Chapter 4      Integrated      Wideband-Narrowband Antenna**

### **4.1      Introduction**

One of the main requirements of the emerging wireless technologies is the multiband operation. The main focus of this thesis is to propose multiband antenna solutions which can satisfy some of the requirements of such networks. Several techniques were introduced in the last chapter to design antennas with multiband functionality. Each method has its own advantages and limitations and might be more appropriate in some applications comparing to the other methods. Among the previously introduced methods, the multi element technique is the main focus of this chapter.

In this technique multiband operation is fulfilled by employing multiple antenna elements. In some cases this approach requires more space. However, it adds to the versatility of the solution since the antennas can be designed separately. On the other hand for an effective design more knowledge, understanding of the system and experience is required. In multiple antenna system the antenna interaction with its environment might be more complicated than a single antenna. The mutual coupling between the ports also needs to be considered. This is not an issue in multiband antenna design using filtering or extra resonating structure approach. Although developing a multi element antenna system might be demanding, it has more degrees of freedom in comparison to the other methods. The antenna

elements can be selected from a wide range of various types of antennas according to the desired radiation characteristics such as frequency of operation, radiation pattern and polarization or desired manufacturing technology such as printed, wire or volumetric antennas. Moreover, various bandwidth scenarios can be developed using this technique. Narrowband-narrowband, wideband-narrowband and wideband-wideband can be achieved due to the variety of antennas which can be used in this technique.

A multi element antenna solution is presented in this chapter. An integration concept is introduced to efficiently use the allocated space of the antenna while supporting multiband operation. In this concept the space assigned for one antenna is shared for use of additional antennas. This integration concept will be elaborated in the next section. To demonstrate the benefits of this technique for antenna solutions with multiple bandwidth scenarios, a hybrid wideband-narrowband antenna will be presented as a demonstrator for this concept. A printed UWB antenna is selected as the main antenna and then a shorted patch antenna is integrated into the main structure. Details of the design procedure and the final integrated wideband-narrowband configuration will be described. Finally, the important parameters which affect the antenna performance will also be investigated to obtain some insight into the antenna operation principles.

## **4.2 Integration Concept**

In a typical multiple antenna system, the space required for the antennas grows with the number of antennas. This is more significant for wideband antennas, since they are generally larger in size comparing to narrowband antennas. To tackle this problem an integration solution is introduced in this section. The main concept is to use one antenna or part of it as part of the additional antennas. In this way a section of one antenna can be shared between several antennas. For instance, an antenna with a relatively large metallization area can be used as a ground plane for an additional antenna which requires large ground plane. Depending on the application and the amount of available space, the second antenna can be selected from a wide range of antennas, such as a vertical conventional monopole, or very

popular inverted L or F antenna or a slot antenna among others. A section of one antenna can also be used as parasitic element or reflector for the other antenna. Therefore, this technique offers a variety of combinations to efficiently utilize the space. This integration technique can be applied to various types of antennas including printed antennas to include more services in the limited space especially for small portable devices.

For a successful integration, the operation principles of each antenna should be considered. Importantly, in order to avoid design complexity the interaction between the antenna sections should be taken into account. By selecting an electromagnetically-quiet zone for integrating the second antenna, each antenna can be designed independently and issues such as mutual coupling and radiation pattern degradation can be controlled.

In the next section the design procedure of a hybrid wideband-narrowband antenna will be explored. A planar circular disc monopole antenna, which was used as a benchmark, will be first studied. Furthermore, the second antenna will be integrated with the main antenna. Subsequently, the improved integrated wideband-narrowband antenna will be discussed.

## **4.3 Antenna Geometry and Design**

### **4.3.1 Wideband Antenna- Circular Disc Monopole Antenna**

Printed monopoles are basically evolved from vertical monopoles. In general, printed UWB monopoles are composed of two major printed parts, namely the radiator and the ground plane. The feeding system is either a coplanar waveguide (CPW) or a microstrip line [1]-[2]. Impedance matching is optimized by shaping the radiator and controlling the height of the gap between radiator and the ground plane. To improve the bandwidth of the antenna, various configurations of the radiator and ground plane have been documented [1]-[4]. These include circular [1], [2], square [3], and elliptical shapes [4]. Feeding structures based on microstrip or CPW lines are most suitable for printed antennas. In microstrip feeding, the

excitation signal is carried by a finite length line, printed above a ground plane. On the other hand, the CPW line consists of three coplanar finite length metallic sections as shown in Fig. 4.1. The centre line carries the excitation signal and the other two sections are grounded. Both techniques benefit from ease of fabrication. However, in CPW fed antennas there is lower crosspolarized radiation from the feed comparing to conventional microstrip patch antenna [5]. Moreover, weak cross talk effects between adjacent lines and the possibility to make denser CPW circuits comparing to microstrip circuits, makes CPW ideally suited for microwave integrated circuit applications [6]. Taking all these advantages into account, a CPW feeding structure is preferred for UWB printed antenna in this thesis.

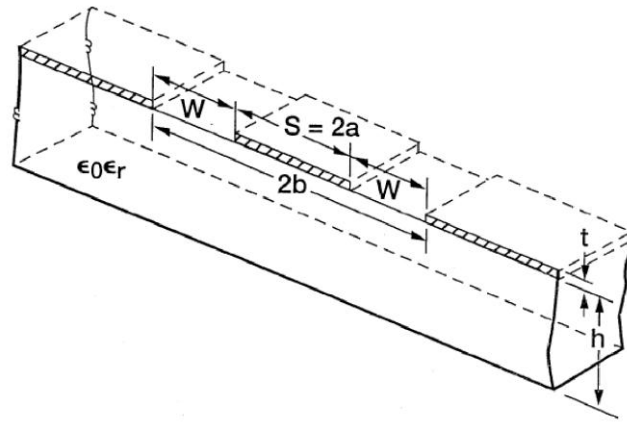


Fig. 4.1 Coplanar waveguide configuration [6].

A planar disc monopole antenna with a CPW feeding is first designed as the base of the hybrid wideband-narrowband antenna. In a CPW fed antenna, the centre strip conductor is elongated and connected to the radiating element. The impedance of the line can be tuned by varying the gap between the centre and side conductors and also the width of the centre strip. The circular disc patch and feeding are both printed on the top layer of dielectric substrate. This configuration is designed on a Taconic TLC laminate with a relative permittivity of  $\epsilon_r=3\pm0.05$  and a thickness of 0.79 mm. The disc diameter determines the lower cut-off frequency and the gap between the feeding and the disc has more influence on the higher end of the frequency band. The width and length of the ground plane also influences the antenna matching [2]. Fig. 4.2 shows the detailed dimensions of the structure. The antenna is

modelled using the CST Microwave Studio™ package, which utilizes the finite integration technique for electromagnetic computation.

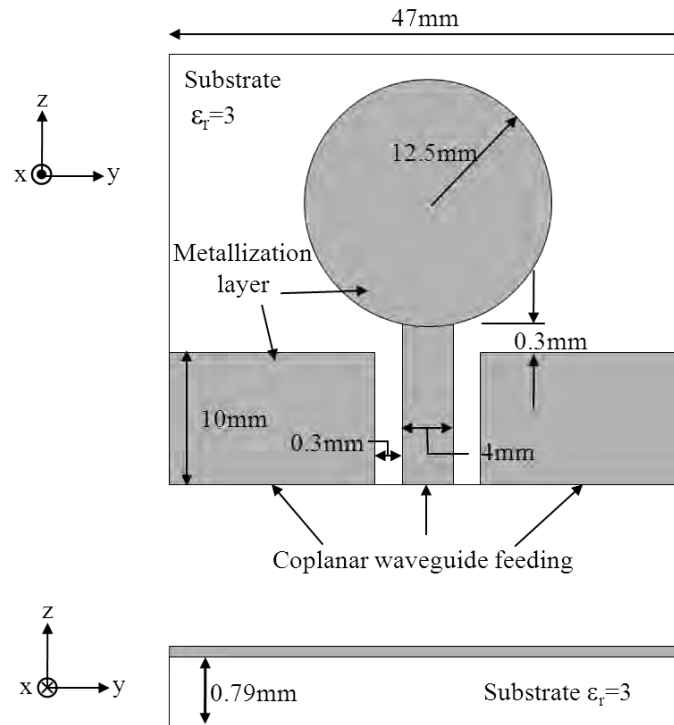


Fig. 4.2 The geometry of the CPW fed circular disc monopole antenna.

The simulated reflection coefficient of the circular disc monopole antenna is presented in Fig. 4.3. Multiple dips in the reflection coefficient curve are indications of closely distributed resonances in this configuration.



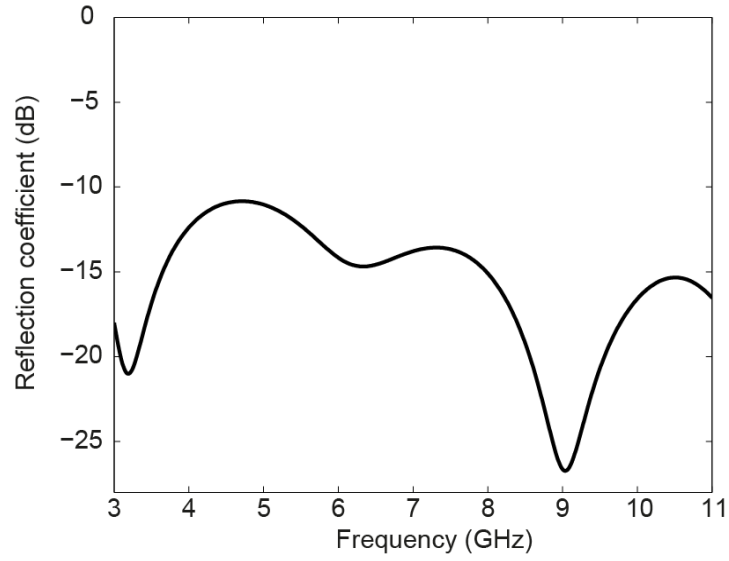


Fig. 4.3 Simulated reflection coefficient of circular disc monopole antenna shown in Fig. 4.2.

Subdividing the operating frequency band to three, low, mid and high bands, the antenna operates as a resonant structure in the low band and hence the radiation is based on standing wave mode. In the mid band the antenna starts to operate in a hybrid mode of standing and travelling waves. At the high band, the travelling wave becomes more critical to the antenna operation. The lower edge of the disc and upper edge of the CPW ground section forms a slot which supports the travelling wave (see Fig. 4.4 ).

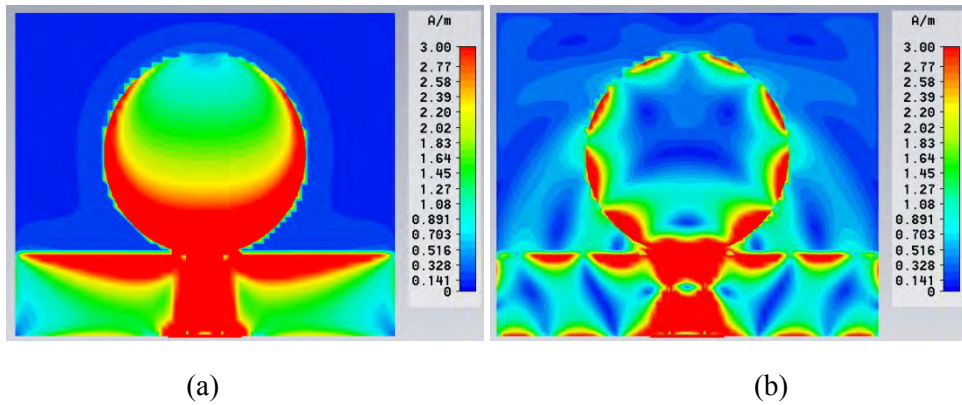


Fig. 4.4 H-field distribution at (a) 3GHz and (b) 17 GHz.

### 4.3.2 Narrowband Antenna

The narrowband antenna is an adoption from the planar inverted F antenna (PIFA) concept. A microstrip patch is printed on the reverse side of the substrate, above the large metallization of the monopole. The patch is then shorted to the monopole radiator by means of a via. Hence, the UWB antenna is used as the ground plane for the shorted patch.

As mentioned in the Chapter 2, PIFAs are classified as resonant antennas. For a typical PIFA as shown in Fig. 4.5, the resonant frequency is defined by (4.1)

$$f_r = \frac{C}{4(L + W + h)} \quad (4.1)$$

where  $C$  is the speed of light and  $L$ ,  $W$  and  $h$  are length, width and height of the planar element, respectively.

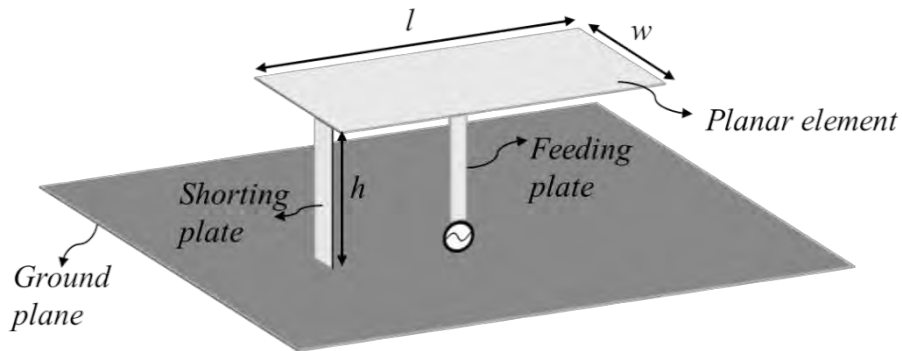


Fig. 4.5 The geometry of a PIFA.

For this arrangement the narrowband antenna is designed for operation in IEEE 802.11a 5GHz sub-bands, specifically,  $f_r = 5.15$  GHz. Therefore, the length and width of the patch are set to be 7mm and 5mm, respectively.

### 4.3.3 Integrated Antenna-Circular Disc Monopole and PIFA Design

The geometry of the integrated disc monopole and shorted patch is shown in Fig. 4.6. The patch is printed above the circular disc on the rear side of the substrate, 7mm away from the board centre and is edge fed through a microstrip line. The 50  $\Omega$  microstrip feeding starts

from the edge of the board above the CPW ground and linearly tapers to  $100\Omega$  before it crosses the gap formed by the disc and the CPW ground and then it reaches the patch. This feeding arrangement adds to the complexity of the system and will be addressed in detail in the next sections.

In this structure in addition to the patch dimensions and shorting pin position, its lateral and vertical position relative to the wideband antenna also influence the resonant frequency of the narrowband antenna. The impact of some parameters on the antenna matching will be studied in the next section in detail.

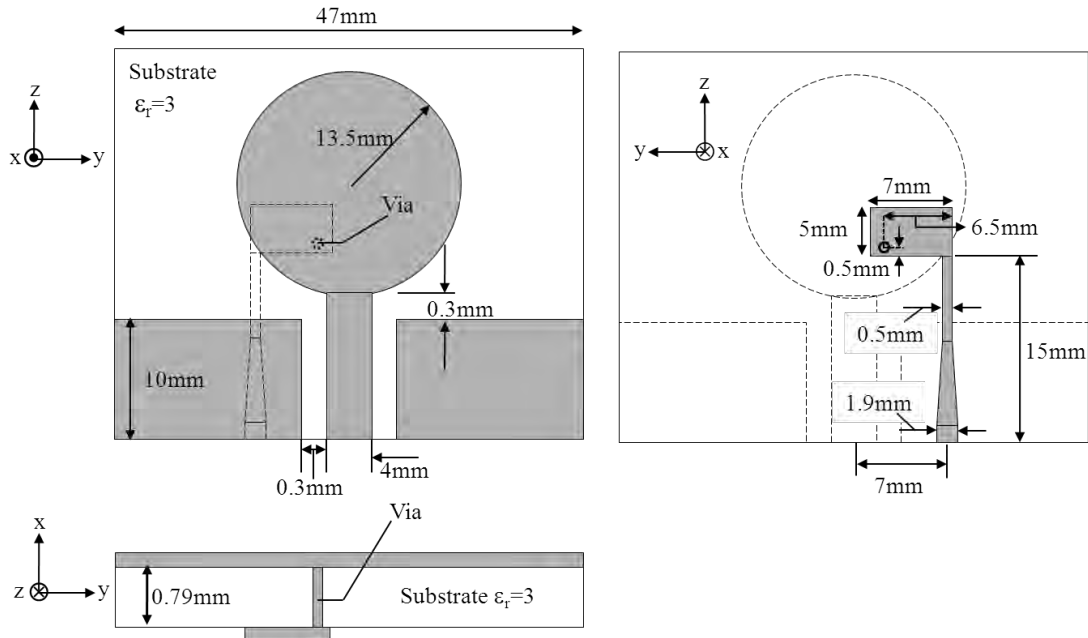


Fig. 4.6 The geometry of the integrated circular disc monopole and PIFA.

Fig. 4.7 shows the reflection coefficient of the disc monopole and shorted patch antennas. These results are achieved by matching one port with a  $50\Omega$  load and exciting the other one. The -10dB impedance bandwidth is reasonably maintained over the whole UWB frequency band, i.e. 3.1 GHz-10.6 GHz. In the range of 6.5-9.5GHz the reflection coefficient is more than -10dB but still less than -7dB, and that is acceptable as a fairly good performance in practical mobile communication. For the narrowband antenna, the -10dB impedance bandwidth covers 5-5.5GHz, which is part of the WLAN 802.11a standard. The transmission coefficient between the two ports is depicted in Fig. 4.8 which is a measure of

isolation between the ports. Transmission coefficient is less than -10 dB for the whole band except in the range of 4.7 GHz to 8.5 GHz which is approximately -5dB. Our investigations showed that the high level of coupling is due to the location of the narrowband antenna feeding. This issue will be addressed thoroughly in Chapter 5.

This configuration provides acceptable results; however there are few practical issues in manufacturing such antenna. In this arrangement the feeding of the narrowband antenna is very close to the wideband feedline. This leaves little space for the sub-miniature version A (SMA) connectors to be connected concurrently. In order to provide enough space for both connectors, it is required that the narrowband antenna is shifted away from the centre of the board which consequently degrades the performance of the wideband antenna. Therefore, it is essential to upgrade the wideband structure accordingly.

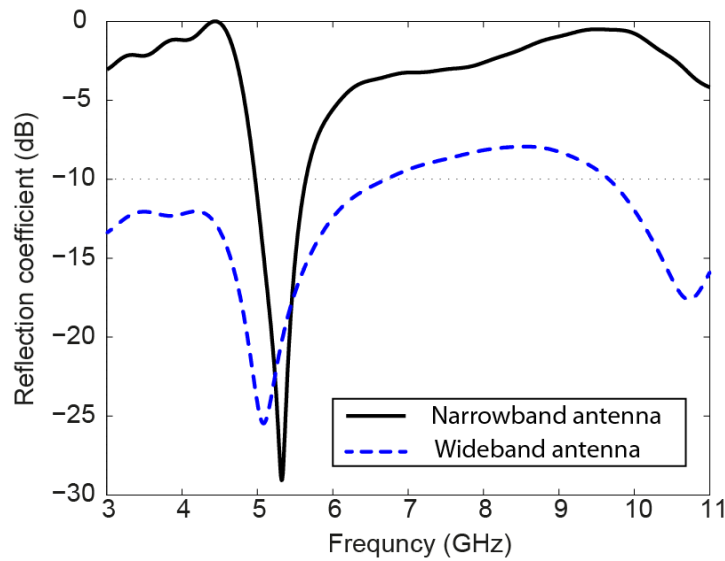


Fig. 4.7 The simulated reflection coefficients of narrowband PIFA and circular disc wideband antennas shown in Fig. 4.6.

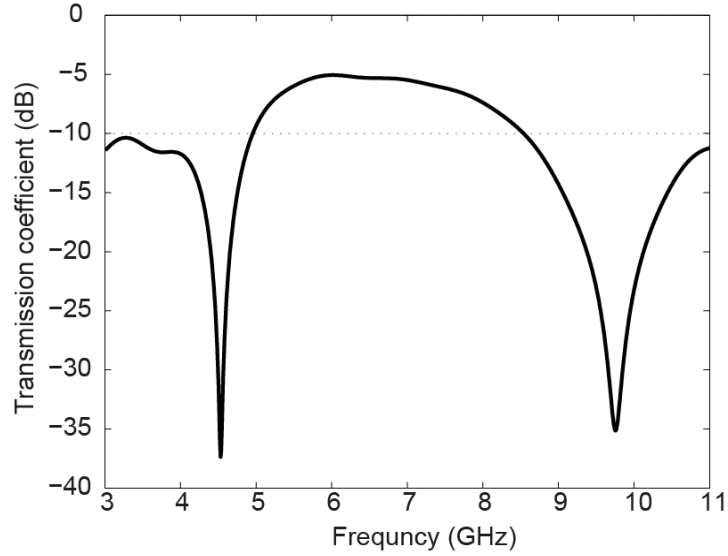


Fig. 4.8 The simulated transmission coefficient of the integrated disc monopole and PIFA shown in Fig. 4.6.

#### **4.3.4 Wideband Antenna - Hour Glass Monopole Antenna Design**

To overcome the feeding problem, a CPW fed hour glass shape UWB monopole antenna has been designed. This shape provides slower transition from 50 $\Omega$  CPW feedline to the monopole radiator. In this structure, a half ellipse has been used for the bottom part and a rectangle for the top part of the monopole radiator. Fig. 4.9 shows the geometry of the upgraded wideband antenna. The antenna has larger radiator and consequently wider ground plane in comparison with the disc monopole version. A prototype of this antenna was manufactured and examined. The reflection coefficient was measured and compared with the simulated result in Fig. 4.10. The measured resonances (at around 4.1GHz, 5.5GHz, 8GHz and 9.4GHz) are very close to those obtained in the simulation. The -10dB bandwidth spans the expected wide frequency range in both simulation and measurement.

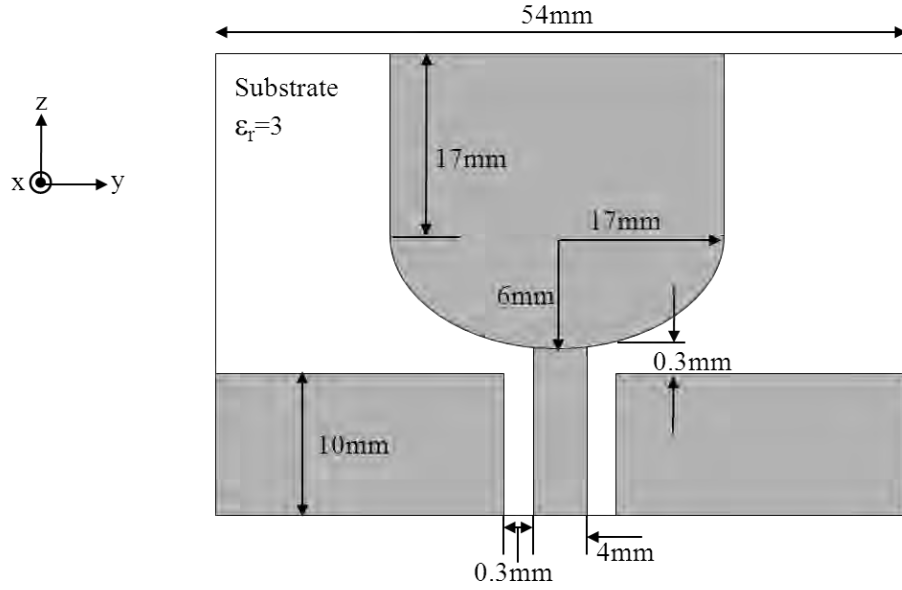


Fig. 4.9 The geometry of the CPW fed hour glass monopole antenna.

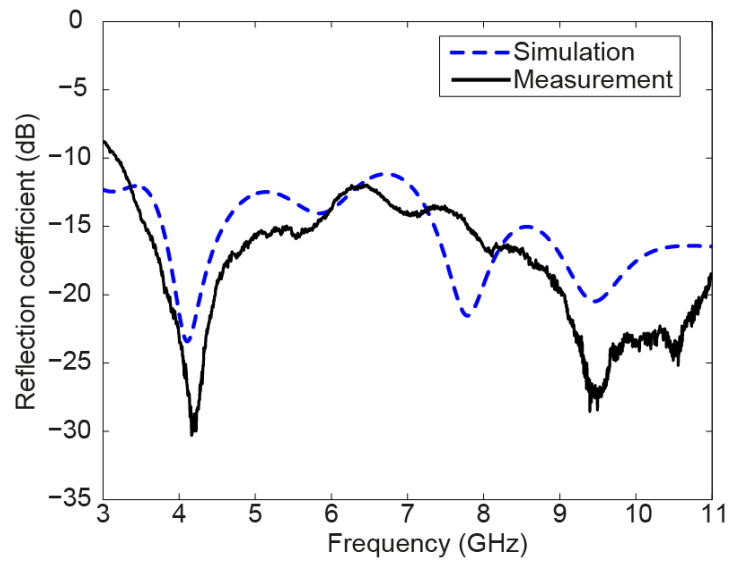


Fig. 4.10 Simulated and measured reflection coefficient of hour glass monopole antenna shown in Fig. 4.9.

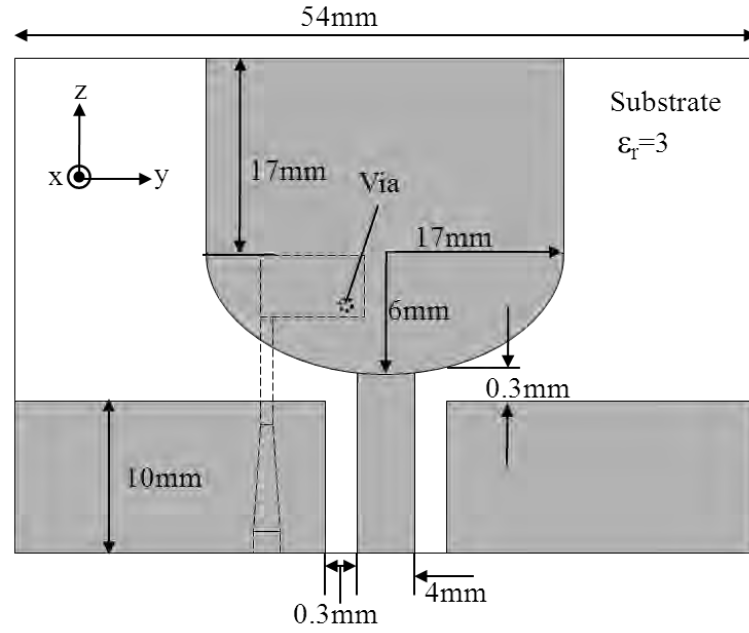
#### 4.3.5 Integrated Antenna-Hour Glass Monopole Antenna and PIFA

After improving the wideband antenna the narrowband shorted patch is integrated into it. Fig. 4.11 shows the top and bottom view of this arrangement. The PIFA feeding was moved away from the board centre to accommodate two connectors and improve the overall performance of the antennas.

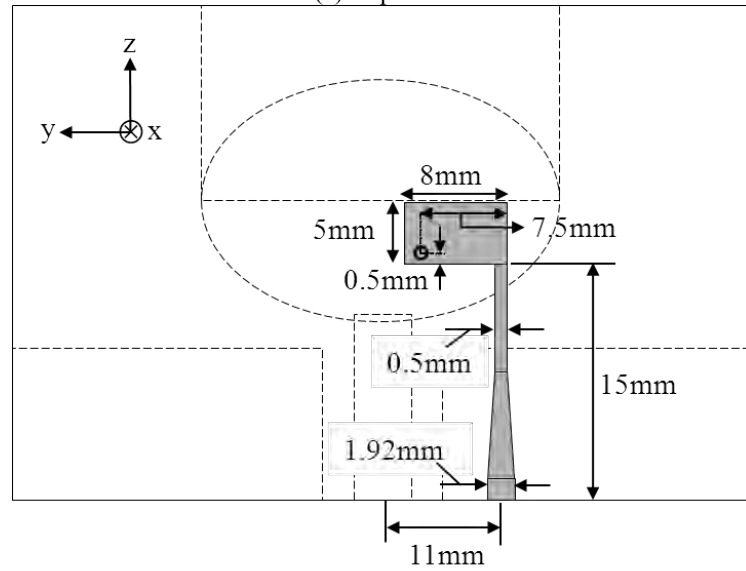
In order to realistically model the antenna, the SMA connectors were also included in the simulations. The effect of the 50 $\Omega$  SMA feeding ports should not be ignored, since they are very close to the antenna and their presence can change the current distribution on the antenna ground plane. Hence, they have been included in the simulation, but this does lead to a substantial computing overhead.

A prototype of the integrated hour glass monopole and PIFA was manufactured and measured. The measured and simulated reflection coefficients for wideband antenna are compared in Fig. 4.12. The wideband antenna provides reasonable match for the whole UWB spectrum. There is a good agreement between the simulated and measured results.

Fig. 4.13 shows the reflection coefficient of the narrowband antenna. The impedance bandwidth (reflection coefficient < -10 dB) is 0.45 GHz (4.9 GHz-5.35 GHz). It is slightly wider than that of the simulated result. This difference may be attributed to the actual substrate having a larger loss tangent than that used in simulation and the tolerance in manufacturing. The transmission coefficient between the ports is depicted in Fig. 4.14. Transmission coefficient is a measure of coupling between the antenna ports. It is less than -10 dB for the whole band except in the range of 4.7 GHz to 7.3 GHz. The coupling peaks (-4 dB) at 5.15 GHz. The investigations showed that the high level of coupling is due to the location of the narrowband antenna. This issue will be discussed in the next chapter.



(a) Top view



(b) Bottom view

Fig. 4.11 The geometry of the integrated hour glass wideband antenna and PIFA.



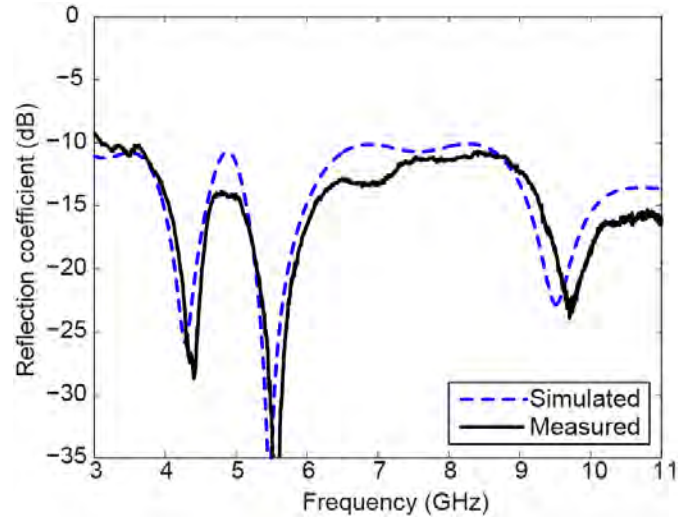


Fig. 4.12 Simulated and measured reflection coefficient of the hour glass wideband antenna shown in Fig. 4.11.

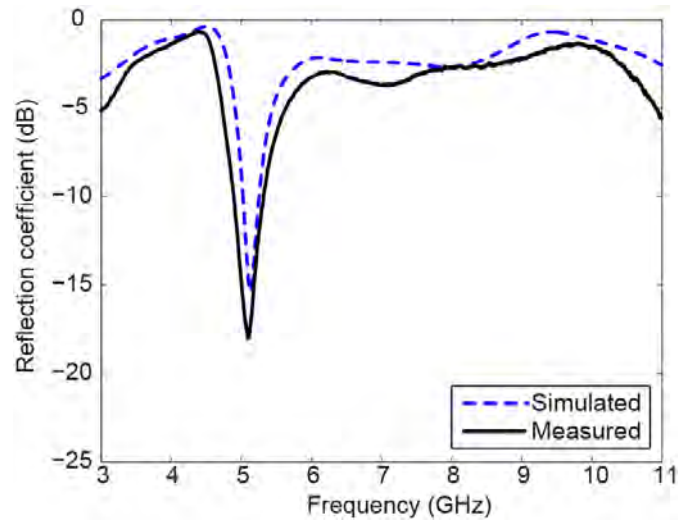


Fig. 4.13 Simulated and measured reflection coefficient of the narrowband PIFA shown in Fig. 4.11.

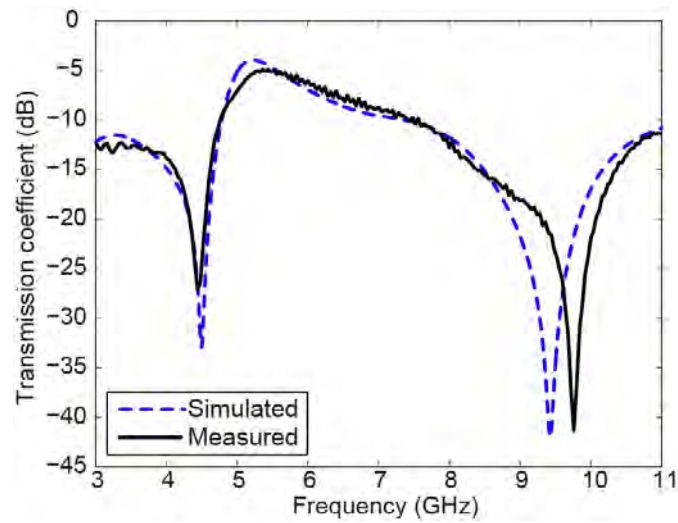


Fig. 4.14 Simulated and measured transmission coefficient of the integrated hour glass monopole and PIFA shown in Fig. 4.11.

The co-polar component of the antenna radiation patterns at the frequencies close to the resonances has been measured inside an anechoic chamber. The measured and simulated radiation patterns at 4.4 GHz and 10GHz are plotted in Fig. 4.15 and Fig. 4.16, respectively. In general the printed symmetrical UWB antennas have an omni-directional radiation pattern in  $xy$ -plane. However, at 4.4 GHz in the  $xy$ -plane an asymmetry with respect to  $x$  axis is noticeable. There is lower level of radiation in the direction of  $\phi = -90^\circ$  in comparison with  $\phi = +90^\circ$ . By referring to the geometry of the antenna in Fig. 4.9, it can be seen that the narrowband antenna is positioned in the direction which affects the radiation pattern. The difference between the simulated and measured result in that region might be due to perturbing effect of the narrowband connector and matched load which are close to the wideband antenna ground plane. In the  $zy$ -plane the pattern shows its monopole characteristics by a significant front lobe comparing to a back lobe. The asymmetry discussion is also valid in this plane.

Unlike the radiation pattern at low frequency, at 10 GHz the radiation pattern in the  $xy$ -plane is symmetrical and agrees well with the simulation. Comparing to the 4.4GHz patterns, the difference is due to the different operating principle of the printed UWB antennas across the operating band. At lower frequencies the antenna operates in the resonant mode, therefore, by placing the narrowband antenna along the resonance length, the original current distribution in that region, and as a result the UWB antenna performance, is significantly affected. However, at higher frequencies, the slot mode happens before it reaches the narrowband antenna. The current distribution will be studied later in this chapter. In the  $zy$ -plane multiple dips have appeared in the front lobe and the back lobe has split into minor lobes.

The simulated radiation patterns of the narrowband antenna at its resonance frequency, 5.15 GHz, are shown in Fig. 4.17. In the  $xy$ -plane, unsurprisingly, the main lobes are towards  $\phi = -90^\circ$  where the narrowband antenna is located. In  $zx$ -plane, with less than 10dB variation in all directions, the  $E_\theta$  component is fairly omni-directional. The  $E_\phi$

component has slightly rotated doughnut shape. In general the measured results convincingly agree with the simulated results.

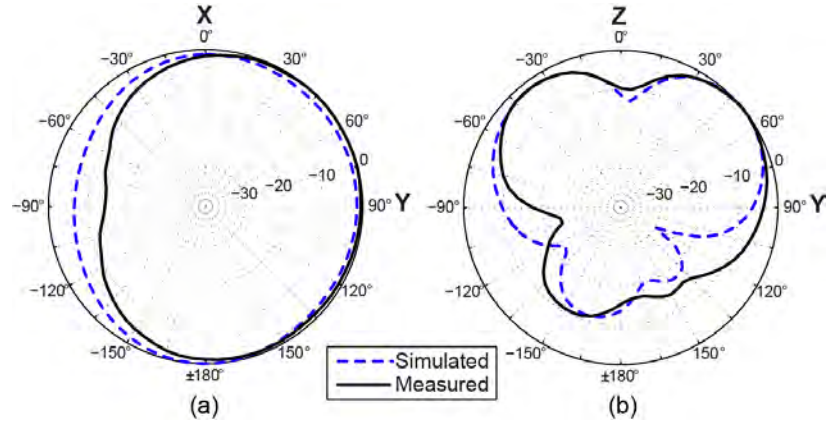


Fig. 4.15 Simulated and measured radiation pattern of the wideband antenna shown in Fig. 4.11 at 4.4 GHz. (a)  $xy$ -plane, (b)  $zy$ -plane.

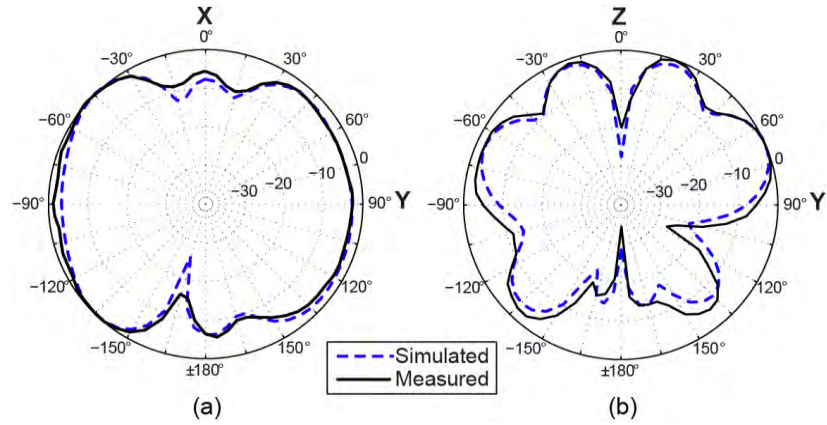


Fig. 4.16 Simulated and measured radiation pattern of the wideband antenna shown in Fig. 4.11 at 10 GHz. (a)  $xy$ -plane, (b)  $zy$ -plane.

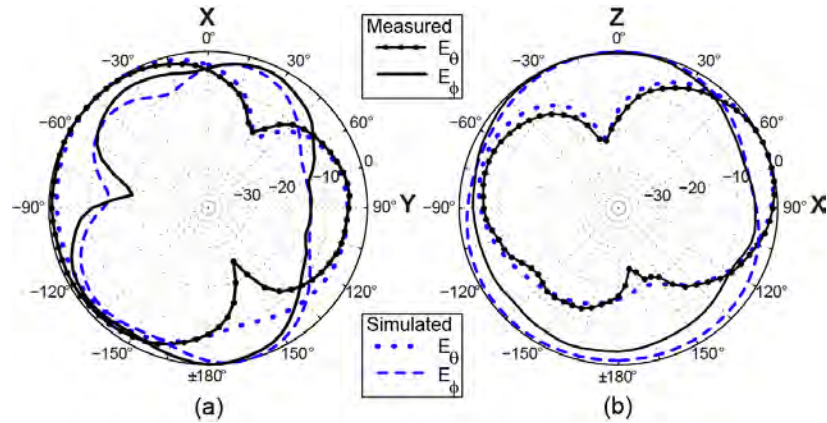


Fig. 4.17 Simulated and measured radiation patterns of the narrowband antenna shown in Fig. 4.11 at 5.15GHz (a)  $xy$ -plane, (b)  $zx$ -plane.

The corresponding impedance behaviour of the wideband and narrowband antennas are demonstrated in Fig. 4.18 and Fig. 4.19, respectively. Resonances occur when the input reactance is close to  $0\Omega$  and the input resistance is close to  $50\Omega$ . In Fig. 4.18, the first resonance happens at around 4.3GHz, the second at around 5.5GHz and the third around 9.5GHz. This agrees well with the reflection coefficient curve in Fig. 4.12. The narrowband antenna is designed for operation at 5.15GHz (Fig. 4.13). As shown in Fig. 4.19, the input reactance at 5.15GHz is close to  $0\Omega$  and input resistance is close to  $50\Omega$ . Another reactance zero crossing occurs at 7.8GHz, however since the resistance peaks to  $330\Omega$  no resonance is excited at 7.8GHz.

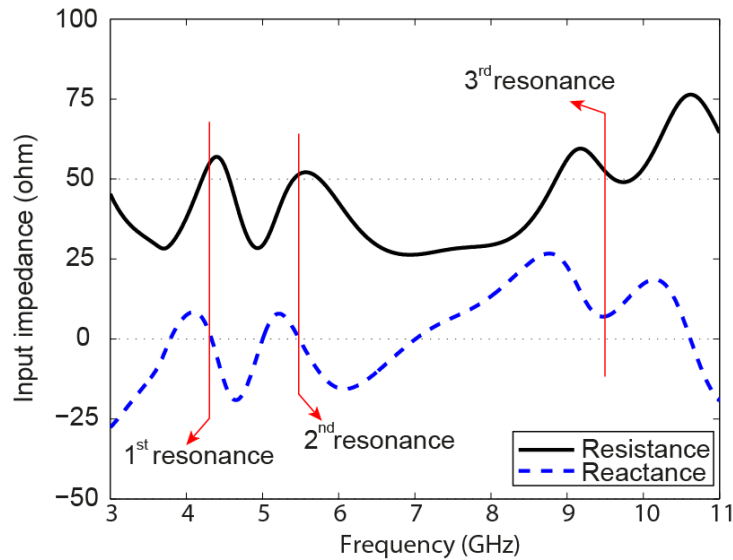


Fig. 4.18 Simulated input impedance of the wideband antenna shown in Fig. 4.11.

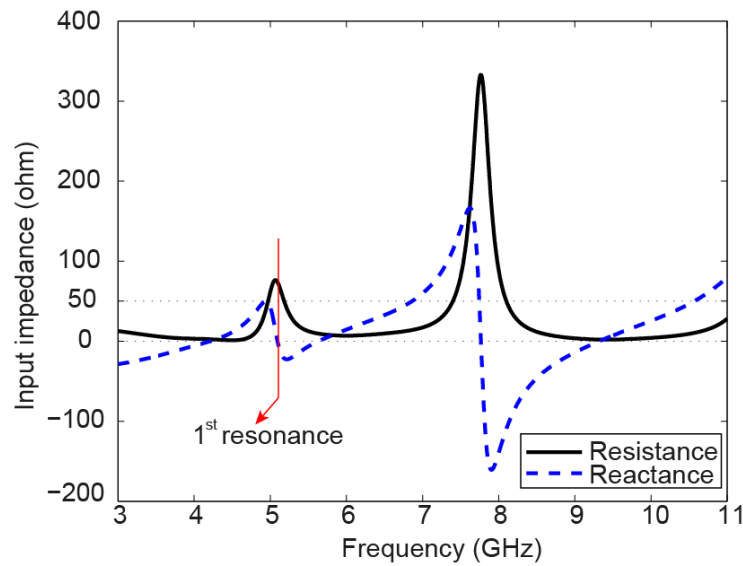


Fig. 4.19 Simulated input impedance of the narrowband antenna shown in Fig. 4.11.

In order to explore the EM behaviour of the antenna, the current distributions on the antenna at different frequencies are shown in Fig. 4.20 and Fig. 4.21. Fig. 4.20 shows the current distribution on both sides of the whole structure when the UWB antenna is excited and the narrowband antenna is terminated to a  $50\Omega$  load. Fig. 4.20a shows the current pattern near the first resonance of UWB antenna at 4.4GHz. Currents are more concentrated on the edge of radiator and ground plane. Hence, a significant amount of power couples to the narrowband antenna. The strong current distributions on the ground plane support the argument that the ground plane contributes to the impedance matching of this structure. The asymmetrical current distribution on the UWB antenna is due to the presence of narrowband antenna.

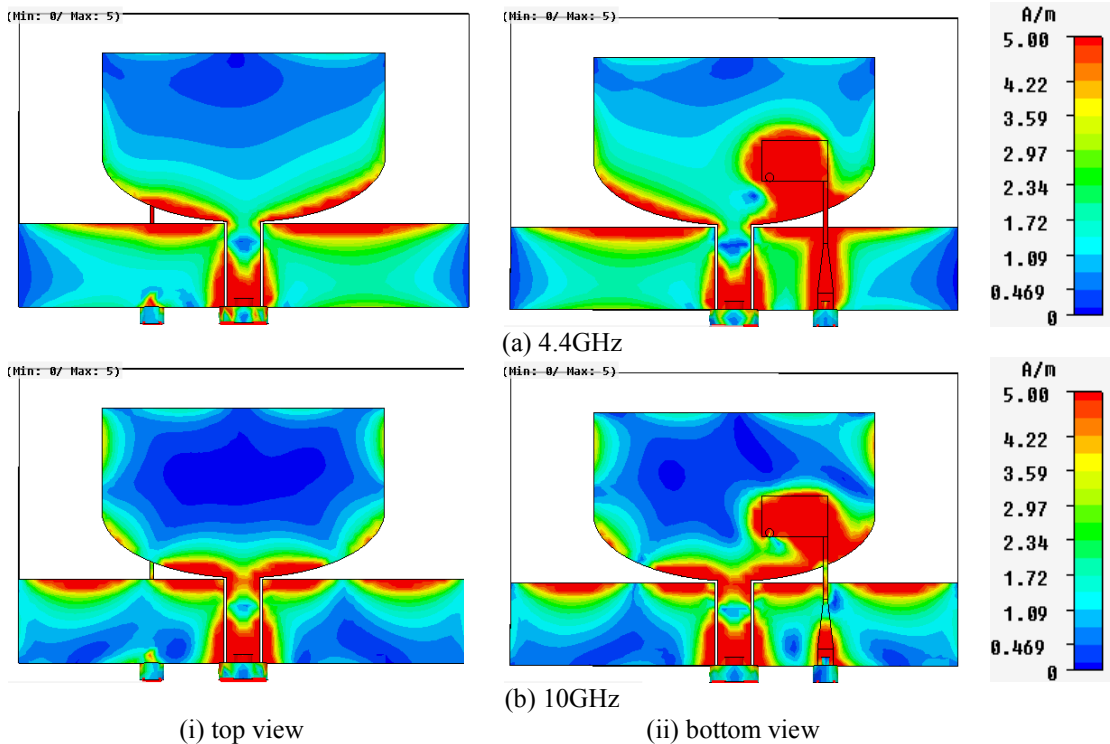


Fig. 4.20 Current distributions when the wideband antenna is excited and the narrowband antenna is terminated to a  $50\Omega$  load.(a) 4.4GHz, (b) 10GHz.

Fig. 4.20b illustrates a more complicated current pattern at 10GHz. As discussed previously, at high frequencies antenna radiates in travelling wave mode and the slot region close to the feeding gap supports travelling waves, therefore the narrowband antenna, which is further away, does not disturb the wideband patterns at 10GHz and the current distribution stays symmetrical.

Fig. 4.21 shows the current distributions on the structure when the narrowband antenna is excited and the UWB antenna is terminated to a  $50\Omega$  load. Since the narrowband antenna is fed in this case, the currents are highly concentrated around it. At the narrowband antenna resonant frequency, 5.15GHz, high concentration of currents can also be observed on the edge of the UWB radiator and ground plane. However, at 10GHz the currents on the edge of UWB antenna is comparably lower. This observation agrees well with the transmission coefficient curve shown in Fig. 4.14, that peaks at 5.15GHz and drops at around 10GHz.

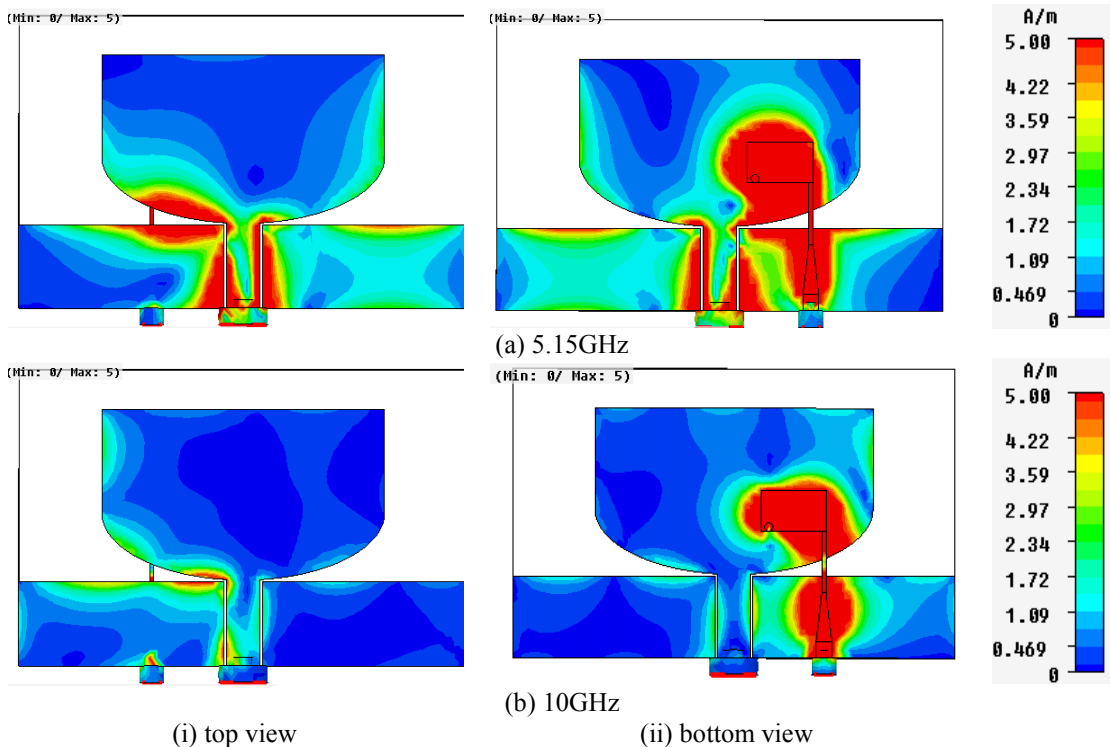


Fig. 4.21 Current distributions when the narrowband antenna is excited and the wideband antenna is terminated to a  $50\Omega$  load.(a) 4.4GHz, (b) 10GHz.

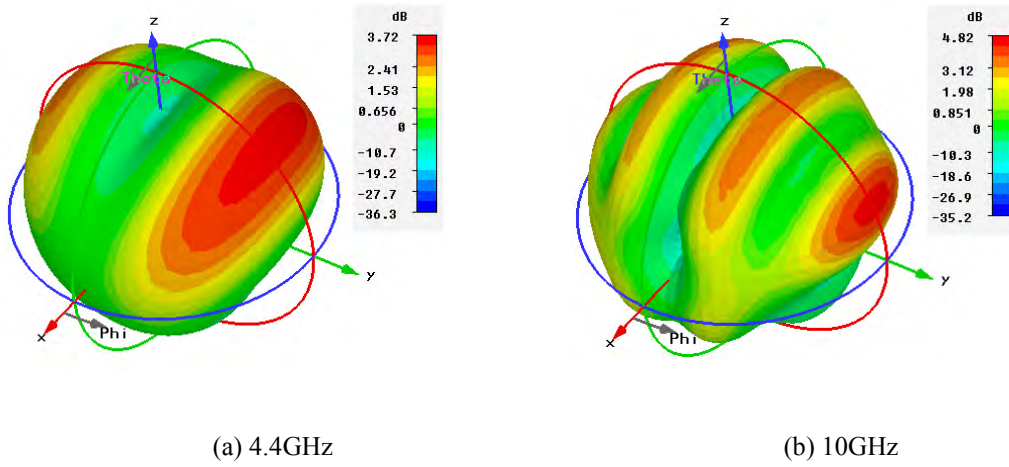


Fig. 4.22 Simulated 3D radiation pattern of wideband antenna shown in Fig. 4.11. (a) 4.4GHz, (b) 10GHz.

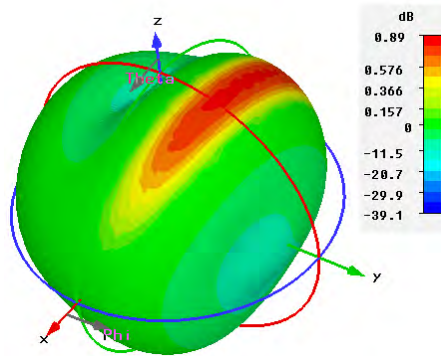


Fig. 4.23 Simulated 3D radiation pattern of narrowband antenna shown in Fig. 4.11 at 5.15GHz.

The simulated 3D radiation patterns of the wideband and narrowband antenna are shown in Fig. 4.22 and Fig. 4.23, respectively. They complement the 2D radiation patterns depicted in Fig. 4.15-Fig. 4.17 by including the contribution of both orthogonal components of the radiation pattern.

## 4.4 Parametric Analysis

In order to gain better understanding of the operating principle of this design, a parametric study has been carried out. The parameters influencing the performance of antenna could be classified into following three groups:



1. parameters that influence the wideband operation. Depending on the structure's shape and feeding mechanism various parameters could be involved. However in general, dimensions of the radiator, the ground plane and the feed gap determine the impedance bandwidth.
2. parameters that influence the narrowband antenna performance. Specifically in this design, the patch dimensions, orientation, position of the shorting pin and the feeding mechanism are critical.
3. integration parameters, e.g. the relative positions of the patch and the feeding structure.

Classifying the parameters into three groups does not imply that the effect of each group is independent. In this section the effect of two fundamental parameters from each group on the antenna impedance matching will be studied and discussed. In order to lower the computational requirements, in this section the 50Ω SMA connector is not included in the simulated model. Through this analysis, the contribution of one parameter at a time is studied while other parameters are set to their suboptimal values showed in Fig. 4.11.

#### **4.4.1 Wideband Antenna Parameters**

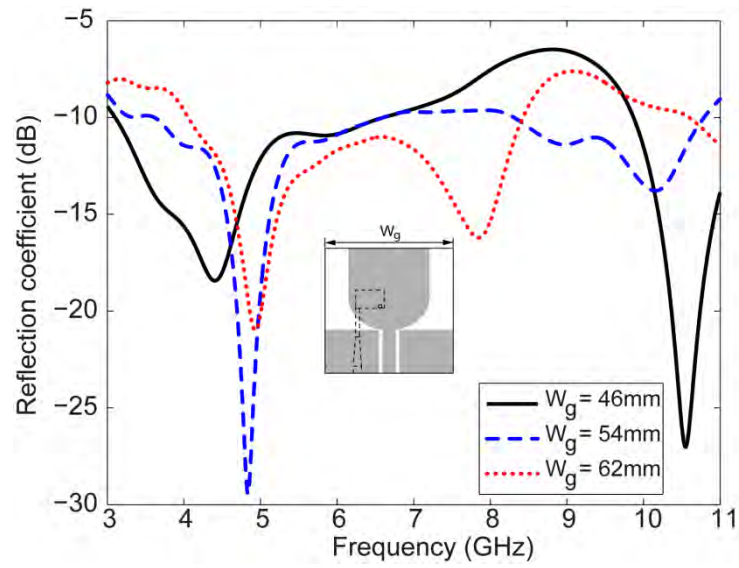
##### **4.4.1.1 Ground Plane Width ( $W_g$ )**

The simulated reflection coefficients curves for different  $W_g$  are presented in Fig. 4.24. Fig. 4.24a and Fig. 4.24b show the reflection coefficient variation for UWB and narrowband antenna, respectively, when  $W_g$  is varied from 46mm to 62mm while other parameters are fixed. It is evident from Fig. 4.24a that both ends of the band are considerably affected by changing the ground width, while the band ranging from 4GHz to 7GHz stay less than -10dB for all values of  $W_g$ . While the first resonance is not significantly affected by the width of the ground plane the second resonance is shifted along the band. Considering that the optimal width of the ground plane is 54mm, it is important to note that the -10dB bandwidth has reduced for both narrower and wider ground plane. This observation implies that the

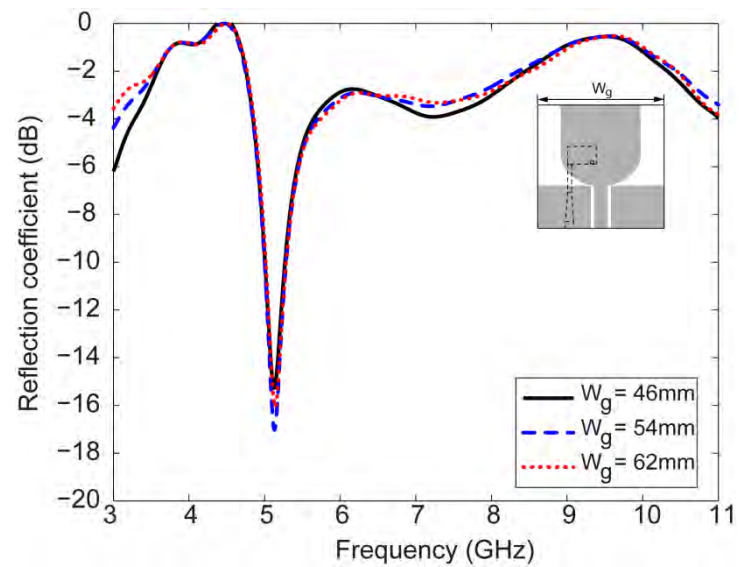


ground plane is considered as part of the antenna and contributes to the radiation. As shown in Fig. 4.20 the currents flow along the edge of the ground plane, hence changing the width of the ground plane changes the length of the current path.

Fig. 4.24b demonstrates that the narrowband antenna reflection coefficient is independent from the width of the ground plane. This is understandable since the wideband antenna ground plane is used as the ground plane for narrowband antenna microstrip feeding and therefore variation of ground plane width does not change the narrowband feeding impedance or the current distribution.



(a)



(b)

Fig. 4.24 Simulated reflection coefficient curves for different  $W_g$  (a) wideband antenna, (b) narrowband antenna.

#### **4.4.1.1 Ground Plane Length ( $L_g$ )**

The reflection coefficient curves for different  $L_g$  for wideband and narrowband antennas are shown in Fig. 4.25a and Fig. 4.25b, respectively. It is observed that increasing the length of the ground plane improves the return loss at lower frequencies and reduces the lower cut-off frequency. Increasing the ground length results in an increment in the number of closely distributed resonances across the band. As previously discussed in the section on the ground plane width, this phenomenon also confirms that the ground plane is part of the antenna. Variation in the size of ground plane changes the current path and therefore antenna matching.

For the narrowband antenna, the curves are shown in Fig. 4.25b. Increasing the length of the ground does not affect the main resonance. However, when  $L_g=40\text{mm}$  a second resonance also appears close to the first resonance.

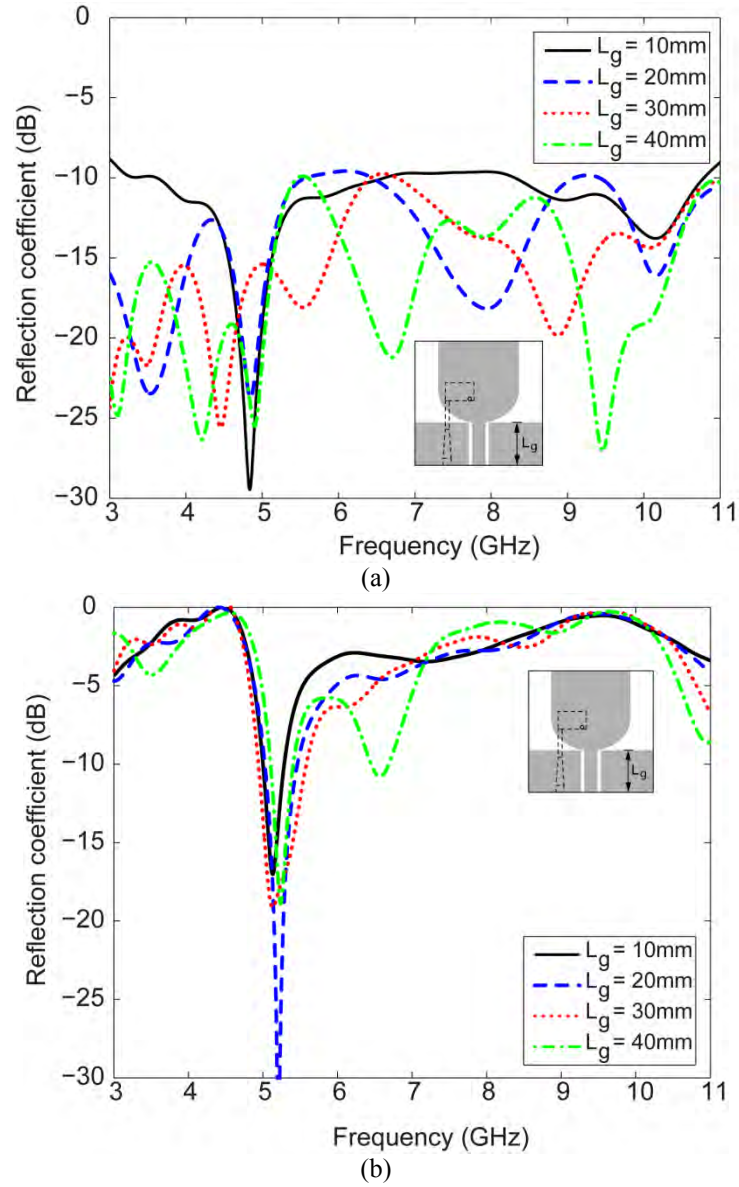


Fig. 4.25 Simulated reflection coefficient curves for different  $L_g$  (a) wideband antenna, (b) narrowband antenna.

## 4.4.2 Narrowband Antenna Parameters

### 4.4.2.1 Patch Length ( $L_p$ )

The patch dimensions determine the resonance frequency of the narrowband antenna. In this structure the length of the patch is a quarter of a wavelength at 5.15GHz. However, to design it for other frequencies, other parameters must also be optimised. It is important to

note that the position of the shorting pin on the patch also has to be tuned to achieve enough matching at the desired resonant frequency.

Fig. 4.26 shows the reflection coefficient curves for different values of patch length while the shorting pin position was fixed at the corner of the patch. As expected the narrowband resonance can be tuned by the length of the patch. However, surprisingly, the first resonance of the wideband antenna also follows the same trend, i.e. it shifts towards lower frequency when the patch becomes longer. The strong coupling between the narrowband and wideband antenna might cause this phenomenon. The coupling between the wideband and narrowband antenna changes the resonant current path around the narrowband antenna region and therefore affects the wideband matching and resonance.

#### **4.4.2.2 Patch Width ( $W_p$ )**

As previously pointed out in equation (4.1), both dimensions of the patch ( $L_p$  and  $W_p$ ) contribute in tuning the operating frequency. The impedance matching variation caused by increasing the width of the patch is shown Fig. 4.27. In addition to lowering the main resonance frequency, increasing the patch width shifts the out of band higher resonances towards lower frequencies for both antennas. As observed in Fig. 4.27b the frequency shifts in second resonances are higher than for first resonances. At  $W_p=7\text{mm}$  the first resonance is at 4.2GHz and the second at 10.9GHz, whereas at  $W_p=11\text{mm}$ , the first resonance shifts down to 3.2GHz and the second to 8.5GHz.

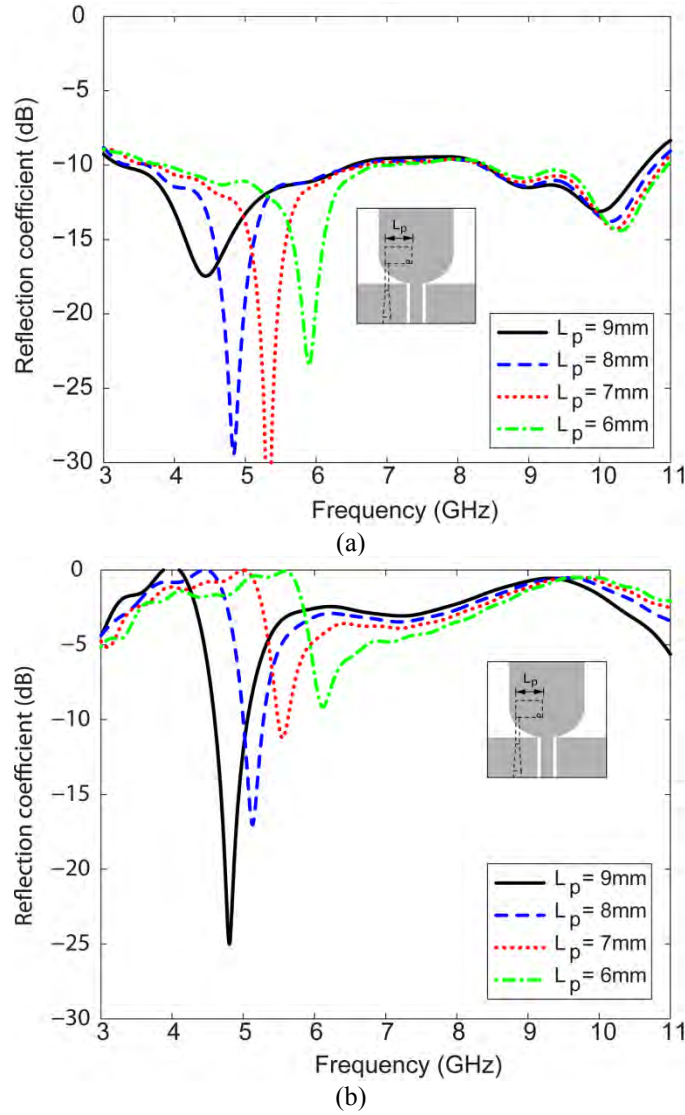


Fig. 4.26 Simulated reflection coefficient curves for different  $L_p$  (a) wideband antenna, (b) narrowband antenna.

### 4.4.3 Integration Parameters

#### 4.4.3.1 Narrowband Antenna Lateral Position ( $d$ )

Fig. 4.28 shows the reflection coefficient variations while the narrowband antenna is placed at different positions relative to the centre of the board. Fig. 4.28a shows that the closer the narrowband antenna is to the centre, the better is the wideband antenna matching in the mid band frequency range, i.e. 5-8GHz. This observation implies that less field coupling occurs when the narrowband feeding is above the narrower section of the wideband slot. Meanwhile, an increase in the value of  $d$  reduces the resonant frequency and -10dB impedance bandwidth of the narrowband antenna (see Fig. 4.28b).

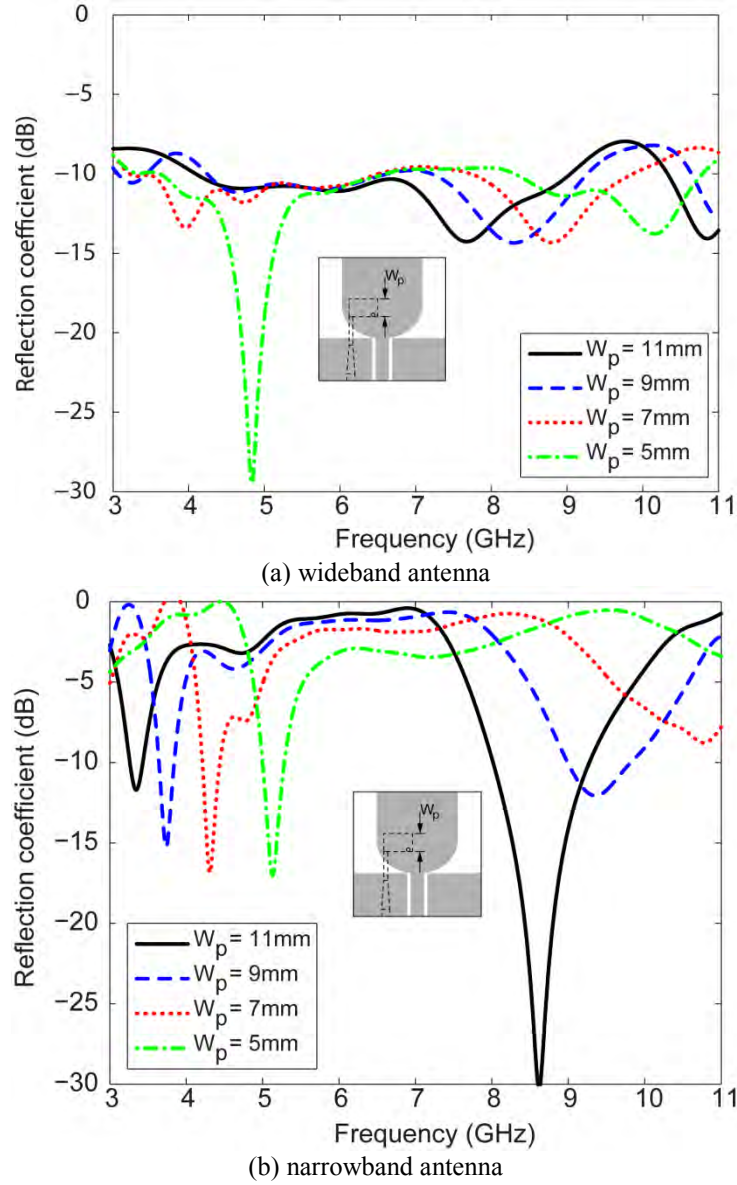


Fig. 4.27 Simulated reflection coefficient curves for different  $W_p$ .

It is important to note that the narrowband antenna feed line runs above the slot formed by the edge of the wideband antenna and its ground plane. Due to its tapered shape the impedance of the slot line varies along its length. Therefore, moving the feed line and thereby placing it above different slot line sections implies that various impedances might be seen from the narrowband antenna port.

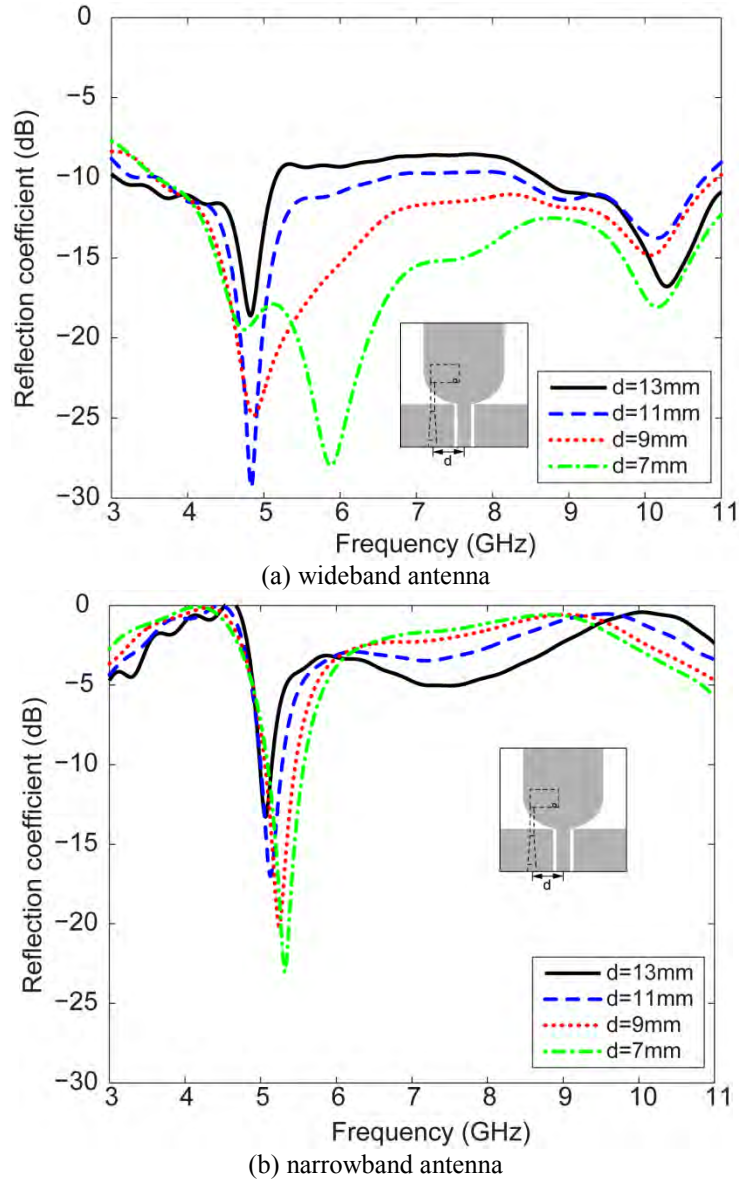
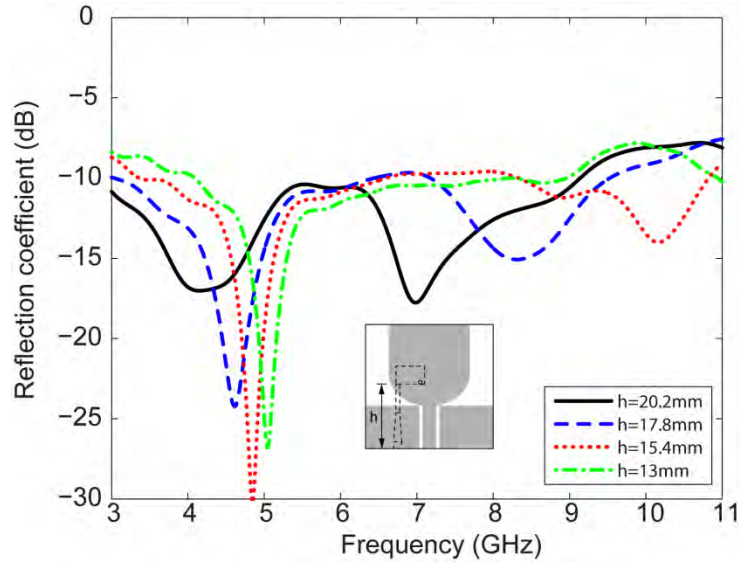


Fig. 4.28 Simulated reflection coefficient curves for different  $d$ .

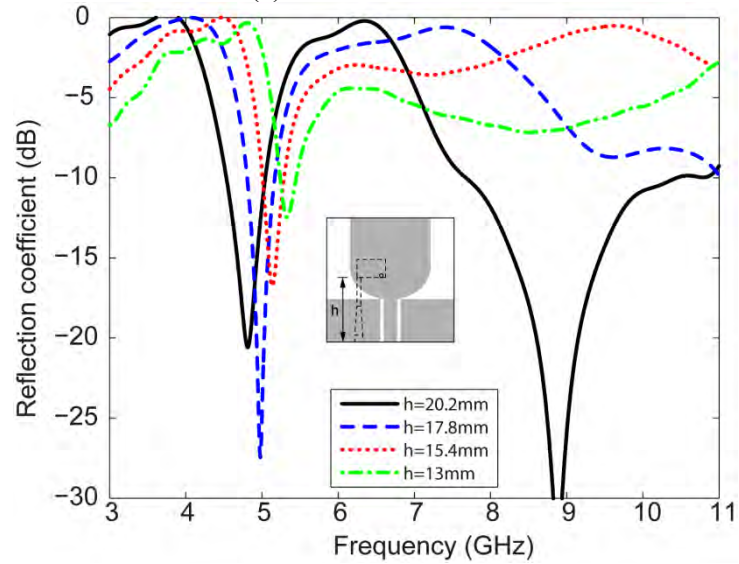
#### 4.4.3.2 Narrowband Antenna Vertical Position ( $h$ )

As previously pointed out, since the current varies across the wideband radiator edge, the performance of the narrowband antenna is influenced by its position relative to the wideband antenna. Fig. 4.29 shows the simulated return loss of the antenna for different vertical positions of the patch. Fig. 4.29a shows that increasing the length of the narrowband antenna feeding ( $h$ ) improves the matching at lower frequencies.





(a) wideband antenna



(b) narrowband antenna

Fig. 4.29 Simulated reflection coefficient curves for different  $h$  (a) wideband antenna, (b) narrowband antenna.

However, it has a reverse effect on the higher end of the frequency band ranging from 9GHz to 11GHz. Increasing the narrowband antenna height relative to the edge of the board introduces considerable variation in the return loss of the patch antenna at the frequency range of 6GHz to 11GHz, depicted in Fig. 4.29b. Increasing the length of the feeding from 13mm to 20.2 mm decreases the expected resonance frequency from 5.5GHz to 4.8GHz. In the frequency range of 6-11GHz it changes dramatically with no clear pattern, such that at  $h = 20.2\text{mm}$  a second resonance appears at approximately 9GHz. Increasing the feeding length changes its impedance; however this does not



follow a clear pattern which might be due to the effect of the feed crossing the gap between the monopole and its ground plane.

## 4.5 Discussion

The design of an integrated wideband-narrowband antenna was explored in this chapter. However, this arrangement is only a demonstrator for the proposed integration concept and numerous antenna structures can be designed using this method. Depending on the application and the space provided plenty of combinations can be designed. Several designs were published on the base of this integration concept. For instance, a similar wideband-narrowband combination is achieved in [7] by replacing the PIFA with a slot antenna as shown in Fig. 4.30. A microstrip resonator is also employed in order to produce a notch band at 5.2 GHz in the UWB frequency response. In [8], a circular disc radiator is shared between two modes of operation: one wideband mode achieved by CPW feeding and one narrowband mode with microstrip feeding from the opposite side as shown in Fig. 4.31.

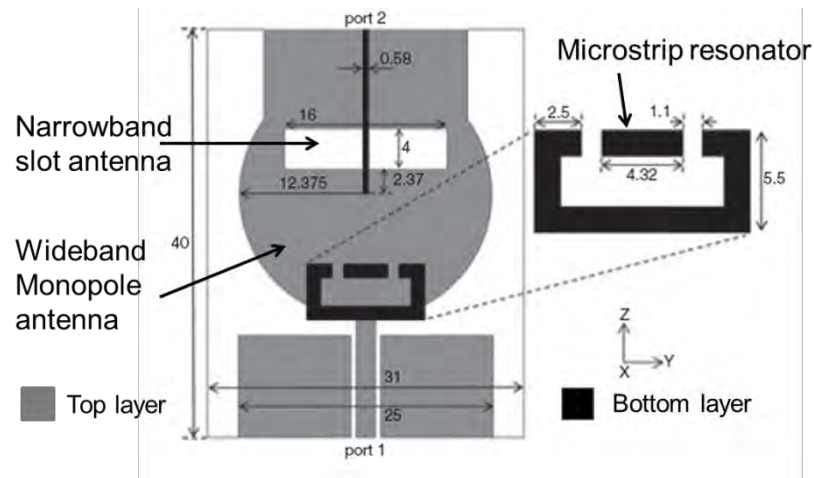


Fig. 4.30 Integrated slot antenna and monopole [7].

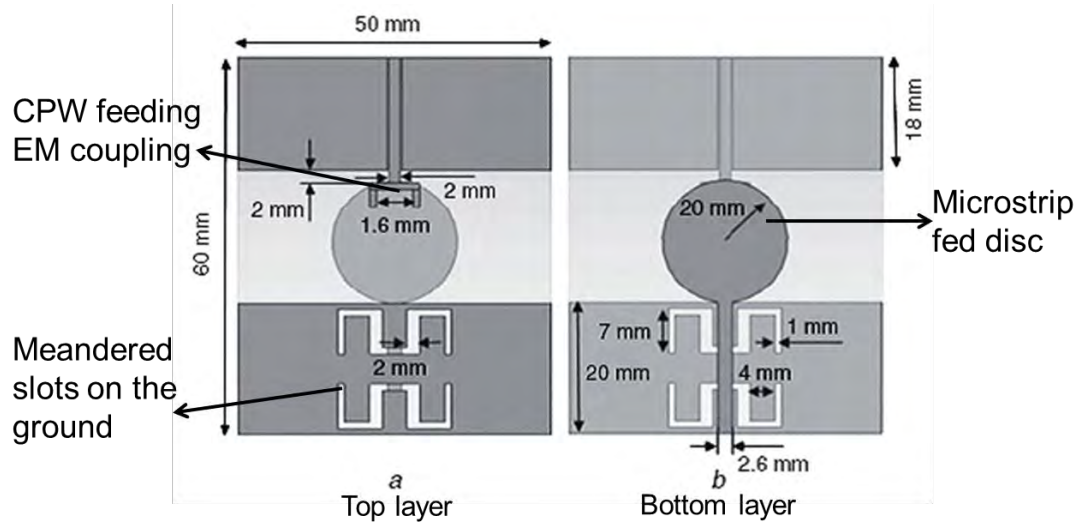


Fig. 4.31 Two port monopole antenna [8].

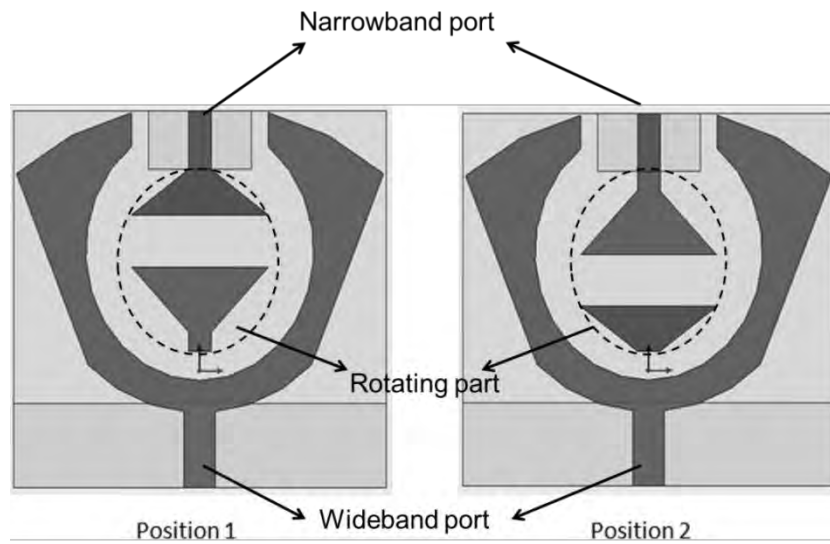


Fig. 4.32 Two port wideband and rotating narrowband antenna [9].

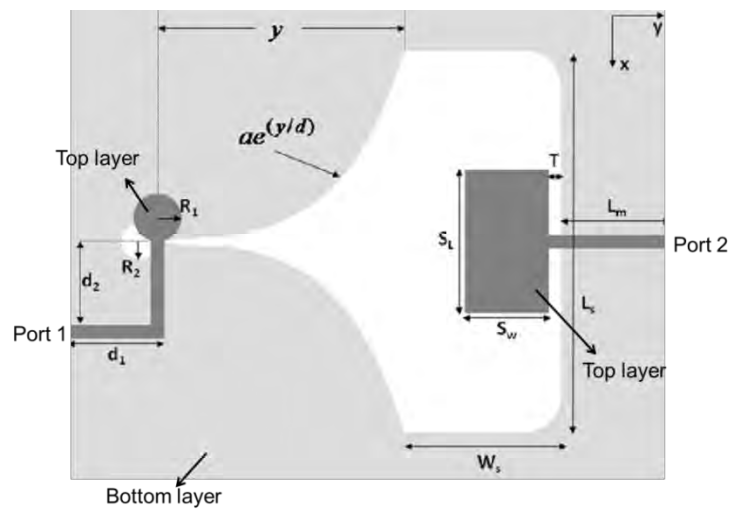


Fig. 4.33 Two port UWB MIMO antenna [10].

This integration technique enables adding extra features to the antenna. For instance in [9] two modes of narrowband functionality is achieved by rotating the narrowband antenna which is integrated in the centre of a wideband monopole. The configuration is shown in Fig. 4.32.

This integration technique is not limited to wideband-narrowband operation. Other combinations such as two wideband antennas or a wideband and a multiband antenna may also be possible. Moreover, the number of antennas is not restricted to two antennas. Multiple antennas can be integrated into the main antenna. For instance, two similar narrowband antennas for MIMO diversity can be integrated into a wideband antenna.

In addition to various bandwidth scenarios, antennas with different polarization can also be integrated together. This could be useful for polarization diversity techniques [10]. Two orthogonal modes are achieved by integrating a Vivaldi and a wide slot antenna as shown in Fig. 4.33.

The additional antennas can be integrated into the main antenna in various forms. In order to avoid high interaction between the antennas, the additional antennas should not disrupt each other's original radiation. In practice the ground plane is saved for RF front end, therefore, it is better not to place the additional antennas on the ground plane. Several modified configurations of the proposed integrated wideband-narrowband antenna will be presented in the next chapter. Improving the port isolation is the main goal in these modifications.

The wideband-narrowband combination could be of value in other scenarios as well. It is well known that a very reliable technique for outdoor positioning is GPS however it is not appropriate for indoor positioning. The UWB technology however, is capable of indoor tracking with acceptable accuracy. Therefore, the UWB-GPS combination enables the sought after continuous tracking for indoor and outdoor.

Covering a wide range of frequencies with quasi-omnidirectional radiation pattern the UWB antenna is a good candidate for RF energy harvesting. This would be a back-up approach for emergency cases when individual battery servicing becomes impractical.

## 4.6 Summary

An integration concept for multi-standard radios was proposed in this chapter. The method is based on sharing some parts of one antenna between additional antennas. An integrated wideband-narrowband antenna was presented as a demonstrator for this concept. The system consists of a wideband monopole and a narrowband shorted patch. The patch is printed above the main radiator of the wideband antenna on the reverse side of the substrate and fed by a microstrip line. A prototype of the demonstrator was manufactured and examined. A parametric study was carried out to provide design guidelines. The recent publications based on this technique are also reviewed.

## References

- [1] C. J. Liang, C.C. Chiau, X. Chen and C. G. Parini, "Study of a printed circular disc monopole antenna for UWB systems," *IEEE Trans. Antennas Propag.*, vol. 53, pp. 3500–3504, Nov. 2005.
- [2] J. Liang, L. Guo, C.C. Chiau, X. Chen and C.G. Parini, "Study of CPW-fed circular disc monopole antenna for ultra wideband applications," in *Proc. IEE Microw. Antennas Propag.*, vol. 152, pp.520-526, Dec. 2005.
- [3] S. W. Su, J.H. Chou and K. L. Wong, "Internal ultra wideband monopole antenna for wireless USB dongle applications," *IEEE Trans. Antennas Propag.*, vol. 55, no. 4, pp. 1180–1183, Apr. 2007.
- [4] K. Bahadori and Y. R. Samii, "A miniaturized elliptic-card UWB antenna with WLAN band rejection for wireless communications," *IEEE Trans. Antennas Propag.*, vol. 55, no. 11, pp. 3326–3332, Nov. 2007.
- [5] J. W. Greiser, "Coplanar stripline antenna," *Microwave J.*, vol. 19, no. 10, pp. 47-49, Oct. 1976.
- [6] R. N. Simons, "Coplanar Waveguide Circuits, Components, and Systems," John Wiley & Sons, 2001.

- [7] J.R. Kelly, P.S. Hall, P. Gardner, F. Ghanem, "Integrated narrow/band-notched UWB," *Electron. Lett.*, vol. 46, no. 12, pp. 814 - 816, 2010.
- [8] F. Ghanem, P.S. Hall, J.R. Kelly, "Two port frequency reconfigurable antenna for cognitive radios," *Electron. Lett.*, vol. 45, no. 11, pp. 534 - 536, 2009.
- [9] Y. Tawk, C.G. Christodoulou, "A new reconfigurable antenna design for cognitive radio," *IEEE Ant. Wireless Propag. Lett.*, vol. 8, pp. 1378-1381, 2009.
- [10] Y.-C.Lu and Y.-C. Lin, "A compact dual-polarized UWB antenna with high port isolation," *IEEE International Symposium Antennas Propagation Society (APSURSI)*, pp.1-4, 11-17 July 2010.

## **Chapter 5      Port Isolation**

### **5.1      Introduction**

A hybrid two port wideband-narrowband antenna was presented in the previous chapter. In addition to the conventional antenna parameters, the mutual field coupling between the antenna ports should also be studied in multiport antenna systems. For most systems low port coupling is essential. In Chapter 3 several major techniques for improving the isolation between antenna ports in multiple antenna systems were reviewed. Each decoupling mechanism has its own advantages and limitations which should be considered together with other factors such as antenna topology, manufacturing technology and system requirements prior to start the design process.

In order to enable simultaneous wideband and narrowband functionality in the previously proposed antenna, it is required that the antenna ports are isolated. In this chapter first the coupling phenomenon between the ports will be studied. Consequently several solutions for enhancing the port isolation in this antenna will be introduced.

## 5.2 Field Coupling in the Wideband-Narrowband Antenna

In Chapter 4, it was shown that the transmission coefficient between the ports peaks at the resonance frequency of the narrowband antenna. This phenomenon is caused by the field coupling between the narrowband feeding and wideband antenna. The narrowband feeding is orthogonal to the tapered slot formed by the monopole radiator and the ground plane on the top side of the substrate as it is shown in Fig. 5.1. In fact, this arrangement forms a microstrip to slot line transition. Considering  $S_{21} = \frac{V_2^-}{V_1^+} = -4dB$ , it is possible to calculate that approximately 40% ( $10^{-4/10}$ ) of the power is coupled from one antenna into the other. This analysis can also be confirmed by studying the current distribution on the antenna at the resonance frequency of the narrowband antenna as shown in Fig. 5.2.

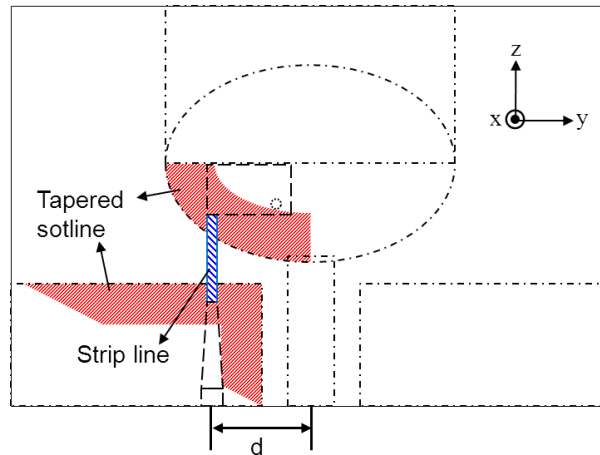


Fig. 5.1 The schematic of the antenna with highlighted microstrip to tapered slot transition.

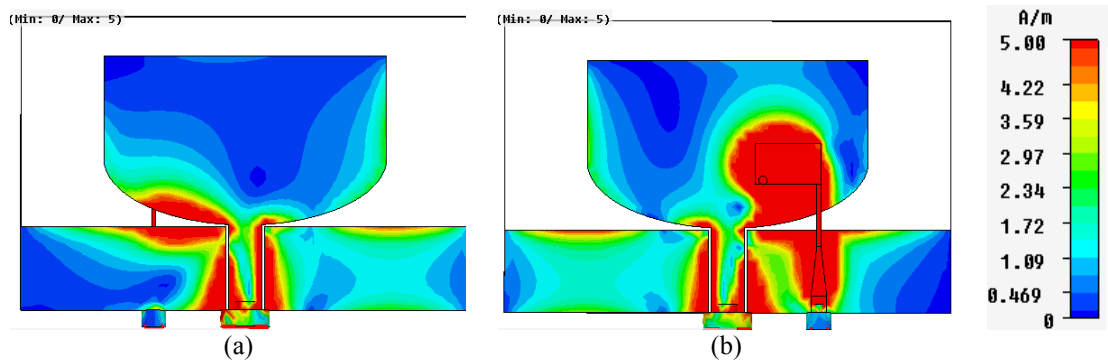


Fig. 5.2 Simulated current distribution at 5.15GHz. (a) top view (b) bottom view.

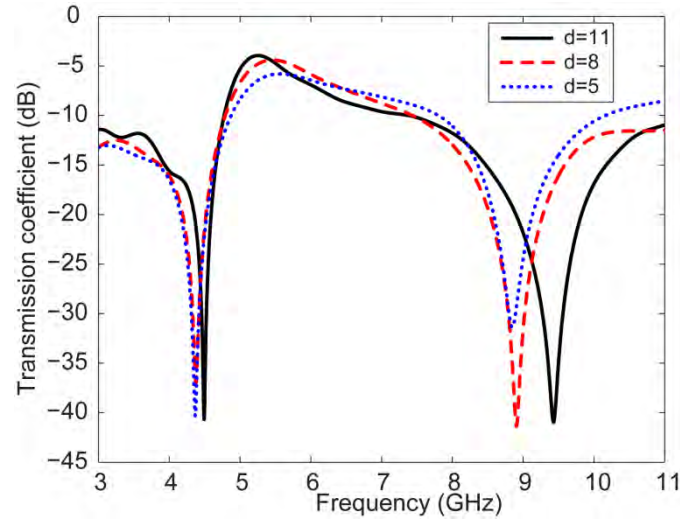


Fig. 5.3 Simulated transmission coefficient curves for different d.

In Fig. 5.2 high concentration of currents can be observed around the antenna feeding. The width of the tapered slot varies along its length and so does its impedance. At the beginning of the slot where the gap is smaller, the impedance is relatively low (approximately  $50\Omega$ ) and it increases when the gap grows (up to about  $200\Omega$ ). Strong field coupling in this region is perhaps a result of impedance matching between the strip and slot line. Considering the complicated field coupling in that region it is difficult to completely quantify this effect. Simulations show that when the narrowband antenna is shifted towards the board centre line the peak transmission coefficient drops a few dBs and therefore the isolation increases (see Fig. 5.3). However, as explained earlier it is not practically possible to place the narrowband antenna very close to the centre of the board where the wideband antenna is fed through.

In the conventional multiple antenna scenarios the antennas normally share a common ground plane which supports the coupled fields. Therefore, by modifying the ground plane it is possible to improve the coupling. However, in the proposed integrated wideband-narrowband antenna the field coupling is directly between the antennas and not a third element. Hence, it is challenging to isolate the ports in this configuration. One approach is to carefully avoid areas with high concentration of currents in the design procedure. This can be achieved by relocating the second antenna. However, it can always be useful to take into account practical considerations. There is less concentration of the surface current on the



ground plane of the wideband antenna which suggests that the second antenna can be placed at that region. However, in a typical mobile phone or a USB dongle, the ground plane is mainly used for mounting the RF front-end and baseband circuitry. Therefore, this area is normally tightly packed with elements and chipsets which make it not only unhelpful but impractical to be used as the ground plane for the additional antenna. In section 5.3 several modifications of the wideband-narrowband antenna with less coupling but based on the same integration concept are introduced.

The other approach to tackle the port isolation problem is to use external circuits or networks. This might add to the size of the antenna system which is not affordable for every application. On the other hand, the advantage of this technique is that it is possible to design the decoupling network independent from the antenna. The design principle of such network will be elaborated in the section 5.4.

### **5.3 Isolation Enhanced Wideband-Narrowband Antenna**

In this section several modified configurations of the antenna with improved transmission coefficient will be introduced. All these configurations are based on avoiding the regions with strong field interactions.

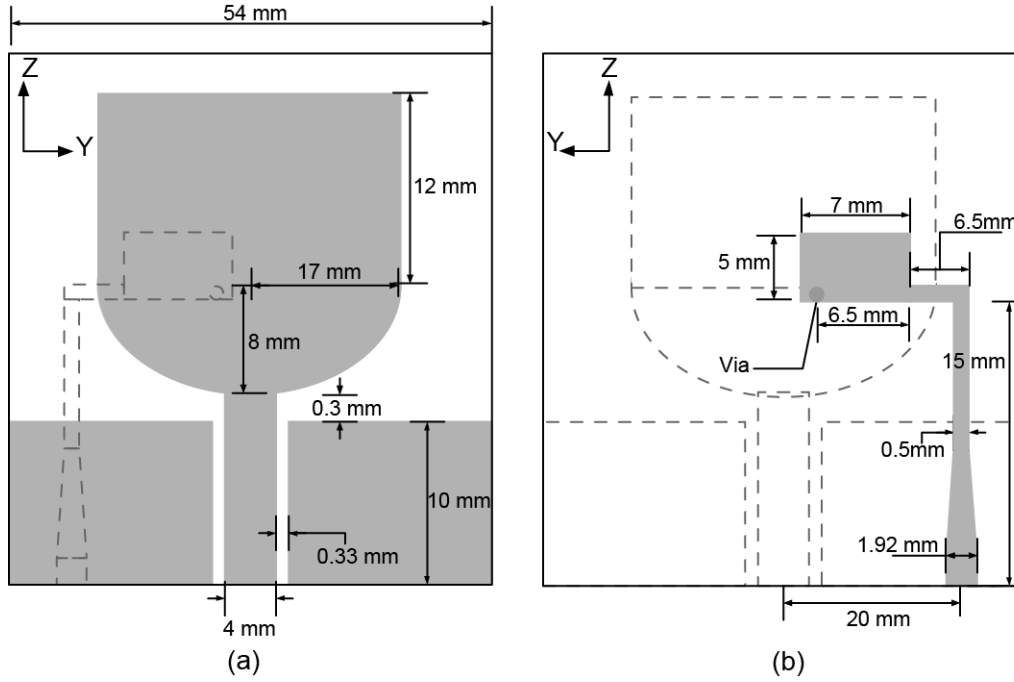


Fig. 5.4 Geometry of configuration A, (a) top view, (b) bottom view.

### 5.3.1 Configuration A

Following the discussion in the previous section, in the first modification the narrowband antenna feeding is shifted away from the wideband tapered slot. Fig. 5.4 demonstrates the geometry of the first configuration (Configuration A). The modification involves shifting the patch feed line away from the tapered slot and bending it at a right angle.

Using this method, the peak value of mutual coupling drops from -4 dB to below -7 dB (see Fig. 5.5a). The reflection coefficients of the wideband and narrowband antenna are shown in Fig. 5.5b and c, respectively.

The reflection coefficient of the wideband port is better than -8dB at the whole UWB band. It is important to note that, considering that the main aim in this section is to demonstrate the coupling reduction, no attempt was made to optimise the wideband reflection coefficient. The narrowband antenna has a resonance at 4.81 GHz and a higher order resonance appears at the top end of the band. The second resonance might not be a problem since it is far enough from the first resonance.

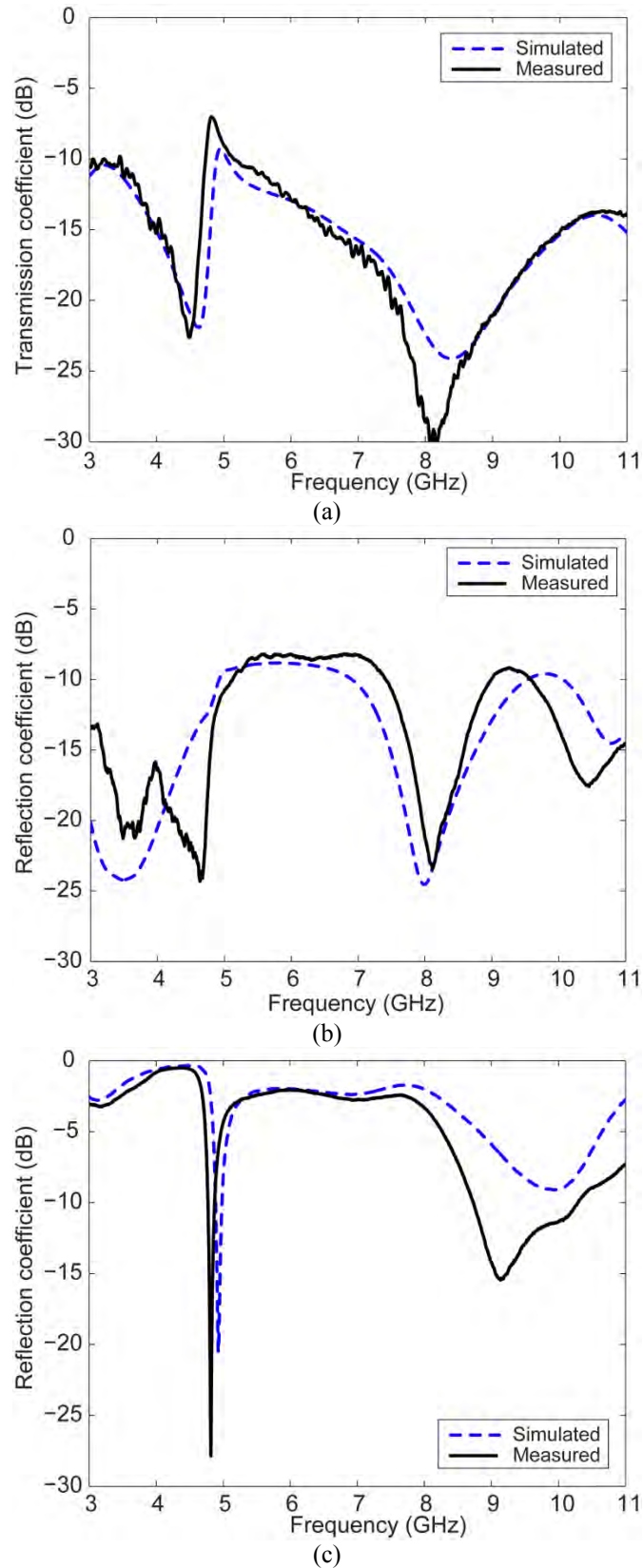


Fig. 5.5 Simulated and measured S parameter of configuration A antenna. (a) Transmission coefficient, (b) wideband antenna reflection coefficient, (c) narrowband antenna reflection coefficient.

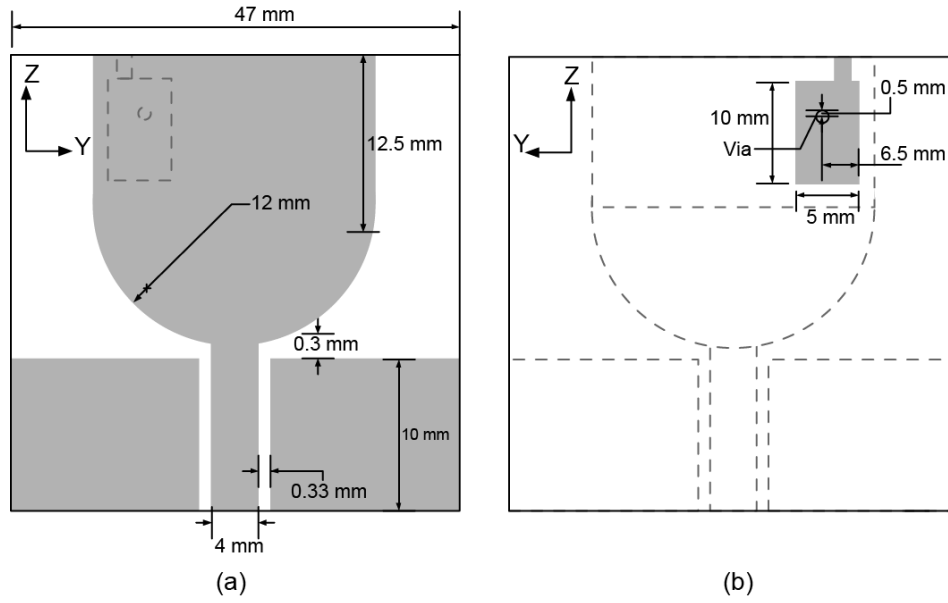


Fig. 5.6 Geometry of configuration B, (a) top view, (b) bottom view.

### 5.3.2 Configuration B

Investigating the current distribution reveals that there are less currents on the upper part of the monopole radiator representing a good location for the second antenna. Fig. 5.6 illustrates the second modified antenna (denoted Configuration B). The monopole radiator is elongated so that it extends to the edge of the board. The narrowband patch is printed on the reverse side of the substrate. The simulated and measured S parameters are demonstrated in Fig. 5.7a. In this configuration, the peak transmission coefficient is  $-18$  dB. It remains below  $-25$  dB throughout the majority of the UWB band. The discrepancy between simulated and measured data might be perhaps due to the tolerances in the manufacturing and manual assembling the shorting pin and connector in the final prototype. The reflection coefficient of the wideband antenna, in this configuration, is well below  $-10$  dB from 3-11 GHz as shown in Fig. 5.7b. The narrowband antenna operates at 5.26 GHz where the reflection coefficient is  $-7.5$  dB (see Fig. 5.7c).

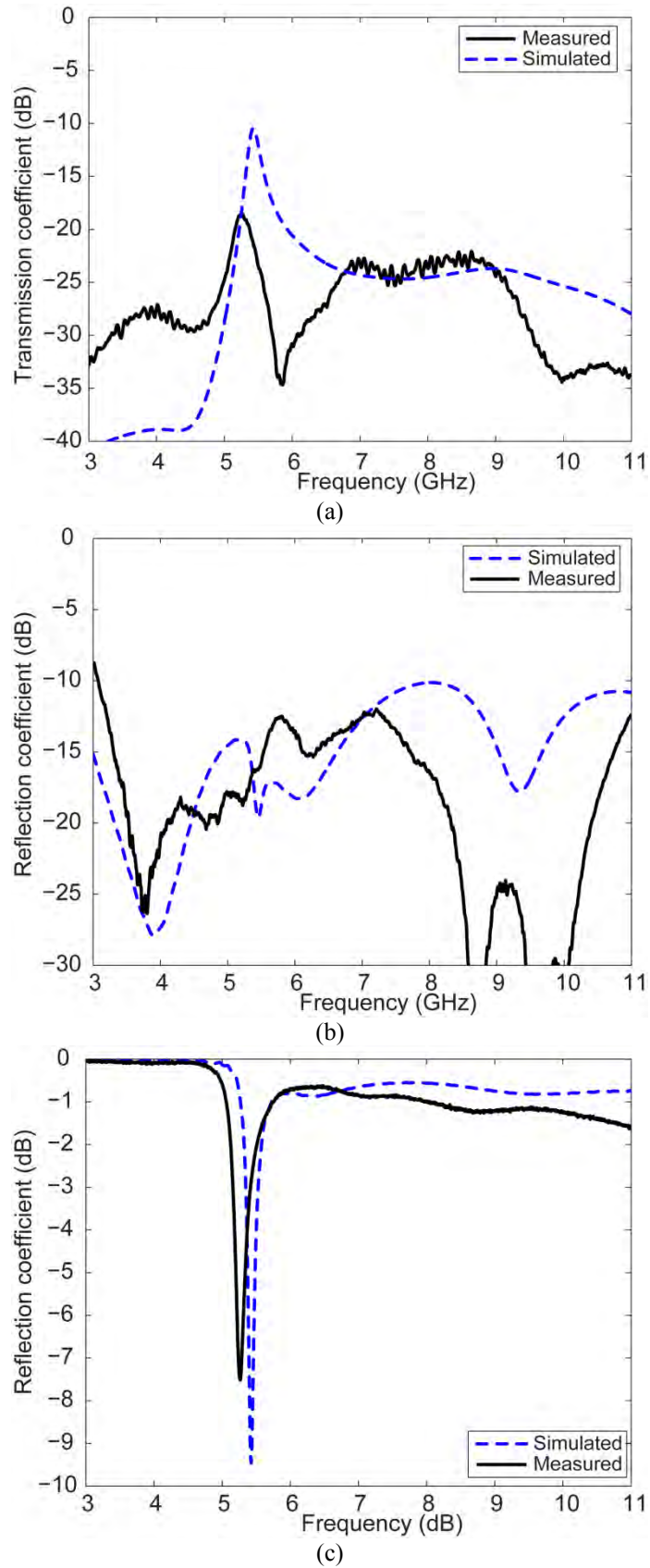


Fig. 5.7 Simulated and measured S parameter of configuration B antenna. (a) Transmission coefficient, (b) wideband antenna reflection coefficient, (c) narrowband antenna reflection coefficient.

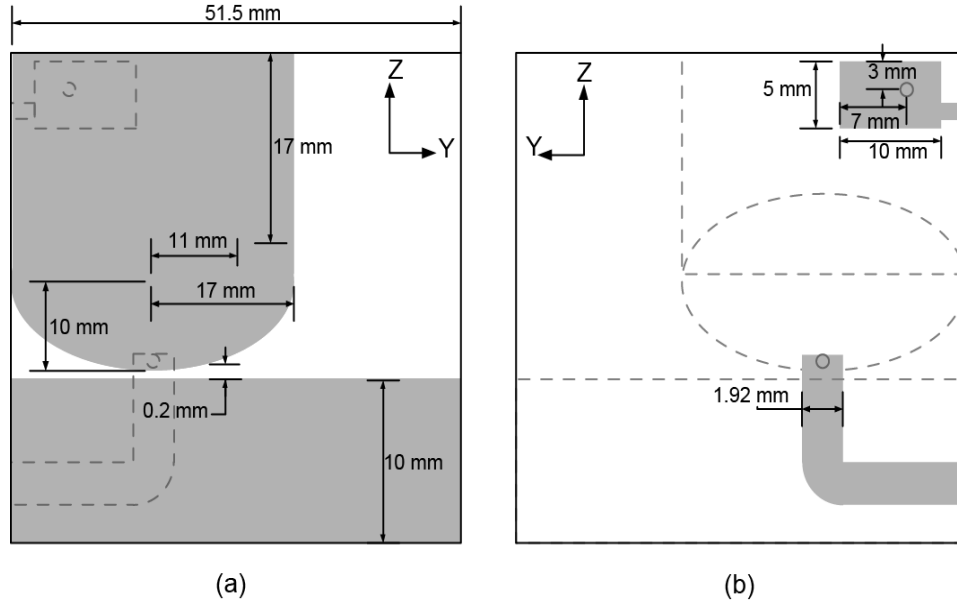


Fig. 5.8 Geometry of configuration C, (a) top view, (b) bottom view.

### 5.3.3 Configuration C

For some applications, it may not be physically affordable for the designer to have ports on opposite sides of the board. Thus in the third arrangement of this structure the goal is to have two ports on the same side, while maintaining a good level of isolation. The geometry of the third antenna (Configuration C) is presented in Fig. 5.8. In this structure the wideband monopole has been shifted along the  $x$ -axis, from the middle of the substrate to one side. The UWB radiator and ground plane are printed onto the upper surface of the substrate. The UWB monopole is fed through a bent section of microstrip line which is printed onto the back of the substrate. The feed line is connected to the monopole radiator through a via hole. The narrowband antenna is located above the rectangular part of the monopole. The simulated and measured S parameters are shown in Fig. 5.9. This configuration provides approximately 18 dB of isolation between the two ports (see Fig. 5.9a). The -10dB impedance bandwidth of the wideband antenna has not been significantly changed. The narrowband antenna operates at 5.4 GHz. The discrepancy between the measured and simulated result might be due to human errors in manufacturing the printed antenna and assembling the connectors and shorting vias .

It is expected that the antenna radiation patterns will be affected due the integration arrangement. However, in the target applications i.e. portable wireless devices due to rich multipath fading the radiation pattern are not of such importance.

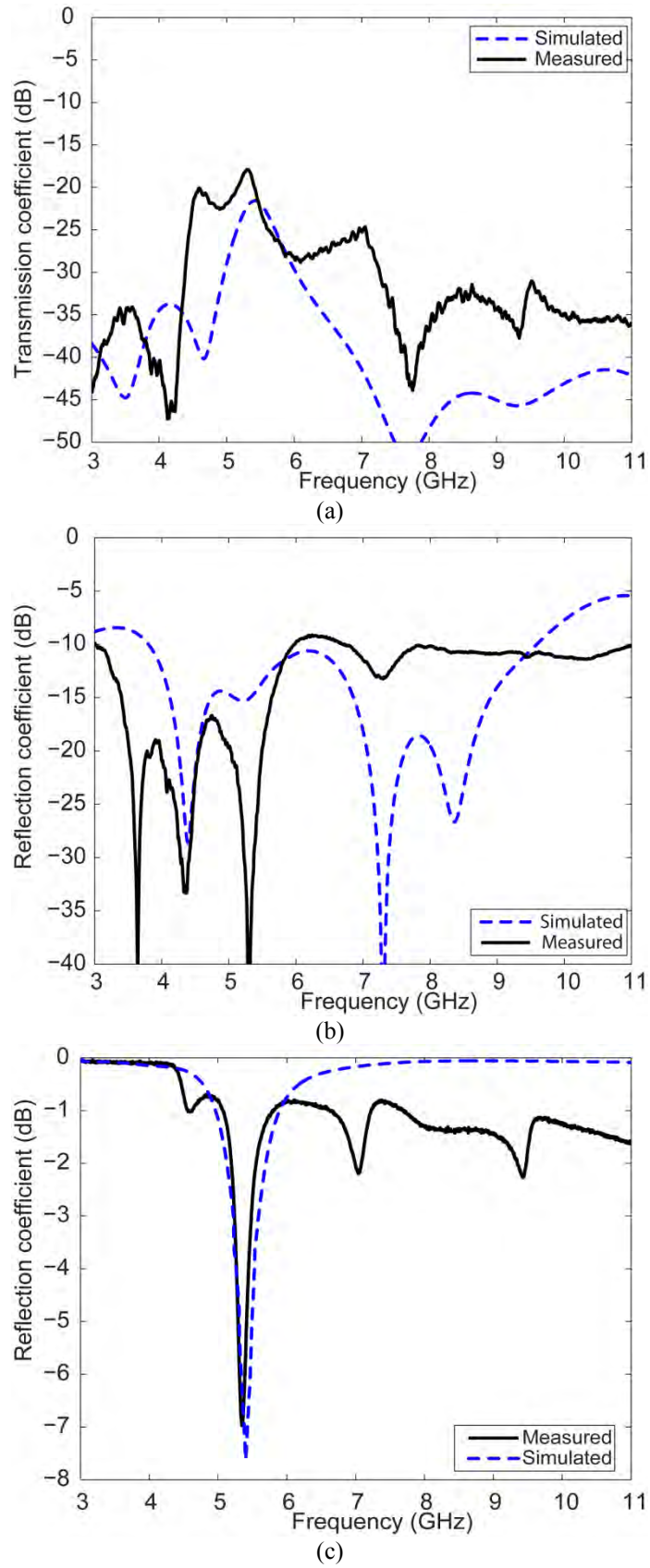


Fig. 5.9 Simulated and measured S parameter of configuration C antenna. (a) Transmission coefficient, (b) wideband antenna reflection coefficient, (c) narrowband antenna reflection coefficient.

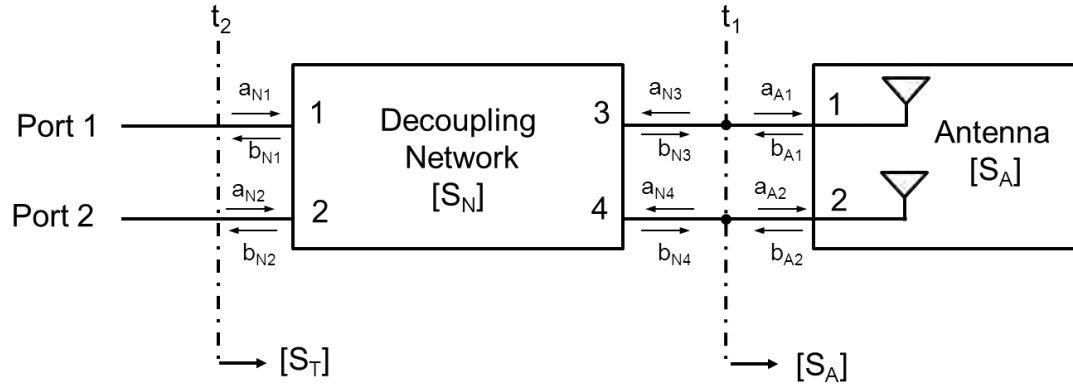


Fig. 5.10 Block diagram of the antenna with the decoupling network.

## 5.4 External Decoupling Feed Network Error! Switch argument not specified.

In addition to the internal modifications that can be applied to the antenna structure, it is also possible to add external decoupling circuits to the antenna ports to improve the isolation. In this section the theory and calculations behind a linear decoupling feed network will be elaborated. Consequently the antenna together with the network is examined. It is important to note that, in this technique the assumption is to derive the decoupling conditions for a single frequency and there is no constraint on what happens at other frequencies.

### 5.4.1 Decoupling Network Design Theory

A four-port decoupling network, with two output ports connected to the antennas, is first assumed for reducing the coupling between the two resultant new input ports. The block diagram of the two port antenna together with the decoupling network is shown in Fig. 5.10.

Let the scattering matrix of the coupled antennas be denoted as  $[S_A]$  at the reference plane  $t_1$ . After connecting the network with scattering matrix  $[S_N]$ , the new scattering matrix at the reference plane  $t_2$  is expressed as  $[S_T]$ . In this technique we linearly combine the two input signals. Thus at the antenna inputs we would have



$$a_{A1} = b_{N3} = A \times a_{N1} + B \times a_{N2} \quad (5.1)$$

$$a_{A2} = b_{N4} = C \times a_{N1} + D \times a_{N2}$$

Where  $a_{Ai}$  is the incident normalised voltage wave into port  $i$  of antenna and  $b_{Ai}$  is normalised voltage reflected wave coming out of port  $i$  of antenna. ( $i=1, 2$ ).  $a_{Ni}$  and  $b_{Ni}$ , respectively, represent the incident and reflected voltage waves at port  $i$  of the network, where  $i=1, \dots, 4$ . In order to retain the power and satisfy the lossless network requirements [1], (5.2) needs to be satisfied.

$$\begin{aligned} A^2 + B^2 &= 1 \\ C^2 + D^2 &= 1 \end{aligned} \quad (5.2)$$

A simple solution for (5.2) would use *Sine* and *Cosine-basis* functions. Therefore A, B, C and D can be written as follows

$$\begin{bmatrix} A & B \\ C & D \end{bmatrix} = \begin{bmatrix} \cos \theta & -\sin \theta \\ \sin \theta & \cos \theta \end{bmatrix}. \quad (5.3)$$

Using (5.3), (5.1) can be written in matrix form as (5.4)

$$\begin{bmatrix} a_{A1} \\ a_{A2} \end{bmatrix} = \begin{bmatrix} b_{N3} \\ b_{N4} \end{bmatrix} = \begin{bmatrix} \cos \theta & -\sin \theta \\ \sin \theta & \cos \theta \end{bmatrix} \begin{bmatrix} a_{N1} \\ a_{N2} \end{bmatrix}. \quad (5.4)$$

It is assumed that the four ports of the feed network are matched and isolated. This indicates that  $S_{N11}$ ,  $S_{N22}$ ,  $S_{N33}$ ,  $S_{N44}$ ,  $S_{N12}$ ,  $S_{N21}$ ,  $S_{N34}$ , and  $S_{N43}$  are all zero. Therefore, by assuming the whole feed network to be symmetrical and reciprocal the scattering matrix of the decoupling network can be written as (5.5).

$$S_N = \begin{bmatrix} 0 & 0 & \cos \theta & \sin \theta \\ 0 & 0 & -\sin \theta & \cos \theta \\ \cos \theta & -\sin \theta & 0 & 0 \\ \sin \theta & \cos \theta & 0 & 0 \end{bmatrix} \quad (5.5)$$

Using (5.4), the scattering matrix of the whole system (antenna and network) could be derived as (5.6).

$$\begin{aligned}
 \begin{bmatrix} b_{N1} \\ b_{N2} \end{bmatrix} &= \begin{bmatrix} \cos \theta & \sin \theta \\ -\sin \theta & \cos \theta \end{bmatrix} \begin{bmatrix} a_{N3} \\ a_{N4} \end{bmatrix} \\
 &= \begin{bmatrix} \cos \theta & \sin \theta \\ -\sin \theta & \cos \theta \end{bmatrix} \begin{bmatrix} b_{A1} \\ b_{A2} \end{bmatrix} \\
 &= \begin{bmatrix} \cos \theta & \sin \theta \\ -\sin \theta & \cos \theta \end{bmatrix} S_A \begin{bmatrix} a_{A1} \\ a_{A2} \end{bmatrix} \\
 &= \begin{bmatrix} \cos \theta & \sin \theta \\ -\sin \theta & \cos \theta \end{bmatrix} S_A \begin{bmatrix} b_{N3} \\ b_{N4} \end{bmatrix} \\
 &= \begin{bmatrix} \cos \theta & \sin \theta \\ -\sin \theta & \cos \theta \end{bmatrix} S_A \begin{bmatrix} \cos \theta & -\sin \theta \\ \sin \theta & \cos \theta \end{bmatrix} \begin{bmatrix} a_{N1} \\ a_{N2} \end{bmatrix}
 \end{aligned} \tag{5.6}$$

Since the specific element of any general scattering matrix can be determined as (5.7) the scattering matrix for the composite two port system, i.e. the antenna and decoupling network can be defined as (5.8).

$$S_{ij} = \left. \frac{V_j^-}{V_j^+} \right|_{V_k^+ = 0 \text{ for } k \neq j} \tag{5.7}$$

$$\begin{aligned}
 S_T &= \begin{bmatrix} \cos \theta & \sin \theta \\ -\sin \theta & \cos \theta \end{bmatrix} S_A \begin{bmatrix} \cos \theta & -\sin \theta \\ \sin \theta & \cos \theta \end{bmatrix} \\
 &= \begin{bmatrix} \cos \theta & \sin \theta \\ -\sin \theta & \cos \theta \end{bmatrix} \begin{bmatrix} S_{A11} & S_{A12} \\ S_{A21} & S_{A22} \end{bmatrix} \begin{bmatrix} \cos \theta & -\sin \theta \\ \sin \theta & \cos \theta \end{bmatrix}
 \end{aligned} \tag{5.8}$$

$$S_{T11} = S_{A11} \cos^2 \theta + S_{A22} \sin^2 \theta + S_{A12} \sin 2\theta$$

$$S_{T21} = S_{T12} = (S_{A11} - S_{A22}) \sin 2\theta - 2 \cos 2\theta S_{A12}$$

$$S_{T22} = S_{A22} \cos^2 \theta + S_{A11} \sin^2 \theta - S_{A12} \sin 2\theta$$

To decouple the two ports of the composite network and force  $S_{T12}$  and  $S_{T21}$  to be zero,  $\theta$  should satisfy (5.9).

$$\theta = \frac{1}{2} \tan^{-1}(2S_{A12}/(S_{A11} - S_{A22})) \quad (5.9)$$

Since the antennas are reciprocal we have  $S_{A12} = S_{A21}$ .

In general,  $\theta$  is complex and it will be real if the argument of the inverse tangent function in (5.9) , i.e. (5.10), is real.

$$(2S_{A12}/(S_{A11} - S_{A22})) \quad (5.10)$$

In order to compensate the imaginary part of (5.10) two pieces of transmission lines are required to be added to the input ports of the antennas before connecting to the network. The schematic diagram of the antenna with the compensating transmission lines is shown in Fig. 5.11. The new antenna scattering matrix at the reference plane  $t'_1$  can be written as (5.11). Using (5.11), (5.10) can be rewritten as (5.12)

$$S'_A = \begin{bmatrix} S_{A11}e^{j2\phi_1} & S_{A12}e^{j(\phi_1+\phi_2)} \\ S_{A21}e^{j(\phi_1+\phi_2)} & S_{A22}e^{j2\phi_2} \end{bmatrix} \quad (5.11)$$

$$\frac{2S'_{A12}}{S'_{A11} - S'_{A22}} = \frac{2S_{A12}e^{j(\phi_1+\phi_2)}}{S_{A11}e^{2j\phi_1} - S_{A22}e^{2j\phi_2}} \quad (5.12)$$

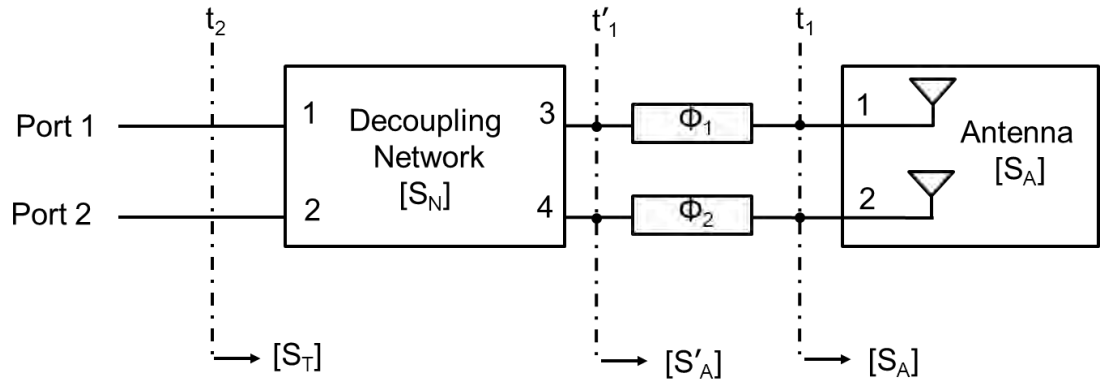


Fig. 5.11 Block diagram of the antenna with the decoupling network and compensating transmission lines.

By substituting  $S_{Aij} = |S_{Aij}|e^{j\alpha_{ij}}$ , where  $\alpha_{ij}$  is the phase value of the  $ij$  component of the scattering matrix of the antenna, into (5.12), it can be rewritten as (5.13).

$$\begin{aligned} & \frac{|S_{A12}|e^{j\alpha_{12}}e^{j(\phi_1+\phi_2)}}{|S_{A11}|e^{j\alpha_{11}}e^{2j\phi_1} - |S_{A22}|e^{j\alpha_{22}}e^{2j\phi_2}} \\ &= \frac{|S_{A12}|}{|S_{A11}|e^{(\phi_1-\phi_2+\alpha_{11}-\alpha_{12})} - |S_{A22}|e^{(\phi_2-\phi_1+\alpha_{22}-\alpha_{12})}} \end{aligned} \quad (5.13)$$

The numerator in (5.13) is real, so just the denominator needs to be real. By setting the imaginary part of the denominator to zero we have

$$|S_{A22}|\sin(\phi_2 - \phi_1 + \alpha_{22} - \alpha_{12}) = |S_{A11}|\sin(\phi_1 - \phi_2 + \alpha_{11} - \alpha_{12})$$

and the above then reduces to

$$\begin{aligned} & \sin(\phi_2 - \phi_1) (|S_{A22}|\cos(\alpha_{22} - \alpha_{12}) + |S_{A11}|\cos(\alpha_{11} - \alpha_{12})) \\ &= \cos(\phi_2 - \phi_1) (|S_{A11}|\sin(\alpha_{11} - \alpha_{22}) - |S_{A22}|\sin(\alpha_{22} - \alpha_{12})) \end{aligned}$$

The phase difference we require to apply between the antenna ports would be as

$$\begin{aligned} & (\phi_2 - \phi_1) \\ &= \tan^{-1} \left( \frac{(|S_{A11}|\sin(\alpha_{11} - \alpha_{12}) - |S_{A22}|\sin(\alpha_{22} - \alpha_{12}))}{(|S_{A22}|\cos(\alpha_{22} - \alpha_{12}) + |S_{A11}|\cos(\alpha_{11} - \alpha_{12}))} \right) \end{aligned} \quad (5.14)$$

The absolute values of  $\phi_1$  and  $\phi_2$  are not critical, but  $\phi_2 - \phi_1$  must be calculated. Finally the new  $\theta'$  can be recalculated from (5.15).

$$\theta' = \frac{1}{2} \tan^{-1} \left( \frac{2S_{A12}e^{j(\phi_1+\phi_2)}}{S_{A11}e^{2j\phi_1} - S_{A22}e^{2j\phi_2}} \right) \quad (5.15)$$

The scattering matrix of the decoupling network can then be recalculated from (5.16).

$$S_N = \begin{bmatrix} 0 & 0 & \cos \theta' & \sin \theta' \\ 0 & 0 & -\sin \theta' & \cos \theta' \\ \cos \theta' & -\sin \theta' & 0 & 0 \\ \sin \theta' & \cos \theta' & 0 & 0 \end{bmatrix} \quad (5.16)$$

It is important to once more note that the only goal in the above design procedure is to minimize the mutual coupling between the two antennas at a certain frequency and there is no constraint on the performance of the antennas at other frequencies. In other words, this technique does not guarantee to maintain the original radiation characteristics of the antennas.

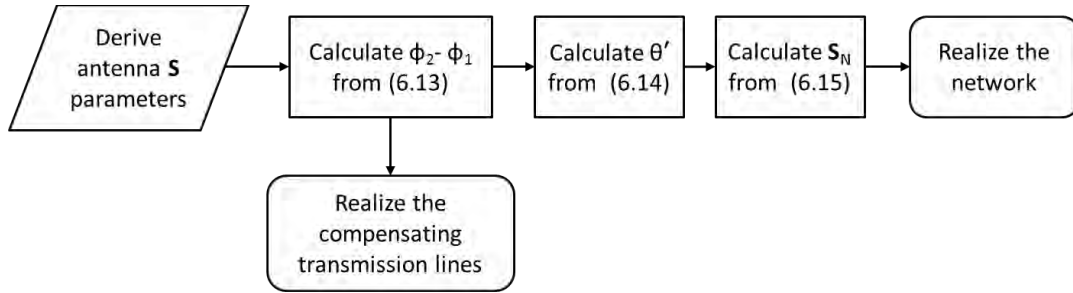


Fig. 5.12 Decoupling network design steps.

#### 5.4.2 Decoupling Network for Integrated Wideband-Narrowband Antenna

The design procedure of decoupling network is summarized in Fig. 5.12. The scattering matrix of the antenna is first utilized to calculate the electrical length of the compensating transmission lines,  $\phi_1$  and  $\phi_2$ . Consequently the  $\theta'$  and  $S_N$  can be calculated and the network can then be realized accordingly.

In this section this procedure is carried out for the integrated wideband-narrowband antenna. The original S parameters of the antenna are shown in Fig. 5.13. It is important to note that since the antenna scattering parameters vary with frequency the resulting parameters i.e.  $\theta'$ ,  $\phi_2$  and  $\phi_1$  are also functions of frequency. Fig. 5.14 shows the calculated value for  $\phi_2 - \phi_1$ . It varies significantly across the band and there is no distinct pattern in this variation. The calculated  $\theta'$  is shown in Fig. 5.15. Similar to Fig. 5.14, the  $\theta'$  varies significantly with frequency. In these figures  $\theta'$  and  $\phi_2 - \phi_1$  are both calculated for the whole frequency range. However, this is not a practical case and it is not possible to design a single network which satisfies such variations of  $\theta'$ . These results are shown here to demonstrate that this theory

provides at least one solution for any frequency and any value of scattering parameters. Fig. 5.16 shows the scattering parameters for the new two port system i.e. the antenna and network combination.

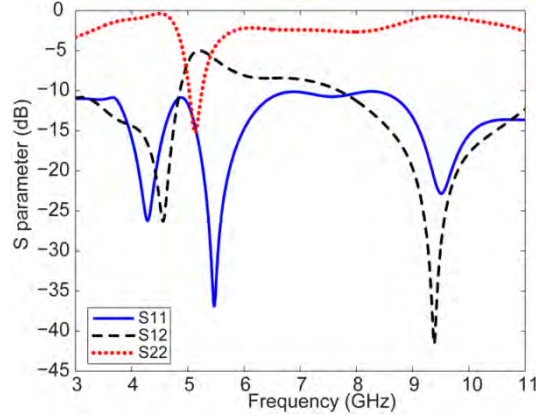


Fig. 5.13 S parameters of the integrated wideband-narrowband antenna.

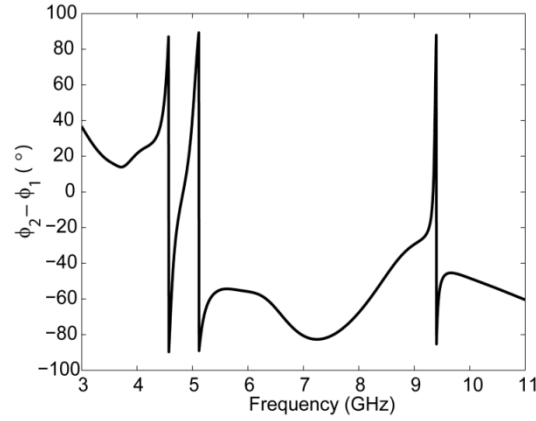


Fig. 5.14 Calculated  $\phi_2 - \phi_1$ .

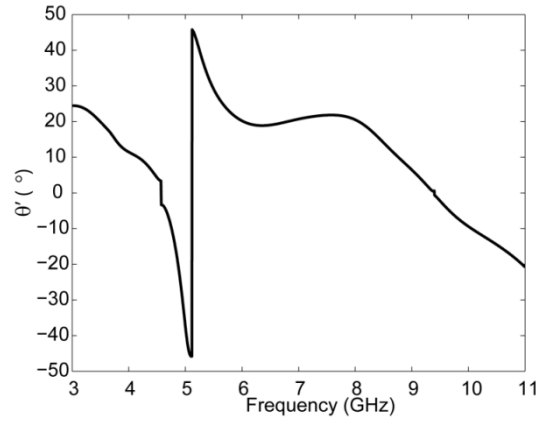
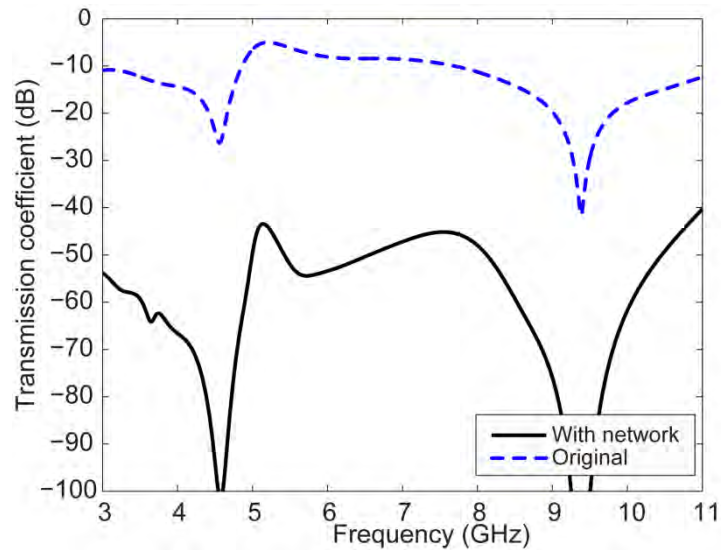
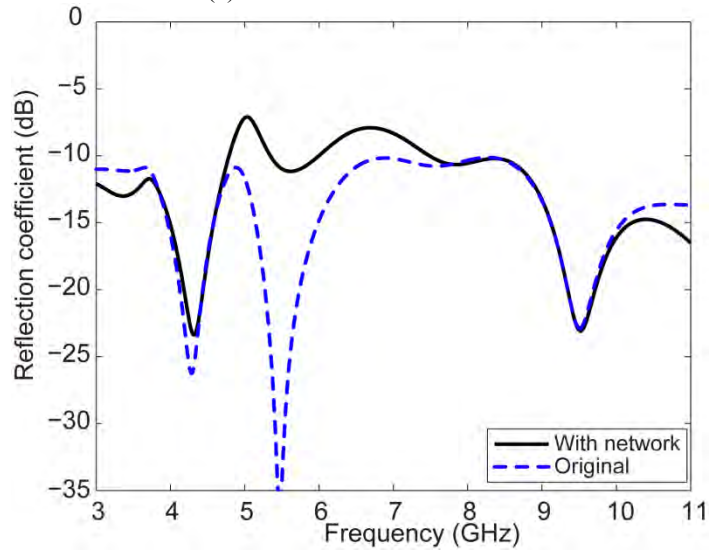


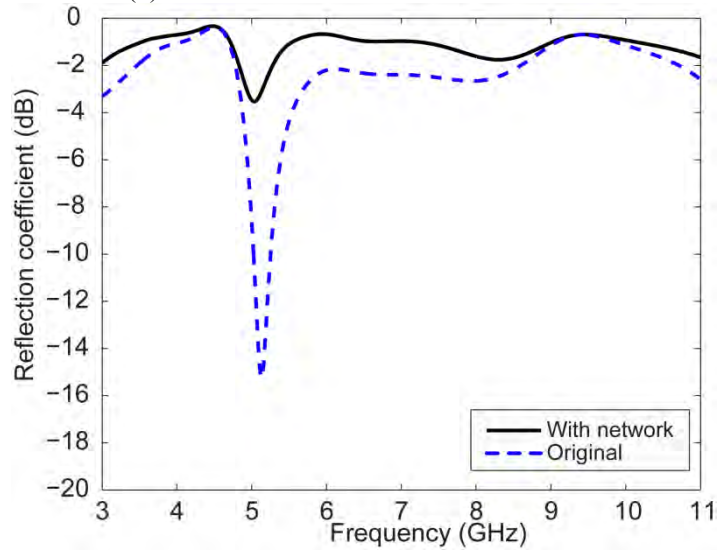
Fig. 5.15 Calculated  $\theta'$ .



(a) Transmission coefficient.



(b) Wideband antenna reflection coefficient.



(c) Narrowband antenna reflection coefficient.

Fig. 5.16 Calculated scattering parameter with and without network for the whole 3-11GHz band.

As shown in Fig. 5.16a, the transmission coefficient has dropped to less than -45dB across the whole band. The wideband reflection coefficient is less than -10dB across the whole band except in a bandwidth of 4.8-5.35 GHz and 6-7.5 GHz where it peaks to -7 GHz (see Fig. 5.16b). Fig. 5.16c shows the reflection coefficient of the narrowband antenna with and without network. Although the main resonance is distinguishable, it is slightly detuned and not well-matched.

It is important to note that in this technique the calculated  $\theta'$  and  $\phi_2-\phi_1$  only satisfy the  $S_{T12}=S_{T21}=0$  condition and there is no control over the port matching. The matching variations can be elaborated by expanding the elements of the  $[S_T]$  matrix. In calculating each element, the calculated values for  $\theta'$  and  $\phi_2-\phi_1$  at each frequency are substituted to the corresponding formulation. In other words, at any frequency  $f$  the total scattering parameters are calculated from (5.17).

$$S_{T12} = S_{T21} = 0 \quad (5.17)$$

$$S_{T11}(f) = S'_{A11}(f) \cos^2 \theta'(f) + S'_{A22}(f) \sin^2 \theta'(f) + S'_{A12} \sin 2\theta'(f)$$

$$S_{T22}(f) = S'_{A22}(f) \cos^2 \theta'(f) + S'_{A11}(f) \sin^2 \theta'(f) - S'_{A12} \sin 2\theta'(f)$$

It can be seen from (5.17) that the antenna matching is affected after adding the network. Depending on the value of  $\theta'$ ,  $S_{A22}$  ( $S_{A11}$ ) and  $S_{A12}$ , the overall port matching i.e.  $S_{T11}$  ( $S_{T22}$ ) would get better or worse. The effects of the network on antenna port matching with reference to (5.17) are shown in Fig. 5.17.

It can be concluded from the above analysis that this method is frequency dependant. Therefore, it is required to read the values of  $\theta'$  and  $\phi_2-\phi_1$  at the desired frequency and realize the network and compensating transmission lines. For instance, in the integrated wideband-narrowband antenna configuration the narrowband antenna is designed for the 5-5.3GHz in which the coupling peaks to -4dB. Therefore it is important to reduce the coupling specifically at this region.



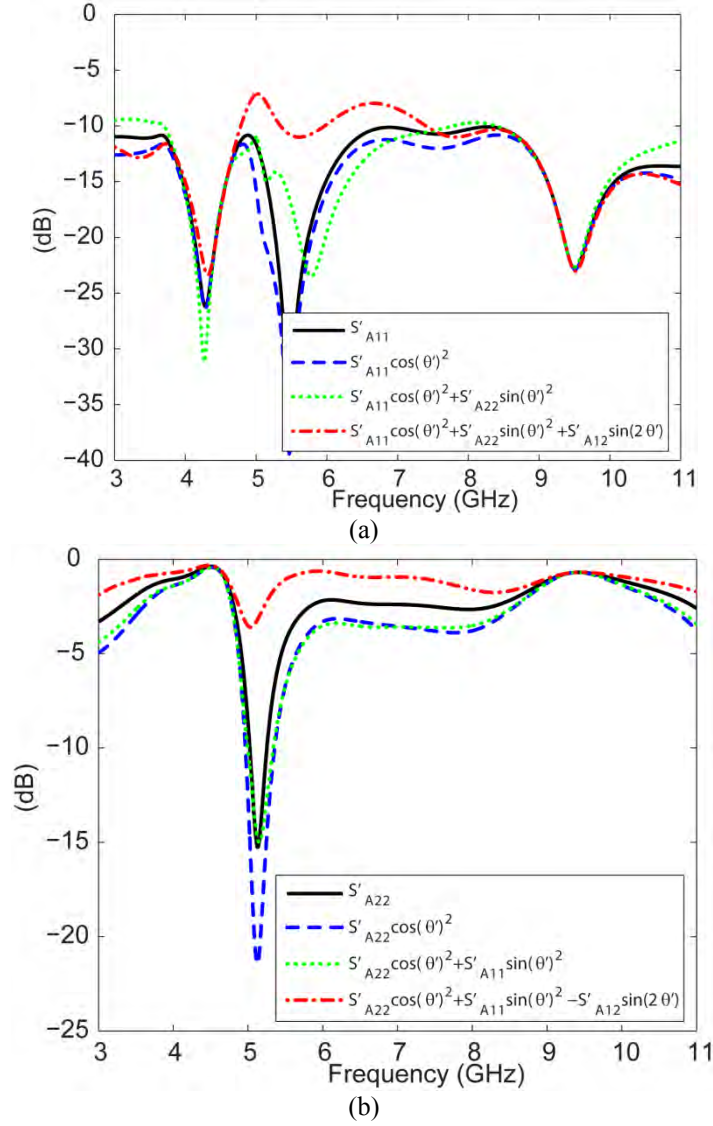


Fig. 5.17 Port matching variation after adding the network (a) wideband antenna (b) narrowband antenna.

For the integrated wideband-narrowband antenna the value of  $\phi_2 - \phi_1$  and  $\theta'$  can be extracted from Fig. 5.14 and Fig. 5.15, respectively. The value for  $\phi_2 - \phi_1$  is about  $90^\circ$ .  $\theta'$  is about  $45^\circ$ . Therefore the scattering matrix of the network can be written as (5.18).

$$S_N = \frac{1}{\sqrt{2}} \begin{bmatrix} 0 & 0 & 1 & 1 \\ 0 & 0 & -1 & 1 \\ 1 & -1 & 0 & 0 \\ 1 & 1 & 0 & 0 \end{bmatrix} \quad (5.18)$$

The resulting matrix is the representation of the ideal 3 dB  $180^\circ$  hybrid or rat-race coupler. The  $180^\circ$  hybrid junction is a four port network which can be used as power combiner or divider [1]. With reference to the  $180^\circ$  hybrid schematic shown in Fig. 5.18, in the combiner mode port 1 and 2 are excited. The signals are added in phase at port 4 ( $\Sigma$ ) and

out of phase ( $\Delta$ ) at port 3. In divider mode if port 1 is excited then the signal will be evenly split into two out of phase components at ports 3 and 4, and port 2 is isolated. If port 2 is excited then the power is split into two in phase component at port 3 and 4 and port 1 is isolated. The ring hybrid or rat-race could be constructed in planar (microstrip or stripline) form, although waveguide version is also possible. The bandwidth of the ring hybrid is limited by the frequency dependence of the ring lengths, but is generally on the order of 20-30% [1]. In order to match the technology of the antenna a microstrip 180° hybrid has been modelled in AWR Microwave Office. It is modelled on the Taconic TLC-30 RF laminate with a relative permittivity of  $\epsilon_r=3\pm0.05$  and a thickness of 0.79 mm. The ports impedance are 50 $\Omega$ . The ring has a characteristic impedance of factor  $\sqrt{2}$  compared to port impedance.

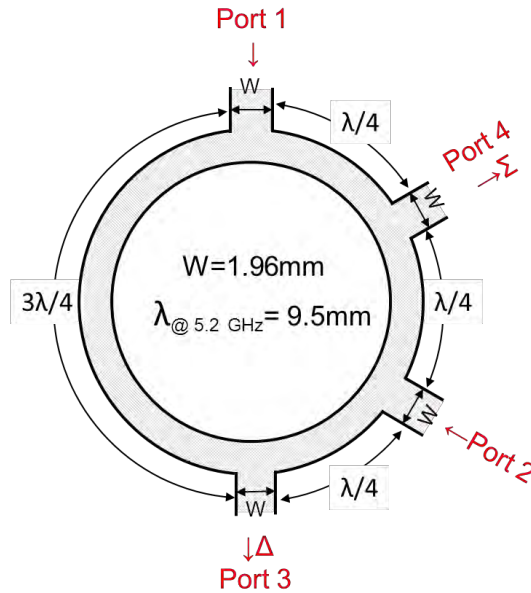


Fig. 5.18 The geometry of the 180° hybrid.

Fig. 5.19a shows the simulated  $S$  parameter magnitude for the 180° hybrid coupler designed at 5.2GHz. All four ports are matched. The 3dB power coupling is achieved between the input and output ports. The input ports are isolated from each other ( $S_{12} < -10$  @ 5.2GHz). The  $S$  parameters phase variations are shown in Fig. 5.19b. The 180° phase difference can be observed between  $S_{13}$  and  $S_{14}$ . The rat race is then connected to the antenna ports.

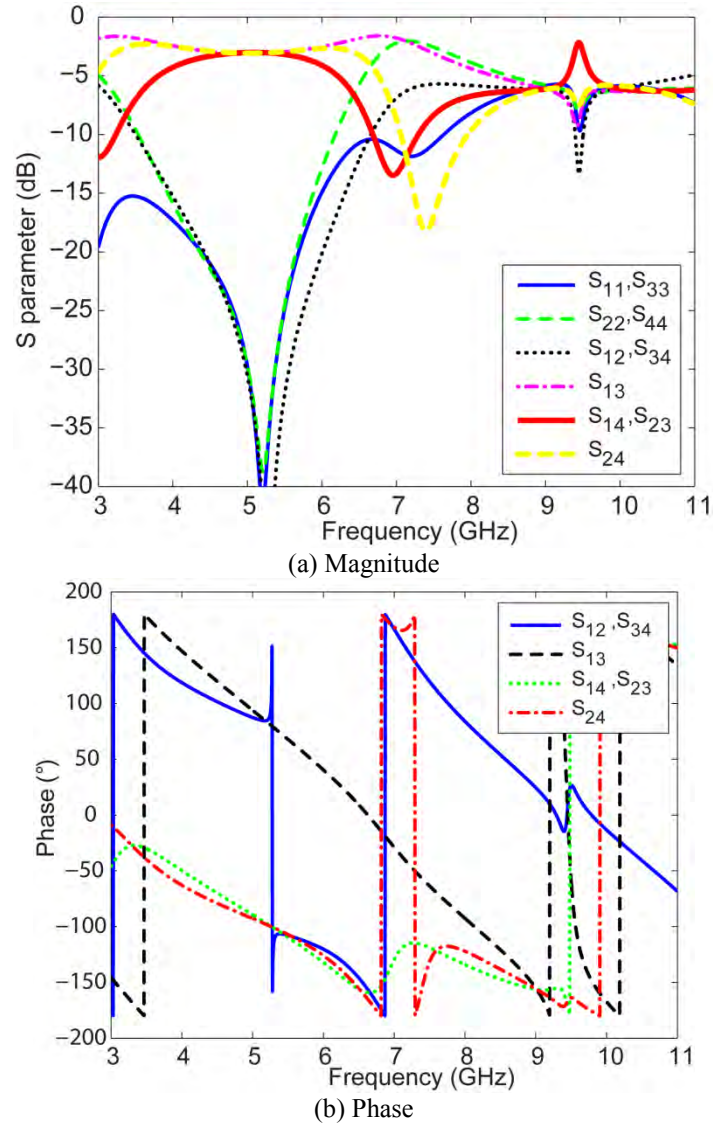


Fig. 5.19 Simulated 180° hybrid coupler S parameter.

The antenna together with the 180° hybrid coupler is simulated in AWR Microwave Office. The simulated S parameters are shown in Fig. 5.20. Very good isolation (-30dB) is achieved between the ports at 5.2GHz. This value is comparable with the calculated results shown in Fig. 5.16 at 5.2GHz. Both narrowband and wideband matching is affected by the network. This is due to the fact that the range of  $\theta'$  and  $\phi_2 - \phi_1$  variation against frequency is quite large. This condition cannot be satisfied by a single network. Referring to Fig. 5.14 and Fig. 5.15  $\theta'$  and  $\phi_2 - \phi_1$  variations versus frequency can be quantified.

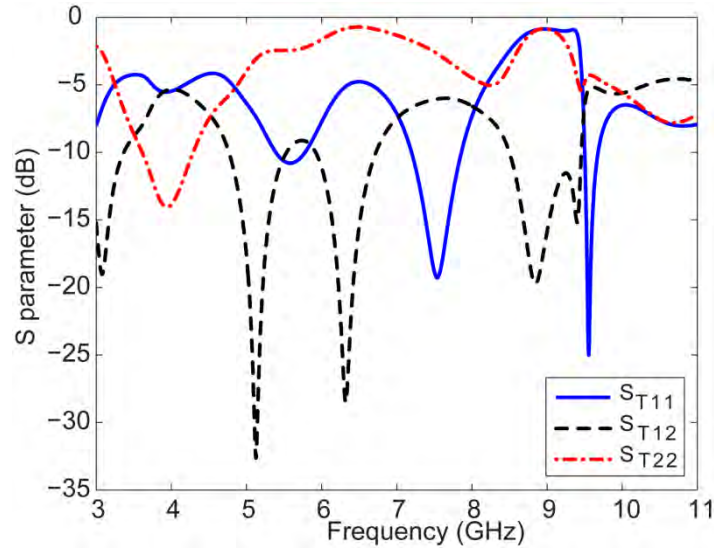


Fig. 5.20 Simulated S parameters of the antenna and decoupling network.

## 5.5 Concluding Remarks and Summary

In the previous sections two main methods of isolating the highly coupled ports were studied. In the first method the relative arrangement of the antennas are modified to achieve good isolation. In order to find the arrangement with higher isolation, the current distributions on the antennas are studied. The regions with high concentration of currents are avoided. In choosing the right location for the antennas it is important to take the practical issues into account. Some areas such as the ground plane, in practice, are reserved for mounting the RF components and are not suitable for antennas. Connecting the antennas to the RF circuit should be technically and economically achievable. In configuration B this might not be easily achievable. Therefore the level of isolation is not the only issue in choosing the right antenna arrangement. It is important to note that in developing these antennas the main application considered was portable wireless devices in which the radiation pattern is not of particular importance. However, depending on the application the influence of the antenna arrangement on the radiation patterns should also be taken into consideration. Fig. 5.21 compares the level of isolation achieved with each configuration.

In some cases changing the antenna arrangements is not possible. Therefore, an external decoupling technique is required. For this case, a design method was described in the

last section. In this method the goal is to achieve maximum isolation and no condition is applied on the port matching. The scattering parameters of a four port decoupling network at each frequency can be calculated. However, it is not possible to realize a single network which satisfies required scattering parameters at all frequencies in a wide frequency band. Therefore, this technique is more suitable for narrowband antennas, where a network can be specifically designed for the desired narrow bandwidth. For the integrated wideband-narrowband antenna configuration, the decoupling network appeared to be a  $180^\circ$  hybrid coupler at 5.2GHz. The coupler together with the antenna was simulated; however, it was not realized at this stage since the simulation results were not convincing enough. This was due to high variation of  $\theta'$  and  $\phi_2 - \phi_1$  versus frequency. As mentioned earlier in this method the condition is upon the transmission coefficient. To improve the input port matching results it is possible to add two more conditions on the ports matching. Otherwise, extra matching circuits are required to compensate the matching. This might be a challenge for wideband antennas. All these are planned for future extension of the method. This technique is more suitable for scenarios with less limitation on space. The radiation from the network and connecting transmission lines should also be taken care of.

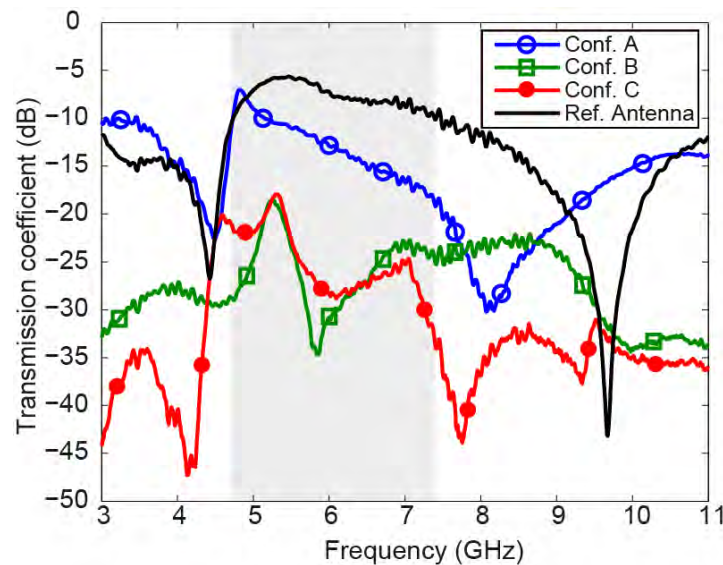


Fig. 5.21 Measured transmission coefficient for all three configurations and the reference antenna.

This study confirms the fact that integrating multiple antennas in small space results in high level of interaction between the antennas. Therefore, when designing multiband antennas it is important to make sure that the isolation level stays in the acceptable range. It is important to consider that regardless of the technique used to reduce the antenna port coupling the field interaction between the antennas can result in radiation pattern deformation. In some applications such as wireless communication this might not be of high importance due to the multipath effects. However, in other applications such as global positioning service or satellite radio, maintaining the shape of the pattern is very important. It is necessary to reemphasise that although integrating multiple antennas into small space might add to the versatility of the antenna it might also result in degradation of other radiation parameters.

## **References**

- [1] D. M. Pozar, *Microwave Engineering*, 2nd ed., Wiley & Sons, Inc, New York, United States, 1998.
- [2] P. Gardner, *Private communication*, 2008.

# **Chapter 6      Reconfigurable                      Wideband- Narrowband Antenna**

## **6.1      Introduction**

Antennas with reconfiguration capabilities (frequency, bandwidth, pattern, polarization) have the potential to open up a world of new possibilities for system performance, flexibility, and robustness. In current wireless networks reconfigurable antennas can be utilized to improve the system robustness in today's harsh and time varying electromagnetic environments. In future, flexible transceivers are required for dynamically accessing the spectrum in CR networks. Reconfiguration can be achieved at different levels. Reconfigurable antennas might however, relax the reconfiguration complexities at the RF front end.

The combination of wideband and narrowband functionality adds to the versatility of the antenna systems in various wireless scenarios. This unique feature can be advantageous in CR networks for spectrum sensing and communication procedure. As such, wideband simultaneous spectrum sensing can be carried out using the wideband antenna, and once the vacant frequency is detected the narrowband antenna can be tuned accordingly. As it was reviewed in Chapter 3, there are various techniques to tune a narrowband antenna. The main technique for tuning the resonant antennas is to change the effective electrical length of the antenna which largely determines the operating frequency, its associated bandwidth and

radiation pattern. This can be carried out by modifying the length of the resonant paths in the antenna structure or loading the antenna internally or externally. Using switches (microelectromechanical systems (MEMS), PIN diode) for discrete tuning and varactors for continuous tuning or the combination for coarse and fine tuning are the very popular tuning mechanisms [1]. For the success of these techniques the compatibility of the antenna topology with the intended reconfiguration mechanism should also be considered. Sometimes, the only way to include a particular switch is to design the antenna around the switch's geometry. Switches and varactors can also be used to design external tuning networks in case internally modifying the resonant path is not possible. This technique can be applied to wider range of antennas and is not necessarily restricted to resonant antennas. Moreover, the compatibility with the antenna topology is less limiting in this approach. Therefore, in this chapter tuning the narrowband antenna by means of external tuning circuits are examined.

For the CR application the narrowband antenna should be tuneable across a wide range of frequencies. Therefore, either a bank of matching circuits or several reconfigurable matching circuits need be used. Either of these techniques has both advantages and challenges. A continuously reconfigurable matching network would probably require less space. However, it would be more complicated to design. Most continuously reconfigurable matching circuits are based around a non-linear tuning element such as varactor diodes. This leads to intermodulation products, which are highly undesirable. It would also be necessary to design a bias circuit for varactor diode and that adds to the cost and complexity of the system. Although a bank of switched matching networks may require more space, it would be much easier to design. In a mass produced commercial system these matching circuits could be housed within a microwave integrated circuit (MIC) and that can be optimized to enhance performance and minimize the required space. A microprocessor would then be used to switch between each of the different circuits. It would be important to investigate the effect of component and switch losses, on the total efficiency of the antenna. If this is a problem it may be necessary to use a low loss component, such as a MEMS switch.



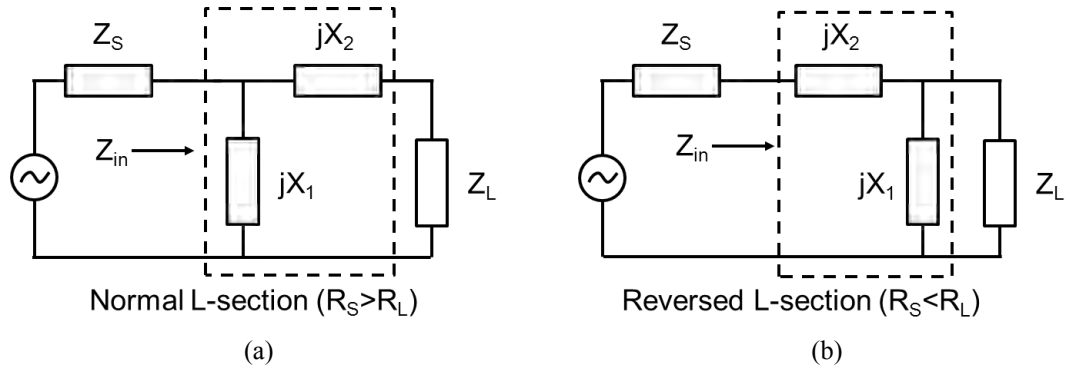


Fig. 6.1 Circuit diagrams L-section matching network, (a) normal (b) reversed.

In view of the above, the possibility for tuning the narrowband antenna across the wide bandwidth (spectrum sensing range) is investigated in this chapter. For this purpose three tuning circuits based on fixed elements are designed and the measured and simulated results are studied.

## 6.2 Impedance Matching Circuit Design

In RF circuits the maximum transfer of power from a source to its load occurs when the load impedance  $Z_L$  is equal to the complex conjugate of the source impedance. This refers to a condition in which any source reactance is resonated with an equal and opposite load reactance; thus, leaving only equal resistor values for the source and the load terminations. The primary objective in any impedance matching scheme, then, is to force a load impedance to be the complex conjugate of the source impedance. Hereby, we briefly overview the design principles of L and  $\Pi$  matching circuits.

### 6.2.1 The L Network

Probably the simplest and most widely used matching circuit is the L network shown in Fig. 6.1 where  $Z_L = R_L + jX_L$ ,  $Z_S = R_S + jX_S$ ,  $Z_1 = jX_1$  and  $Z_2 = jX_2$ . This circuit receives its name because of the component orientation which resembles the shape of an L.

In order to transfer the maximum power to the load the condition in (6.1) should be satisfied.

$$Z_{in} = Z_S^* \quad (6.1)$$

$Z_{in}$  is the input impedance looking into the L-section and can be written for both normal and reversed cases (see Fig. 6.1) as shown in (6.2).

$$\begin{aligned} Z_{in} &= \frac{Z_1(Z_2 + Z_L)}{Z_1 + Z_2 + Z_L} & (\text{normal}) \\ Z_{in} &= Z_2 + \frac{Z_1 Z_L}{Z_1 + Z_L} & (\text{reversed}) \end{aligned} \quad (6.2)$$

In order to calculate the unknown elements of the network (6.2) is substituted into (6.1) and by equating the real and imaginary parts of the two sides two sets of values can be obtained for  $X_1$  and  $X_2$  [2]:

$$\begin{aligned} X_1 &= \frac{X_S \pm R_S Q}{\frac{R_S}{R_L} - 1} & X_1 &= \frac{X_L \pm R_L Q}{\frac{R_L}{R_S} - 1} \\ X_2 &= -(X_L \pm R_L Q) & X_2 &= -(X_S \pm R_S Q) \\ Q &= \sqrt{\frac{R_S}{R_L} - 1 + \frac{X_S^2}{R_S R_L}} & Q &= \sqrt{\frac{R_L}{R_S} - 1 + \frac{X_L^2}{R_S R_L}} \end{aligned} \quad (\text{normal}) \quad (\text{reversed}) \quad (6.3)$$

According to (6.3) there is always at least one solution for any source and load impedance. When  $R_S > R_L$  a normal L-section always exists, and when  $R_S < R_L$  a reversed one always exists.

Equation (6.3) reveals a limitation of the two-element L-section matching network. The  $Q$ -factor and therefore the bandwidth of such circuits are fixed by the source and load impedance. In fact an L matching network provides the minimum achievable  $Q$ -factor. A third element in the network adds an extra degree of freedom to design a circuit with desired  $Q$ -factor.

### 6.2.2 The $\Pi$ Network

A three-element  $\Pi$  network and its equivalent T network are shown in Fig. 6.2. In this section the design procedure for a  $\Pi$  network will be explained and the equivalent T network parameters can be derived using circuit transformation equation sets [2].

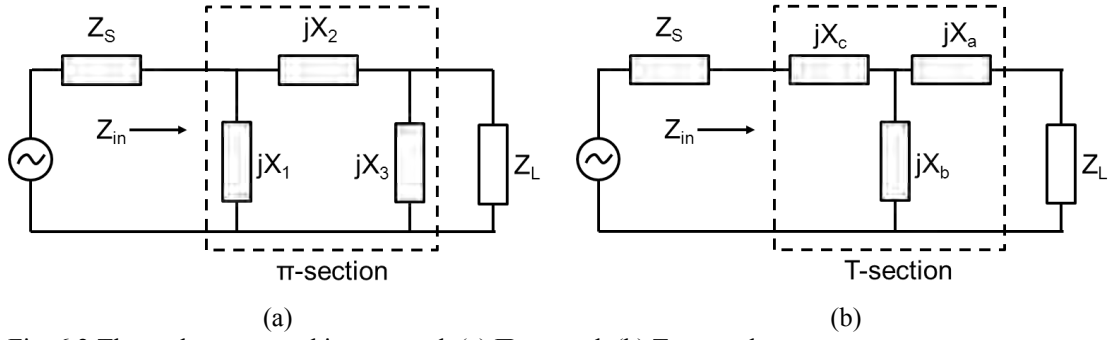


Fig. 6.2 Three-element matching network (a)  $\Pi$  network (b) T network.

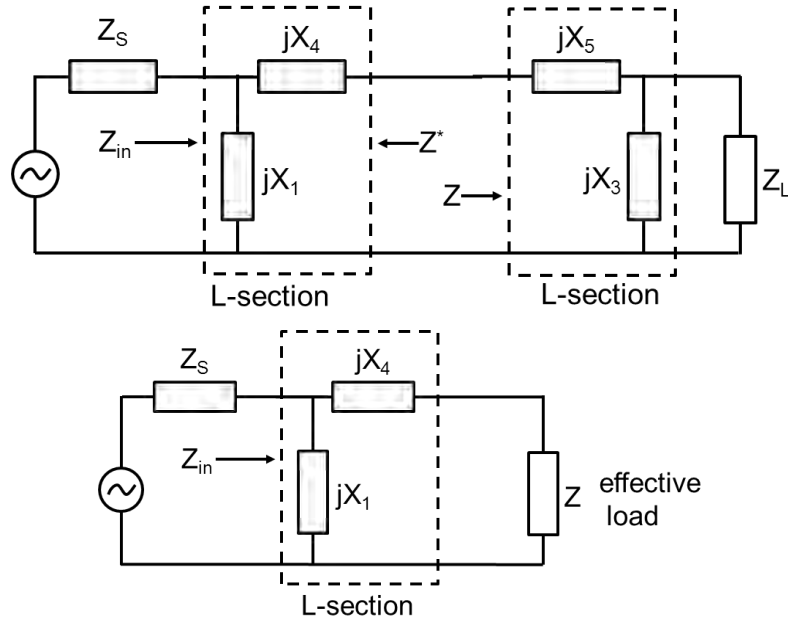


Fig. 6.3 Equivalent L network for a  $\Pi$  network.

A  $\Pi$  network can be considered as two back-to-back  $L$  networks as shown in Fig. 6.3 where the series reactance is split to two parts;  $X_2 = X_4 + X_5$ . Referring to the Fig. 6.3 the impedance looking into the right  $L$ -section is  $Z$  and the impedance looking into the left  $L$ -section is  $Z^*$ . Considering that  $Z_1 = jX_1$ ,  $Z_4 = jX_4$ ,  $Z_3 = jX_3$  and  $Z_5 = jX_5$ ,  $Z$  and  $Z^*$  can be written as (6.4).

$$Z_{left} = Z_4 + \frac{Z_1 Z_S}{Z_1 + Z_S} = Z^* \quad Z_{right} = Z_5 + \frac{Z_3 Z_L}{Z_3 + Z_L} = Z \quad (6.4)$$

As shown in Fig. 6.3 the right section and the load impedance can be replaced by an effective load  $Z_{right} = Z$ . The conjugate matching condition can be rewritten as

$$Z_{in} = \frac{Z_1(Z_4 + Z)}{Z_1 + Z_4 + Z} = Z_S^* \quad (6.5)$$

From (6.4) and (6.5), it can be understood that in a  $\Pi$  network the matching is carried out in two stages: one that matches the source  $Z$  to the load  $Z_S$  using a reversed L-section and the other that matches the source  $Z^*$  to the load  $Z_L$  using a normal L-section,

In order to satisfy the conditions for both matching sections we need to match each section to a virtual resistance  $R$  located at the junction between the two sections. Therefore, it is required to have  $R < R_S$  and  $R < R_L$  or

$$R < R_{min} \quad R_{min} = \min(R_L, R_S) \quad (6.6)$$

The network Q-factor would then be

$$Q = \sqrt{\frac{R_{max}}{R} - 1} \quad R_{max} = \max(R_L, R_S) \quad (6.7)$$

and the Q-factor of each section can be calculated from (6.8).

$$Q_S = \sqrt{\frac{R_S}{R} - 1} = \sqrt{\frac{R_S}{R_{max}}(Q^2 + 1) - 1} \quad , \quad (6.8)$$

$$Q_L = \sqrt{\frac{R_L}{R} - 1} = \sqrt{\frac{R_L}{R_{max}}(Q^2 + 1) - 1}$$

The reactances can then be calculated similar to an L-section network.

### **6.2.3 Tuned Integrated Wideband-Narrowband Antenna**

Based on the design equations reviewed in the last section, in this section the matching circuits are designed to tune the narrowband antenna across a wide bandwidth. In

order to reduce the complexity of the manufacturing process, the matching circuit is designed to be fabricated on the same substrate as the antenna. For the purpose of accommodating the matching circuits on the antenna, the antenna ground plane was elongated by 10mm (see Fig. 6.4). The impedance reference plane was then shifted back to its original point and the data was exported for matching circuit design. Using the CPW ground as the ground for the circuits, the elements can be placed around the narrowband antenna feeding on the reverse side of the substrate. The circuits are designed to retune the antenna from 5.2 GHz to 4, 8 and 10 GHz.

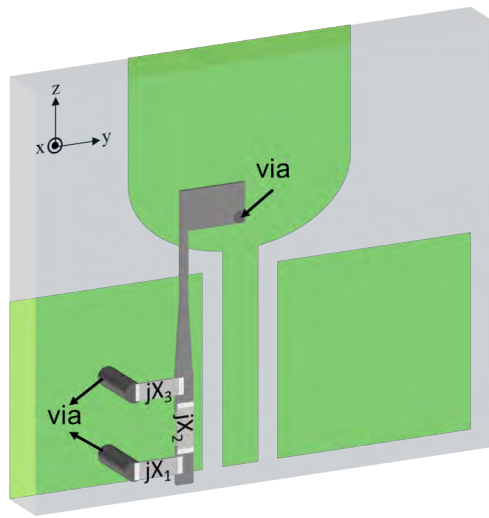


Fig. 6.4 The topology of the antenna with an integrated matching circuit.

A Matlab code was developed to calculate the matching network elements. They were then replaced with the realistic model of the components provided by the manufacturer in AWR Microwave office and CST Microwave Studio to achieve better prediction of the final measured results. To cover some issues in matching circuit design, three different types of matching circuits are designed in this section: two L networks, one low pass which is normal and one high pass which is reversed and one  $\Pi$  network. As it was pointed out previously in the design procedure of L networks, (6.3) gives two sets of results for any circuit. In choosing between the elements their costs, dimensions and availability in the market were taken into account. All three circuits are composed of just lumped element inductors and capacitors. All components are surface mount and chosen from 0402 (1.0 mm  $\times$  0.5 mm), 0603 (1.6 mm  $\times$

0.8 mm) and 0805 (2.0 mm × 1.25 mm) series. In some cases several components were used in series or parallel to build up the required value.

### 6.2.3.1 4 GHz-Normal Low Pass L Network

The antenna impedance at 4GHz was taken as the input to the design procedure. With reference to Fig. 6.1, the calculated parallel reactance  $X_1$  and series reactance  $X_2$  and their corresponding values based on  $X_1=j\omega L$ ,  $X_2=1/j\omega C$  and  $\omega= 2\pi f$  at 4GHz are demonstrated in Table 6.1

Table 6.1 Element values for the normal L network at 4GHz.

| Reactance ( $\Omega$ ) | Corresponding value at f=4GHz |
|------------------------|-------------------------------|
| $X_1 = -13.75$         | $C = 2.89$ pF                 |
| $X_2 = 46$             | $L = 1.82$ nH                 |

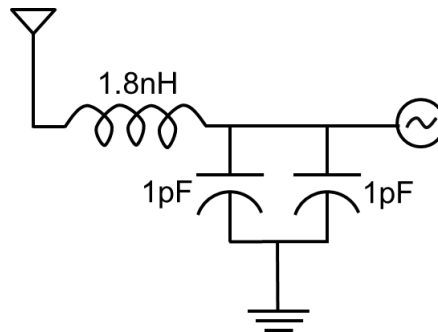


Fig. 6.5 Tuning circuit diagram for 4GHz.

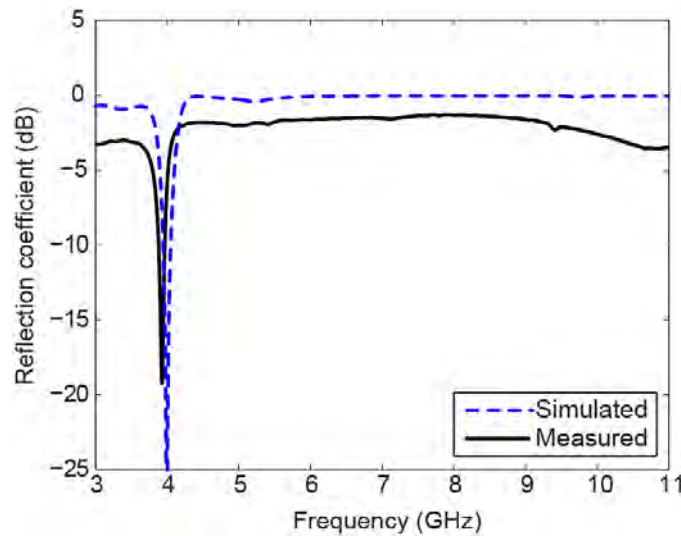


Fig. 6.6 Simulated and measured reflection coefficient of the antenna with a 4 GHz matching circuit.

The realistic models of the elements considering the known parasitic effects were included in the circuit simulation. To realize the circuit, one Coilcraft 1.8nH chip inductor from the 0603 series, and two AVX 1pF thin film capacitors from 0402 series were chosen. Fig. 6.5 shows the schematic diagram of the circuit. Two shorting pins between the top and bottom layer of the board were installed to solder the capacitors. The components were all hand soldered. Fig. 6.6 shows the simulated and measured reflection coefficient for the narrowband antenna. The measured resonance frequency matches very well with the modelled one. However, the discrepancy in the level of measured and simulated results indicates that there are some added losses in the system. Investigations show that the two ground connecting pins are the prime source of such discrepancy. The pin can be considered as a series resonant circuit.

#### **6.2.3.2 8 GHz- High Pass $\Pi$ Network**

A  $\Pi$  network is designed for tuning the antenna to 8 GHz. This circuit is high pass and the element in the series branch is a capacitor. The elements values for achieving the Q-factor 10 are summarized in Table 6.2. However, the closest commercially available values were chosen for the final circuits. Four Coilcraft 0402 chip inductors and one AVX thin film 0402 capacitor were used in the realized circuits. To achieve  $L_T=0.26\text{nH}$ , the three 0.8nH inductors are connected in parallel. For this purpose three shorting pins are included to connect the capacitors to the ground. A 0.3pF capacitor was placed on the feeding line between the port and the antenna. The circuit diagram is shown in Fig. 6.7. The simulated and measured reflection coefficient is shown in Fig. 6.8. The measured resonance frequency matches the predicted one in the simulated model. However, the measured -10dB impedance bandwidth is larger than the expected bandwidth. The difference is believed to be due to the added loss through the prototyping procedure. The four ground connecting vias in this circuit result in more loss and bandwidth.

Table 6.2 Calculated element values for the high pass  $\Pi$  network at 8GHz.

| Reactance ( $\Omega$ ) | Corresponding value at $f=8\text{GHz}$ |
|------------------------|--|
| $X_1 = 13.14$          | $L_1 = 0.26 \text{ nH}$                |
| $X_2 = -44.61$         | $C = 0.44 \text{ pF}$                  |
| $X_3 = 160$            | $L_2 = 3.18 \text{ nH}$                |

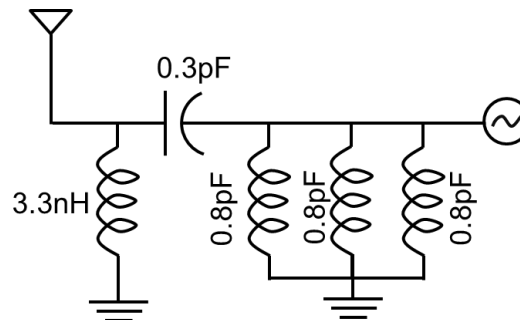


Fig. 6.7 Tuning circuit diagram for 8GHz.

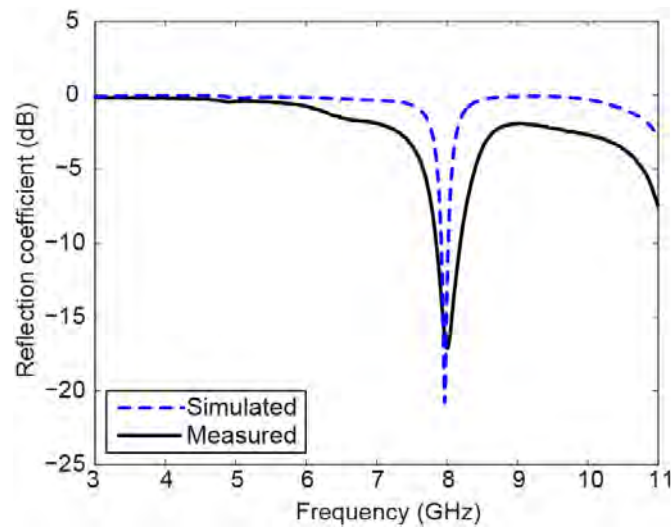


Fig. 6.8 Simulated and measured reflection coefficient of the antenna with a 8 GHz matching circuit.

### **6.2.3.3 10 GHz-Reversed High Pass L Network**

To cover the higher end of the UWB band a two-element network is designed to tune the narrowband antenna to 10GHz. The element values for a reversed high pass L network are calculated and shown in Table 6.3. In the actual circuit a 0402 Coilcraft 0.8nH chip inductor was shorted to the ground as the shunt element and an AVX 0603 0.1pF capacitor is placed in



the gap on the feeding line between the connector and the antenna as the series element. The circuit diagram with final values is shown in Fig. 6.9. The measured and simulated reflection coefficients are compared in Fig. 6.10. Unlike the other two circuits 900MHz difference is observed between the results. This might be due to other unknown parasitics of the elements which are not considered in the simulation. Since the elements are not placed with a pick and place machine on the PCB, positional errors also might give rise to this discrepancy. The hand-made grounding vias can increase the loss and change the reactive values in each branch.

Table 6.3 Calculated element values for the reversed high pass L network at 10GHz.

| Reactance ( $\Omega$ ) | Corresponding value at $f=10\text{GHz}$ |
|------------------------|---|
| $X_1 = 52.85$          | $L = 0.84 \text{ nH}$                   |
| $X_2 = -116.77$        | $C = -0.13 \text{ pF}$                  |

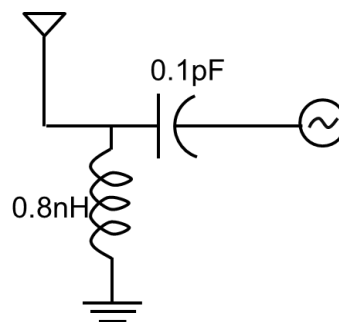


Fig. 6.9 Tuning circuit diagram for 10GHz.

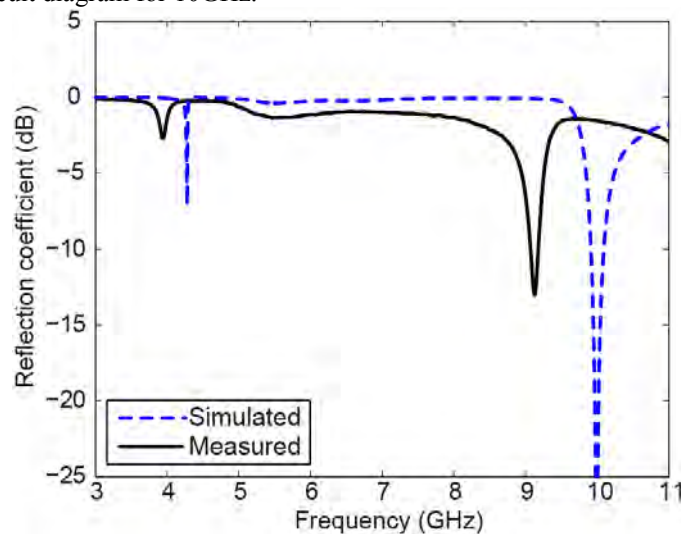


Fig. 6.10 Simulated and measured reflection coefficient of the antenna with a 10 GHz matching circuit.

### 6.3 Discussion

It is important to note that since external matching circuits were used in this study the wideband matching was not affected by the narrowband matching networks.

Table 6.4 compares the total efficiency and realized gain of the tuning circuit when integrated with the original antenna. The total efficiency is defined as the ratio of radiated to stimulated power. The difference between the input power and the stimulated power is that the latter includes any reflections that may occur at the feeding location. The realized gain includes this impedance mismatch loss and is defined by  $G \cdot (1 - S_{11}^2)$ , where  $G$  is the IEEE gain defined in [3]. The antenna becomes electrically larger as the frequency increases, and so the efficiency and gain increase. However, at lower frequencies the structure is electrically small and the level of total efficiency and realized gain is lower which agrees with the Chu-Harrington expression.

In developing and analysing the tuning networks for this structure several issues have been taken into account. A low pass network was chosen for matching at 4GHz in which the series inductor in the circuit filters out the higher frequency resonances. Similarly, at high frequencies a high pass structure with a series capacitor is more suitable for suppressing any low frequency resonances. The circuits were all manufactured manually and no pick and place technique is used in the manufacturing procedure. Considering the small dimensions of

Table 6.4 Efficiency and gain of various narrowband antennas.

|           | Efficiency<br>(%) | Realized gain*<br>(dB) |
|-----------|-------------------|------------------------|
| 5.15GHz** | 54.6              | 0.6                    |
| 4GHz      | 37.2              | 0.2                    |
| 8GHz      | 56.7              | 1.9                    |
| 10GHz     | 75                | 4.4                    |

\* Realized gain = Gain  $\cdot (1 - S_{11}^2)$  \*\* Original antenna

the components, accurately placing them on the feeding or between the feeding and shorting pins and soldering them were challenging. Therefore, errors in the components placement was inevitable. Due to practical limitations in prototyping of the antennas at the time, the ground connecting pins were also inserted manually by drilling through the board and filling them with thin wires. Moreover, the tolerances in the values of components when added to the other effects might be considerable. Although the best effort was made to include all the available information about the frequency behaviour of the elements in the circuit simulation, there might be still unknown effects which were not modelled.

Although the focus of this study was narrowband reconfigurability, specifically for this antenna configuration the matching circuits can also be of benefit in the design procedure. Given that the narrowband antenna is a resonant structure; its operation frequency is determined by its dimensions. Subsequently, for lower frequencies the required dimensions grow and therefore designing the antenna becomes challenging. Specifically for PIFA monopole combination, if the size of the PIFA plate is increased the dimensions of its ground plane, i.e. monopole in this case also needs to be increased which might not be feasible in some applications. In such cases, one solution can be to design the antenna for higher frequency with affordable dimensions and then tune it down to the desired frequency via a matching circuit.

## **6.4 Summary**

The hybrid wideband-narrowband antenna supports two fixed modes of operation. The frequency agile functionality would add to the versatility of the antennas performance. In this chapter the possibility of tuning the narrowband antenna by means of an external matching circuit and maintain the wideband operation is demonstrated. Three sets of lumped elements tuning circuits were designed and examined. To cover the various types of circuits, a low pass L network for 4GHz, a high pass  $\Pi$  network for 8GHz and a high pass reversed L network for 10GHz were developed and examined.

## References

- [1] J. T. Bernhard, *Reconfigurable Antennas*, Morgan and Claypool, ISBN 9781598290271, 2007.
- [2] C. Bowick, *RF Circuit Design*, Newnes, ISBN 0-7506-9946-9, 1982.
- [3] IEEE standard definitions of terms for antennas, June 1983.

# **Chapter 7    Device    Integrated    Printed    UWB**

## **Antenna**

### **7.1    Introduction**

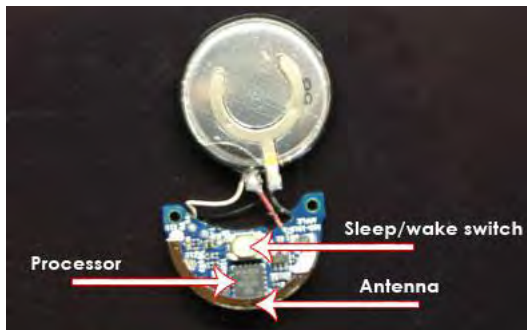
The recent advances in wireless technology have had a huge impact on our life. The mobile phone is no longer one of the modern technology's wonders. Wireless technology is nowadays utilized in various applications such as health and care systems, home media networks, logistics and security. Antennas play the key role in wirelessly enabled devices. Depending on the application, the antennas need to have certain characteristics. Their size and shape are mostly influenced by the *form factor* of the device. First generation wireless devices normally have external antennas. As the demand for an aesthetic industrial design (ID) increases, so does the trend towards device-integrated antennas. "Internal", "embedded" or "device-integrated" antennas are designed to fit inside the device casing. Selecting a suitable antenna concept involves considering both the system technical requirements and the device physical requirements. In other words, in order to ensure device optimal performance, it is important to take into account several parameters such as the device volume, shape and form factor. For instance, the Nike+ iPod sport set [1] has two components; a sensor and a receiver, both of which are about a 2.5 cm long (see Fig. 7.1). The sensor fits into a small space under the insole of a Nike+ shoe. The receiver plugs into an iPod Nano. A planar inverted F antenna

(PIFA) is fit into the shoe sensor, however for the receiver which is packed with RF and electronic components a chip antenna is used. Importantly, for mass produced products all components including antenna need to be light and inexpensive.

Considering that the antenna is a radiating device that interacts with other components in its vicinity, it needs to be customized to operate in a specific assembly of different components in the device. In this stage the size of the device determines the complexity of the antenna integration procedure and the possible antenna technology. These basic rules are applicable to all wireless technologies and there is no exception for UWB communication.



(a)



(b)



(c)

Fig. 7.1 (a) The Nike+ iPod sport set (b) a PIFA antenna on the sensor component (c) chip antenna on the receiver [2].

In previous chapters some of the capabilities of the UWB technology have been pointed out. Benefiting from low power communication and large bandwidth UWB communication offers both performance and high data rate to a wide range of applications from military to commercial products [3],[4]. Various types of UWB antennas have been

studied in the literature [5]-[11]. Taking into account the costs, size, manufacturing technology and technical requirements, certain antenna solutions might be preferred. With the increasing demand for smaller wireless devices in recent years, small-size UWB antennas have received a considerable amount of attention [7]-[11].

Typically, the antenna characteristics are investigated in an ideal “isolated scenario” in which the effect of other structures in the vicinity of the antenna is undermined. However, ultimately the antenna must be mounted close to a (plastic) casing, camera, and/or battery, or onto a PCB. This case is addressed as “integrated” or “device-integrated scenario” in this chapter. As mentioned earlier, for proper integration of the antenna within the industrial design, one should take into account a variety of factors to ensure optimal device performance. Each application also introduces various restrictions for the antenna design and integration.

In some cases the designers can benefit from the structure of the final industrial design. Recently there has been significant increase in the number of radio systems built in handheld devices. Due to physical limitations, designing antennas for services such as digital TV (DTV) is very challenging. In order to avoid large and external antennas for such applications, a well-known technique is to excite the device PCB by a simple coupling element [12]. The coupling element introduces resonances across the length of the PCB. Studies show that the interaction between the antenna and the mobile phone chassis is quite strong. Hence, the antenna needs to be designed together with the chassis [13].

UWB antennas on the other hand are mostly designed without considering the mounting platform. This results in further modification after integration. Thevenard et. al in [14] suggested using a four sector Vivaldi antenna on a television camera shown in Fig. 2. They placed the antenna which occupies a volume of 90 mm × 90 mm × 39 mm at the rear of the camera. Despite choosing a relatively quiet location for the antenna, the camera structure affects the antenna radiation. The multi sector antenna radiation patterns are tilted when integrated. They also are more directive when compared to the isolated case (see Fig. 7.2).

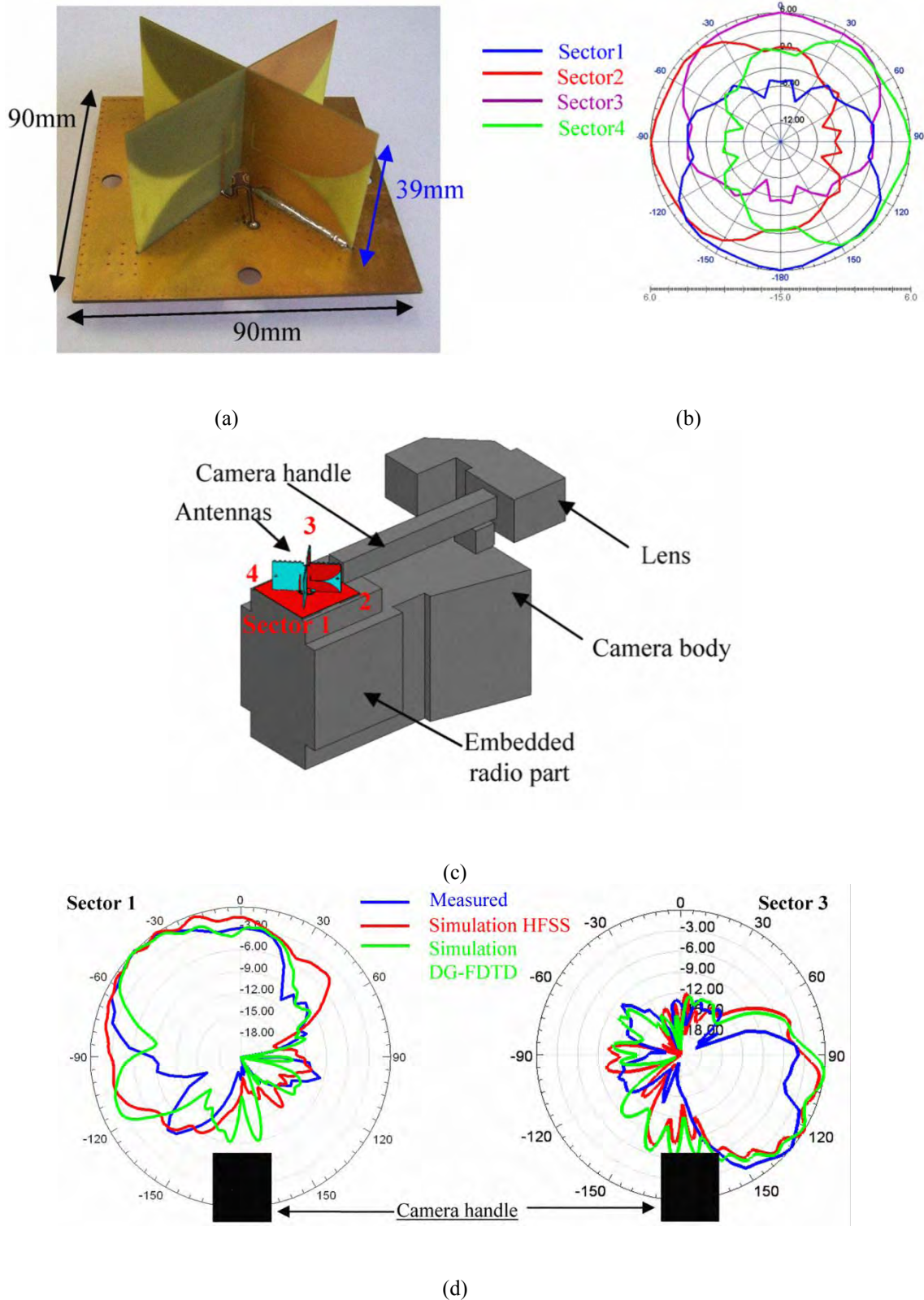


Fig. 7.2 (a) Four sector Vivaldi antenna, (b) isolated antenna radiation pattern, (c) the four sector Vivaldi antenna mounted on a television camera (d) integrated antenna radiation patterns [14].

In [15] a vertical UWB monopole is integrated into the casing of a home entertainment device, a DVD player, as depicted in Fig. 7.3. The integration mainly affects



the radiation patterns. Despite of having a quasi-omnidirectional pattern in the isolated case the antenna shows a strong directive pattern in the integrated case. In this case the internal volume of the DVD player box is utilized to accommodate the antenna and its ground plane. However, the bulky structure and the need for a reasonable size ground plane limit the application of vertical monopole antennas for integration in small and thin devices.

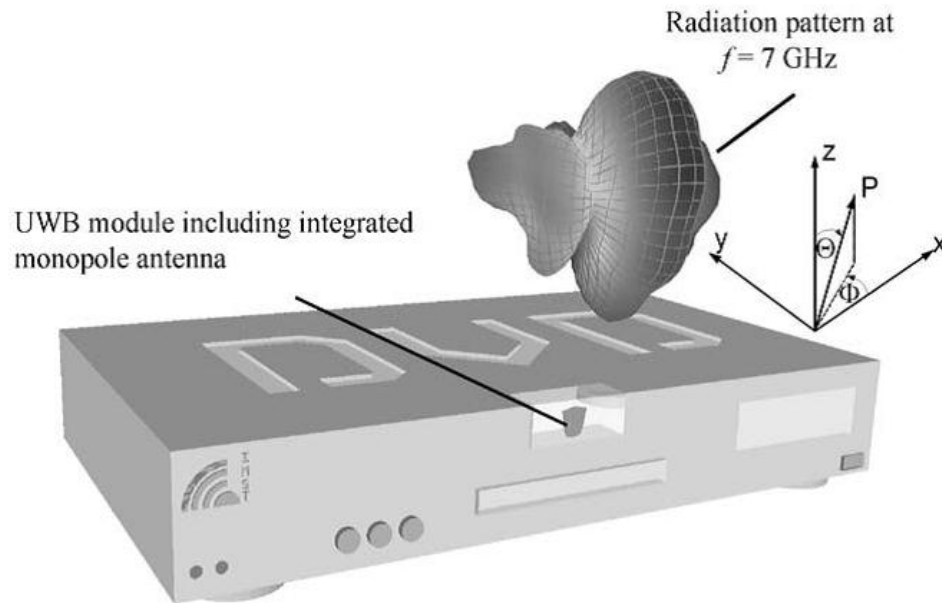


Fig. 7.3 UWB mono-cone antenna integrated into a DVD player and the calculated radiation pattern at 7GHz [15].

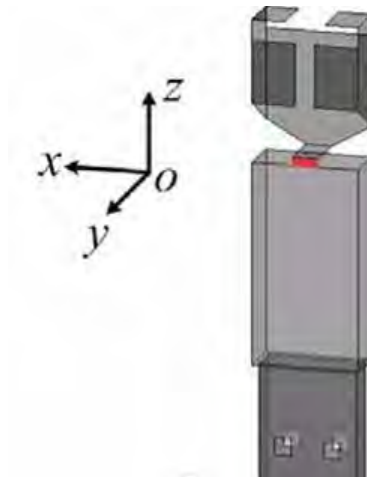


Fig. 7.4 Internal 2.4 GHz UWB antenna for wireless dongle applications [16].

A small internal UWB antenna for a USB dongle was proposed in [16]. The antenna is a folded radiator with bent stubs mounted on the top of the PCB. The integrated antenna is

shown in Fig. 7.4. The interaction between the antenna and the PCB were controlled by covering the PCB with a small grounded metal box. This technique might solve the PCB and antenna interaction; however, the metal box contributes to the radiation as the antenna ground plane. Furthermore mass producing a folded antenna might not be very cost effective. Unlike folded monopoles and vertical monopoles, printed UWB antennas are low profile and suitable for compact devices. Such antennas provide good radiation characteristics while they are low cost and easy to manufacture.

As it has been discussed in previous chapters, the operation principle in printed UWB monopole antennas is based on the overlapping of the closely distributed resonance modes. At low frequency the antenna operates in a standing wave mode. With increasing frequency, the antenna operates in a hybrid mode of standing and travelling waves. At high frequencies, the travelling wave becomes more critical to the antenna operation. The structures formed by the lower edge of the radiating element and the upper edge of the ground plane support the travelling wave [11]. This implies that other than the main radiating element, the ground plane also contributes to the radiation. Thus, varying the dimensions and shape of the ground plane alters the antenna matching. This makes such antennas ground-dependant. Furthermore, when measuring the antenna characteristics, the currents on the ground plane leak to the measurement cable. Consequently the cable radiates and influences the measurement. Several techniques are reported in the literature to overcome this problem [17]- [32]. A well-known method is to use ferrite magnetic chokes to suppress the currents on the cable (see Fig. 7.5) [17]. By introducing two leakage blocking narrow slots on the antenna ground, the currents can be controlled, but not completely stopped [18]. If an omnidirectional symmetrical radiation pattern is not the system requirement, the ground surface currents can be reduced by asymmetrically feeding the antenna. In [32], the antenna is fed asymmetrically and a notch is cut off from the radiator while a strip is asymmetrically attached to the radiator.

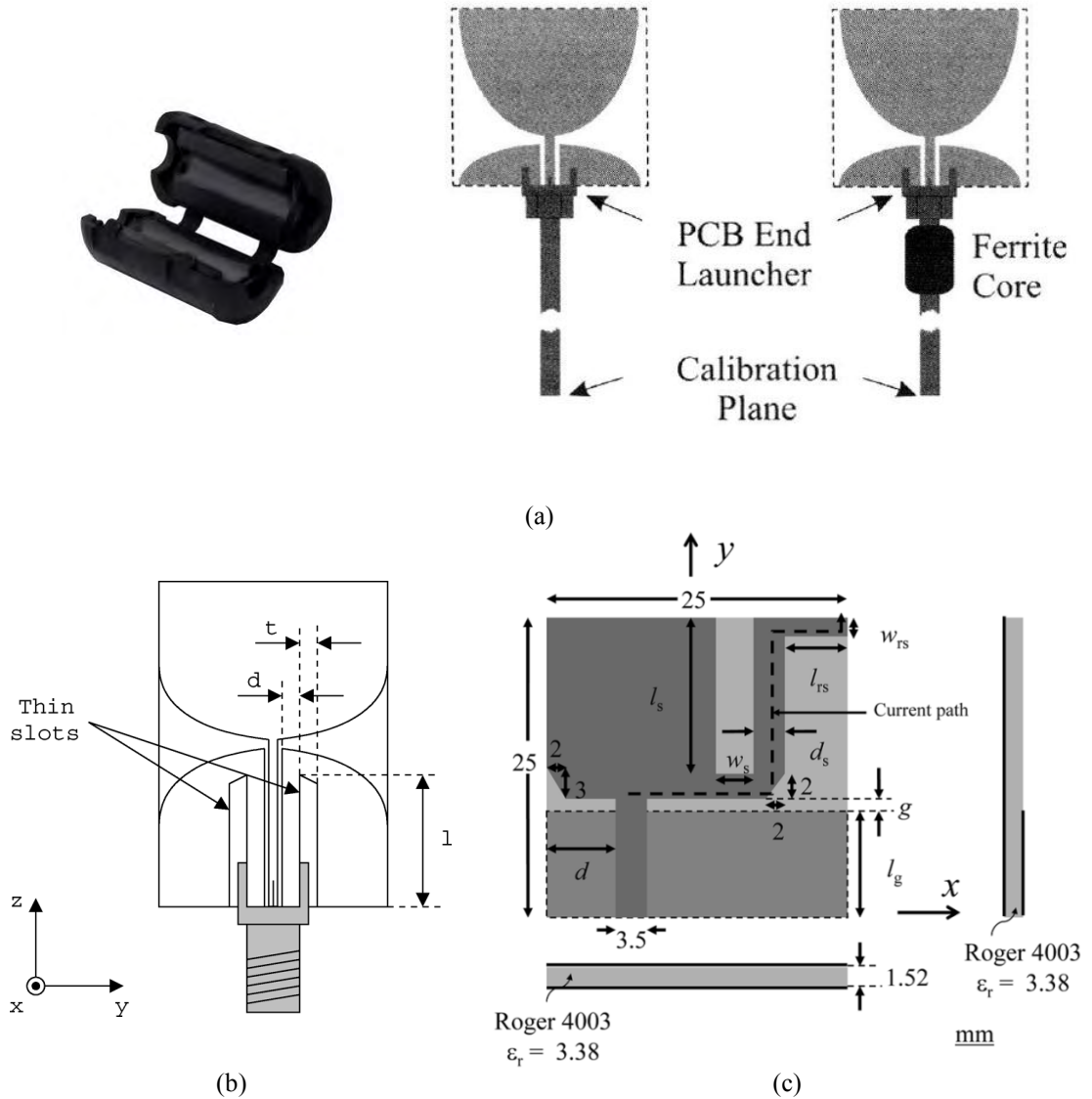


Fig. 7.5 Reported solutions for ground plane surface current in UWB antennas. (a) Ferrite choke [17] (b) ground plane slots [18] (c) asymmetric feeding and radiator [32].

Ferrite chokes cannot be used when the antennas are integrated into the device. However, by some modifications the other two methods can be very useful for suppressing the unwanted RF currents in integrated cases. In integrated scenarios if the currents are not suppressed properly, further electromagnetic compatibility (EMC) problems might occur [31]. Like [16] the PCB can be covered by a metal box to avoid EMC problems. However, in that case the antenna excites the metal box or the chassis. Unlike mobile terminal antenna design [12], [13], chassis excitation is not desired in UWB applications. Chassis excitation would result in multiple radiation points on the structure and consequent alteration of radiation

parameters. Hence, PCB or chassis originated resonances caused by RF interaction of the antenna and its surrounding need to be controlled in UWB applications.

In order to attenuate the RF currents, methods such as defect ground structures (DGS) [20], [21] and electromagnetic band gap (EBG) materials [22] have been utilised in the literature. A DGS structure operates as a low pass filter stopping the high frequency signal and an EBG structure is basically a notch filter that stops the specified frequency band. These structures might be costly and add to the complexity of the design. The “RF choke” or “wavetrap” is also another method to block the unwanted RF currents. It is widely used to prevent RF signal from flowing in the DC bias circuits. The RF choke is usually implemented by distributed elements. High impedance points implemented by short-circuited quarter-wavelength transmission lines can enforce current minima and reduce the flow of RF currents. RF choke structures are also used in antenna design for improving antenna performance, such as bandwidth enhancement, multiple band operation, gain enhancement, and the radiation pattern shaping. The sleeve (or bazooka) balun for dipole antenna feed is a best example of using the short-circuited quarter-wavelength coaxial cable as an RF choke [23]. A similar technique was also used in horn antennas- the coaxial cable choke was used to prevent the current from flowing over the outer conductor of the horn [24]-[26]. These chokes mounted on horns can improve the radiation patterns [24], [25] or enhance the antenna gain [26]. Furthermore, a combination of ring chokes and EBG structures to reduce the surface wave for a good radiation pattern was presented in [27], [28]. Since the RF choke can change the current resonant length, the concept was also adopted to achieve multiband or wideband operation. In [29] a choke, formed by a short-circuited quarter-wavelength microstrip stub, was introduced to divide a monopole antenna into two sections so as to create two resonant paths and thus achieve dual band operation. In [30] a bandwidth enhancement technique for mobile phone antennas was developed by introducing a quarter-wavelength choke to the chassis edge. By accurately determining the position of the choke, the bandwidth can be improved dramatically.

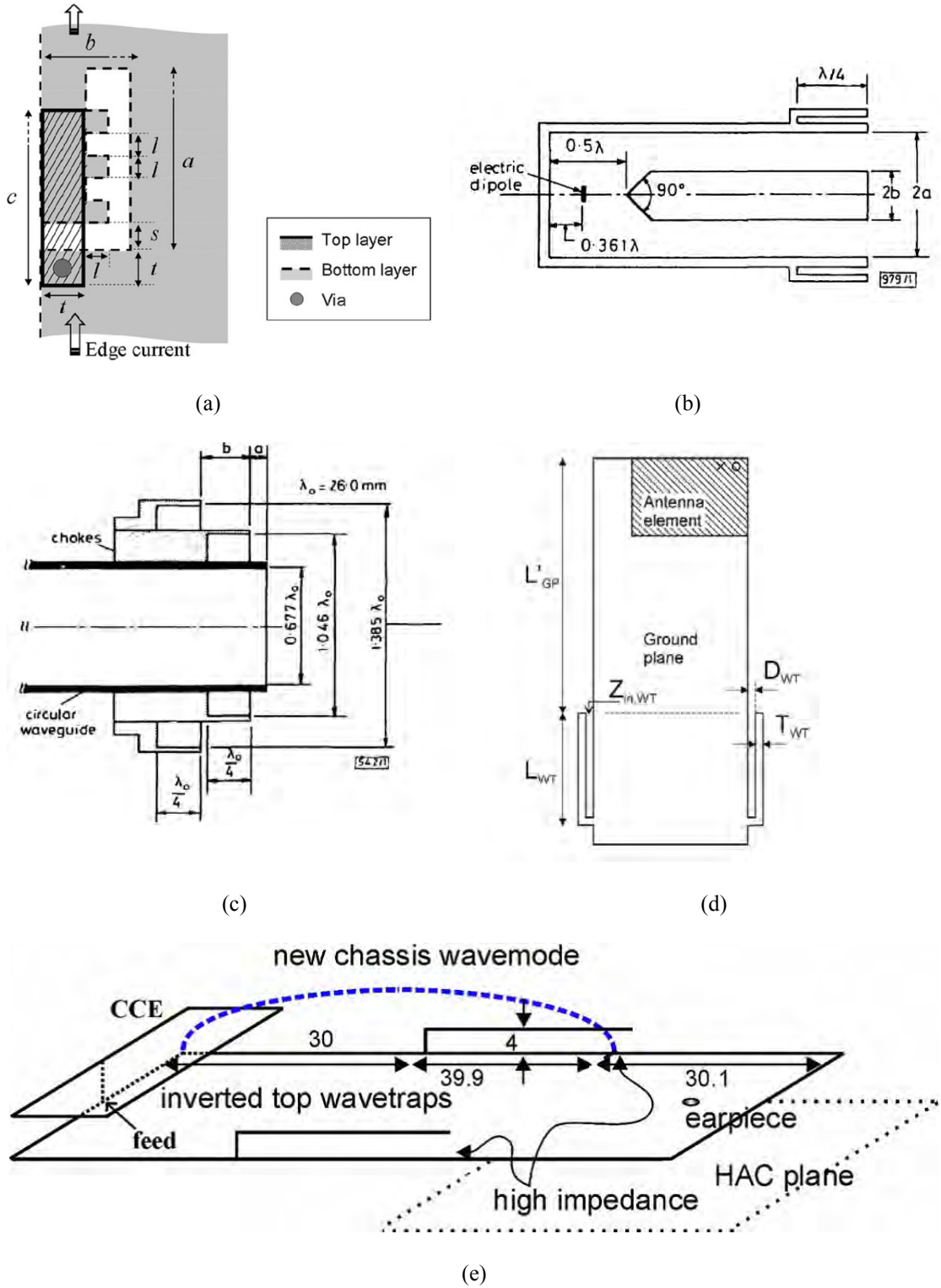


Fig. 7.6 (a) edge current RF choke [32] (b) coaxial cable RF choke [23] (c) RF chokes on horn antenna [25] (d) RF choke on handset antenna [30] (e) RF choke on handset antenna [31].

In mobile phone application a pair of RF chokes is also used to control the near-fields of a mobile terminal antenna [31]. The local reduction of the near-fields is especially important for the operation of the hearing aid of the user. The reshaping of the near-fields may also enable reduced specific absorption rate (SAR) values [31]. In [32] an RF choke is

implemented using a printed inductor and a capacitor. This choke can be fabricated on the periphery of the PCB ground plane for surface current blocking and thus shaping the ground edge current. Most of the above mentioned methods (some shown in Fig. 7.6) are useful for certain type of applications. Thus, it is important to consider the system requirements and limitations when developing the integrated antenna.

An antenna is required for indoor positioning application. High data rate, low equipment costs, multipath immunity, high penetration capability and low power consumption are the outstanding features of UWB technology and make it suitable for indoor positioning. The positioning procedure is based on radio ranging which basically is measuring the distance between two terminals by recording the time of transmitted and received signal and then converting them to distance.

The received signal arrives after a delay that is proportional to the distance it has travelled, so each time a signal goes from one unit to another the distance between them can be measured. Given the distances from one mobile unit to several other “reference” units at known positions, as well as the positions of all the references, the mobile unit can be located by triangulation. Multipath does not affect the UWB positioning accuracy since the direct pulses are received prior to the reflected pulses and therefore they can be detected easily.

In this chapter the integration of a UWB antenna into a device PCB will be studied. This follows the studies on UWB antennas in the previous chapters. To keep it consistent a printed CPW fed UWB antenna has been selected as the basis of this integration. A relatively large PCB represents the device PCB. The antenna feeding mechanism and its ground-dependant behaviour need to be customized for the purpose of integration. In order to mitigate the unwanted effects of surface currents on the edge of the PCB, two pairs of shorted RF chokes are introduced into the design. By creating current minima the RF chokes reduce the PCB contribution to the radiation. The important parameters which affect the antenna performances will be investigated both numerically and experimentally. This study is carried out for the European UWB frequency mask, which is partly focused on the frequencies between 6-8.5 GHz [33].

## **7.2 Antenna Design**

In order to model the device-integrated antenna in this study, the antenna is placed on a 100 mm by 160 mm PCB. For the indoor position application the system has the following key requirements:

- the operating frequency band is the European UWB mask i.e. 6-8.5 GHz.
- the antenna should occupy the smallest space possible within the device.
- the PCB should have a minimal effect on the antenna radiation performance.
- the antenna should have a quasi-omnidirectional radiation pattern in the plane in which the PCB is situated.
- the antenna should possess a fairly constant group delay across the frequency range of interest.

In this section, the antenna concept selected for this study is briefly reviewed and then the integrated structure is presented. The antennas have been modelled using the finite-difference time-domain (FDTD)-based field solver EMPIRE™ [34].

### **7.2.1 The Isolated Antenna**

Similar to the previous chapter, for this application a printed CPW fed circular disc monopole antenna is selected [7]. The antenna is printed on the top layer of the PCB. The geometry of the antenna structure is depicted in Fig. 7.7. The dimensions such as disc radius, width and length of the antenna ground plane sections and the feed gap are optimized to achieve -10 dB input impedance matching across the 6-8.5 GHz band. The antenna is designed on a RO4350B substrate with 1.52 mm of thickness and  $\epsilon_r=3.48$ .

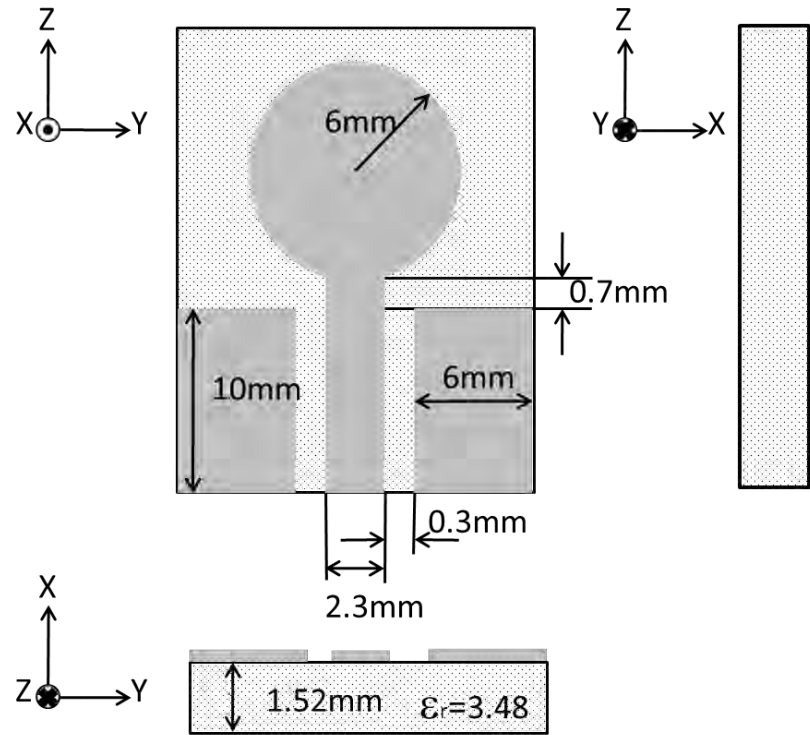


Fig. 7.7 The geometry of the isolated antenna.

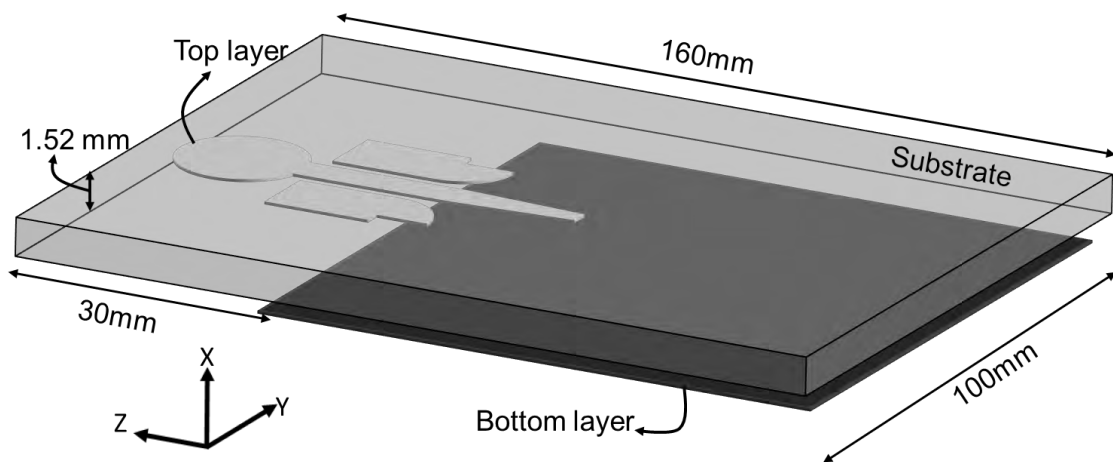


Fig. 7.8 The 3D view of the integrated antenna.

## 7.2.2 Antenna Integration with the PCB

### 7.2.2.1 Feeding Mechanism

The 3D view of the integrated antenna is depicted in Fig. 7.8. The antenna is printed on top of the substrate and the bottom layer is the ground. In order to maintain the



symmetrical radiation pattern, the antenna symmetry line is aligned with the vertical symmetry line of the board. The metal layer of the top 30 mm by 100 mm part of the PCB is removed from the bottom side of the substrate in order to accommodate the antenna on the top side. The geometry and dimensions of the antenna are demonstrated in Fig. 7.9.

The antenna needs to be eventually connected to the off-the-shelf RF components on the board. Therefore, it is required to specially design a proper feeding mechanism. To achieve that, the CPW ground sections and centre strip conductor are extended to form a conductor-backed CPW (CBCPW) [35]. Fig. 7.10 is the schematic of a CBCPW. The CBCPW is basically a CPW with a lower ground plane. In order to attain a good matching the size and shape of the CPW ground sections are smoothly modified. The centre strip is then further extended and linearly tapered to get a  $50\Omega$  microstrip line. Fig. 7.11 shows the electric field variation at each section along the CPW to microstrip transition. In the microstrip line section, the electric field lines are mostly vertical as terminating perpendicularly at the ground of the substrate as shown in the A-A' plot. In the CPW section, the electric field lines are mostly horizontal and concentrated between the centre strip and two ground strips as shown in C-C'. In order to gradually match the field distributions between the microstrip line and the CPW, a CBCPW (B-B') is inserted. In this feeding technique there is no need to directly connect the antenna ground to the PCB.

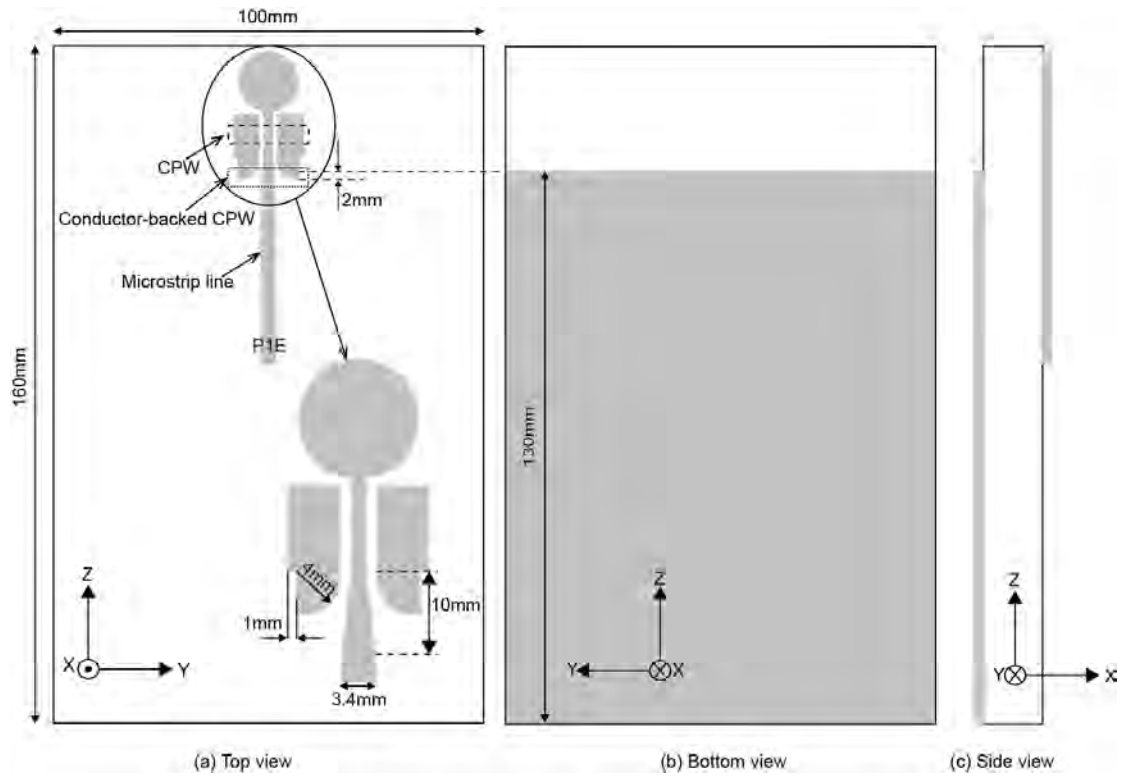


Fig. 7.9 The geometry of the antenna integrated with PCB. (The dotted rectangles represent areas of conventional CPW and conductor-backed CPW)

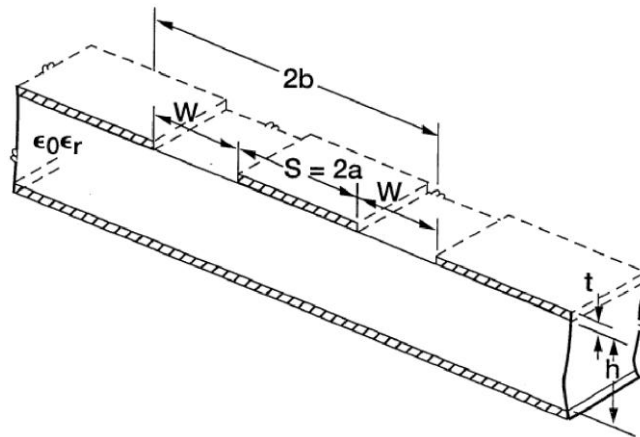


Fig. 7.10 Schematic of conductor-backed CPW on a dielectric substrate of a finite thickness [35].

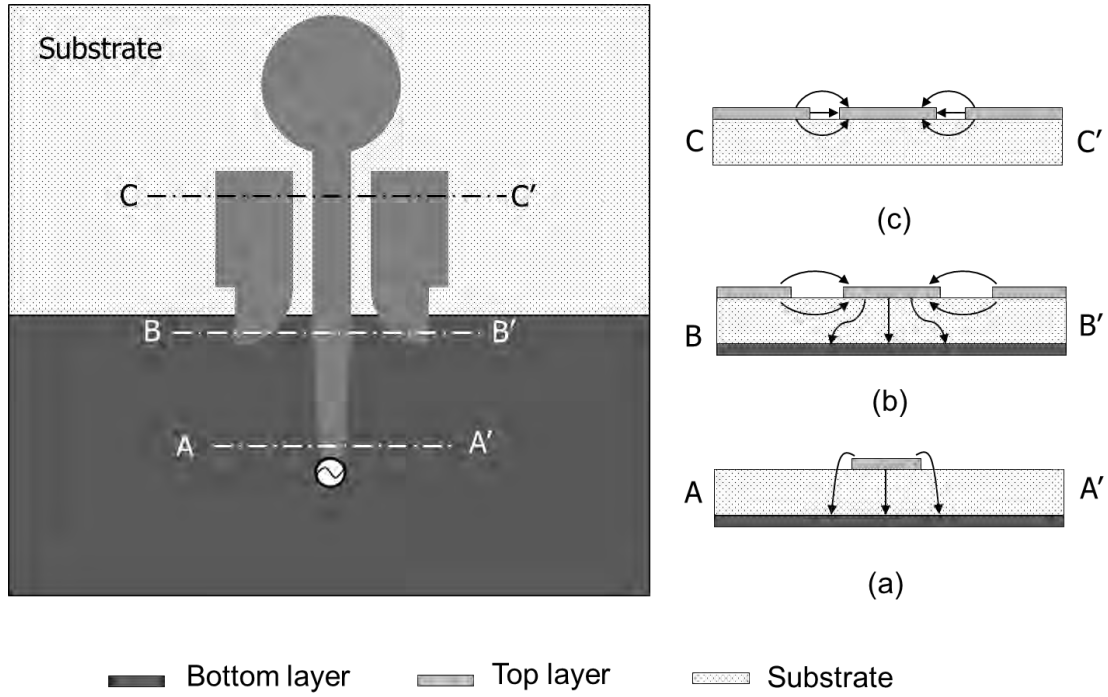


Fig. 7.11 The CPW to microstrip transition feeding. Electric field at each cross-section along the transition, (a) microstrip, (b) CBCPW, (c) CPW.

#### 7.2.2.2 RF Chokes

Once the antenna is integrated, it is possible to study the interaction between the antenna and PCB. Fig. 7.12 shows the surface current distribution in the integrated scenario at 7.25 GHz. There is high concentration of currents on the edge of the PCB. Thus, this structure is very ground dependent. To simplify, the arrangement can also be thought of having similarities to an asymmetrically fed dipole (see Fig. 7.13a). In this case, the current distribution is a combination of a standing and travelling wave [36]. The travelling wave mode affects the radiation pattern, in that the pattern is more directive towards the longer leg of the dipole. In order to reduce the PCB contribution to radiation it is important to force the currents to be concentrated around the antenna (see Fig. 7.13b). For this reason, two pairs of short circuit transmission lines, RF chokes, are printed at the top short edge of the PCB symmetrically. The currents on the PCB encounter a high-impedance interface at the open ends, enforcing current minima. The idea is similar to the well-known coaxial sleeve (or bazooka) balun [37] that chokes the unbalanced current flowing on the outside of a feeding coaxial cable.

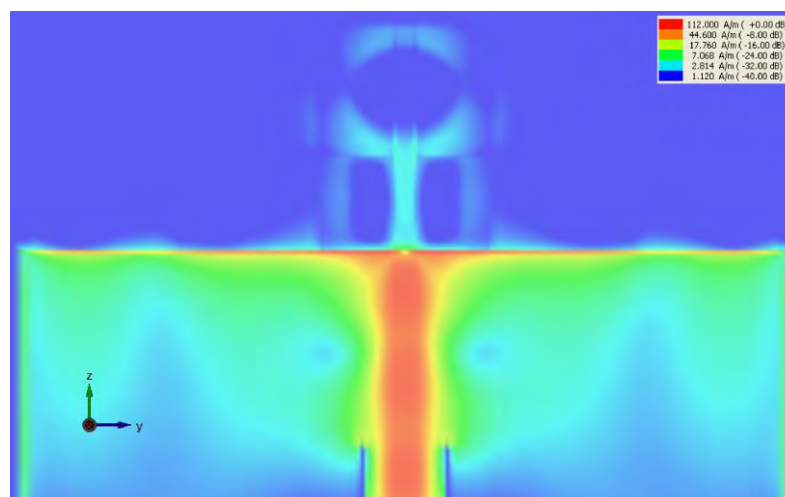


Fig. 7.12 Surface current distribution on the ground plane of the integrated antenna at 7.25 GHz.

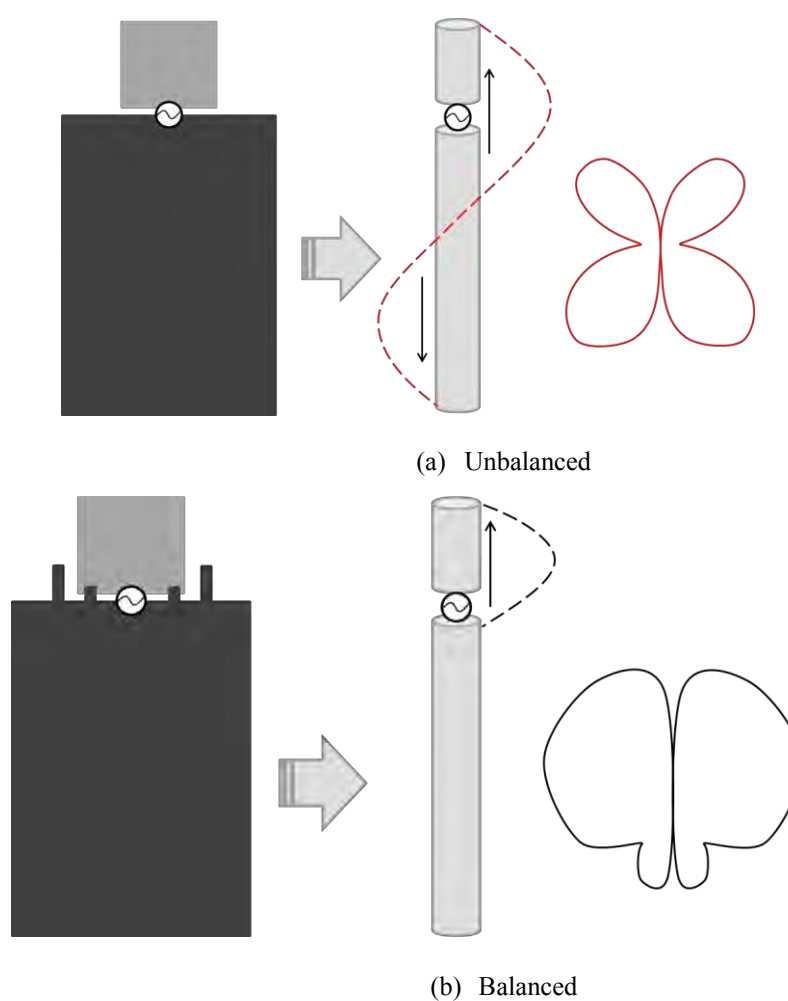


Fig. 7.13 Modeling the integrated antenna with an asymmetrically-fed dipole.

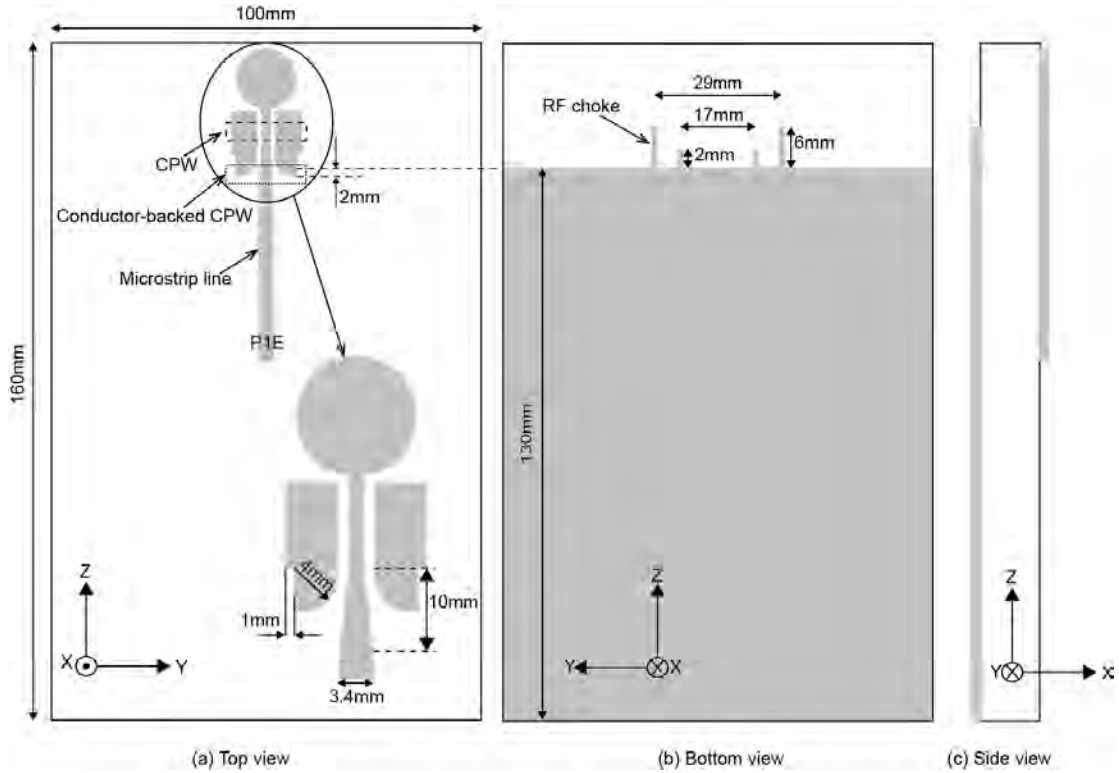


Fig. 7.14 The geometry of the antenna integrated with PCB with RF chokes.

In determining the length and positions of the chokes, it is required to maintain the good matching and stable gain and radiation pattern of the original antenna. Therefore, in this application the filtering function of the chokes is not desired. The goal is to concentrate all the radiating currents around the antenna and avoid scattered radiation points around the PCB. In order to cover the whole band of interest (6-8.5GHz) two pairs of shorted transmission lines are printed on the PCB side of the structure. The longer pair is further away from the centre and feeding. It suppresses the low frequency currents on the PCB. The shorter pair is closer to the centre where high frequency field coupling is stronger.

Extensive simulations were conducted in order to find a trade-off between the matching, stable gain and omni-directional radiation patterns. The best result was achieved when the length of the longer pair was a quarter of the guided wavelength at 6 GHz and the shorter pair was less than a quarter of the guided wavelength at 8.5 GHz. The dimensions of the final antenna with the RF chokes are presented in Fig. 7.14. In the next section the effects of integration and RF choke utilization are discussed.

## 7.3 Analysis

In this section the isolated antenna characteristics are compared with the PCB integrated antenna. The effectiveness of the RF chokes is also studied in this section.

### 7.3.1 Surface Currents

Once the antenna is integrated with the PCB, incorporating the RF chokes helps to electrically shorten the surface currents paths on the edge of the PCB. The surface current distributions on the PCB in the integrated antenna with RF chokes are shown in Fig. 7.15. Comparing Fig. 7.12 and Fig. 7.15, it is clear that by using RF chokes it is possible to concentrate the currents around the antenna and not the PCB.

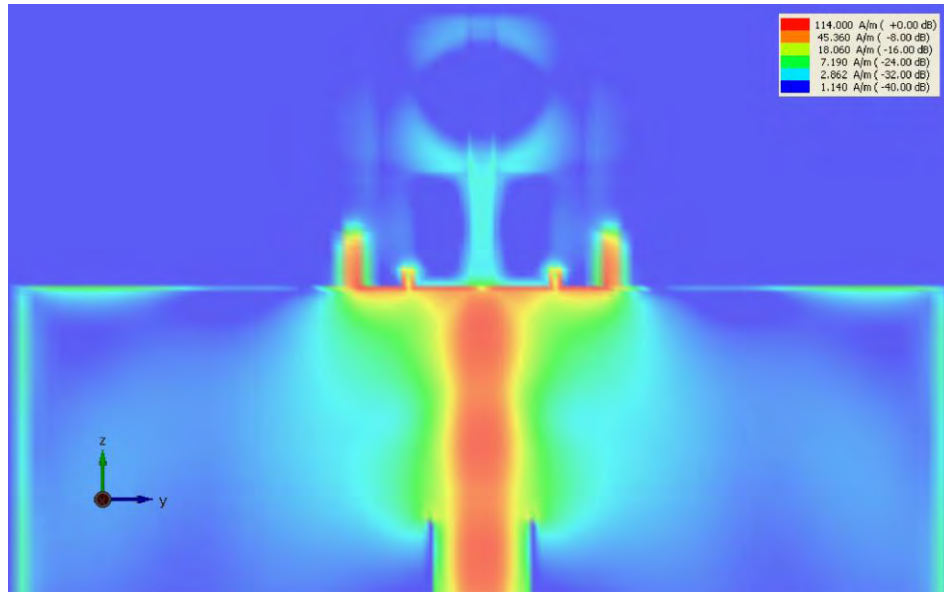


Fig. 7.15 Surface current distribution on the PCB for integrated antenna with RF chokes at 7.25GHz.

### 7.3.2 Impedance Matching

The reflection coefficients of the antenna in isolated and integrated scenarios are compared in Fig. 7.16. The required -10 dB impedance bandwidth is satisfied in all cases for the required bandwidth i.e. 6-8.5GHz. However, it can be observed that the matching is affected by the integration. The overall bandwidth has reduced, and new resonances have

appeared in the reflection coefficient curve. RF chokes enhance the integrated antenna bandwidth at high frequency.

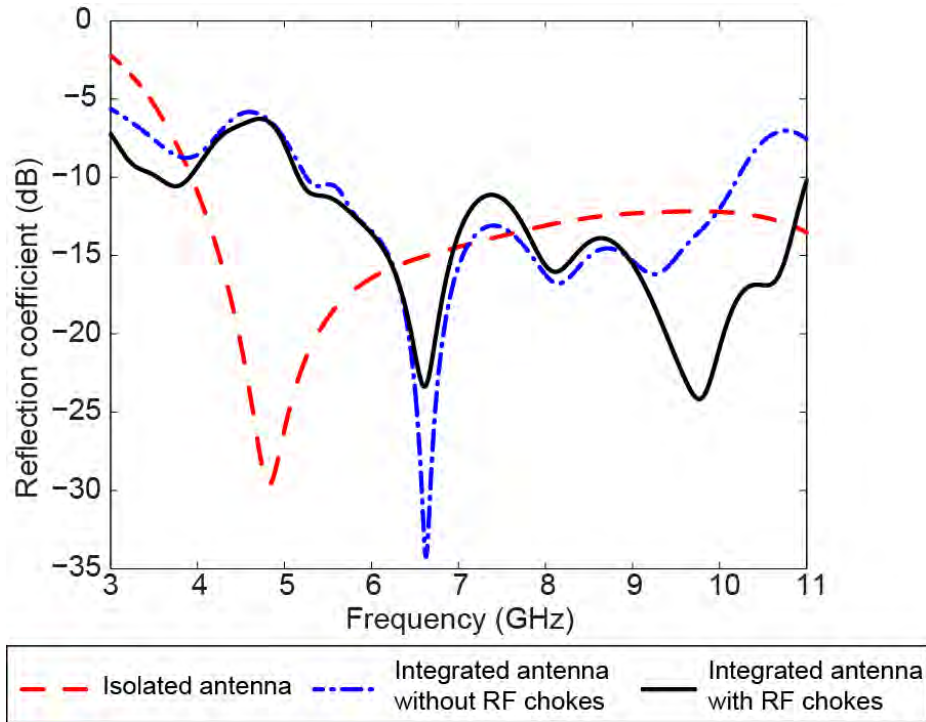


Fig. 7.16 Simulated reflection coefficients of the isolated antenna and integrated antenna with and without RF chokes.

### 7.3.3 Radiation Pattern

As expected, the integration process alters the radiation patterns [14]-[16]. Fig. 7.17 compares the simulated gain patterns of the antenna in an isolated and integrated scenario with and without RF chokes at 6, 7.25 and 8.5 GHz. It is required that the antenna has stable gain and omni-directional pattern across the 6-8.5GHz band. In the  $H$ -plane, there are improvements in the pattern at all frequencies when utilizing the chokes. For the integrated antenna without chokes, the pattern variation increases with the increase of frequency. Introduction of higher modes are clearly visible at 8.5 GHz. In the  $xy$ -plane the radiation pattern of the antenna without chokes has got two dips at  $\phi=\pm 90^\circ$  which are in the direction of the PCB edge. However, the dips disappear when the chokes are utilized confirming that the currents at the edges are reduced. Comparing the  $H$ -plane patterns, the chokes successfully stabilize the pattern across the frequency band. In the  $E$ -plane, the integration results in

Table 7.1 Gain variations for the three cases.

|                                      | Min<br>(dBi) | Max<br>(dBi) | Diff<br>(dBi) |
|--------------------------------------|--------------|--------------|---------------|
| Isolated antenna                     | -0.56        | 4.58         | 5.15          |
| Integrated antenna without RF chokes | -8.93        | 1.03         | 9.97          |
| Integrated antenna with RF chokes    | -1.84        | 2.86         | 4.71          |

slightly directive patterns at all frequencies. It also introduces dips at  $\theta=\pm 90^\circ$ . However, the patterns can be smoothed to some extent and improved to look more similar to the isolated antenna patterns by using the chokes. Fig. 7.17 also shows that chokes improve the back radiation in the  $xz$ -plane. Overall, it can be confirmed that employing quarter wavelength chokes reduces the effect of the PCB surface currents in all planes of observation.

The simulations also show that (not presented here) the level of cross-polar component is higher in integrated case comparing to the isolated case. We interpret this due to the increase in the overall size of the complete structure.

#### **7.3.4 Gain**

A stable gain across the frequency band of interest (6-8.5 GHz) and in all directions is one of the main advantages of the small printed UWB monopoles. Therefore, it is important to maintain this characteristic to some extent after the integration. The gain-frequency and angle plot in the horizontal plane ( $\theta=90^\circ$ ,  $0<\varphi<360$ ) is displayed in Fig. 7.18.

The isolated antenna has a nearly omni-directional gain pattern (see Fig. 7.18a). Fig. 7.18b shows the gain versus frequency and angle for the integrated antenna without RF chokes. The integration clearly affects the antenna gain pattern. Comparing with the isolated antenna for the 6-8.5 GHz band, gain drops significantly. The minima are at  $\varphi=\pm 90^\circ$ . Fig. 7.18c demonstrates the gain improvement after introducing the RF chokes in the design. Across the frequency range of interest, the gain has increased. It shows fairly stable gain for 6-8.5 GHz and along various directions and more than 50% improvement was achieved



comparing to the integrated case without chokes (see Table 7.1). Table 7.1 shows the minimum and maximum values in all planes/

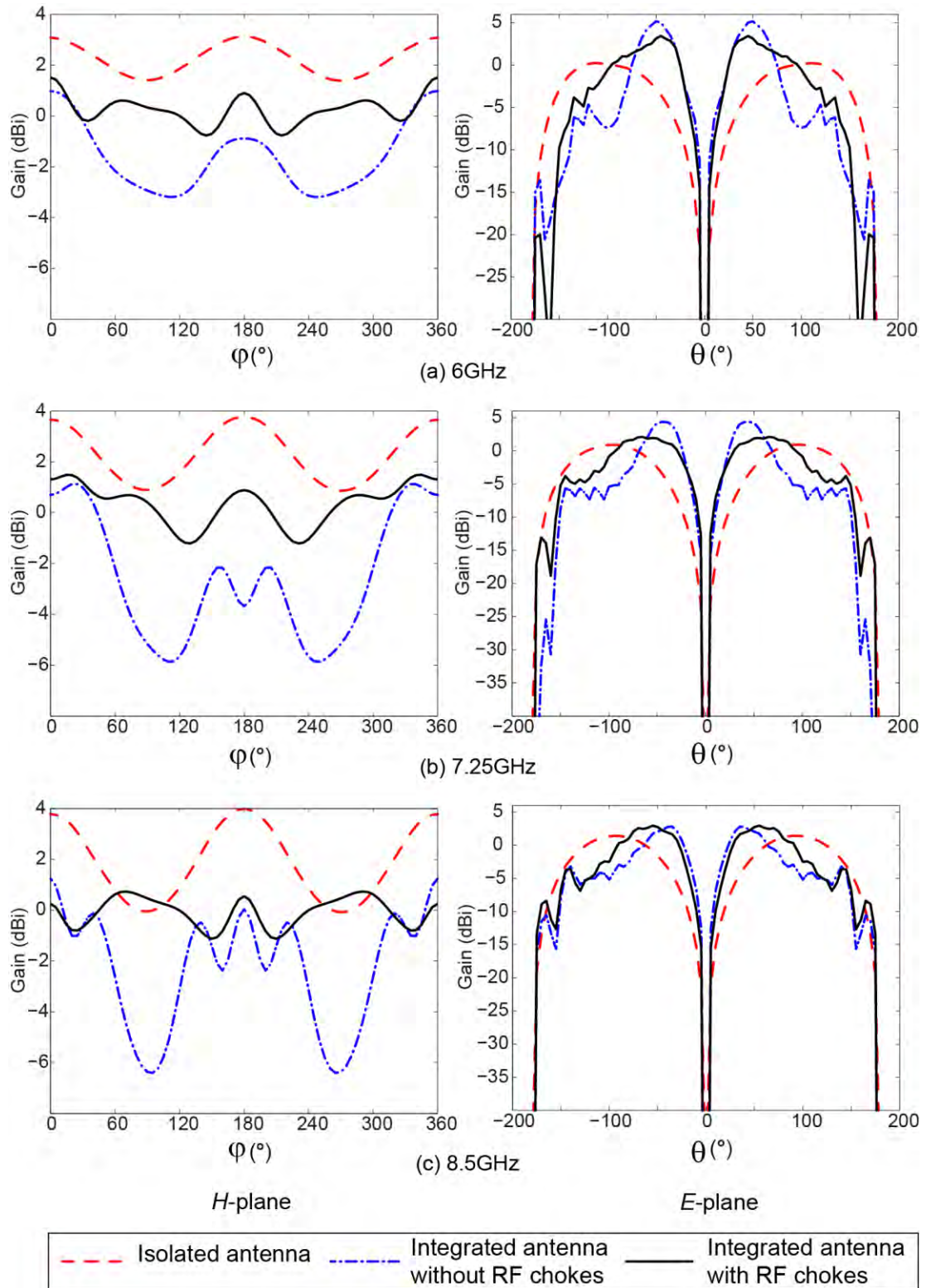


Fig. 7.17 Simulated antenna gain patterns in H and E planes, (a)6 GHz, (b)7.25 GHz, (c) 8.5 GHz.

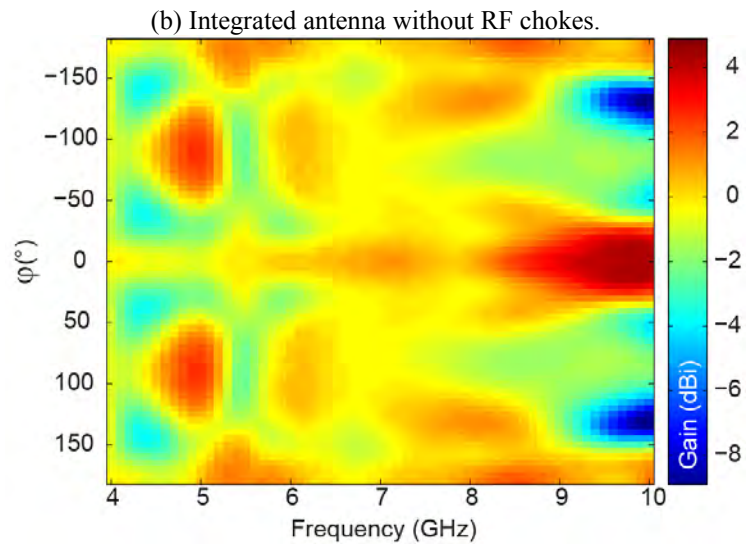
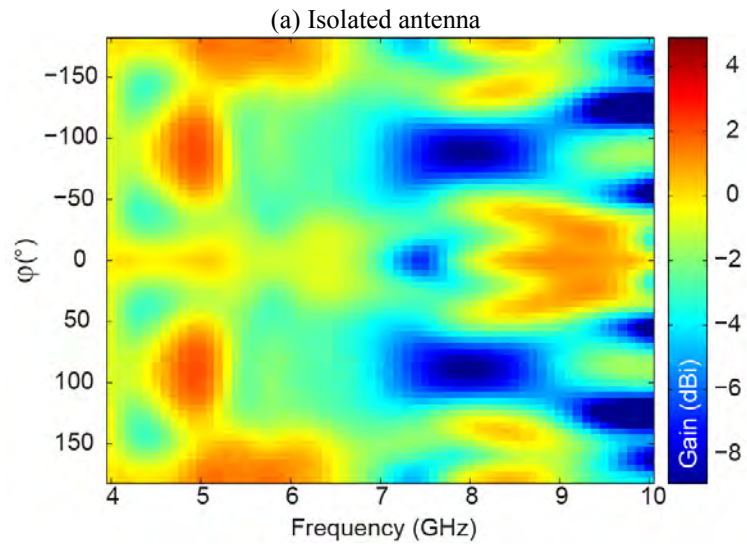
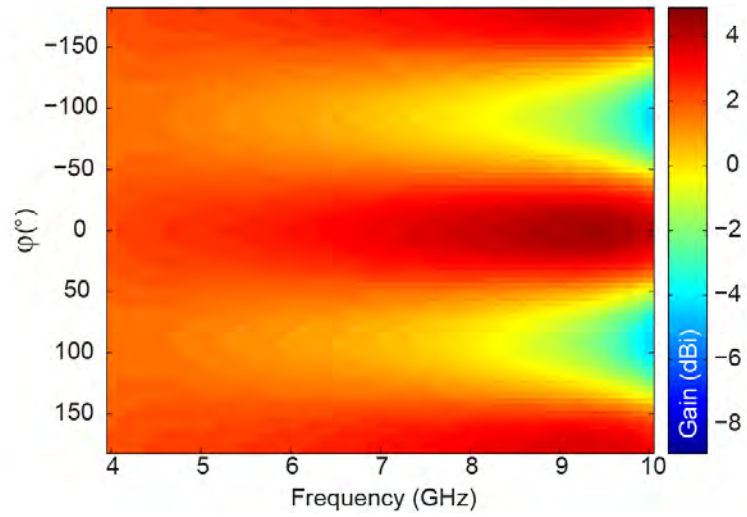


Fig. 7.18 The antenna gain pattern in  $xy$ -plane. RF chokes improve and stabilize the radiation pattern in  $H$ - plane in all frequencies.

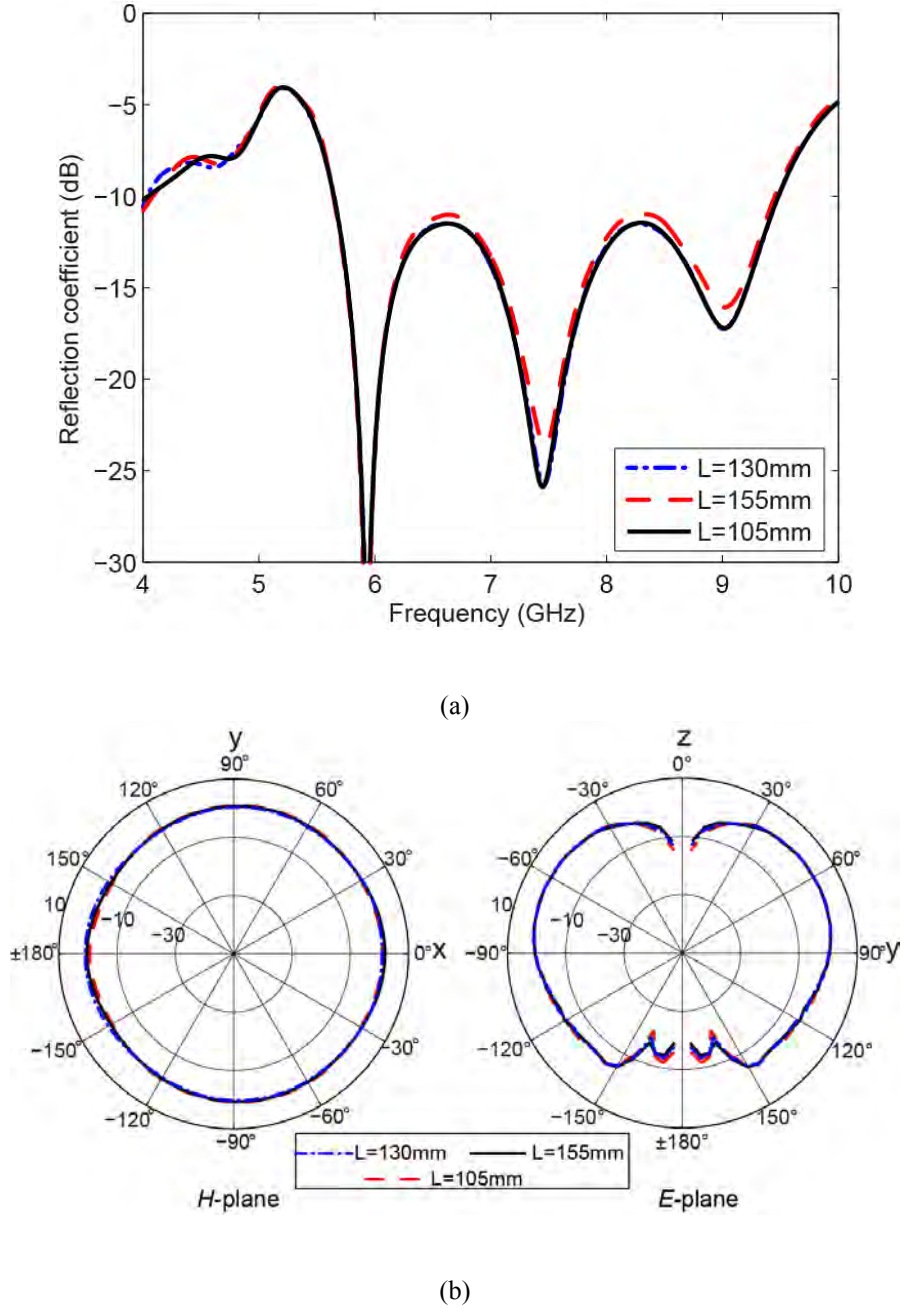


Fig. 7.19 Simulated (a) reflection coefficient (b) radiation patterns of the integrated antenna for different lengths of the PCB. The stable results show that the PCB radiation is controlled.

### 7.3.5 Field Coupling to the PCB

In order to demonstrate that the coupling between the PCB and antenna has been minimised, a parametric study was conducted by varying the length and width of the PCB. Fig. 7.19a shows the simulated reflection coefficient for different lengths of the PCB. The differences caused by varying the PCB length are insignificant since the different curves are indistinguishable. This indicates that the approach described above works efficiently. A similar trend is observed in the radiation patterns. The radiation patterns for different lengths

of the PCB at centre frequency, 7.25 GHz are illustrated in Fig. 7.19b. A similar study has been carried out by varying the width of the PCB in which a same trend can be detected (see Fig. 7.20). These observations confirm that the PCB contribution to the overall radiation is well controlled.

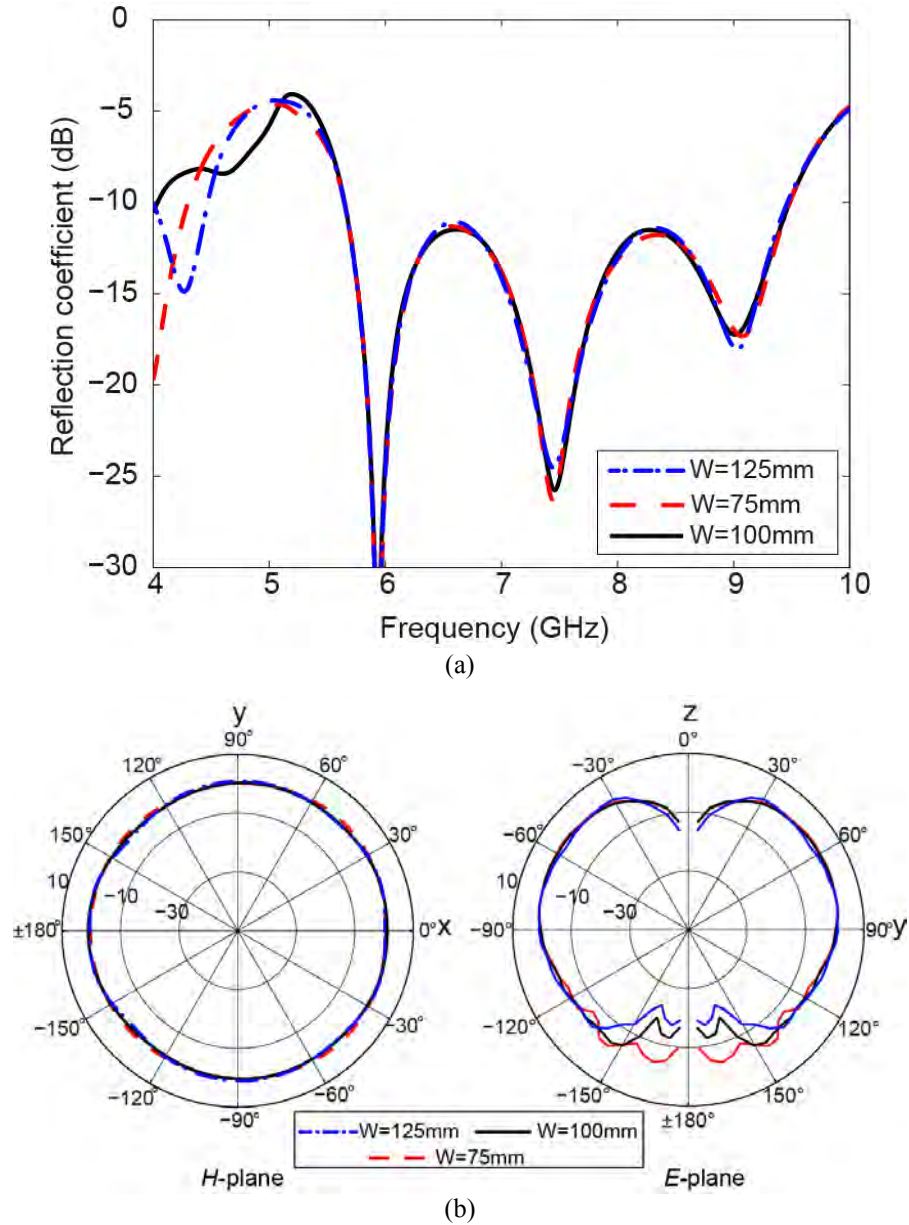


Fig. 7.20 Simulated (a) reflection coefficient (b) radiation patterns of the integrated antenna for different widths of the PCB. The stable results show that the PCB radiation is controlled.



Table 7.2 Group delay variation comparison for the two scenarios.

| Group delay (nsec)                   | Min  | Max  | Diff |
|--------------------------------------|------|------|------|
| Isolated antenna                     | 2.3  | 2.4  | 0.1  |
| Integrated antenna without RF chokes | 2.58 | 3.45 | 0.86 |
| Integrated antenna with RF chokes    | 3.02 | 3.40 | 0.38 |

### 7.3.6 Group Delay

Small printed UWB antennas are reported to have low dispersive behaviour [8]. Group delay is the parameter that can be used to quantitatively evaluate the dispersive performance of the antenna. It is defined as the derivative of far-field phase with respect to the frequency [38]. It quantifies the pulse distortion and far-field phase linearity.

The effect of integration on the group delay is studied by simulating a two antenna system excited by a Gaussian signal. The antennas face towards each other ( $\theta=90^\circ$ ,  $\varphi=0^\circ$ ) and are separated by 60 cm. The transmission coefficient  $S_{21}(\omega)=|S_{21}(\omega)|e^{j\psi(\omega)}$  of the two antenna system is then calculated. The group delay can then be calculated with (7.1)

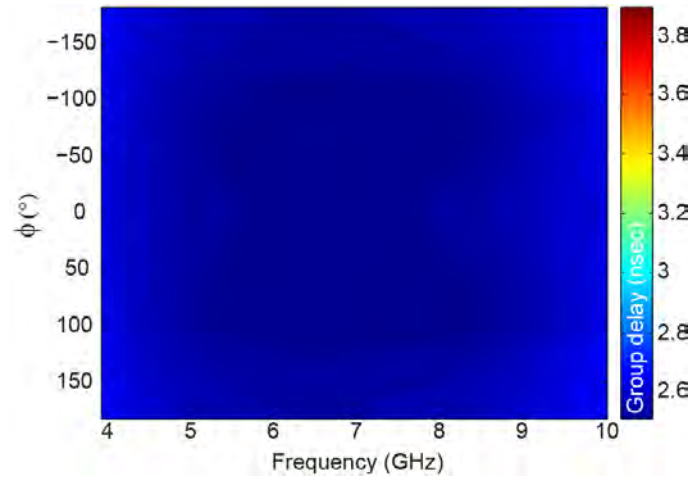
$$\tau(\omega) = -\frac{d\psi(\omega)}{d\omega} = -\frac{d\psi(f)}{2\pi df}. \quad (7.1)$$

The plots of group delay versus frequency and angle for the antenna with and without RF chokes are compared in Fig. 7.21. The isolated antenna shows a flat group delay [11] (not shown). As mentioned before, for the localization system, it is important to have a fairly constant group delay across the frequency range of interest (6-8.5 GHz). This is achieved by controlling the currents on the ground by utilizing the RF chokes. The improvement is more significant for 7-9 GHz. As shown in Table 7.2 incorporating the RF chokes results in more than 50% improvement comparing to the antenna without RF chokes.

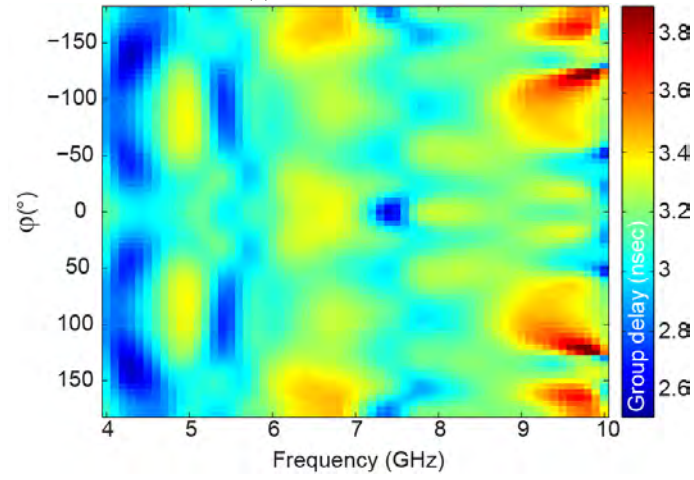
### 7.3.7 Time Signals

The effect of integration on the time signals is studied. As mentioned in the

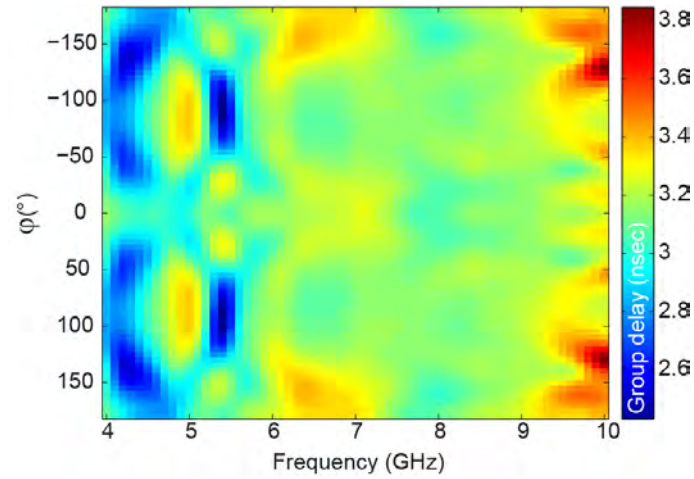
previously, a configuration of two similar antennas which are separated by 60 cm is simulated. The antennas face each other ( $\theta=90^\circ$ ,  $\phi=0^\circ$ ). The transmitting antenna is excited by the pulse depicted in Fig. 7.22a. The received signal is shown in Fig. 7.22b. The same configuration is simulated for all three antennas. Fig. 7.22b shows that the ringing effect is more significant in the integrated case as compared to the isolated case. The amplitude of the signal is lower for the integrated antenna case than the isolated one. The RF chokes do not influence the received signal. The signal distortion in the integrated case can be due to the impedance bandwidth mismatch between the antenna and the excitation signal. The antenna impedance bandwidth is less than the -10 dB bandwidth of the excitation signal and therefore not all of the frequency components of the pulse can be transmitted efficiently. This leads to distortion.



(a) Isolated antenna



(b) Integrated antenna without RF chokes.



(c) Integrated antenna with RF chokes.

Fig. 7.21 The antenna group delay in  $xy$ -plane, (a) isolated antenna, (b) integrated antenna without RF chokes, (c) integrated antenna with RF chokes.

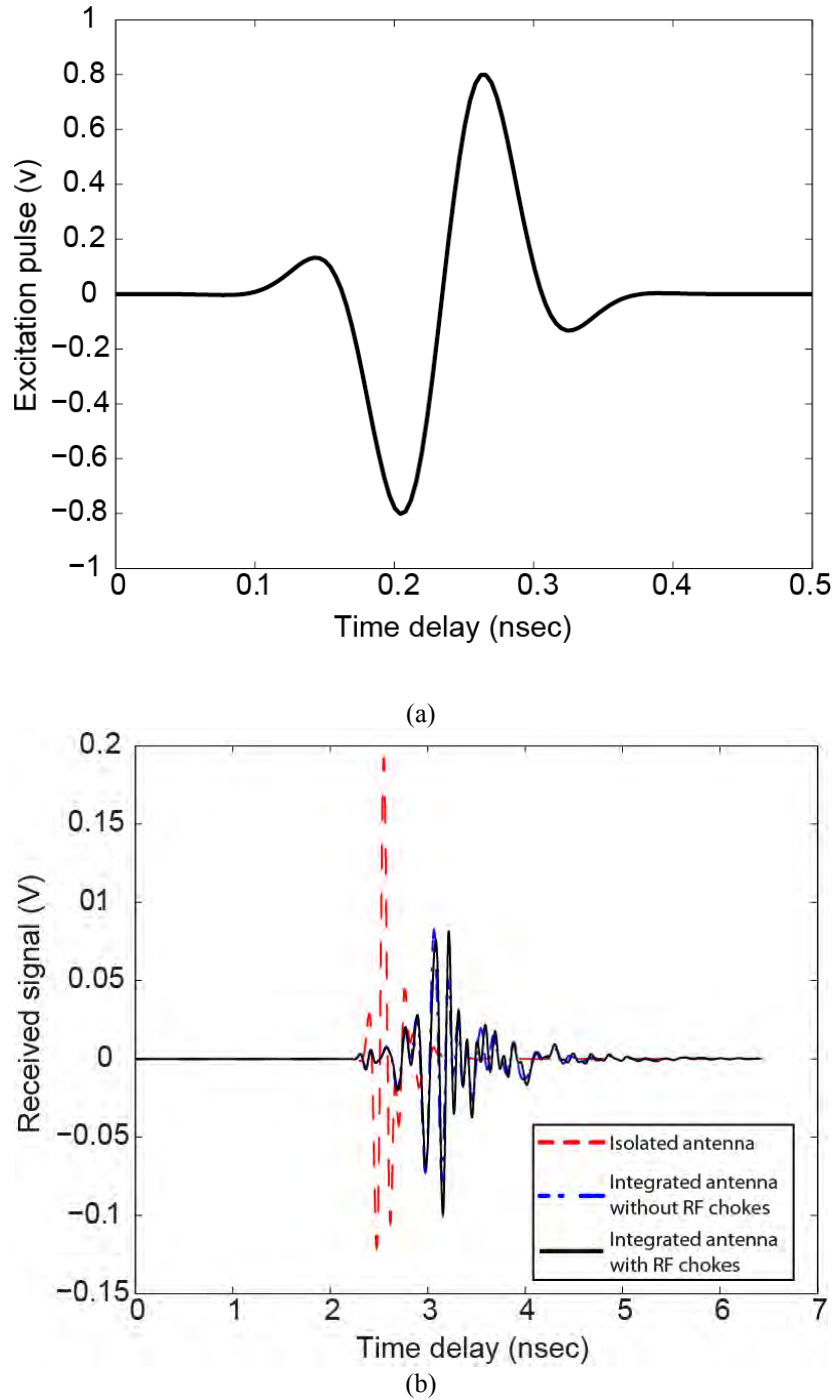


Fig. 7.22 The time signals (a) excitation pulse (b) received signal at  $\theta=90^\circ$ ,  $\phi=0^\circ$ . Integration results in smaller received signal level and stronger ringing effect.

## 7.4 Experimental Verification

The structure introduced in previous sections was developed on one layer of RO4350B with 1.52mm thickness and two layers of metallisation on top and bottom of the substrate. However, for the final product it is important to consider the multilayer structure of



the RF and digital board. The final board consisted of five dielectric layers with the total height of 1.23 mm. Fig. 7.23 shows a cross-section of the board layout. The width of the 50 $\Omega$  microstrip feedline on a substrate with the height of 1.23mm and  $\epsilon_r=3.48$  would be 2.88 mm - this is wide enough for connecting to the RF chipset pin. Therefore, the width of the microstrip line is further tapered to 0.4 mm. To retain the 50 $\Omega$  impedance the height of the substrate needs to be subsequently reduced. In order to save more space for the RF front end, the shape of the four inner layers i.e. L02, 3, 3b, 4b are modified. Fig. 7.24 demonstrates the final prototype of the antenna.

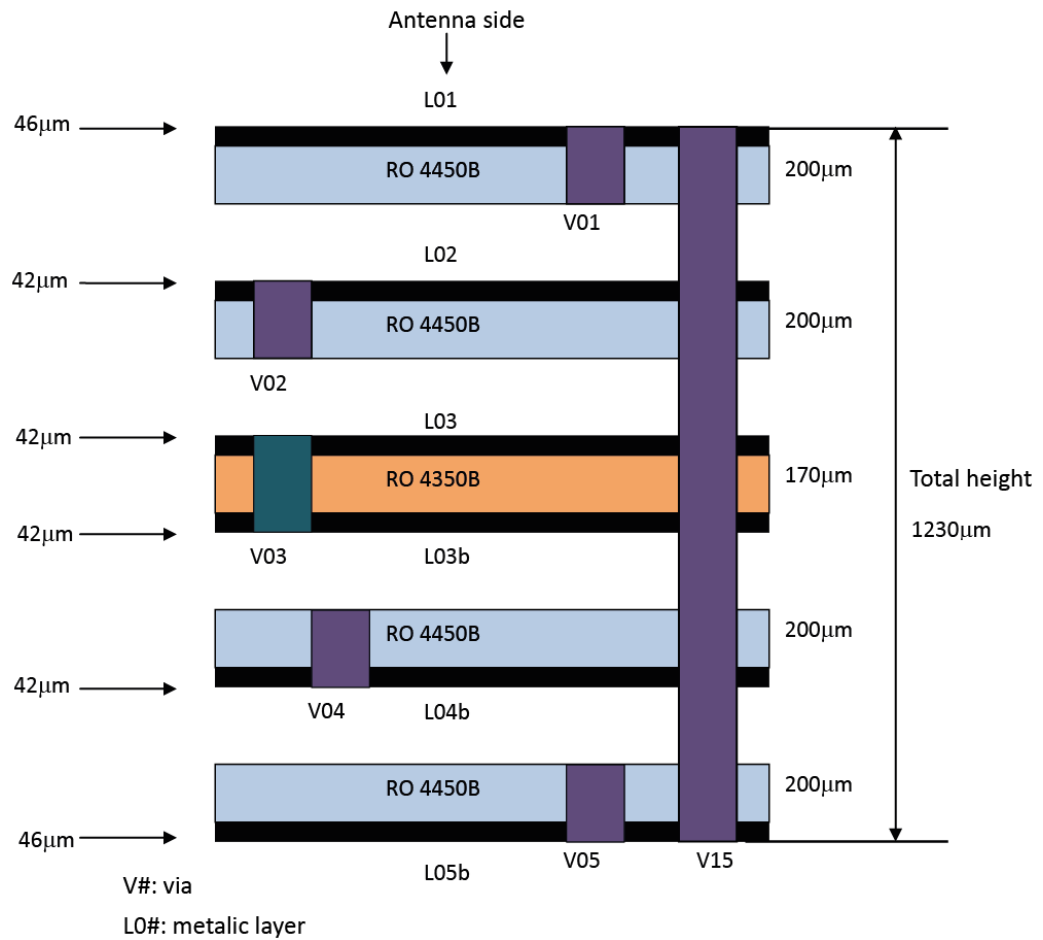


Fig. 7.23 Final prototype board cross-section.

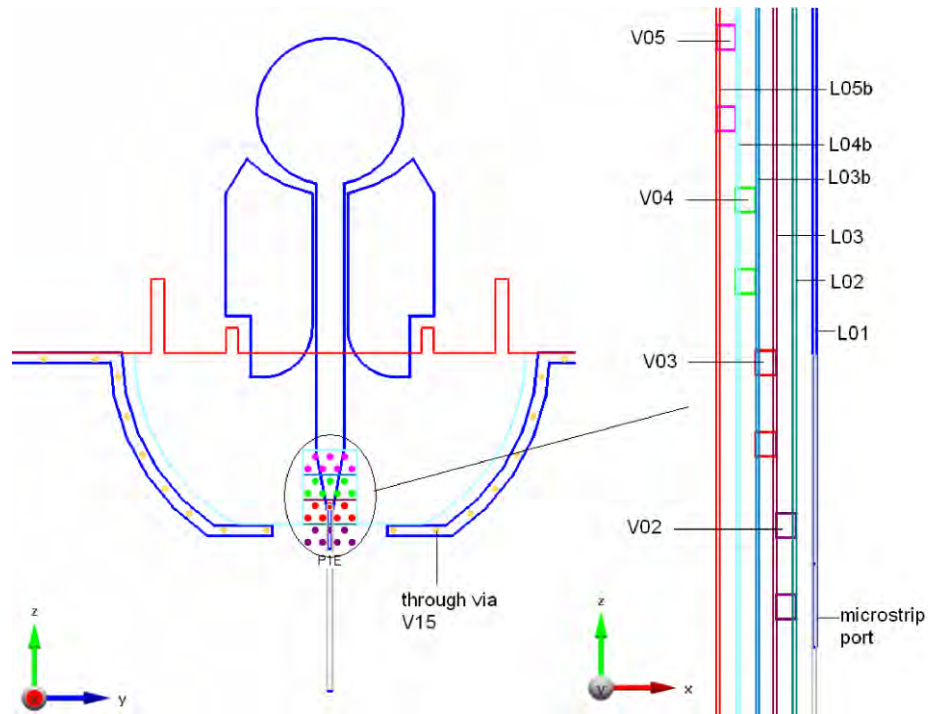
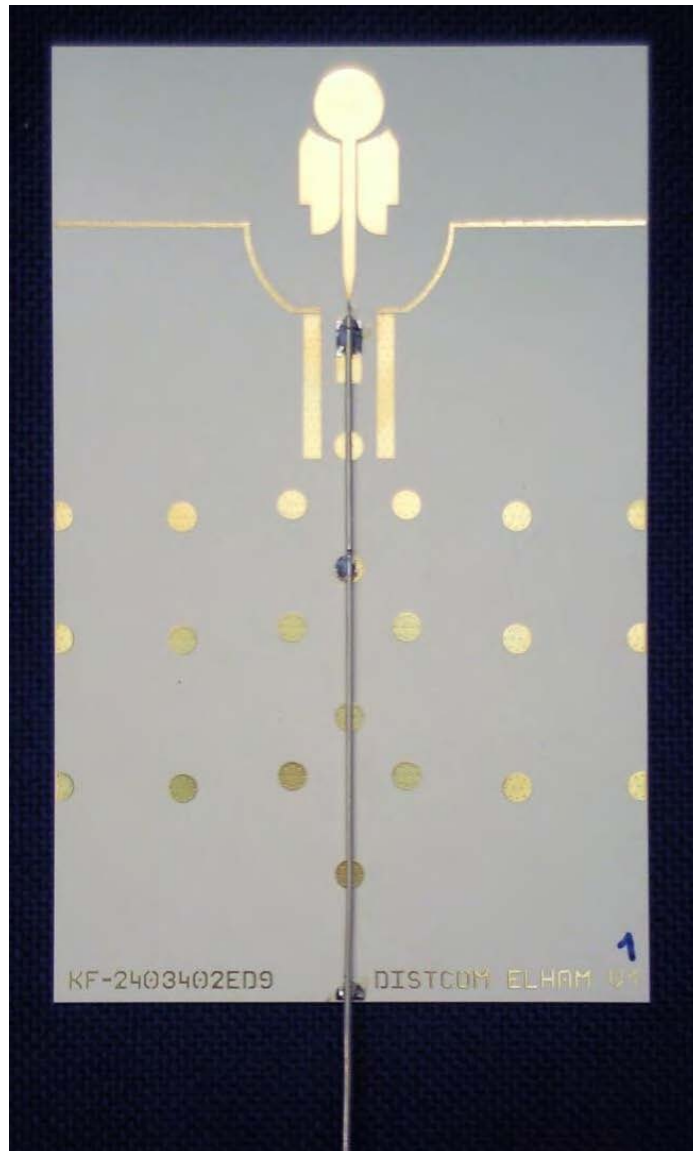
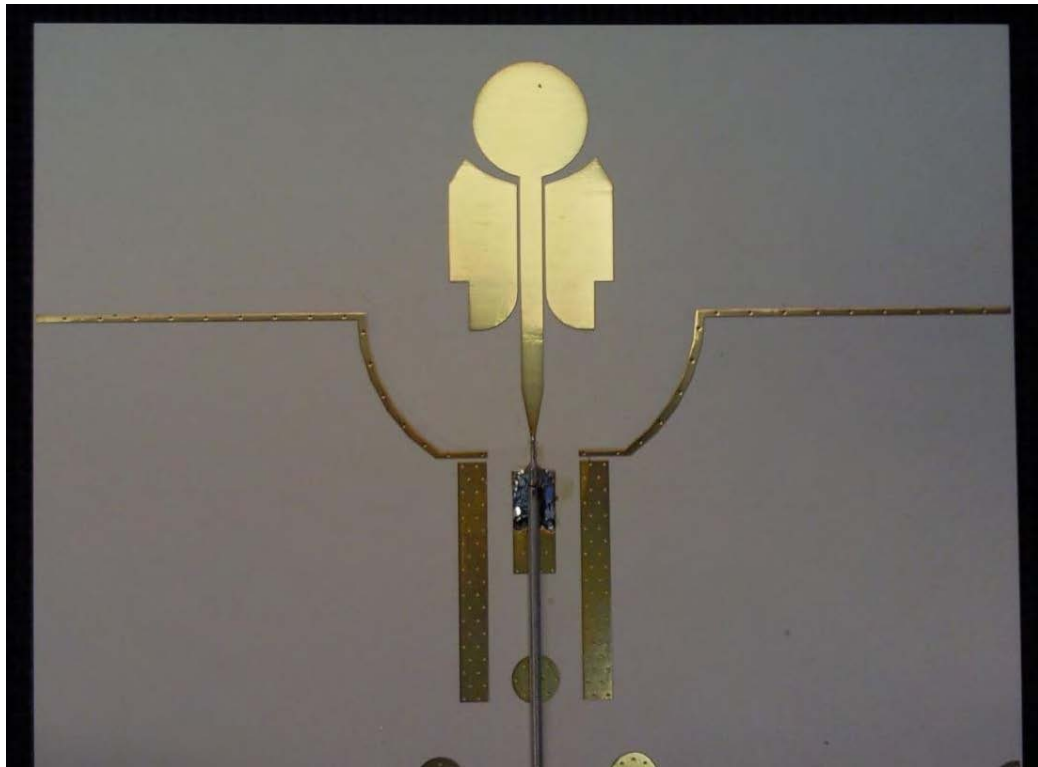


Fig. 7.24 Final antenna prototype and the feedline cross section.

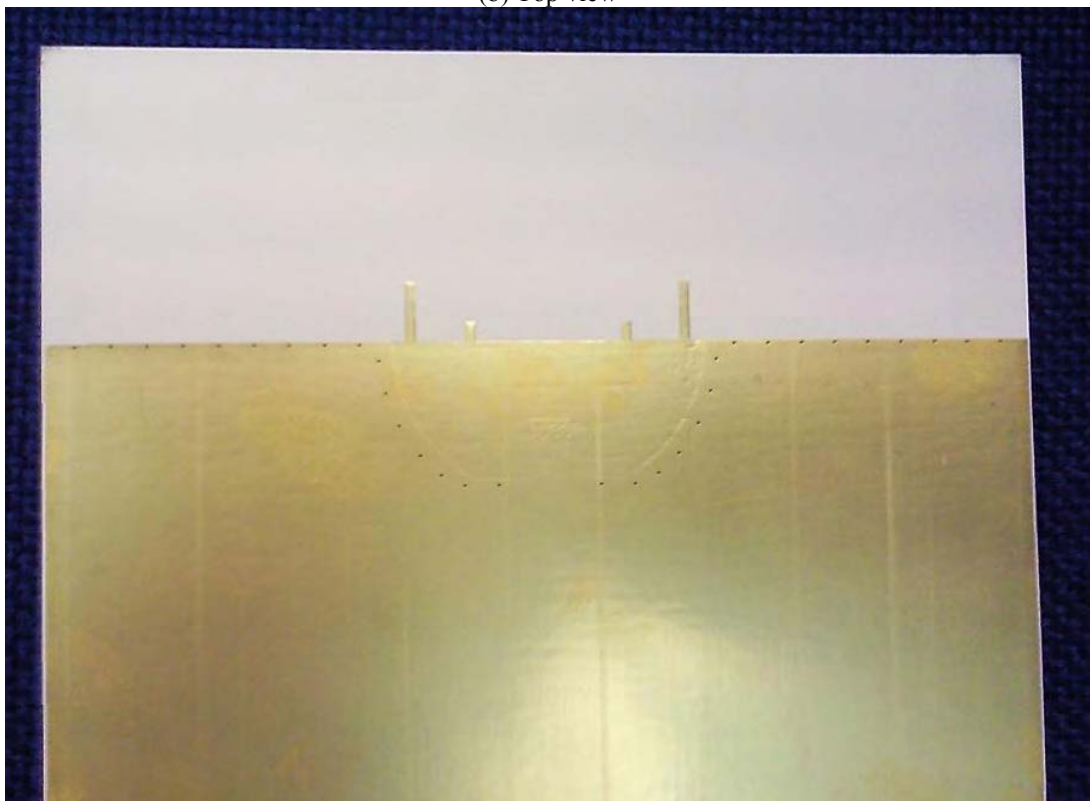
In the simulation procedure the antenna is designed to be excited through a microstrip port. However, for the purpose of test and measurement by a coaxial cable, several pads are printed on the top side and shorted by via pins to the PCB ground. The inner conductor of the coax can then be connected to the microstrip line and the outer to the shorted pads. The antenna geometry needs to be optimized again with the multilayer layout. The upper edge of the CPW ground of the antenna was modified to provide wider bandwidth after the integration. The photo of the fabricated prototype is shown in Fig. 7.25.



(a) Full view of the final prototype



(b) Top view



(c) Bottom view

Fig. 7.25 Photos of the final prototype.

In order to measure the antenna characteristics, the antenna was end fed by a 13cm coaxial cable. Since the length of the cable is significant, the mismatch between the connector and cable was reflected back and forth along the cable. For this reason, multiple resonances can be detected in the measured scattering parameter. Time domain gating was carried out to remove the effects of discontinuities in S-parameter data caused by the test connector and the cable in the post processing [39]. Advanced network analysers can automatically perform the gating and remove the effect of connector mismatch. The frequency domain S-parameters were first converted to the time domain. Time domain gating was then used to remove reflections due to end connector or other discontinuities. The gated time domain result was then transformed back to the frequency domain. By removing the unwanted resonances the S-parameter data will be improved .

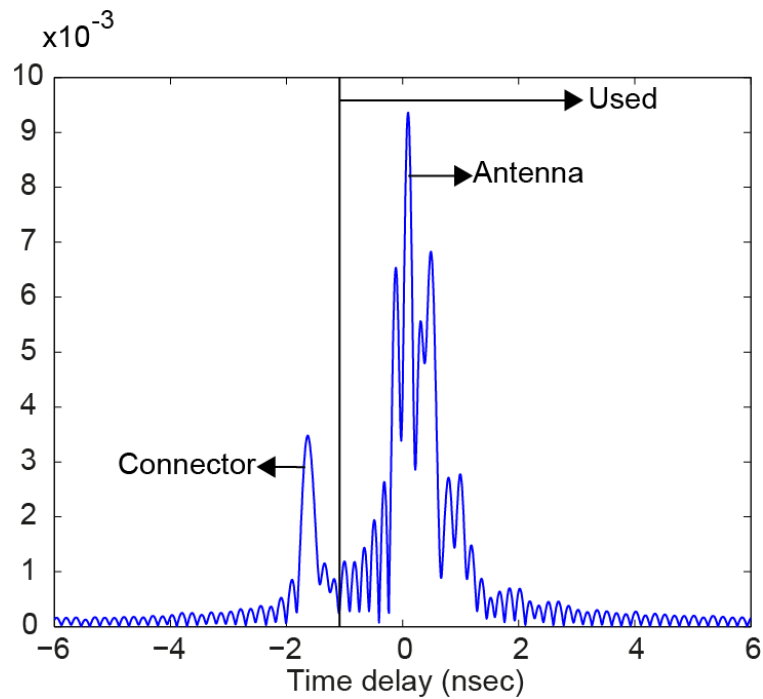


Fig. 7.26 Antenna reflection coefficient in time domain.

The reflection coefficient of the antenna in time domain is depicted in Fig. 7.26. The main peak which can be detected in Fig. 7.26 represents the antenna radiation. The mismatch at the connector can be detected as a peak happening before the main peak of the antenna. In

order to remove the effect of connector mismatch the connector data has been replaced with zeros in the post processing calculation. The new set of data has then been transformed to frequency domain. The measured reflection coefficient before and after gating is demonstrated in Fig. 7.27.

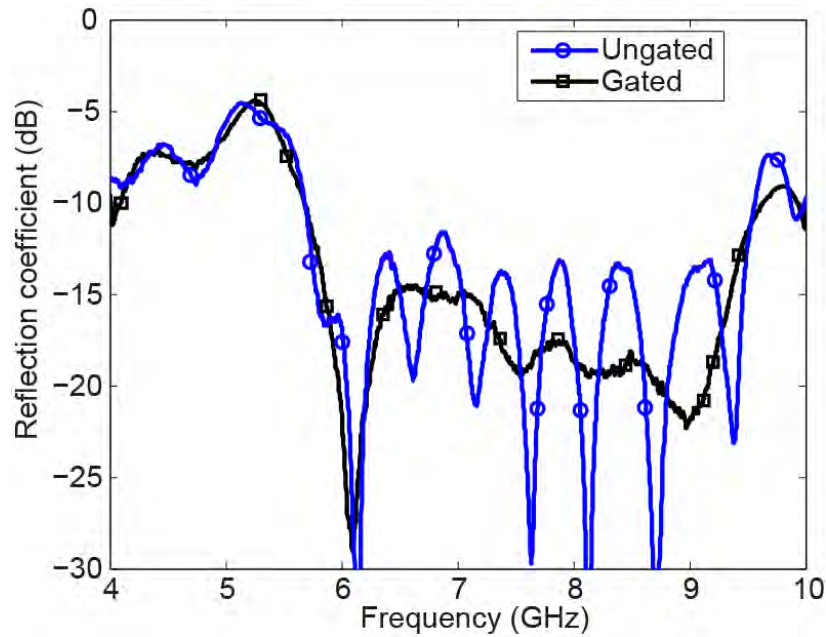


Fig. 7.27 The ungated and gated measured reflection coefficient.

The simulated and measured gated reflection coefficients are compared in Fig. 7.28. The -10 dB impedance bandwidth covers the whole band of interest (6- 8.5 GHz). The gated measured reflection coefficient agrees well with the simulated result. The measured efficiency and peak gain are presented in Fig. 7.29. While the efficiency varies between 75% and 95%, the gain increases from 3dBi at 6GHz up to 8dBi at 8.75GHz. The efficiency is derived through 3D gain measurement. Fig. 7.30 compares the simulated and measured co-polar ( $E_\theta$ ) component of the radiation pattern at 6, 7.25 and 8GHz, in the two main planes. Typical monopole behaviour can be observed in both planes over the whole frequency range.

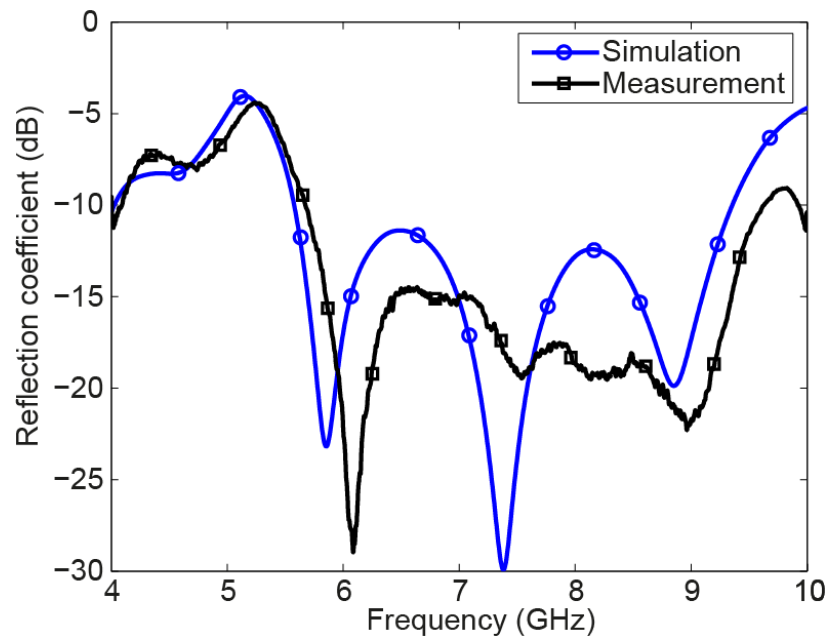


Fig. 7.28 Simulated and measured reflection coefficient.

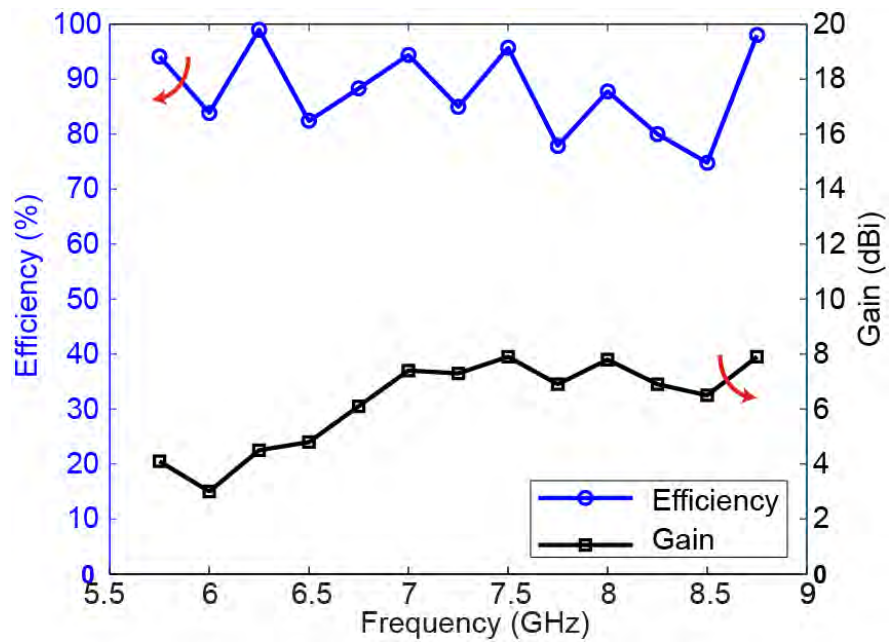
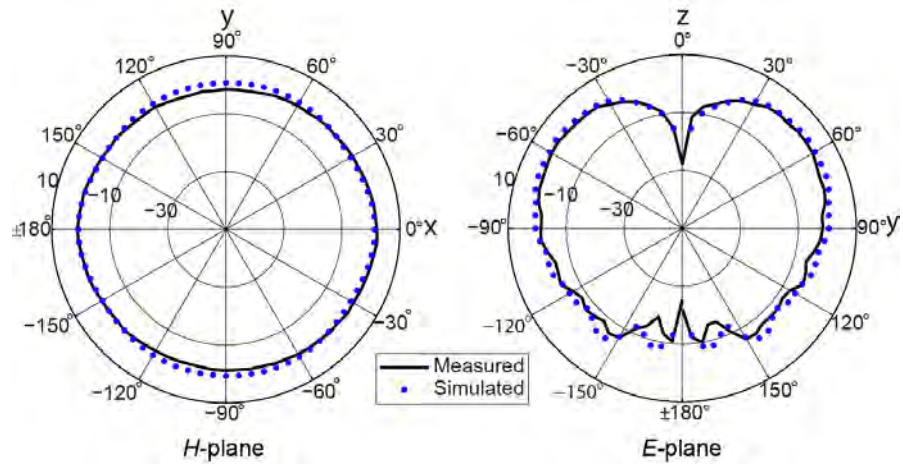
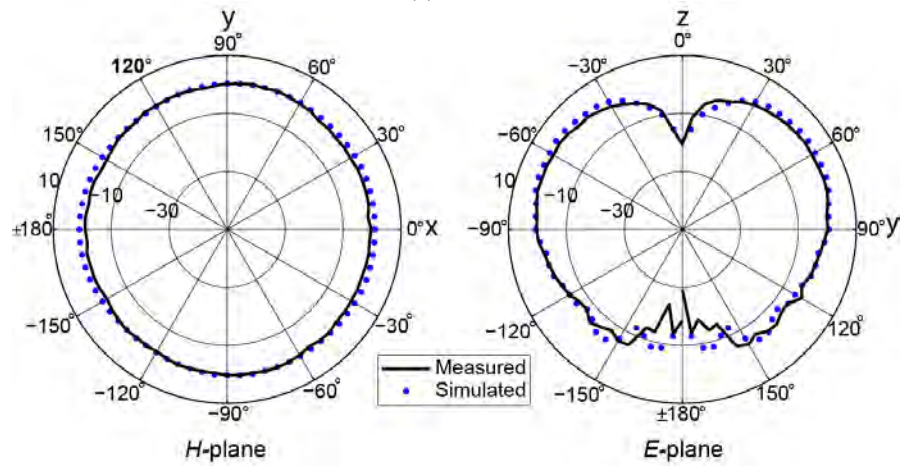


Fig. 7.29 The measured efficiency and peak gain.

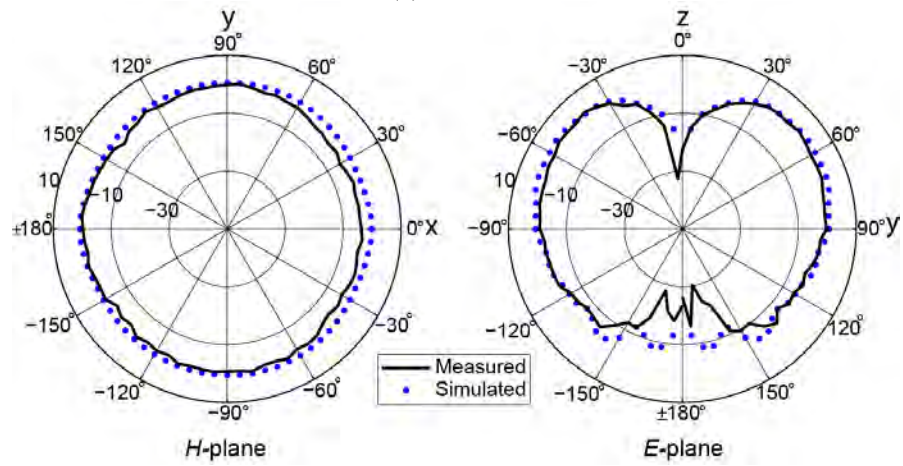




(a) 6GHz



(b) 7.25GHz



(c) 8.5GHz

Fig. 7.30 The simulated and measured radiation patterns at 8.5GHz, (a) 6 GHz, (b) 7.25 GHz, (c) 8.5 GHz.



## **7.5 Summary**

Design challenges of integrating a printed CPW fed UWB antenna into a PCB are elaborated in this chapter. In order to facilitate connecting the antenna to the off-the-shelf components, the original antenna feeding is transformed to a CCPW and then to a microstrip line. The PCB contribution to radiation is controlled by introducing two pairs of RF chokes to the arrangement. The RF chokes suppress the surface currents on the edge of the PCB and enhance the antenna radiation without degrading the matching. The study confirms that the antenna is well decoupled from the PCB. A five-layered prototype of the integrated antenna is manufactured and tested. The results show that the proposed technique significantly reduces the pattern degradation due to the presence of PCB.

## **References**

- [1] <http://www.apple.com/ipod/nike/run.html>
- [2] <http://health.howstuffworks.com/wellness/diet-fitness/information/nike-ipod1.htm>
- [3] S. Colson and H. Hoff, "Ultra-wideband technology for defence applications", in *Proc. IEEE Int. Ultra-Wideband Conf.*, Sept. 2005.
- [4] I.Y. Immoreev, "Practical applications of UWB technology", *IEEE Aerospace Electronic Systems Mag.*, vol. 25, no. 2, pp. 36-42, Feb. 2010.
- [5] C. Nguyen, J. S. Lee and J. S. Park, "Ultra-wideband microstrip quasi-horn antenna", *Electron Lett.*, vol. 37, no. 12, pp. 731-732, 2001.
- [6] Z N. Chen, M. J. Ammann, X. Qing, X. H. Wu, T. S. P. See and A. Cai, "Planar antennas," *IEEE Microwave Magazine*, vol. 7, no. 6 pp. 63 – 73, Dec. 2006.
- [7] J. Liang, L. Guo, C.C.Chiau, X. Chen and C.G.Parini, "Study of CPW-fed circular disc monopole antenna for ultra wideband applications", *IEE Proc. Microw., Antennas Propag.*, vol. 152, no. 6, pp. 520-526, Dec 2005.

- [8] J. Liang, C Chiau, X. Chen and C.G. Parini, "Study of a printed circular disc monopole antenna for UWB systems," *IEEE Trans. Antennas Propag.*, vol. 53, no. 11, pp.3500-3504, Nov. 2005.
- [9] K. L. Wong; C. H. Wu and S. W. Su, "Ultra wide-band square planar metal-plate monopole antenna with a trident-shaped feeding strips," *IEEE Trans. Antenna. Propag.*, vol. 53 , no. 4, pp.1262 – 1269, 2005.
- [10] C.-C. Lin, Y.-C. Kan, L.-C. Kuo and H.-R. Chuang, "A planar triangular monopole antenna for UWB communication," *IEEE Microw. Wireless Compon. Lett.*, vol. 15, no. 10, pp. 624-626, Oct. 2005.
- [11] B. Allen, M. Dohler, E. Okon, W. Malik, A. Brown and D. Edwards, *Ultra Wideband Antennas and Propagation for Communications, Radar and Imaging*, John Wiley and Sons, Ltd, 2007.
- [12] P. Vainikainen, J. Ollikainen, O. Kivekas, and K. Keltner, "Resonator-based analysis of the combination of mobile handset antenna and chassis," *IEEE Trans. on Antennas Propag.*, vol. 50, no 10, pp. , 1433-1444, 2002.
- [13] J. Holopainen, O. Kivekäs, C. Icheln, and P. Vainikainen, "Internal broadband antennas for digital television receiver in mobile terminals," *IEEE Trans. on Antennas and Propagat.*, vol. 58 ,no 10, pp. 3363-3374, 2010.
- [14] J. Thevenard, A. Louzir, D.L.H. Tong, C. Nicolas, C. Person, J. P. Coupez, R. Pascaud, R. Gillard and R. Loison, "Integration of a multi-sector antenna system on a wireless camera," *IEEE Int. Symp. Antennas Propag.*, 2009.
- [15] D. Manteuffel, "Considerations on antennas and propagation aspects for UWB consumer applications," in *Proc. Loughborough Antennas Propag. Conference*, pp. 145-150, April 2006.
- [16] S. Tu, Y.C. Jiao, Z. Zhang, Y. Song, and S.M. Ning "Small internal 2.4 GHz/UWB antenna for wireless dongle applications," *IEEE Antennas Wireless Propag Lett.*, vol. 9 , pp. 284-287, 2010.

- [17] T.W. Hertel, "Cable-current effects of miniature UWB antennas," *IEEE Int. Symp. Antennas Propag.*, vol. 3A, pp. 524 – 527.
- [18] D.-H. Kwon and Y. Kim, "Suppression of cable leakage current for edge-fed printed dipole UWB antennas using leakage-blocking slots," *IEEE Antennas Wireless Propag. Lett.*, vol. 5, no. 1, pp. 183 – 186, 2006.
- [19] Z. N. Chen, T. S. P. See and X. Qing, "Small printed ultra wideband antenna with reduced ground plane effect," *IEEE Trans. Antennas Propag.*, vol. 55, no. 2, pp. 383-388, 2007.
- [20] Y.-C. Jeong, S.-G. Jeong, J.-S. Lim and S. Nam, "A new method to suppress harmonics using  $\lambda/4$  bias line combined by defected ground structure in power amplifiers," *IEEE Microw. Wireless Compon. Lett.*, vol. 13, no. 4, pp. 538–540, Dec. 2003.
- [21] Y. Chung, S.-S. Jeon, D. Ahn, J.-I. Choi and T. Itoh, "High isolation dual-polarized patch antenna using integrated defected ground structure," *IEEE Microw. Wireless Compon. Lett.*, vol. 14, no. 1, pp. 4–6, Jan. 2004.
- [22] Choi, V. Govind and M. Swaminathan, "A novel electromagnetic bandgap (EBG) structure for mixed-signal system applications," in *Proc. IEEE Radio Wireless Conf.*, Sep. 19-22, 2004, pp. 243-246.
- [23] W. L. Stutzman and G. A. Thiele, *Antenna Theory and Design*. New York: Wiley, 1998.
- [24] A. A. Kishk, L. Shafai and A. Ittipiboon, "Improvement in radiation characteristic of coaxial feds using a quarter-wavelength choke," *Electron. Lett.*, vol. 20, no. 12, pp. 522–523, 1984.
- [25] K. Miyata and M. Suzuki, "Effects of choked-load position on radiation properties in double-choked small horn antennas," *Electron. Lett.*, vol. 19, no. 9, pp. 329–330, 1983.
- [26] S. Noghianian and L. Shafai, "Gain enhancement of annular slot antennas," *Proc. Inst. Elect. Eng. Microw Antennas Propag.*, vol. 148, no. 2, pp. 109–114, Apr. 2001.

- [27] L. I. Basilio, J. T. Williams, D. R. Jackson and M. A. Khayat, "A comparative study of a new GPS reduced-surface-wave antenna," *IEEE Antennas Wireless Propag. Lett.*, vol. 4, pp. 233–236, 2005.
- [28] C. C. Tchapwou and T. Bertuch, "Investigation of EBG surface performance for high-precision GPS applications," *Electron. Lett.*, vol. 43, no. 24, Nov. 2007.
- [29] K. T. Chen, Y. S. Wang and S.-J. Chung, "A new printed dual-band monopole antenna with a short stub," *presented at the Int. Conf. on Antennas, Radar, and Wave Propag.*, Banff, Canada, Jul. 19–21, 2005.
- [30] P. Lindberg and E. Ojefors, "A bandwidth enhancement technique for mobile handset antennas using wavetraps," *IEEE Trans. Antenna Propag.*, vol. 54, no. 8, pp. 2226–2233, Aug. 2006.
- [31] J. Holopainen, J. Ilvonen, O. Kivekas, R. Valkonen, C. Icheln and P. Vainikainen, "Near-field control of handset antennas based on inverted-top wavetraps: focus on hearing-aid compatibility," *IEEE Antennas Wireless Propag. Lett.*, vol. 8, pp. 592-595, 2009.
- [32] Y. S. Wang, J. C. Lu, S. J. Chung, "A miniaturized ground edge current choke—design, measurement, and applications," *IEEE Trans Antennas and Propag.*, vol. 57 ,no. 5, pp. 1360 – 1366, 2009.
- [33] The Commission of the European Communities, "Commission decision on allowing the use of the radio spectrum for equipment using ultra-wideband technology in a harmonised manner in the Community", *Official Journal of the European Union*, 21 Feb. 2007.
- [34] EMPIRE XCcel Reference Manual, <http://www.empire.de/>.
- [35] R. N. Simons, *Coplanar Waveguide Circuits, Components, and Systems*, John Wiley & Sons, Inc., 2001.
- [36] E. C. Jordan and K. G. Balmain, *Electromagnetic Waves and Radiating Systems*, Prentice-Hall, Inc., 1968.
- [37] C. A. Balanis, *Antenna Theory*, 2nd ed. New York: Wiley, 1997.

- [38] W. Wiesbeck, G. Adamiuk, C. Sturm, “Basic properties and design principle of UWB antennas”, *Proceedings of the IEEE*, vol. 97, no. 2, 372-385, 2009.
- [39] B. Archambeault, S. Connor, J.C. Diepenbrock, “Time domain gating of frequency domain S-parameter data to remove connector end effects for PCB and cable applications”, in *Proc. IEEE Int. Electromagnetic Compatibility Symp.*, 2006.
- [40] F. Gustrau, D. Manteuffel, *EM modelling of antennas and RF components for wireless communication system*, Springer-Verlag, 2006.
- [41] J. Kunisch, J. Pamp, “UWB radio channel modelling considerations”, in *Proc. Int. Conf. Electro. Adv. App.*, Italy, 2003.

## **Chapter 8      Conclusions and Future Work**

### **8.1      Conclusions**

The wireless industry market has been witnessing unprecedented growth mainly driven by increasing number of emerging services and applications. As a result, regulatory bodies and designers face looming challenges in spectrum management and hardware implementation.

The newly-introduced standards together with the earlier generations of wireless services are collocated within a limited part of the spectrum. While these bands are heavily crowded other parts of the spectrum are under-utilized. The spectrum under-utilization occurs when either only a fraction of an assigned band is used at a time or the whole bandwidth is used but very occasionally. Hence, responding to the growing demand for bandwidth hungry applications such as online multimedia streaming appears to be challenging. All the above leads to the conclusion that the fixed and regulated access to the spectrum holds only limited promise for the expansion of wireless technology.

Aiming at the efficient use of spectrum, the regulatory bodies have considered sharing the spectrum between several standards. Following the same ambition, the unlicensed use of the 3.1-10.6 GHz band for UWB emission was authorized in 2002. Transmission of low power short impulses is the enabling principle for reliable, high data rate, multipath-tolerant and non-invasive communication in UWB technology. Prior to that, in 2000, Mitola

had introduced an intelligent and self-aware radio concept known as cognitive radio which has dynamic access to the spectrum for optimum performance. While this approach creates new opportunities to pursue the main goals, it comes with its own set of challenges, in particular the antennas.

For an optimum performance, the CR needs to be aware of its own state, collect information about the surrounding environment (i.e. spectrum sensing), process the new information together with the data fed back from previous operations and select the best standard accordingly (i.e. spectrum allocation). Successful completion of this cycle necessitates the collaborative use of software and hardware components (i.e. antenna and RF front end circuitry). Spectrum sensing and allocation procedure can be realized by means of two communications links; spectrum sensing link and communication link. In the sensing link, a wideband antenna may continuously monitors the spectrum in search of vacant or idle frequency bands (spectrum holes) while a narrowband reconfigurable antenna with wide tuning range is in charge of communication in the other link. Hence, an antenna solution with wideband and reconfigurable narrowband functionality is required for spectrum sensing and allocation task in CR.

The widespread deployment of wireless connectivity in various applications has resulted in strong demand for multi standard portable platforms. Antennas that can operate over several frequency bands are essential in order to support multi standard operation. The antenna bandwidth requirements vary for low, medium and high data rate applications. Hence, as well as supporting multiple frequency bands, the antennas need to satisfy several bandwidth requirements.

In view of the above argument on the necessity of developing antennas with wideband and narrowband functionality for current and future wireless networks, a hybrid wideband-narrowband antenna was designed in Chapter 4. The antenna is designed based on an integration concept aiming at efficiently using the spaced allocated for the antennas. The efficient integration relies on sharing part(s) of one antenna between other additional antennas. In the demonstrator antenna, a CPW fed UWB printed monopole was etched on the

top layer of the Taconic substrate. On the bottom layer, above the UWB antenna radiator, a microstrip fed shorted patch antenna was printed. It was then shorted through a via pin to the UWB antenna radiator. In this configuration the UWB radiator was also used as the ground plane for the narrowband shorted patch antenna. Therefore, the space of one antenna was used for two antennas. A prototype of this antenna was fabricated and measured. Good agreement was observed between the simulated and measured results. A parameter study was conducted to explain the antenna performance.

Other than the conventional parameters of each antenna in this configuration their relative position also affects the performance. Specifically, the transmission coefficient is strongly influenced by the position of the narrowband antenna. This issue was addressed in Chapter 5. Investigating the surface current distribution on the edge of the UWB radiator and the microstrip feeding of the narrowband antenna indicates that some percentage of power is coupled between the ports causing high transmission coefficient. To resolve this problem two techniques were applied; modifying the antenna structure and designing an external decoupling feeding network. In the first approach, the aim was to avoid the area that caused the power coupling; therefore, the narrowband feeding was shifted away from the board centre and a few dB reduction in the transmission coefficient was achieved. To further improve the port isolation, the narrowband antenna was placed on the top part of the radiator and fed from the opposite edge of the board. The resulting transmission coefficient was -18dB.

The design procedure of an external decoupling network was elaborated as the second approach. An unknown four port network is connected to the two port antenna. The scattering matrix of the total system was extracted and the unknowns were derived on the condition of no coupling. Considering that the antenna scattering matrix which was taken as the input data for this procedure was varying with frequency the resulting network scattering matrix was also a function of frequency. Therefore, realizing such network with frequency dependant components such as transmission lines is challenging.



For a reliable wireless service in interference-rich harsh electromagnetic environments, the antennas should be robust and versatile. Reconfigurable antennas are the key components to increase the system tolerance against variations in the environment. Antenna frequency detuning due to the interaction with the user's head or hand, variation of the interference signal or traffic can be under control with the help of reconfigurable antennas as they can react to the changes in the system and environment. Systems with reconfigurable antennas can be considered as preliminary models of intelligent and self-organizing networks such as CR. It can be envisaged that reconfigurable antennas and filters along with vast use of software controlled algorithms at different levels facilitate the realization of CR.

Reconfiguration is achievable by means of banks of external matching circuits and switching between them with when necessary. This feature was examined in Chapter 6. Three sets of matching circuits were designed to tune the narrowband antenna across the UWB band. The circuit antennas were fabricated and verified. Considering the manufacturing tolerance the measured and simulated results agreed well.

From the early large heavy terminals with protrusive external antennas to today's trendy compact devices with unobtrusive antennas, the mobile handset have gone through an evolutionary journey which is now being followed by the other wireless enabled devices for various applications such as health and care system, public safety and logistics. Since they are installed on the terminal chassis, the external antennas have less interaction with other components of the device and therefore it is possible to design the antenna in isolation and afterwards add it to the final product with small variation in the desired characteristics. However, the internal antennas have to be placed in close vicinity of components such as screen, battery or the highly populated PCB where unsurprisingly their interaction might result in degradation of antenna characteristics. Hence, it is concluded that for a successful compact antenna design, the impact of other components on the antenna should be determined and reflected in the design procedure.

Taking to account, the unique features of UWB technology, a UWB antenna was designed to operate at 6-8.5GHz (European UWB mask) for indoor positioning application. It

was necessary that the antenna provided good impedance matching, stable radiation pattern and gain across the operating band. A printed disc monopole was selected for integration into a relatively large PCB. High concentration of the currents on the antenna ground plane resulted in strong field interaction between the antenna and the PCB which degrades the gain and radiation pattern of the antenna. Field coupling between the antenna and PCB is controlled in two stages. Firstly the antenna is fed by a CPW mechanism to separate the antenna (virtual) ground plane and the PCB. The CPW feeding is then transformed to microstrip feeding. In order to facilitate smooth field transition a conductor backed CPW was used between CPW and microstrip feeding. In the second stage, two pairs of RF chokes were printed on the PCB to reduce the flow of current on the edge of the PCB. This decreased the contribution of PCB in the radiation and therefore, the original radiation characteristics of the antenna were successfully maintained. A multilayer prototype of the antenna on the PCB was fabricated and measured and simulated results were compared. The performance of the final design was compared with the original antenna in isolation and the integrated antenna without RF chokes. The investigations showed that the RF chokes create high impedance point forcing the current minima.

Overall it can be concluded that in modern wireless applications the antenna performance is linked with other parameters such as the device industrial design, RF and digital circuitry sensitivity and complexity. Therefore, in order to propose a promising antenna solution, it is beneficial to take the corresponding system requirements into considerations. Fig. 8.1 summarizes the goals and achievements in this thesis.

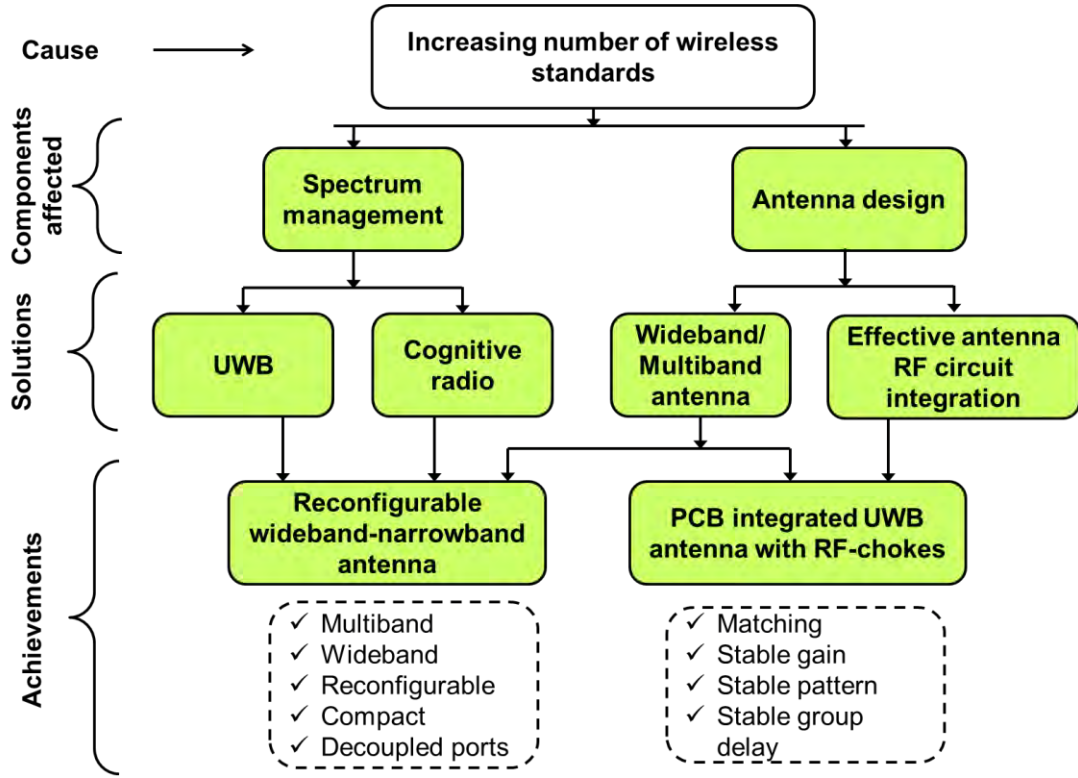


Fig. 8.1 Summary of the areas covered and the main achievements in this dissertation.

## 8.2 Future Work

Although it has been more than a decade since Mitola introduced the cognitive radio concept the debates on its required regulations, architecture and algorithms is still on-going. To this time, most researchers have focused on developing intelligent software algorithms for spectrum sensing, sharing or allocation and significantly less interest was directed towards hardware implementation of CR in particular antennas. Therefore, it is assumed that there may be many more antenna designs suitable for CR. Increasing the versatility of the antenna and relaxing the RF front end by combining different bandwidth scenarios and including the filtering and tuning functions into the antenna to reduce the pressure of the RF front end.

The presented integration technique can be applied to wide range of antennas for different combinations, such as polarization or pattern combination. It is also not limited to two antennas; as with the right choice of antennas and arrangement, multiple antennas can be integrated using this technique. The principle can also be applied to low frequency antennas however, some miniaturization approaches will be necessary.

It is important to consider the arrangements which cause the least coupling between the ports. Otherwise decoupling feeding networks are necessary. Since the antennas are not similar (as in MIMO) and have different frequency response, matching and decoupling at the same time over different range of frequencies is challenging. For more practical solution, there should be a trade-off between the required coupling and matching. This means instead of setting the condition to zero coupling, a higher feasible coupling together with an acceptable matching should be taken as the network design condition. Moreover, if required wideband matching techniques might be considered.

Reconfiguration in this antenna is an added feature and can vary for different choices of antennas. To increase the tuning range several matching circuits together with a decision making unit can be used. MEMS can also be used to reduce the loss. Circuits with variable components are suitable for continuously tuning.

The printed monopoles have been studied extensively in the literature and most authors report that the current distribution on the ground plane is quite strong. This makes the antenna integration into PCBs challenging. A PCB integration solution was presented in this dissertation for the European UWB mask i.e. 6-8.5GHz band. As an extension, various techniques for increasing the operating bandwidth can be studied. For instance using multiple RF chokes or reshaping the chokes (e.g. radial chokes) for wide band operation might be considered. Controlling the surface currents on the antenna ground plane before integration to the PCB is also another issue worth investigating. Finally, balanced antennas with minimum common mode currents on the ground might be an alternative solution to this problem.

## Appendix A Simulation Software

The exact knowledge of electromagnetic fields and the propagation of waves is a prerequisite for the design of radio frequency (RF) elements. In former times, RF design tasks were based on measurement and simple models, leading to time and costs consuming design procedures. Today, affordable computer hard- and software have established and simulation programs can accurately predict the electromagnetic behaviour of new products. So, field simulators have become a new standard for RF calculations.

### A.1 Computer Simulation Technology (CST) [1]

Simulation plays an essential role regarding the evaluation and expectation of the antenna characteristics and behaviour. One of the commercial simulation software employed in this work is CST Microwave Studio®, which is the product of CST-Computer Simulation Technology [9]. The software package will be briefly introduced from its user manual, as well as the fundamental theory behind them.

CST Microwave Studio® is a fully featured electromagnetic software package based on the Finite Integration Technique (FIT). This numerical method provides a universal spatial discretization scheme, applicable to various electromagnetic analysis and design, ranging from static field calculations to high frequency applications whether in time or frequency domain.

The background theory of CST Microwave Studio so called Finite Integration Technique was first introduced by Weiland in 1977 [2]. FIT discretizes the *integral* form of

## Appendix

Maxwell's equations, rather than the differential one which is employed by Finite Difference Time Domain (FDTD) method. The FIT equations are presented in equation (A.1).

$$\text{Faraday's Law: } \oint_{\partial A} \vec{E} \cdot d\vec{s} = - \int_A \frac{\partial \vec{B}}{\partial t} \cdot d\vec{A}$$

$$\text{Ampere's Law: } \oint_{\partial A} \vec{H} \cdot d\vec{s} = - \int_A \left( \frac{\partial \vec{D}}{\partial t} + \vec{J} \right) \cdot d\vec{A}$$

$$\text{Gauss's Law for electricity: } \oint_{\partial V} \vec{D} \cdot d\vec{A} = - \int_V \rho \cdot dV$$

$$\text{Gauss's Law for magnetism: } \oint_{\partial V} \vec{B} \cdot d\vec{A} = 0 \quad (\text{A.1})$$

$E [V/m]$  =electric field vector;  $B [Wb/m^2]$  =magnetic flux density vector;

$H [A/m]$  =magnetic field vector;  $D [C/m^2]$  =electric flux density vector;

$J [A/m^2]$  =displacement current density;  $\rho [C/m^3]$  =volume charge density.

In order to solve these equations numerically, a finite calculation domain must be defined, enclosing the necessary space region. The next step is to decompose the computational domain into a finite number of tetra- or hexahedra unit cells, and electric and magnetic field vectors can be aligned on the facet of these cells, as shown in Fig. A- 1. Under the decomposition, all the cells have to fit exactly to each other. This decomposition yields the finite simplified cells complex G, which serves as computational grid [3]. The spatial discretization of Maxwell's equations is finally performed on these grid systems. The calculation process is repeated for all grid cells within the boundary until the desired accuracy is reached.

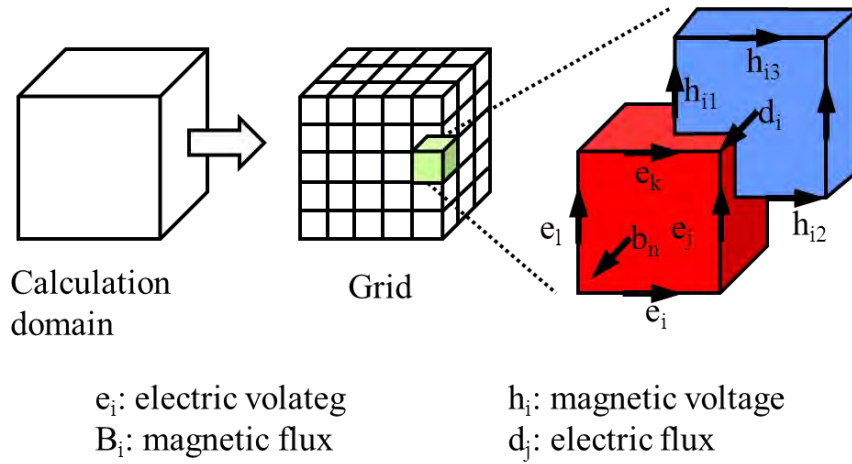


Fig. A- 1 Decomposition of the computational domain in FIT [4].

CST Microwave Studio contains three different simulation tools (transient solver, frequency domain solver, eigenmode solver) to best fit particular applications. The most flexible tool, transient solver, is a time domain simulator, which is also the mainly used solver in this project. It is remarkably efficient for the most kinds of high frequency applications. The entire broadband frequency behaviour of the simulated object can be obtained from only one calculation run. CST is also distinctive on its windows-based operating interface and graphic feedback for the definition of object that is being developed. Another outstanding feature of CST is that the mesh properties can be very flexible. The mesh of an objective can be defined in high density to achieve high accuracy result, or sub-grid mesh system can be used to save computational resources when processing electrically large objects.

Like other 3-D full wave simulation softwares, there are some disadvantages in CST Microwave Studio. For example, the software is based on a method which requires the discretization of the entire calculation volume; therefore the application is limited by the electrical size of the structure. In general, CST Microwave Studio is a reliable software tool for most microwave applications.

## A.2 Empire XCcel [5]

Unlike the Finite Element Method, which has long been established in computing electromagnetic fields, the FDTD method had its breakthrough in the late 80's when extensive research and development lead to a number of improvements in applying advanced boundary conditions, e.g. free space or waveguides, and, therefore, reducing significantly the area of simulation. Today, its applicability covers the whole area of three-dimensional (3D) field simulations for RF designer.

The EMPIRE XCcel<sup>TM</sup> simulator is another tool for solving Maxwell's equations and modelling antenna structures used in this work. It is based on the Finite Difference Time Domain method (FDTD), which means that the equations are discretized in space and time. This is accomplished by mapping the structure of interest onto a rectangular grid where the unknown field components are located in each cell.

Because of the nature of the electromagnetic problem<sup>1</sup>, an initial value problem has to be solved. This means that the unknown field for a certain time is calculated from the field values before. The FDTD method employs an efficient time stepping algorithm, known as the Yee's leapfrog scheme [6]. The size of the time steps is related to the size of the grid for stability reasons and cannot, therefore, be defined independently. So the definition of a suitable grid is an important task for efficient simulation.

The aim of the FDTD method is to solve Maxwell's equations and its associated material relations for a given structure and boundary conditions. Those equations yield

$$\begin{aligned}\nabla \times \vec{H} &= \vec{D} + \vec{J}, & \vec{B} &= \mu \vec{H}, \\ \nabla \times \vec{E} &= -\vec{B}, & \vec{J} &= \sigma \vec{E}. \\ \vec{D} &= \epsilon \vec{E},\end{aligned}\tag{A.2}$$

where  $\vec{E}$  and  $\vec{H}$  are the electric and magnetic field vectors,  $\vec{D}$  and  $\vec{B}$  are the electric and magnetic flux density vectors and  $\epsilon$ ,  $\mu$ , and  $\sigma$  are permittivity, permeability, and conductivity



of the material, respectively. Some assumptions have to be made to derive the algorithm to solve these equations with numerical methods:

- Passivity

The structure does not contain any active element. These elements cannot be described by Maxwell's equations and, therefore, have to be excluded from the simulation.

- Linearity

Non-linear elements, like semi-conductors and some dielectric or permeable materials, need special treatment in the algorithm, which is not considered here.

- No remedy effects

Hysteresis effects, which can occur in highly permeable materials, are not considered in the simulator.

- Isotropy

Anisotropic materials can be taken into account in the algorithm as long the material tensor can be described by a diagonal matrix which must coincide with the co-ordinate system of the grid. Because of higher memory requirements, this feature is not implemented yet.

- Absence of free charges

Free charges can be accelerated by electromagnetic fields and, therefore, have to be calculated with a combined set of Maxwell's equations and movement equations, which is often implemented in so called Particle in Cell Codes.

- Frequency independent materials

For the applied algorithm, the material properties are assumed to be independent of frequency, because often a whole frequency range is covered by exciting with Gaussian-like pulses. If the frequency dependence can be described by simple differential equations in the time domain it can be considered but the algorithm has to be changed for those regions.

### **A.2.1 The Yee algorithm [6]**

No assumptions have to be made for the shape and material distribution of the structure. The only limitation is that the structure has to be subdivided into cells in which the

material properties are constant. For the Finite Difference scheme, these cells are formed by intersecting planes of a Cartesian co-ordinate system. The basic idea of the algorithm is to place the unknown field components in a certain position of each cell so that every electrical field component  $\vec{E}$  is surrounded by four circulating magnetic field components  $\vec{H}$  and vice versa, as shown in Fig. A- 2, and to approximate Maxwell's differential equations by central differences.

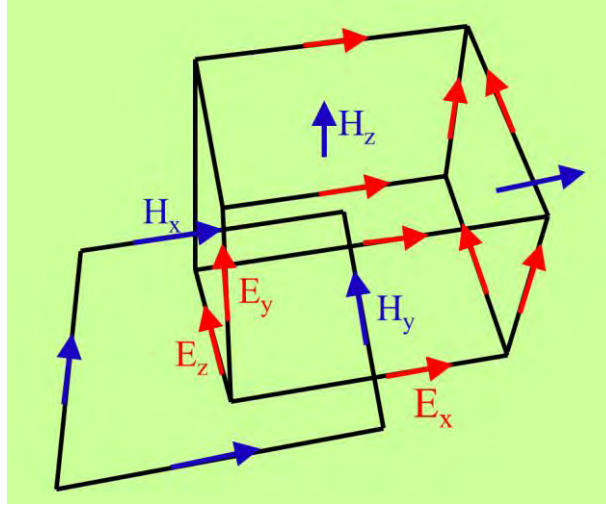


Fig. A- 2 Arrangement of field components in a Yee cell.

For example, the corresponding approximate equation for the  $\dot{B}_x$  component gives

$$\dot{B}_x = \frac{E_y\left(x, y, z + \frac{\delta z}{2}\right) - E_y\left(x, y, z - \frac{\delta z}{2}\right)}{\delta z} - \frac{E_z\left(x, y + \frac{\delta y}{2}, z\right) - E_z\left(x, y - \frac{\delta y}{2}, z\right)}{\delta y} \quad (\text{A.3})$$

Also the time derivative is approximated by central differences and arranged in such a way, that the computed values for  $\vec{B}$  and  $\vec{E}$  are shifted for a half step in time, yielding the well-known leapfrog scheme. For any component  $A$ , a numbering according to

$$A(x, y, z, t) = A\left(\sum_i \delta x_i, \sum_j \delta y_j, \sum_k \delta z_k, n\delta t\right) \triangleq A_{i,j,k}^n \quad (\text{A.4})$$

is introduced. The FDTD scheme can then be written as:

$$\begin{aligned} E_{x_{i^+,j,k}}^{n+1} &= \frac{1 - \frac{\sigma_{ijk}\delta t}{2\varepsilon_{ijk}}}{1 + \frac{\sigma_{ijk}\delta t}{2\varepsilon_{ijk}}} E_{x_{i^+,j,k}}^n + \frac{2\delta t}{\varepsilon_{ijk}} \left( \frac{H_{x_{i^+,j,k}^+}^{n+1/2} - H_{x_{i^+,j,k}^-}^{n+1/2}}{\delta y_j + \delta y_{j-1}} - \frac{H_{x_{i^+,j,k}^+}^{n+1/2} - H_{x_{i^+,j,k}^-}^{n+1/2}}{\delta z_k + \delta z_{k-1}} \right) \\ E_{y_{i,j^+,k}}^{n+1} &= \frac{1 - \frac{\sigma_{ijk}\delta t}{2\varepsilon_{ijk}}}{1 + \frac{\sigma_{ijk}\delta t}{2\varepsilon_{ijk}}} E_{y_{i,j^+,k}}^n + \frac{2\delta t}{\varepsilon_{ijk}} \left( \frac{H_{x_{i,j^+,k}^+}^{n+1/2} - H_{x_{i,j^+,k}^-}^{n+1/2}}{\delta z_k + \delta z_{k-1}} - \frac{H_{z_{i,j^+,k}^+}^{n+1/2} - H_{z_{i,j^+,k}^-}^{n+1/2}}{\delta x_i + \delta x_{i-1}} \right) \\ E_{z_{i,j,k^+}}^{n+1} &= \frac{1 - \frac{\sigma_{ijk}\delta t}{2\varepsilon_{ijk}}}{1 + \frac{\sigma_{ijk}\delta t}{2\varepsilon_{ijk}}} E_{z_{i,j,k^+}}^n + \frac{2\delta t}{\varepsilon_{ijk}} \left( \frac{H_{y_{i,j,k^+}}^{n+1/2} - H_{y_{i,j,k}^-}^{n+1/2}}{\delta x_i + \delta x_{i-1}} - \frac{H_{x_{i,j,k^+}}^{n+1/2} - H_{x_{i,j,k}^-}^{n+1/2}}{\delta y_j + \delta y_{j-1}} \right) \\ H_{x_{i,j^+,k^+}}^{n+1/2} &= H_{x_{i,j^+,k^+}}^{n-1/2} + \frac{\delta t}{\mu_{ijk}} \left( \frac{E_{y_{i,j^+,k+1}}^{n+1/2} - E_{y_{i,j^+,k}}^{n+1/2}}{\delta z_k} - \frac{E_{z_{i,j+1,k^+}}^{n+1/2} - E_{z_{i,j,k^+}}^{n+1/2}}{\delta y_j} \right) \\ H_{y_{i^+,j,k^+}}^{n+1/2} &= H_{y_{i^+,j,k^+}}^{n-1/2} + \frac{\delta t}{\mu_{ijk}} \left( \frac{E_{z_{i+1,j,k^+}}^{n+1/2} - E_{z_{i,j,k^+}}^{n+1/2}}{\delta x_i} - \frac{E_{x_{i^+,j,k+1}}^{n+1/2} - E_{x_{i^+,j,k}}^{n+1/2}}{\delta z_k} \right) \\ H_{z_{i^+,j^+,k}}^{n+1/2} &= H_{z_{i^+,j^+,k}}^{n-1/2} + \frac{\delta t}{\mu_{ijk}} \left( \frac{E_{x_{i^+,j+1,k}}^{n+1/2} - E_{x_{i^+,j,k}}^{n+1/2}}{\delta y_j} - \frac{E_{y_{i+1,j^+,k}}^{n+1/2} - E_{y_{i,j^+,k}}^{n+1/2}}{\delta x_i} \right) \end{aligned} \quad (\text{A.5})$$

Here, the superscripts  $i^\pm$  denote a spatial shift of half a cell size. The discrete material parameters  $\sigma_{ijk}$ ,  $\varepsilon_{ijk}$ ,  $\mu_{ijk}$ , are obtained from the continuous ones by a special averaging scheme. They are stored in an efficient way, so that the memory requirement is approximately limited to the 6 components.

These equations can now be solved recursively if initial values  $\vec{E}^0$  and  $\vec{H}^{1/2}$  and proper boundary conditions are given.

## Appendix

The field values are updated in each time step and lost, if they are not explicitly saved as done when recording voltages, currents or field plots. As can be seen, no matrix inversion is needed and so the calculation with numbers having medium precision (4 Bytes) is sufficient for most applications, thus leading to a very low memory requirement (approximately 24 Bytes per cell) for the simulation.

## **Appendix B Antenna Measurement Techniques**

### **B.1 Background to Antenna Measurement**

Antenna measurement is an important part for evaluating and verifying an antenna's performance during the designing procedure. All the antennas can be specified by a common set of parameters. Typical parameters used in antenna evaluation include the input impedance, polarization, radiation pattern, radiation efficiency and gain. All of these parameters can be measured through various means.

### **B.2 Antenna Test Range**

The choice of an antenna test range depends on many factors, such as the directivity of the antenna under test, frequency range and desired test parameters. Often the physical features of the antenna (size, weight and volume) can also have influence on the selection of an antenna range. During selecting an antenna range to evaluate antenna performance, care must be taken to ensure the performance metrics are measured with sufficient accuracy. Some commonly used antenna test ranges are shown in the Figure D-1.

### **B.3 Antenna Range Instrumentation [2]**

Regardless of the type of antenna range to be chosen, the instruments which operate the range are very similar. The instrumentation for antenna measurement consists of four subsystems; 1) positioning and control, 2) signal source, 3) receiving and 4) recording and processing.

The test antenna is installed on a positioner and is usually tested as the receiving mode. The motion of the positioner, such as rotation of the test antenna, is controlled by a positioner control device which is usually located in the control room. The positioner control device provides position data for the positioner and the recording/processing subsystem. A signal source provides the RF signal for the remote receiving antenna. The signal source can

be permanently fixed on the ground or floor, or located on a table near the source antenna, depending on the frequency of operation and mechanical considerations. The source control device is usually located in the control room with the measurement and control instrumentation.

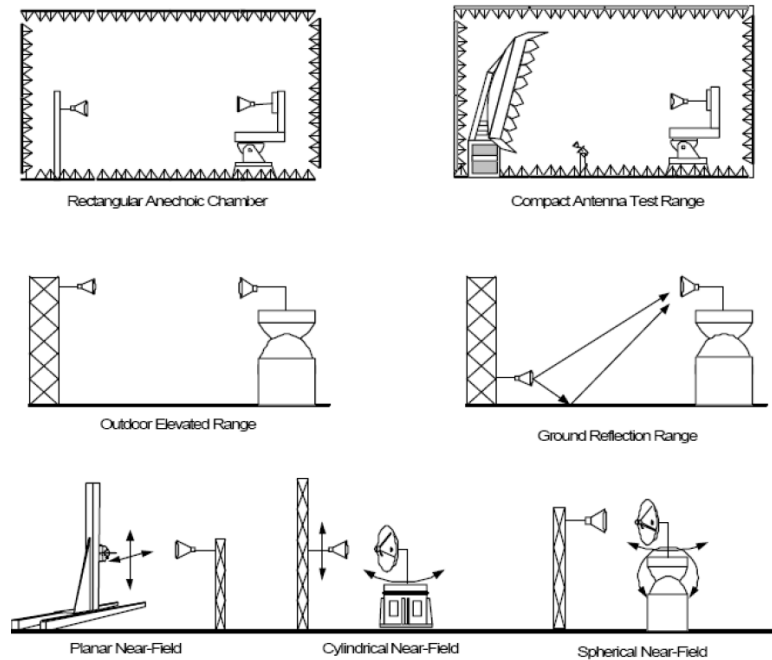


Fig. B. 1 Antenna test ranges.

To process the received signal for recording, microwave receivers are employed on the antenna range to accept the receiving signals from the test antenna and to convert these signals to lower frequencies for processing. Since the signals are usually low level, microwave receivers offer many advantages including improved dynamic range, better accuracy, and rejection of unwanted signals that may be present in the area. Data storage is conveniently handled by a variety of media including a floppy disk, local hard drive, removable drives or bulk data storage on a local network. After data acquisition is completed, an analysis software can plot the measured data, such as return loss, radiation pattern, gain, and so on, into a variety of data plotting formats such as rectangular, polar and three-dimensional plots. Often, a computer subsystem is added to the instrumentation to automate the entire measurement procedure.

## **B.4 Typical Applications of Antenna Range Instrumentation**

### **B.4.1 Near-Field Range**

Near-field ranges are used where large antennas are to be tested indoors in a relatively small space. This type of range uses a small RF probe antenna that scans over a surface surrounding the antenna under test. Typically separation between the probe and the antenna structure is about 4 to 10 wavelengths. During the measurement, near-field amplitude and phase information is collected over a discrete matrix of points. This data is then transformed to the far-field using Fourier techniques. The resulting far-field data can then be displayed in the same formats as conventional far-field antenna measurements. Near-field ranges usually are configured for automatic control. Both the large numbers of measurements and the need of transformation from the near-field data to the far-field, require the use of a computer system for data acquisition, reduction and display. The antenna may be tested in the transmit mode, receive mode, or both. There are many scanning coordinate systems possible for collecting the near-field data. Three techniques are in common usage:

1. Planar near- field method
2. Cylindrical fear-field method
3. Spherical near-field method

### **B.4.2 Indoor Far-Field Range**

Anechoic chambers can be configured for either manual or automatic control. The RF anechoic chamber is covered with radiation absorbent material (RAM) and instrumented the same way as outdoor ranges except that the range length is much shorter since these systems are located indoors. The receiver front end is typically positioned near the positioner with the mixer connected directly to the test antenna port. The source is located near the source antenna. The control room is generally centrally located and connected to both ends of the

antennas via cables. Usually the source antenna requires only polarization control, so a single positioner control unit is used to control all the range axes as well as the short range length.

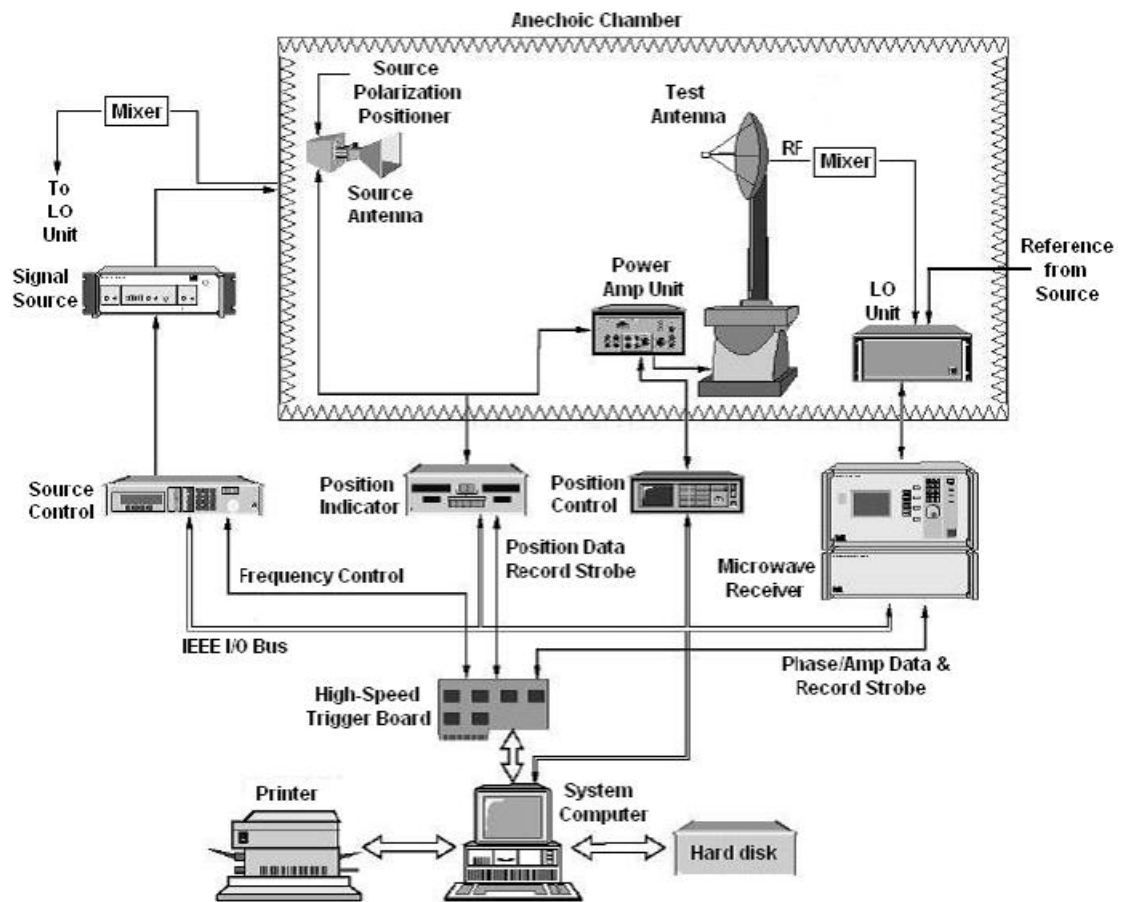


Fig. B. 2 Indoor far-field range.

## B.5 Special Precautions for Measurements

The measurement techniques are similar for most antennas however, depending on the application, size or manufacturing technology some special care needs to be taken. For instance for handset antennas, not only the antenna characteristics are measured in free space, they are also measured in in-hand and head positions. Moreover, parameters such as specific absorption rate (SAR) or hearing aid compatibility should also be specified. The following gives a brief overview on the precautions required for small antenna measurement.

Due to the large effects of the antenna mounting platform, the handset or laptop antennas are not normally measured in free space. It is common that the antenna is mounted on the simplified model of the final product and measured through a cable of minimum



diameter (usually around 1mm). If necessary the outer conductor of cable is soldered at regular intervals to the ground plane. For handset antennas it should exit the PCB close to the mid-point of the long edge of the ground plane, and the terminating connector (often type SMA) should project as little as possible. The reason for these important precautions is that the bandwidth available from an antenna is strongly dependent on its volume, so if the connection between the antenna and the measurement system will allow ground plane currents to flow along its outer conductor, the bandwidth will be enhanced by the presence of the cable. When the cable is removed the performance will be significantly changed – often for the worse [17]. This effect is less significant at the high bands, where performance is less dependent on length. It is usual to connect a quarter-wavelength sleeve choke (often referred to as a balun) directly to the connector on the handset Fig. B. 3 to prevent currents flowing in the outer conductor of the connecting cable [9]. Ferrite beads are lossy at the frequencies of the mobile radio bands; their use may create errors in efficiency measurements, so a choke is to be preferred. Positioning the point of connection at the centre of the PCB places it at the point of minimum voltage (minimum impedance) so the projecting connector has less influence on the measurements than it would if the cable were positioned at the end. It is often convenient to place the feed cable on the reverse side of the PCB to avoid any local influences on the fields surrounding the antenna.

Input impedance measurements are usually made using a vector network analyser (VNA). Two methods are available to allow accurate calibration to a reference plane at the input to the antenna matching circuit (P2 in Fig. B. 3).

- The VNA is calibrated to the end of the balun (P1). It is then connected to the feed cable while the cable is still open-circuit at the antenna matching circuit P2 and the electrical delay parameter of the VNA is adjusted to coalesce the trace to a point at the open-circuit point on the Smith chart. The value of electrical delay is recorded so the system can be recalibrated later without having to detach the measurement cable.
- Two identical feed cables are cut and terminated at one end. One is then fitted to the handset as shown, and the other is reserved for use as a calibrating cable. The same

internal cable and external balun are used for input impedance, radiation pattern and efficiency measurements.

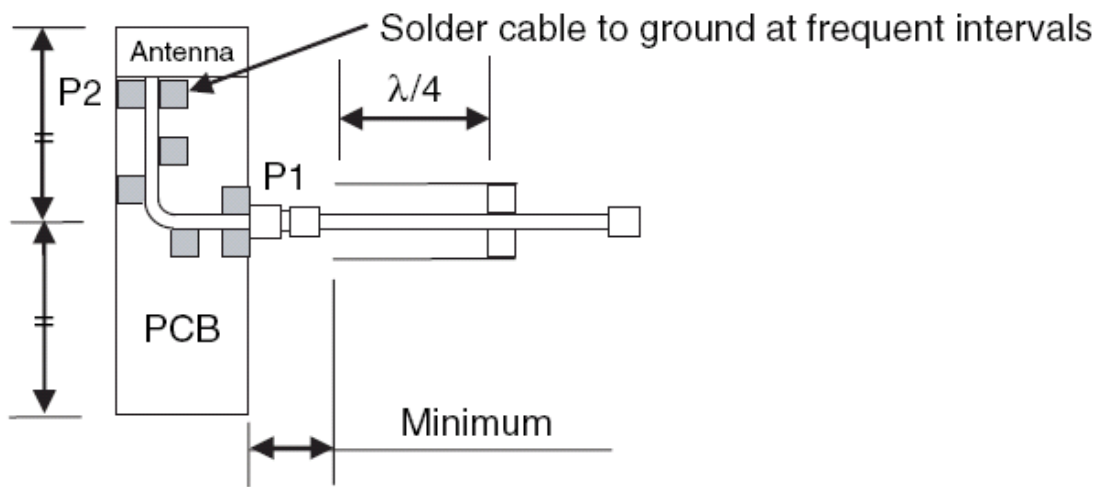


Fig. B. 3 Antenna on PCB with measurement cable and chokes [].

## Appendix C Component Datasheets

### Capacitors

# 1

## Accu-F® / Accu-P®

### Thin-Film Technology


#### THE IDEAL CAPACITOR

The non-ideal characteristics of a real capacitor can be ignored at low frequencies. Physical size imparts inductance to the capacitor and dielectric and metal electrodes result in resistive losses, but these often are of negligible effect on the circuit. At the very high frequencies of radio communication (>100MHz) and satellite systems (>1GHz), these effects become important. Recognizing that a real capacitor will exhibit inductive and resistive impedances in addition to capacitance, the ideal capacitor for these high frequencies is an ultra low loss component which can be fully characterized in all parameters with total repeatability from unit to unit.

Until recently, most high frequency/microwave capacitors were based on fired-ceramic (porcelain) technology. Layers of ceramic dielectric material and metal alloy electrode paste are interleaved and then sintered in a high temperature oven. This technology exhibits component variability in dielectric quality (losses, dielectric constant and insulation resistance), variability in electrode conductivity and variability in physical size (affecting inductance). An alternate thin-film technology has been developed which virtually eliminates these variances. It is this technology which has been fully incorporated into Accu-F® and Accu-P® to provide high frequency capacitors exhibiting truly ideal characteristics.

The main features of Accu-F® and Accu-P® may be summarized as follows:

- High purity of electrodes for very low and repeatable ESR.
- Highly pure, low-K dielectric for high breakdown field, high insulation resistance and low losses to frequencies above 40GHz.
- Very tight dimensional control for uniform inductance, unit to unit.
- Very tight capacitance tolerances for high frequency signal applications.



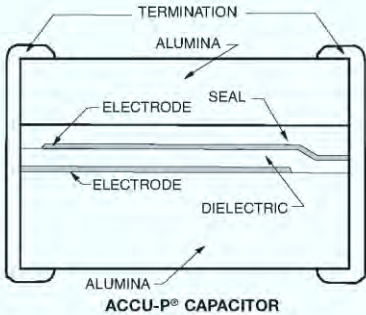
This accuracy sets apart these Thin-Film capacitors from ceramic capacitors so that the term Accu has been employed as the designation for this series of devices, an abbreviation for "accurate."

#### THIN-FILM TECHNOLOGY

Thin-film technology is commonly used in producing semiconductor devices. In the last two decades, this technology has developed tremendously, both in performance and in process control. Today's techniques enable line definitions of below 1µm, and the controlling of thickness of layers at 100Å (10<sup>-3</sup>µm). Applying this technology to the manufacture of capacitors has enabled the development of components where both electrical and physical properties can be tightly controlled.


The thin-film production facilities at AVX consist of:

- Class 1000 clean rooms, with working areas under laminar-flow hoods of class 100, (below 100 particles per cubic foot larger than 0.5µm).
- High vacuum metal deposition systems for high-purity electrode construction.
- Photolithography equipment for line definition down to 2.0µm accuracy.
- Plasma-enhanced CVD for various dielectric depositions (CVD=Chemical Vapor Deposition).
- High accuracy, microprocessor-controlled dicing saws for chip separation.
- High speed, high accuracy sorting to ensure strict tolerance adherence.



ACCU-P® CAPACITOR

6



## Accu-F® / Accu-P®

### Thin-Film Chip Capacitors



#### ACCU-F® TECHNOLOGY

The use of very low-loss dielectric materials, silicon dioxide and silicon oxynitride, in conjunction with highly conductive electrode metals results in low ESR and high Q. These high-frequency characteristics change at a slower rate with increasing frequency than for ceramic microwave capacitors.

Because of the thin-film technology, the above-mentioned frequency characteristics are obtained without significant compromise of properties required for surface mounting.

The main Accu-F® properties are:

- Internationally agreed sizes with excellent dimensional control.
- Small size chip capacitors (0603) are available.
- Tight capacitance tolerances.
- Low ESR at VHF, UHF and microwave frequencies.
- High stability with respect to time, temperature, frequency and voltage variation.
- Nickel/solder-coated terminations to provide excellent solderability and leach resistance.

#### ACCU-F® FEATURES

Accu-F® meets the fast-growing demand for low-loss (high-Q) capacitors for use in surface mount technology especially for the mobile communications market, such as cellular radio of 450 and 900 MHz, UHF walkie-talkies, UHF cordless telephones to 2.3 GHz, low noise blocks at 11-12.5 GHz and for other VHF, UHF and microwave applications.

Accu-F® is currently unique in its ability to offer very low capacitance values (0.1pF) and very tight capacitance tolerances ( $\pm 0.05\text{pF}$ ). Typically Accu-F® will be used in small signal applications in VCO's, matching networks, filters, etc.

Inspection test and quality control procedures in accordance with ISO 9001, CECC, IECQ and USA MIL Standards yield products of the highest quality.

#### APPLICATIONS

Cellular Communications  
CT2/PCN (Cordless Telephone/Personal Comm. Networks)  
Satellite TV  
Cable TV  
GPS (Global Positioning Systems)  
Vehicle Location Systems  
Vehicle Alarm Systems  
Paging  
Military Communications

Radar Systems  
Video Switching  
Test & Measurements  
Filters  
VCO's  
Matching Networks

#### APPROVALS

ISO 9001

#### ACCU-P® TECHNOLOGY

As in the Accu-F® series the use of very low-loss dielectric materials (silicon dioxide and silicon oxynitride) in conjunction with highly conductive electrode metals results in low ESR and high Q. At high frequency these characteristics change at a slower rate with increasing frequency than conventional ceramic microwave capacitors. Using thin-film technology, the above-mentioned frequency characteristics are obtained without significant compromise of properties required for surface mounting. The use of high thermal conductivity materials results in excellent RF power handling capabilities.

The main Accu-P® properties are:

- Enhanced RF power handling capability.
- Improved mechanical characteristics.
- Internationally agreed sizes with excellent dimensional control.
- Ultra Small size chip capacitors (0201) are available.
- Tight capacitance tolerances.
- Low ESR at UHF, VHF, and microwave frequencies.
- High-stability with respect to time, temperature, frequency and voltage variation.
- High temperature nickel/solder-coated terminations as standard to provide excellent solderability and leach resistance.

#### ACCU-P® FEATURES

- Minimal batch to batch variability of parameters at high frequency.
- The Accu-P® has the same unique features as the Accu-F® capacitor such as low ESR, high Q, availability of very low capacitance values and very tight capacitance tolerances.
- The RF power handling capability of the Accu-P® allows for its usage in both small signal and RF power applications.
- Inspection, test and quality control procedures in accordance with ISO 9001, CECC, IECQ and USA MIL Standards guarantee product of the highest quality.
- Hand soldering Accu-P®: Due to their construction utilizing relatively high thermal conductivity materials, Accu-P's have become the preferred device in R & D labs and production environments where hand soldering is used. Accu-P's are available in all sizes and are electrically identical to their Accu-F counterparts.

#### APPLICATIONS

Cellular Communications  
CT2/PCN (Cordless Telephone/Personal Comm. Networks)  
Satellite TV  
Cable TV  
GPS (Global Positioning Systems)  
Vehicle Location Systems  
Vehicle Alarm Systems  
Paging  
Military Communications

Radar Systems  
Video Switching  
Test & Measurements  
Filters  
VCO's  
Matching Networks  
RF Amplifiers

#### APPROVALS

ISO 9001





## Accu-P®

## Signal and Power Type Capacitors



## Accu-P® Capacitance Ranges (pF)

## TEMP. COEFFICIENT CODE

"J" =  $0 \pm 30 \text{ ppm}/^\circ\text{C}$  (-55°C to +125°C)<sup>(1)</sup>

## TEMP. COEFFICIENT CODE

"K" =  $0 \pm 60 \text{ ppm}/^\circ\text{C}$  (-55°C to +125°C)<sup>(1)</sup>

1

| Size                     |          | 0201 |    |    |    |    | 0402 |    |    |    |    | 0603 |    |    |     |    | 0805 |     |    |    |     | 1210 |     |    |     |    |
|--------------------------|----------|------|----|----|----|----|------|----|----|----|----|------|----|----|-----|----|------|-----|----|----|-----|------|-----|----|-----|----|
| Size Code                |          | 100  | 50 | 25 | 16 | 10 | 100  | 50 | 25 | 16 | 10 | 100  | 50 | 25 | 100 | 50 | 25   | 100 | 50 | 25 | 100 | 50   | 100 | 50 | 100 | 50 |
| Cap in pF <sup>(1)</sup> | Cap code |      |    |    |    |    |      |    |    |    |    |      |    |    |     |    |      |     |    |    |     |      |     |    |     |    |
| 0.1                      | — 0R1    |      |    |    |    |    |      |    |    |    |    |      |    |    |     |    |      |     |    |    |     |      |     |    |     |    |
| 0.2                      | — 0R2    |      |    |    |    |    |      |    |    |    |    |      |    |    |     |    |      |     |    |    |     |      |     |    |     |    |
| 0.3                      | — 0R3    |      |    |    |    |    |      |    |    |    |    |      |    |    |     |    |      |     |    |    |     |      |     |    |     |    |
| 0.4                      | — 0R4    |      |    |    |    |    |      |    |    |    |    |      |    |    |     |    |      |     |    |    |     |      |     |    |     |    |
| 0.5                      | — 0R5    |      |    |    |    |    |      |    |    |    |    |      |    |    |     |    |      |     |    |    |     |      |     |    |     |    |
| 0.6                      | — 0R6    |      |    |    |    |    |      |    |    |    |    |      |    |    |     |    |      |     |    |    |     |      |     |    |     |    |
| 0.7                      | — 0R7    |      |    |    |    |    |      |    |    |    |    |      |    |    |     |    |      |     |    |    |     |      |     |    |     |    |
| 0.8                      | — 0R8    |      |    |    |    |    |      |    |    |    |    |      |    |    |     |    |      |     |    |    |     |      |     |    |     |    |
| 0.9                      | — 0R9    |      |    |    |    |    |      |    |    |    |    |      |    |    |     |    |      |     |    |    |     |      |     |    |     |    |
| 1.0                      | — 1R0    |      |    |    |    |    |      |    |    |    |    |      |    |    |     |    |      |     |    |    |     |      |     |    |     |    |
| 1.1                      | — 1R1    |      |    |    |    |    |      |    |    |    |    |      |    |    |     |    |      |     |    |    |     |      |     |    |     |    |
| 1.2                      | — 1R2    |      |    |    |    |    |      |    |    |    |    |      |    |    |     |    |      |     |    |    |     |      |     |    |     |    |
| 1.3                      | — 1R3    |      |    |    |    |    |      |    |    |    |    |      |    |    |     |    |      |     |    |    |     |      |     |    |     |    |
| 1.4                      | — 1R4    |      |    |    |    |    |      |    |    |    |    |      |    |    |     |    |      |     |    |    |     |      |     |    |     |    |
| 1.5                      | — 1R5    |      |    |    |    |    |      |    |    |    |    |      |    |    |     |    |      |     |    |    |     |      |     |    |     |    |
| 1.6                      | — 1R6    |      |    |    |    |    |      |    |    |    |    |      |    |    |     |    |      |     |    |    |     |      |     |    |     |    |
| 1.7                      | — 1R7    |      |    |    |    |    |      |    |    |    |    |      |    |    |     |    |      |     |    |    |     |      |     |    |     |    |
| 1.8                      | — 1R8    |      |    |    |    |    |      |    |    |    |    |      |    |    |     |    |      |     |    |    |     |      |     |    |     |    |
| 1.9                      | — 1R9    |      |    |    |    |    |      |    |    |    |    |      |    |    |     |    |      |     |    |    |     |      |     |    |     |    |
| 2.0                      | — 2R0    |      |    |    |    |    |      |    |    |    |    |      |    |    |     |    |      |     |    |    |     |      |     |    |     |    |
| 2.1                      | — 2R1    |      |    |    |    |    |      |    |    |    |    |      |    |    |     |    |      |     |    |    |     |      |     |    |     |    |
| 2.2                      | — 2R2    |      |    |    |    |    |      |    |    |    |    |      |    |    |     |    |      |     |    |    |     |      |     |    |     |    |
| 2.3                      | — 2R3    |      |    |    |    |    |      |    |    |    |    |      |    |    |     |    |      |     |    |    |     |      |     |    |     |    |
| 2.4                      | — 2R4    |      |    |    |    |    |      |    |    |    |    |      |    |    |     |    |      |     |    |    |     |      |     |    |     |    |
| 2.5                      | — 2R5    |      |    |    |    |    |      |    |    |    |    |      |    |    |     |    |      |     |    |    |     |      |     |    |     |    |
| 2.6                      | — 2R6    |      |    |    |    |    |      |    |    |    |    |      |    |    |     |    |      |     |    |    |     |      |     |    |     |    |
| 2.7                      | — 2R7    |      |    |    |    |    |      |    |    |    |    |      |    |    |     |    |      |     |    |    |     |      |     |    |     |    |
| 2.8                      | — 2R8    |      |    |    |    |    |      |    |    |    |    |      |    |    |     |    |      |     |    |    |     |      |     |    |     |    |
| 2.9                      | — 2R9    |      |    |    |    |    |      |    |    |    |    |      |    |    |     |    |      |     |    |    |     |      |     |    |     |    |
| 3.0                      | — 3R0    |      |    |    |    |    |      |    |    |    |    |      |    |    |     |    |      |     |    |    |     |      |     |    |     |    |
| 3.1                      | — 3R1    |      |    |    |    |    |      |    |    |    |    |      |    |    |     |    |      |     |    |    |     |      |     |    |     |    |
| 3.2                      | — 3R2    |      |    |    |    |    |      |    |    |    |    |      |    |    |     |    |      |     |    |    |     |      |     |    |     |    |
| 3.3                      | — 3R3    |      |    |    |    |    |      |    |    |    |    |      |    |    |     |    |      |     |    |    |     |      |     |    |     |    |
| 3.4                      | — 3R4    |      |    |    |    |    |      |    |    |    |    |      |    |    |     |    |      |     |    |    |     |      |     |    |     |    |
| 3.5                      | — 3R5    |      |    |    |    |    |      |    |    |    |    |      |    |    |     |    |      |     |    |    |     |      |     |    |     |    |
| 3.6                      | — 3R6    |      |    |    |    |    |      |    |    |    |    |      |    |    |     |    |      |     |    |    |     |      |     |    |     |    |
| 3.7                      | — 3R7    |      |    |    |    |    |      |    |    |    |    |      |    |    |     |    |      |     |    |    |     |      |     |    |     |    |
| 3.8                      | — 3R8    |      |    |    |    |    |      |    |    |    |    |      |    |    |     |    |      |     |    |    |     |      |     |    |     |    |
| 3.9                      | — 3R9    |      |    |    |    |    |      |    |    |    |    |      |    |    |     |    |      |     |    |    |     |      |     |    |     |    |
| 4.0                      | — 4R0    |      |    |    |    |    |      |    |    |    |    |      |    |    |     |    |      |     |    |    |     |      |     |    |     |    |
| 4.1                      | — 4R1    |      |    |    |    |    |      |    |    |    |    |      |    |    |     |    |      |     |    |    |     |      |     |    |     |    |
| 4.2                      | — 4R2    |      |    |    |    |    |      |    |    |    |    |      |    |    |     |    |      |     |    |    |     |      |     |    |     |    |
| 4.3                      | — 4R3    |      |    |    |    |    |      |    |    |    |    |      |    |    |     |    |      |     |    |    |     |      |     |    |     |    |
| 4.4                      | — 4R4    |      |    |    |    |    |      |    |    |    |    |      |    |    |     |    |      |     |    |    |     |      |     |    |     |    |
| 4.5                      | — 4R5    |      |    |    |    |    |      |    |    |    |    |      |    |    |     |    |      |     |    |    |     |      |     |    |     |    |
| 4.6                      | — 4R6    |      |    |    |    |    |      |    |    |    |    |      |    |    |     |    |      |     |    |    |     |      |     |    |     |    |
| 4.7                      | — 4R7    |      |    |    |    |    |      |    |    |    |    |      |    |    |     |    |      |     |    |    |     |      |     |    |     |    |
| 5.1                      | — 5R1    |      |    |    |    |    |      |    |    |    |    |      |    |    |     |    |      |     |    |    |     |      |     |    |     |    |
| 5.6                      | — 5R6    |      |    |    |    |    |      |    |    |    |    |      |    |    |     |    |      |     |    |    |     |      |     |    |     |    |
| 6.2                      | — 6R2    |      |    |    |    |    |      |    |    |    |    |      |    |    |     |    |      |     |    |    |     |      |     |    |     |    |
| 6.8                      | — 6R8    |      |    |    |    |    |      |    |    |    |    |      |    |    |     |    |      |     |    |    |     |      |     |    |     |    |
| 7.5                      | — 7R5    |      |    |    |    |    |      |    |    |    |    |      |    |    |     |    |      |     |    |    |     |      |     |    |     |    |
| 8.2                      | — 8R2    |      |    |    |    |    |      |    |    |    |    |      |    |    |     |    |      |     |    |    |     |      |     |    |     |    |
| 9.1                      | — 9R1    |      |    |    |    |    |      |    |    |    |    |      |    |    |     |    |      |     |    |    |     |      |     |    |     |    |
| 10.0                     | — 10R0   |      |    |    |    |    |      |    |    |    |    |      |    |    |     |    |      |     |    |    |     |      |     |    |     |    |
| 11.0                     | — 11R0   |      |    |    |    |    |      |    |    |    |    |      |    |    |     |    |      |     |    |    |     |      |     |    |     |    |
| 12.0                     | — 12R0   |      |    |    |    |    |      |    |    |    |    |      |    |    |     |    |      |     |    |    |     |      |     |    |     |    |
| 13.0                     | — 13R0   |      |    |    |    |    |      |    |    |    |    |      |    |    |     |    |      |     |    |    |     |      |     |    |     |    |
| 14.0                     | — 14R0   |      |    |    |    |    |      |    |    |    |    |      |    |    |     |    |      |     |    |    |     |      |     |    |     |    |
| 15.0                     | — 15R0   |      |    |    |    |    |      |    |    |    |    |      |    |    |     |    |      |     |    |    |     |      |     |    |     |    |
| 16.0                     | — 16R0   |      |    |    |    |    |      |    |    |    |    |      |    |    |     |    |      |     |    |    |     |      |     |    |     |    |
| 17.0                     | — 17R0   |      |    |    |    |    |      |    |    |    |    |      |    |    |     |    |      |     |    |    |     |      |     |    |     |    |
| 18.0                     | — 18R0   |      |    |    |    |    |      |    |    |    |    |      |    |    |     |    |      |     |    |    |     |      |     |    |     |    |
| 19.0                     | — 19R0   |      |    |    |    |    |      |    |    |    |    |      |    |    |     |    |      |     |    |    |     |      |     |    |     |    |
| 20.0                     | — 20R0   |      |    |    |    |    |      |    |    |    |    |      |    |    |     |    |      |     |    |    |     |      |     |    |     |    |
| 21.0                     | — 21R0   |      |    |    |    |    |      |    |    |    |    |      |    |    |     |    |      |     |    |    |     |      |     |    |     |    |
| 22.0                     | — 22R0   |      |    |    |    |    |      |    |    |    |    |      |    |    |     |    |      |     |    |    |     |      |     |    |     |    |
| 24.0                     | — 24R0   |      |    |    |    |    |      |    |    |    |    |      |    |    |     |    |      |     |    |    |     |      |     |    |     |    |
| 27.0                     | — 27R0   |      |    |    |    |    |      |    |    |    |    |      |    |    |     |    |      |     |    |    |     |      |     |    |     |    |
| 30.0                     | — 30R0   |      |    |    |    |    |      |    |    |    |    |      |    |    |     |    |      |     |    |    |     |      |     |    |     |    |
| 33.0                     | — 33R0   |      |    |    |    |    |      |    |    |    |    |      |    |    |     |    |      |     |    |    |     |      |     |    |     |    |
| 39.0                     | — 39R0   |      |    |    |    |    |      |    |    |    |    |      |    |    |     |    |      |     |    |    |     |      |     |    |     |    |
| 47.0                     | — 47R0   |      |    |    |    |    |      |    |    |    |    |      |    |    |     |    |      |     |    |    |     |      |     |    |     |    |
| 56.0                     | — 56R0   |      |    |    |    |    |      |    |    |    |    |      |    |    |     |    |      |     |    |    |     |      |     |    |     |    |
| 68.0                     | — 68R0   |      |    |    |    |    |      |    |    |    |    |      |    |    |     |    |      |     |    |    |     |      |     |    |     |    |

<sup>(1)</sup> For capacitance values higher than listed in table, please consult factory.<sup>(2)</sup> TC shown is per EIA/IEC Specifications.

These values are produced with "K" temperature coefficient code only.

| Size                     |          | 805 |    |    |     |    | 1210 |    |     |    |     |
|--------------------------|----------|-----|----|----|-----|----|------|----|-----|----|-----|
| Size Code                |          | 100 | 50 | 25 | 100 | 50 | 100  | 50 | 100 | 50 | 100 |
| Cap in pF <sup>(1)</sup> | Cap code |     |    |    |     |    |      |    |     |    |     |
| 0.1                      | — 0R1    |     |    |    |     |    |      |    |     |    |     |
| 0.2                      | — 0R2    |     |    |    |     |    |      |    |     |    |     |
| 0.3                      | — 0R3    |     |    |    |     |    |      |    |     |    |     |
| 0.4                      | — 0R4    |     |    |    |     |    |      |    |     |    |     |
| 0.5                      | — 0R5    |     |    |    |     |    |      |    |     |    |     |
| 0.6                      | — 0R6    |     |    |    |     |    |      |    |     |    |     |
| 0.7                      | — 0R7    |     |    |    |     |    |      |    |     |    |     |
| 0.8                      | — 0R8    |     |    |    |     |    |      |    |     |    |     |
| 0.9                      | — 0R9    |     |    |    |     |    |      |    |     |    |     |
| 1.0                      | — 1R0    |     |    |    |     |    |      |    |     |    |     |
| 1.1                      | — 1R1    |     |    |    |     |    |      |    |     |    |     |
| 1.2                      | — 1R2    |     |    |    |     |    |      |    |     |    |     |
| 1.3                      | — 1R3    |     |    |    |     |    |      |    |     |    |     |
| 1.4                      | — 1R4    |     |    |    |     |    |      |    |     |    |     |
| 1.5                      | — 1R5    |     |    |    |     |    |      |    |     |    |     |
| 1.6                      | — 1R6    |     |    |    |     |    |      |    |     |    |     |
| 1.7                      | — 1R7    |     |    |    |     |    |      |    |     |    |     |
| 1.8                      | — 1R8    |     |    |    |     |    |      |    |     |    |     |
| 1.9                      | — 1R9    |     |    |    |     |    |      |    |     |    |     |
| 2.0                      | — 2R0    |     |    |    |     |    |      |    |     |    |     |
| 2.1                      | — 2R1    |     |    |    |     |    |      |    |     |    |     |
| 2.2                      | — 2R2    |     |    |    |     |    |      |    |     |    |     |

Accu-P®

AVX RF

## 0402 Typical Electrical Tables

1

| Capacitance<br>& Tolerance*<br>@ 1 MHz<br>(pF) | Self<br>Resonance<br>Frequency<br>(GHz)<br>Typical | Ref<br>Freq<br>(MHz) | Typ.<br>C(eff)<br>(pF) | Typ.<br>Q | Typ.<br>ESR<br>(Ω) | Ref<br>Freq<br>(MHz) | Typ.<br>C(eff)<br>(pF) | Typ.<br>Q | Typ.<br>ESR<br>(Ω) | Ref<br>Freq<br>(MHz) | Typ.<br>C(eff)<br>(pF) | Typ.<br>Q | Typ.<br>ESR<br>(Ω) | Ref<br>Freq<br>(MHz) | Typ.<br>C(eff)<br>(pF) | Typ.<br>Q | Typ.<br>ESR<br>(Ω) | Ref<br>Freq<br>(MHz) | Typ.<br>C(eff)<br>(pF) | Typ.<br>Q | Typ.<br>ESR<br>(Ω) |
|--|--|----------------------|------------------------|-----------|--------------------|----------------------|------------------------|-----------|--------------------|----------------------|------------------------|-----------|--------------------|----------------------|------------------------|-----------|--------------------|----------------------|------------------------|-----------|--------------------|
| 0.1±0.05                                       | 19.4   | n/a                  | n/a                    | n/a       | n/a                | n/a                  | n/a                    | n/a       | n/a                | n/a                  | n/a                    | n/a       | n/a                | n/a                  | n/a                    | n/a       | n/a                | n/a                  | n/a                    | n/a       | n/a                |
| 0.2±0.05                                       | 16.4   | n/a                  | n/a                    | n/a       | n/a                | n/a                  | n/a                    | n/a       | n/a                | n/a                  | n/a                    | n/a       | n/a                | n/a                  | n/a                    | n/a       | n/a                | n/a                  | n/a                    | n/a       | n/a                |
| 0.3±0.05                                       | 14.6   | n/a                  | n/a                    | n/a       | n/a                | n/a                  | n/a                    | n/a       | n/a                | n/a                  | n/a                    | n/a       | n/a                | n/a                  | n/a                    | n/a       | n/a                | n/a                  | n/a                    | n/a       | n/a                |
| 0.4±0.05                                       | 12.5   | n/a                  | n/a                    | n/a       | n/a                | n/a                  | n/a                    | n/a       | n/a                | n/a                  | n/a                    | n/a       | n/a                | n/a                  | n/a                    | n/a       | n/a                | n/a                  | n/a                    | n/a       | n/a                |
| 0.5±0.05                                       | 11.3   | n/a                  | n/a                    | n/a       | n/a                | n/a                  | n/a                    | n/a       | n/a                | n/a                  | n/a                    | n/a       | n/a                | n/a                  | n/a                    | n/a       | n/a                | n/a                  | n/a                    | n/a       | n/a                |
| 0.6±0.05                                       | 10.4   | n/a                  | n/a                    | n/a       | n/a                | n/a                  | n/a                    | n/a       | n/a                | n/a                  | n/a                    | n/a       | n/a                | n/a                  | n/a                    | n/a       | n/a                | n/a                  | n/a                    | n/a       | n/a                |
| 0.7±0.05                                       | 9.5  | n/a                  | n/a                    | n/a       | n/a                | n/a                  | n/a                    | n/a       | n/a                | n/a                  | n/a                    | n/a       | n/a                | n/a                  | n/a                    | n/a       | n/a                | n/a                  | n/a                    | n/a       | n/a                |
| 0.8±0.05                                       | 9.1  | n/a                  | n/a                    | n/a       | n/a                | n/a                  | n/a                    | n/a       | n/a                | n/a                  | n/a                    | n/a       | n/a                | n/a                  | n/a                    | n/a       | n/a                | n/a                  | n/a                    | n/a       | n/a                |
| 0.9±0.05                                       | 8.8  | n/a                  | n/a                    | n/a       | n/a                | n/a                  | n/a                    | n/a       | n/a                | n/a                  | n/a                    | n/a       | n/a                | n/a                  | n/a                    | n/a       | n/a                | n/a                  | n/a                    | n/a       | n/a                |
| 1.0±0.05                                       | 8  | 247                  | 1.16                   | 1635      | 0.34               | 494                  | 1.15                   | 1283      | 0.22               | 742                  | 1.13                   | 870       | 0.22               | 991                  | 1.12                   | 620       | 0.23               | 1240                 | 1.14                   | 474       | 0.25               |
| 1.1±0.05                                       | 7.8  | 246                  | 1.25                   | 1581      | 0.32               | 492                  | 1.22                   | 1219      | 0.21               | 740                  | 1.21                   | 791       | 0.22               | 989                  | 1.19                   | 561       | 0.24               | 1238                 | 1.21                   | 425       | 0.25               |
| 1.2±0.05                                       | 7.4  | 245                  | 1.34                   | 1538      | 0.30               | 491                  | 1.33                   | 1153      | 0.21               | 738                  | 1.31                   | 727       | 0.22               | 986                  | 1.3                    | 503       | 0.25               | 1234                 | 1.33                   | 372       | 0.25               |
| 1.3±0.05                                       | 7  | 244                  | 1.42                   | 1502      | 0.29               | 490                  | 1.42                   | 1109      | 0.21               | 736                  | 1.4                    | 701       | 0.21               | 983                  | 1.35                   | 480       | 0.24               | 1230                 | 1.41                   | 350       | 0.25               |
| 1.4±0.05                                       | 6.8  | 243                  | 1.53                   | 1476      | 0.28               | 488                  | 1.54                   | 1061      | 0.20               | 733                  | 1.52                   | 680       | 0.21               | 980                  | 1.49                   | 461       | 0.23               | 1229                 | 1.53                   | 333       | 0.25               |
| 1.5±0.05                                       | 6.5  | 242                  | 1.63                   | 1454      | 0.28               | 486                  | 1.63                   | 1002      | 0.20               | 731                  | 1.58                   | 638       | 0.21               | 978                  | 1.6                    | 438       | 0.23               | 1226                 | 1.65                   | 316       | 0.25               |
| 1.6±0.05                                       | 6.5  | 242                  | 1.71                   | 1448      | 0.27               | 485                  | 1.76                   | 986       | 0.20               | 729                  | 1.69                   | 622       | 0.21               | 986                  | 1.71                   | 429       | 0.23               | 1224                 | 1.77                   | 309       | 0.24               |
| 1.7±0.05                                       | 6.4  | 241                  | 1.85                   | 1444      | 0.27               | 483                  | 1.81                   | 970       | 0.19               | 728                  | 1.75                   | 612       | 0.20               | 985                  | 1.75                   | 422       | 0.22               | 1223                 | 1.86                   | 305       | 0.23               |
| 1.8±0.05                                       | 6.2  | 240                  | 1.93                   | 1430      | 0.26               | 482                  | 1.86                   | 931       | 0.19               | 727                  | 1.83                   | 597       | 0.20               | 983                  | 1.8                    | 413       | 0.22               | 1220                 | 1.91                   | 299       | 0.23               |
| 1.9±0.05                                       | 6  | 239                  | 2.01                   | 1421      | 0.25               | 481                  | 1.93                   | 897       | 0.19               | 726                  | 1.91                   | 583       | 0.20               | 972                  | 1.91                   | 401       | 0.21               | 1219                 | 1.97                   | 294       | 0.22               |
| 2.0±0.05                                       | 5.7  | 239                  | 2.11                   | 1410      | 0.24               | 480                  | 2.06                   | 896       | 0.18               | 722                  | 2.11                   | 582       | 0.19               | 969                  | 2.01                   | 400       | 0.20               | 1215                 | 2.11                   | 293       | 0.21               |
| 2.1±0.05                                       | 5.4  | 238                  | 2.21                   | 1406      | 0.23               | 478                  | 2.14                   | 893       | 0.17               | 720                  | 2.21                   | 581       | 0.18               | 966                  | 2.1                    | 398       | 0.19               | 1213                 | 2.22                   | 291       | 0.20               |
| 2.2±0.05                                       | 5.1  | 237                  | 2.28                   | 1406      | 0.22               | 476                  | 2.27                   | 893       | 0.16               | 718                  | 2.26                   | 581       | 0.17               | 964                  | 2.27                   | 396       | 0.18               | 1212                 | 2.35                   | 289       | 0.19               |
| 2.3±0.05                                       | 5  | 237                  | 2.32                   | 1405      | 0.20               | 475                  | 2.36                   | 870       | 0.16               | 716                  | 2.4                    | 549       | 0.17               | 962                  | 2.3                    | 379       | 0.18               | 1209                 | 2.4                    | 262       | 0.20               |
| 2.4±0.05                                       | 4.9  | 236                  | 2.45                   | 1404      | 0.19               | 473                  | 2.48                   | 845       | 0.16               | 715                  | 2.51                   | 501       | 0.17               | 960                  | 2.41                   | 358       | 0.18               | 1208                 | 2.53                   | 253       | 0.20               |
| 2.5±0.05                                       | 4.7  | 235                  | 2.49                   | 1404      | 0.18               | 472                  | 2.6                    | 821       | 0.16               | 714                  | 2.62                   | 486       | 0.17               | 959                  | 2.52                   | 349       | 0.19               | 1205                 | 2.7                    | 240       | 0.20               |
| 2.6±0.05                                       | 4.6  | 234                  | 2.6                    | 1402      | 0.16               | 470                  | 2.71                   | 799       | 0.15               | 712                  | 2.73                   | 477       | 0.17               | 958                  | 2.65                   | 331       | 0.19               | 1204                 | 2.85                   | 231       | 0.20               |
| 2.7±0.05                                       | 4.5  | 233                  | 2.84                   | 1399      | 0.15               | 469                  | 2.83                   | 778       | 0.15               | 711                  | 2.82                   | 464       | 0.17               | 956                  | 2.86                   | 313       | 0.19               | 1203                 | 3                      | 224       | 0.20               |
| 2.8±0.05                                       | 4.5  | 233                  | 2.85                   | 1395      | 0.15               | 468                  | 2.94                   | 769       | 0.15               | 710                  | 2.9                    | 458       | 0.16               | 954                  | 2.91                   | 308       | 0.18               | 1202                 | 3.12                   | 220       | 0.20               |
| 2.9±0.05                                       | 4.4  | 232                  | 2.87                   | 1395      | 0.15               | 467                  | 3.11                   | 751       | 0.15               | 710                  | 2.99                   | 450       | 0.16               | 953                  | 3.15                   | 303       | 0.18               | 1201                 | 3.24                   | 218       | 0.19               |
| 3.0±0.05                                       | 4.4  | 231                  | 2.88                   | 1392      | 0.14               | 466                  | 3.39                   | 746       | 0.15               | 709                  | 3.11                   | 440       | 0.16               | 952                  | 3.41                   | 299       | 0.18               | 1201                 | 3.33                   | 212       | 0.19               |
| 3.1±0.05                                       | 4.4  | 230                  | 2.9                    | 1392      | 0.14               | 465                  | 3.45                   | 733       | 0.15               | 708                  | 3.22                   | 429       | 0.16               | 951                  | 3.48                   | 291       | 0.18               | 1199                 | 3.45                   | 207       | 0.19               |
| 3.2±0.05                                       | 4.3  | 230                  | 2.91                   | 1391      | 0.14               | 464                  | 3.61                   | 725       | 0.15               | 707                  | 3.3                    | 421       | 0.16               | 950                  | 3.68                   | 285       | 0.17               | 1198                 | 3.58                   | 203       | 0.19               |
| 3.3±0.05                                       | 4.3  | 229                  | 2.92                   | 1391      | 0.14               | 462                  | 3.72                   | 711       | 0.14               | 707                  | 3.42                   | 415       | 0.16               | 949                  | 3.8                    | 282       | 0.17               | 1197                 | 3.61                   | 198       | 0.19               |
| 3.4±0.05                                       | 4.3  | 228                  | 2.93                   | 1390      | 0.14               | 461                  | 3.78                   | 705       | 0.14               | 706                  | 3.53                   | 407       | 0.15               | 948                  | 3.79                   | 276       | 0.17               | 1196                 | 3.78                   | 195       | 0.19               |
| 3.5±0.05                                       | 4.2  | 227                  | 2.95                   | 1389      | 0.13               | 460                  | 3.82                   | 693       | 0.14               | 705                  | 3.6                    | 402       | 0.15               | 947                  | 3.85                   | 273       | 0.16               | 1195                 | 3.91                   | 191       | 0.18               |
| 3.6±0.05                                       | 4.2  | 226                  | 2.97                   | 1382      | 0.13               | 459                  | 3.87                   | 688       | 0.14               | 704                  | 3.7                    | 395       | 0.15               | 946                  | 3.89                   | 270       | 0.16               | 1194                 | 4                      | 186       | 0.18               |
| 3.7±0.05                                       | 4.1  | 226                  | 2.99                   | 1381      | 0.13               | 458                  | 3.93                   | 667       | 0.14               | 702                  | 3.81                   | 389       | 0.15               | 945                  | 3.95                   | 262       | 0.16               | 1193                 | 4.1                    | 181       | 0.18               |
| 3.8±0.05                                       | 4  | 225                  | 4                      | 1380      | 0.13               | 458                  | 4                      | 658       | 0.13               | 699                  | 3.9                    | 386       | 0.15               | 944                  | 4.02                   | 256       | 0.16               | 1192                 | 4.23                   | 177       | 0.18               |
| 3.9±0.05                                       | 3.9  | 224                  | 4.01                   | 1379      | 0.13               | 457                  | 4.01                   | 649       | 0.13               | 697                  | 4.02                   | 384       | 0.15               | 943                  | 4.11                   | 251       | 0.16               | 1191                 | 4.37                   | 172       | 0.18               |
| 4.0±0.05                                       | 3.9  | 224                  | 4.09                   | 1372      | 0.12               | 457                  | 4.07                   | 650       | 0.13               | 696                  | 4.11                   | 381       | 0.14               | 942                  | 4.18                   | 250       | 0.16               | 1190                 | 4.46                   | 170       | 0.18               |
| 4.1±0.05                                       | 3.8  | 223                  | 4.18                   | 1370      | 0.12               | 456                  | 4.18                   | 655       | 0.13               | 696                  | 4.2                    | 380       | 0.14               | 941                  | 4.23                   | 248       | 0.15               | 1190                 | 4.52                   | 169       | 0.17               |
| 4.2±0.05                                       | 3.8  | 223                  | 4.27                   | 1356      | 0.12               | 455                  | 4.27                   | 658       | 0.12               | 695                  | 4.29                   | 379       | 0.14               | 940                  | 4.37                   | 247       | 0.15               | 1189                 | 4.66                   | 167       | 0.17               |
| 4.3±0.05                                       | 3.7  | 222                  | 4.36                   | 1355      | 0.12               | 454                  | 4.34                   | 657       | 0.12               | 694                  | 4.43                   | 373       | 0.14               | 939                  | 4.58                   | 246       | 0.15               | 1195                 | 4.75                   | 168       | 0.17               |
| 4.4±0.05                                       | 3.7  | 222                  | 4.44                   | 1351      | 0.11               | 453                  | 4.45                   | 660       | 0.12               | 693                  | 4.5                    | 369       | 0.14               | 939                  | 4.62                   | 246       | 0.14               | 1192                 | 4.82                   | 162       | 0.16               |
| 4.5±0.05                                       | 3.6  | 221                  | 4.53                   | 1350      | 0.11               | 452                  | 4.52                   | 665       | 0.12               | 692                  | 4.6                    | 364       | 0.13               | 938                  | 4.7                    | 245       | 0.14               | 1190                 | 4.96                   | 161       | 0.16               |
| 4.6±0.05                                       | 3.6  | 221                  | 4.62                   | 1347      | 0.11               | 451                  | 4.62                   | 670       | 0.11               | 691                  | 4.72                   | 359       | 0.13               | 938                  | 4.79                   | 244       | 0.14               | 1188                 | 5.07                   | 161       | 0.16               |
| 4.7±0.05                                       | 3.5  | 220                  | 4.75                   | 1343      | 0.11               | 450                  | 4.74                   | 673       | 0.11               | 690                  | 4.74                   | 351       | 0.13               | 937                  | 4.86                   | 244       | 0.14               | 1186                 | 5.18                   | 159       | 0.16               |
| 5.1±0.05                                       | 3.4  | 217                  | 5.19                   | 1310      | 0.11               | 447                  | 5.16                   | 589       | 0.11               | 687                  | 5.23                   | 348       | 0.13               | 934                  | 5.33                   | 230       | 0.14               | 1184                 | 5.82                   | 131       | 0.16               |
| 5.6±0.05                                       | 3.3  | 214                  | 5.74                   | 1297      | 0.11               | 443                  | 5.75                   | 576       | 0.11               | 684                  | 5.81                   | 342       | 0.12               | 932                  | 6.01                   | 201       | 0.14               | 1182                 | 6.62                   | 129       | 0.16               |
| 6.2±0.1  | 3  | 211                  | 6.31                   | 1244      | 0.10               | 440                  | 6.09                   | 585       | 0.10               | 681                  | 6.33                   | 339       | 0.11               | 928                  | 6.68                   | 202       | 0.12               | 1180                 | 7.34                   | 128       | 0.15               |
| 6.8±0.1  | 2.8  | 208                  | 6.92                   | 1202      | 0.09               | 436                  | 6.94                   | 591       | 0.09               | 678                  | 7.04                   | 334       | 0.10               | 926                  | 7.39                   | 203       | 0.11               | 1177                 | 8.22                   | 127       | 0.14               |
| 7.5±0.1  | 2.7  | 205                  | 7.57                   | 1155      | 0.08               | 433                  | 7.51                   | 567       | 0.09               | 675                  | 7.85                   | 320       | 0.10               | 924                  | 8.17                   | 191       | 0.10               | 1176                 | 9.01                   | 129       | 0.13               |
| 8.2±0.1  | 2.6  | 202                  | 8.35                   | 1116      | 0.08               | 430                  | 8.36                   | 542       | 0.08               | 673                  | 8.48                   | 306       | 0.09               | 922                  | 8.93                   | 186       | 0.10               | 1174                 | 10.04                  | 118       | 0.13               |
| 9.1±0.1  | 2.5  | 199                  | 9.23                   | 1059      | 0.09               | 428                  | 9.28                   | 458       | 0.09               | 670                  | 9.97                   | 249       | 0.10               | 920                  | 10.2                   | 152       | 0.11               | 1172                 | 11.98                  | 88        | 0.13               |
| 10.0±1%  | 2.4  | 196                  | 10.14                  | 936       | 0.09               | 424                  | 10.24                  | 385       | 0.10               | 668                  | 10.55                  | 202       | 0.11               | 919                  | 11.49                  | 118       | 0.13               | 1171                 | 13.75                  | 70        | 0.12               |
| 11.0±1%  | 2.3  | 193                  | 11.19                  | 912       | 0.08               | 421                  | 11.17                  | 363       | 0.09               | 666                  | 11.81                  | 185       | 0.11               | 917                  | 12.87                  | 103       | 0.12               | 1170                 | 15.3                   | 61        | 0.12               |
| 12.0±1%  | 2.2  | 189                  | 12.16                  | 889       | 0.08               | 418                  | 12.3                   | 348       | 0.09               | 664                  | 12.77                  | 173       | 0.11               | 915                  | 14.16                  | 96        | 0.13               | 1168                 | 17.63                  | 52        | 0.12               |
| 13.0±1%  | 2.2  | 186                  | 13.3                   | 984       | 0.07               | 416                  | 13.32                  | 363       | 0.08               | 661                  | 14.1                   | 183       | 0.09               | 912                  | 15.8                   | 101       | 0.11               | 1164                 | 23.9                   | 47        | 0.12               |
| 14.0±1%  | 2.1  | 184                  | 14.25                  | 802       | 0.08               | 414                  | 14.44                  | 298       | 0.09               | 660                  | 15.03                  | 149       | 0.12               | 913                  | 16.72                  | 76.7      | 0.14               | 1167                 | 23.1                   | 40        | 0.15               |
| 15.0±1%  | 2.1  | 182                  | 15.34                  | 791       | 0.07               | 413                  | 15.46                  | 283       | 0.08               | 660                  | 16.16                  | 138       | 0.10               | 912                  | 18.51                  | 82        | 0.16               | 1165                 | 23.6                   | 44        | 0.13               |
| 16.0±1%  | 2  | 179                  | 16.3                   | 780       | 0.07               | 410                  | 16.4                   | 270       | 0.08               | 657                  | 17.6                   | 129       | 0.11               | 909                  | 20.2                   | 68        | 0.13               | 1161                 | 34.7                   | 28        | 0.14               |
| 17.0±1%  | 1.9  | 178                  | 17.6                   | 765       | 0.07               | 410                  | 17.7                   | 263       | 0.08               | 657                  | 18.2                   | 130       | 0.11               | 909                  | 21.3                   | 70        | 0.12               | 1163                 | 34.9                   | 28        | 0.14               |
| 18.0±1%  | 1.8  | 176.5                | 18.13                  | 754       | 0.07               | 409                  | 18.42                  | 258       | 0.07               |                      |                        |           |                    |                      |                        |           |                    |                      |                        |           |                    |



# Accu-F® / Accu-P®

## 0603 Typical Electrical Tables



1

| Capacitance & Tolerance*<br>@ 1 MHz<br>(pF) | Self<br>Resonance<br>Frequency<br>(GHz) | Ref<br>Freq.<br>MHz | Effective<br>Capacitance<br>Max/Min<br>(pF) | Max<br>ESR<br>(Ω) | Ref<br>Freq.<br>MHz | Effective<br>Capacitance<br>Max/Min<br>(pF) | Max<br>ESR<br>(Ω) | Ref<br>Freq.<br>MHz | Effective<br>Capacitance<br>Max/Min<br>(pF) | Max<br>ESR<br>(Ω) | Ref<br>Freq.<br>MHz | Effective<br>Capacitance<br>Max/Min<br>(pF) | Max<br>ESR<br>(Ω) |
|---|---|---------------------|---|-------------------|---------------------|---|-------------------|---------------------|---|-------------------|---------------------|---|-------------------|
| 0.1±0.05                                    | 18.0                                    |                     | N/A   | N/A               | N/A                 | N/A   | N/A               | N/A                 | N/A   | N/A               | N/A                 | N/A   | N/A               |
| 0.2±0.05                                    | 12.7                                    |                     | N/A   | N/A               | N/A                 | N/A   | N/A               | N/A                 | N/A   | N/A               | N/A                 | N/A   | N/A               |
| 0.3±0.05                                    | 10.4                                    |                     | N/A   | N/A               | N/A                 | N/A   | N/A               | N/A                 | N/A   | N/A               | N/A                 | N/A   | N/A               |
| 0.4±0.05                                    | 9.0                                     |                     | N/A   | N/A               | N/A                 | N/A   | N/A               | N/A                 | N/A   | N/A               | N/A                 | N/A   | N/A               |
| 0.5±0.05                                    | 8.1                                     |                     | N/A   | N/A               | N/A                 | N/A   | N/A               | N/A                 | N/A   | N/A               | N/A                 | N/A   | N/A               |
| 0.6±0.10                                    | 7.4                                     |                     | N/A   | N/A               | N/A                 | N/A   | N/A               | N/A                 | N/A   | N/A               | N/A                 | N/A   | N/A               |
| 0.7±0.10                                    | 6.8                                     |                     | N/A   | N/A               | N/A                 | N/A   | N/A               | N/A                 | N/A   | N/A               | N/A                 | N/A   | N/A               |
| 0.8±0.10                                    | 6.4                                     |                     | N/A   | N/A               | N/A                 | N/A   | N/A               | N/A                 | N/A   | N/A               | N/A                 | N/A   | N/A               |
| 0.9±0.10                                    | 6.0                                     |                     | N/A   | N/A               | N/A                 | N/A   | N/A               | N/A                 | N/A   | N/A               | N/A                 | N/A   | N/A               |
| 1.0±0.10                                    | 5.7                                     | 245                 | 1.15/0.90                                   | 280               | 491                 | 1.10/0.90                                   | 220               | 738                 | 1.10/0.90                                   | 220               | 987                 | 1.15/0.90                                   | 300               |
| 1.1±0.10                                    | 5.4                                     | 244                 | 1.25/1.00                                   | 270               | 490                 | 1.25/1.00                                   | 210               | 736                 | 1.11/1.00                                   | 210               | 985                 | 1.25/1.00                                   | 290               |
| 1.2±0.10                                    | 5.2                                     | 243                 | 1.35/1.10                                   | 260               | 487                 | 1.35/1.05                                   | 200               | 734                 | 1.40/1.05                                   | 210               | 981                 | 1.35/1.05                                   | 280               |
| 1.3±0.10                                    | 5.0                                     | 242                 | 1.45/1.15                                   | 260               | 486                 | 1.45/1.15                                   | 200               | 732                 | 1.45/1.15                                   | 200               | 974                 | 1.45/1.15                                   | 270               |
| 1.4±0.10                                    | 4.8                                     | 241                 | 1.55/1.25                                   | 250               | 485                 | 1.55/1.25                                   | 190               | 731                 | 1.45/1.25                                   | 200               | 977                 | 1.55/1.25                                   | 260               |
| 1.5±0.10                                    | 4.7                                     | 241                 | 1.65/1.35                                   | 250               | 484                 | 1.65/1.35                                   | 180               | 729                 | 1.65/1.35                                   | 190               | 976                 | 1.70/1.35                                   | 250               |
| 1.6±0.10                                    | 4.5                                     | 240                 | 1.75/1.45                                   | 240               | 483                 | 1.75/1.45                                   | 180               | 727                 | 1.75/1.45                                   | 190               | 973                 | 1.80/1.50                                   | 250               |
| 1.7±0.10                                    | 4.4                                     | 240                 | 1.85/1.55                                   | 230               | 482                 | 1.85/1.60                                   | 170               | 725                 | 1.85/1.60                                   | 180               | 971                 | 1.90/1.60                                   | 250               |
| 1.8±0.10                                    | 4.2                                     | 239                 | 2.10/1.70                                   | 220               | 479                 | 2.10/1.70                                   | 160               | 723                 | 2.10/1.70                                   | 170               | 969                 | 2.15/1.70                                   | 250               |
| 1.9±0.10                                    | 4.1                                     | 239                 | 2.15/1.78                                   | 210               | 478                 | 2.15/1.80                                   | 160               | 721                 | 2.15/1.80                                   | 167               | 967                 | 2.20/1.80                                   | 240               |
| 2.0±0.10                                    | 4.0                                     | 238                 | 2.11/1.80                                   | 205               | 477                 | 2.11/1.80                                   | 155               | 720                 | 2.11/1.80                                   | 165               | 966                 | 2.25/1.90                                   | 230               |
| 2.1±0.10                                    | 3.9                                     | 237                 | 2.25/1.95                                   | 200               | 475                 | 2.25/1.98                                   | 150               | 718                 | 2.35/1.98                                   | 162               | 964                 | 2.35/2.00                                   | 220               |
| 2.2±0.10                                    | 3.8                                     | 236                 | 2.40/2.05                                   | 190               | 474                 | 2.45/2.05                                   | 145               | 717                 | 2.42/2.05                                   | 160               | 962                 | 2.45/2.10                                   | 210               |
| 2.4±0.25                                    | 3.7                                     | 234                 | 2.70/2.15                                   | 175               | 471                 | 2.75/2.15                                   | 140               | 713                 | 2.80/2.15                                   | 150               | 958                 | 2.80/2.15                                   | 200               |
| 2.7±0.25                                    | 3.5                                     | 232                 | 3.00/2.45                                   | 160               | 468                 | 3.10/2.45                                   | 125               | 709                 | 3.10/2.45                                   | 145               | 954                 | 3.15/2.48                                   | 190               |
| 3.0±0.25                                    | 3.3                                     | 230                 | 3.40/2.75                                   | 150               | 465                 | 3.40/2.75                                   | 120               | 706                 | 3.40/2.75                                   | 140               | 951                 | 3.60/2.80                                   | 170               |
| 3.9±0.25                                    | 3.1                                     | 226                 | 3.60/3.05                                   | 130               | 459                 | 3.70/3.05                                   | 120               | 699                 | 3.70/3.05                                   | 130               | 945                 | 3.80/3.10                                   | 165               |
| 3.6±0.25                                    | 3.0                                     | 224                 | 3.90/3.30                                   | 128               | 456                 | 4.25/3.35                                   | 119               | 697                 | 3.90/3.35                                   | 125               | 942                 | 4.10/3.40                                   | 160               |
| 3.9±0.25                                    | 2.9                                     | 223                 | 4.20/3.65                                   | 125               | 455                 | 4.35/3.70                                   | 115               | 695                 | 4.90/3.75                                   | 120               | 940                 | 5.15/3.75                                   | 150               |
| 4.3±0.25                                    | 2.7                                     | 220                 | 4.60/4.00                                   | 122               | 451                 | 4.80/4.05                                   | 117               | 692                 | 5.10/4.05                                   | 115               | 937                 | 5.30/4.05                                   | 150               |
| 4.7±0.25                                    | 2.6                                     | 218                 | 5.00/4.45                                   | 120               | 448                 | 5.20/4.45                                   | 110               | 689                 | 5.30/4.50                                   | 115               | 935                 | 5.50/4.55                                   | 145               |
| 5.1±0.25                                    | 2.5                                     | 216                 | 5.40/4.85                                   | 115               | 445                 | 5.70/4.89                                   | 105               | 686                 | 6.00/4.90                                   | 115               | 931                 | 6.20/5.00                                   | 140               |
| 5.6±0.25                                    | 2.4                                     | 214                 | 5.90/5.35                                   | 110               | 443                 | 6.10/5.35                                   | 100               | 684                 | 6.15/5.40                                   | 110               | 929                 | 6.50/5.50                                   | 135               |
| 6.2±0.25                                    | 2.3                                     | 211                 | 6.50/5.95                                   | 105               | 439                 | 6.90/5.95                                   | 099               | 680                 | 7.10/6.00                                   | 110               | 927                 | 8.00/6.10                                   | 130               |
| 6.8±0.25                                    | 2.2                                     | 208                 | 7.20/6.55                                   | 100               | 435                 | 7.25/6.55                                   | 099               | 677                 | 7.50/6.60                                   | 110               | 925                 | 9.00/6.65                                   | 130               |
| 7.5±0.50                                    | 2.1                                     | 205                 | 8.10/7.00                                   | 095               | 432                 | 8.10/7.00                                   | 099               | 675                 | 8.20/7.00                                   | 110               | 925                 | 9.50/7.05                                   | 125               |
| 8.2±0.50                                    | 2.0                                     | 202                 | 8.80/7.70                                   | 090               | 429                 | 8.80/7.70                                   | 098               | 672                 | 9.00/7.70                                   | 110               | 921                 | 10.00/7.80                                  | 125               |
| 9.1±0.50                                    | 1.9                                     | 200                 | 9.80/8.60                                   | 090               | 425                 | 10.95/8.65                                  | 098               | 670                 | 12.00/9.00                                  | 110               | 919                 | 13.00/9.10                                  | 120               |
| 10±5%                                       | 1.8                                     | 195                 | 10.70/9.50                                  | 085               | 422                 | 11.60/9.50                                  | 097               | 667                 | 12.50/9.60                                  | 110               | 917                 | 16.00/9.90                                  | 120               |
| 11±5%                                       | 1.7                                     | 191                 | 11.60/10.90                                 | 085               | 420                 | 12.20/10.60                                 | 095               | 665                 | 13.20/10.50                                 | 110               | 916                 | 17.00/10.00                                 | 120               |
| 12±5%                                       | 1.6                                     | 189                 | 12.90/11.40                                 | 085               | 418                 | 13.40/11.50                                 | 095               | 663                 | 14.60/11.90                                 | 110               | 914                 | 18.00/12.00                                 | 120               |
| 13±5%                                       | 1.6                                     | 187                 | 13.10/12.90                                 | 080               | 416                 | 14.00/13.00                                 | 095               | 661                 | 16.00/13.50                                 | 110               | 913                 | 21.00/14.00                                 | 120               |
| 14±5%                                       | 1.5                                     | 185                 | 14.90/13.25                                 | 080               | 414                 | 16.90/14.00                                 | 090               | 660                 | 19.00/15.00                                 | 110               | 912                 | 26.00/15.00                                 | 120               |
| 15±5%                                       | 1.5                                     | 182                 | 15.90/14.25                                 | 080               | 412                 | 17.50/15.30                                 | 090               | 659                 | 21.00/16.50                                 | 100               | 911                 | 29.00/17.00                                 | 120               |
| 16±5%                                       | 1.4                                     | 179                 | 17.00/15.15                                 | 070               | 410                 | 18.00/15.90                                 | 085               | 657                 | 22.00/17.00                                 | 100               | 910                 | 30.00/18.00                                 | 120               |
| 18±5%                                       | 1.3                                     | 176                 | 19.50/17.00                                 | 070               | 408                 | 20.20/17.10                                 | 085               | 656                 | 23.70/19.00                                 | 100               | 908                 | 33.00/21.00                                 | 120               |
| 22±5%                                       | 1.2                                     | 170                 | 24.00/20.90                                 | 066               | 404                 | 25.00/20.90                                 | 080               | 654                 | 28.00/21.00                                 | 10                | 906                 | 39.00/21.50                                 | 120               |
| 24±5%                                       | 1.2                                     | 168                 | 26.00/22.80                                 | 066               | 403                 | 30.00/23.00                                 | 080               | 653                 | N/A   | 10                | 905                 | N/A   | 120               |
| 27±5%                                       | 1.1                                     | 165                 | 29.00/25.60                                 | 065               | 402                 | 36.00/27.00                                 | 080               | 652                 | N/A   | 10                | 905                 | N/A   | 120               |
| 30±5%                                       | 1.0                                     | 163                 | 32.00/28.50                                 | 064               | 401                 | 40.00/30.00                                 | 080               | 651                 | N/A   | 10                | 904                 | N/A   | 120               |
| 33±5%                                       | 1.0                                     | 160                 | 37.65/31.35                                 | 064               | 400                 | 45.00/33.00                                 | 080               | 650                 | N/A   | 10                | 904                 | N/A   | 120               |

\* Other tolerances are available, see page 8

## Accu-F®/Accu-P®

### Automatic Insertion Packaging



#### TAPE & REEL

All tape and reel specifications are in compliance with EIA 481-1-A.  
(equivalent to IEC 286 part 3).

- 8mm carrier
- Reeled quantities: Reels of 3,000 per 7" reel or 10,000 pieces per 13" reel  
0201 and 0402 = 5,000 pieces per 7" reel and 20,000 pieces per 13" reel

1

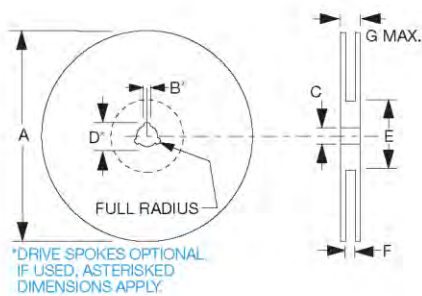
#### REEL

**DIMENSIONS:** millimeters (inches)

| A <sup>(1)</sup>         | B                        | C                         | D                         | E                       | F                          | G                         |
|--------------------------|--------------------------|---------------------------|---------------------------|-------------------------|----------------------------|---------------------------|
| 180±1.0<br>(7.087±0.039) | 1.5 min.<br>(0.059 min.) | 13±0.2<br>(0.512 ± 0.008) | 20.2 min.<br>(0.795 min.) | 50 min.<br>(1.969 min.) | 9.6±1.5<br>(0.370 ± 0.050) | 14.4 max.<br>(0.567 max.) |

Metric dimensions will govern.  
Inch measurements rounded and for reference only.

(1) 330mm (13 inch) reels are available.

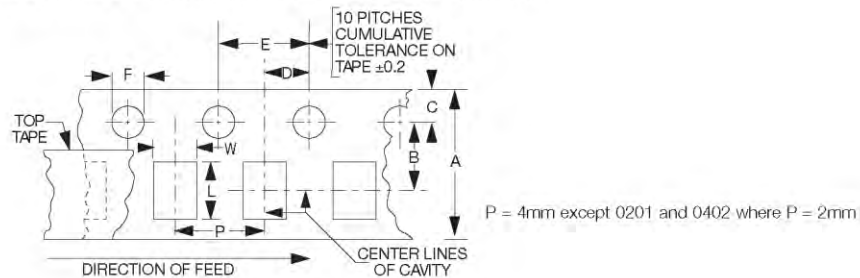


#### CARRIER

**DIMENSIONS:** millimeters (inches)

| A                            | B                             | C                             | D                             | E                            | F   |
|------------------------------|-------------------------------|-------------------------------|-------------------------------|------------------------------|---|
| 8.0 ± 0.3<br>(0.315 ± 0.012) | 3.5 ± 0.05<br>(0.138 ± 0.002) | 1.75 ± 0.1<br>(0.069 ± 0.004) | 2.0 ± 0.05<br>(0.079 ± 0.002) | 4.0 ± 0.1<br>(0.157 ± 0.004) | 1.5 <sup>+0.1</sup> <sub>-0.0</sub><br>(0.059 <sup>+0.004</sup> <sub>-0.000</sub> ) |

NOTE: The nominal dimensions of the component compartment (WL) are derived from the component size.



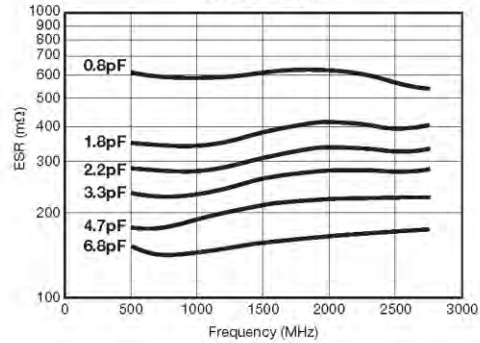
NOTE: AVX reserves the right to change the information published herein without notice.



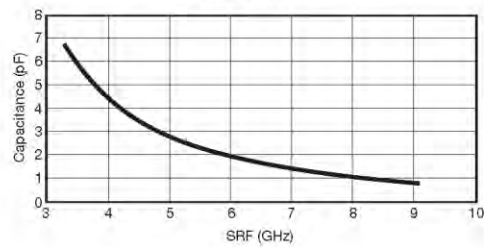
## Accu-F® / Accu-P® High Frequency Characteristics



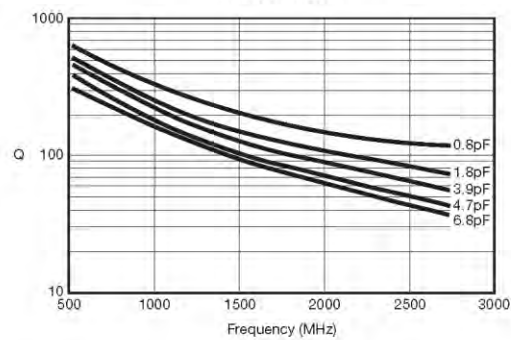
Typical ESR vs. Frequency  
Accu-P® 0201



Typical SRF vs. Capacitance  
Accu-P® 0201



Typical Q vs. Frequency  
Accu-P® 0201

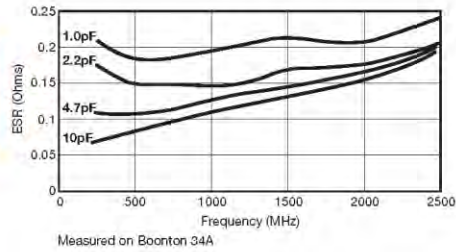


## Accu-F® / Accu-P® High Frequency Characteristics

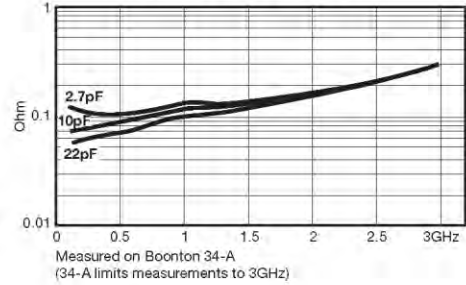


1

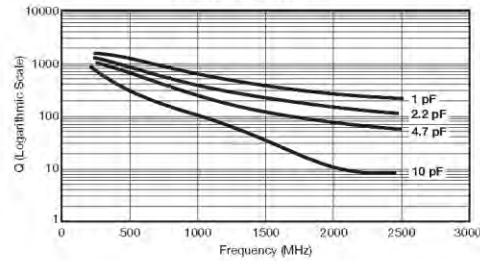
Typical ESR vs. Frequency  
Accu-P® 0402



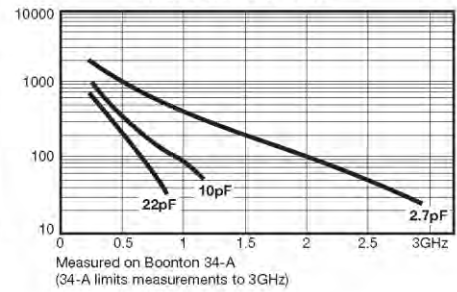
Typical ESR vs. Frequency  
Accu-F®/Accu-P® 0603



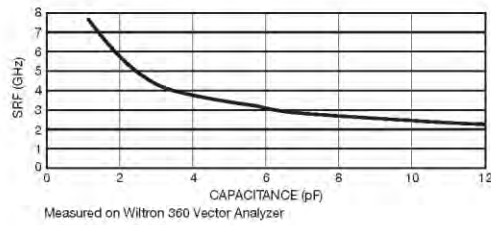
Typical Q vs. Frequency  
Accu-P® 0402



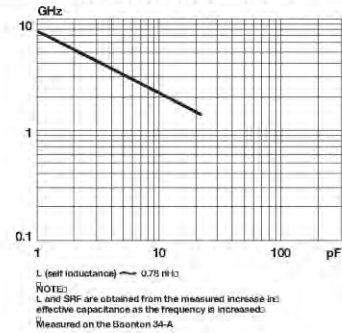
Typical Q vs. Frequency  
Accu-F®/Accu-P® 0603



Typical Self Resonant Frequency vs. Capacitance  
Accu-P® 0402



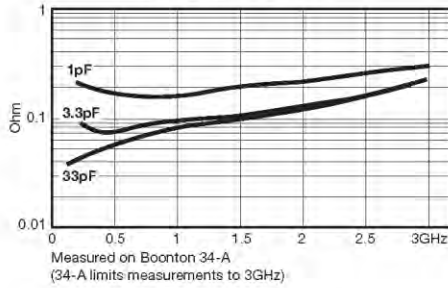
Typical Self Resonant Frequency vs. Capacitance  
Accu-F®/Accu-P® 0603



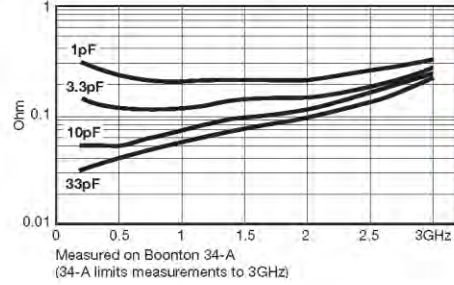
## Accu-F® / Accu-P® High Frequency Characteristics



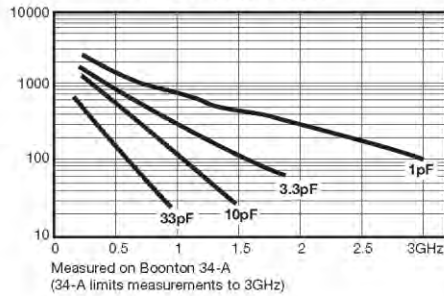
Typical ESR vs. Frequency  
Accu-F®/Accu-P® 0805



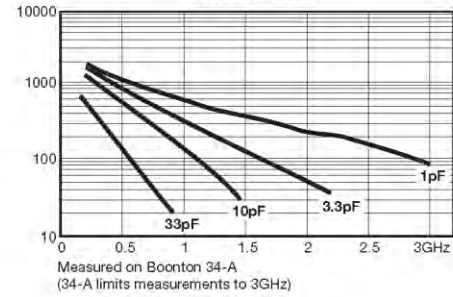
Typical ESR vs. Frequency  
Accu-P® 1210



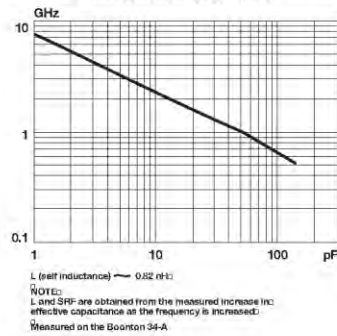
Typical Q vs. Frequency  
Accu-F®/Accu-P® 0805



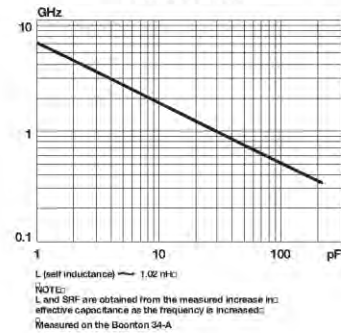
Typical Q vs. Frequency  
Accu-P® 1210



Typical Self Resonant Frequency vs. Capacitance  
Accu-F®/Accu-P® 0805



Typical Self Resonant Frequency vs. Capacitance  
Accu-P® 1210



## Accu-F® / Accu-P®

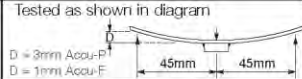


## Environmental / Mechanical Characteristics

## ENVIRONMENTAL CHARACTERISTICS

| TEST  | CONDITIONS  | REQUIREMENT  |
|---|---|--|
| Life (Endurance)<br>MIL-STD-202F Method 108A                                  | 125°C, 2U <sub>B</sub> , 1000 hours   | No visible damage<br>$\Delta C/C \leq 2\%$ for C $\geq 5$ pF<br>$\Delta C \leq 0.25$ pF for C $< 5$ pF |
| Accelerated Damp<br>Heat Steady State<br>MIL-STD-202F Method 103B             | 85°C, 85% RH, U <sub>B</sub> , 1000 hours                                   | No visible damage<br>$\Delta C/C \leq 2\%$ for C $\geq 5$ pF<br>$\Delta C \leq 0.25$ pF for C $< 5$ pF |
| Temperature Cycling<br>MIL-STD-202F Method 107E<br>MIL-STD-883D Method 1010.7 | -55°C to +125°C, 15 cycles – Accu-P®<br>-55°C to +125°C, 5 cycles – Accu-F® | No visible damage<br>$\Delta C/C \leq 2\%$ for C $\geq 5$ pF<br>$\Delta C \leq 0.25$ pF for C $< 5$ pF |
| Resistance to Solder Heat<br>IEC-68-2-58                                      | 260°C $\pm$ 5°C for 10 secs   | C remains within initial limits.   |

## MECHANICAL CHARACTERISTICS

| TEST   | CONDITIONS  | REQUIREMENT  |
|--|---|--|
| Solderability<br>IEC-68-2-58   | Components completely immersed in a solder bath at 235°C for 2 secs.  | Terminations to be well tinned, minimum 95% coverage   |
| Leach Resistance<br>IEC-68-2-58  | Components completely immersed in a solder bath at 260 $\pm$ 5°C for 60 secs.                                   | Dissolution of termination faces $\leq 15\%$ of area<br>Dissolution of termination edges $\leq 25\%$ of length |
| Adhesion<br>MIL-STD-202F Method 211A   | A force of 5N applied for 10 secs.  | No visible damage  |
| Termination Bond Strength<br>IEC-68-2-21 Amend. 2                            | Tested as shown in diagram<br> | No visible damage<br>$\Delta C/C \leq 2\%$ for C $\geq 5$ pF<br>$\Delta C \leq 0.25$ pF for C $< 5$ pF         |
| Robustness of Termination<br>IEC-68-2-21 Amend. 2                            | A force of 5N applied for 10 secs.  | No visible damage  |
| High Frequency Vibration<br>MIL-STD-202F Method 201A,<br>204D (Accu-P® only) | 55Hz to 2000Hz, 20G   | No visible damage  |
| Storage  | 12 months minimum with components stored in "as received" packaging   | Good solderability   |

## QUALITY &amp; RELIABILITY

Accu-P® is based on well established thin-film technology and materials.

## • ON-LINE PROCESS CONTROL

This program forms an integral part of the production cycle and acts as a feedback system to regulate and control production processes. The test procedures, which are integrated into the production process, were developed after long research work and are based on the highly developed semiconductor industry test procedures and equipment. These measures help AVX to produce a consistent and high yield line of products.

## • FINAL QUALITY INSPECTION

Finished parts are tested for standard electrical parameters and visual/mechanical characteristics. Each production lot is 100% evaluated for: capacitance and proof voltage at 2.5 U<sub>B</sub>. In addition, production is periodically evaluated for:

Average capacitance with histogram printout for capacitance distribution;  
IR and Breakdown Voltage distribution;  
Temperature Coefficient;  
Solderability;  
Dimensional, mechanical and temperature stability.

## QUALITY ASSURANCE

The reliability of these thin-film chip capacitors has been studied intensively for several years. Various measures have been taken to obtain the high reliability required today by the industry. Quality assurance policy is based on well established international industry standards. The reliability of the capacitors is determined by accelerated testing under the following conditions:

|                                       |   |
|---------------------------------------|---|
| Life (Endurance)                      | 125°C, 2U <sub>B</sub> , 1000 hours           |
| Accelerated Damp<br>Heat Steady State | 85°C, 85% RH, U <sub>B</sub> ,<br>1000 hours. |



# Accu-F® / Accu-P®



## Performance Characteristics RF Power Applications

### RF POWER APPLICATIONS

In RF power applications capacitor losses generate heat. Two factors of particular importance to designers are:

- Minimizing the generation of heat.
- Dissipating heat as efficiently as possible.

### CAPACITOR HEATING

- The major source of heat generation in a capacitor in RF power applications is a function of RF current (I) and ESR, from the relationship:

$$\text{Power dissipation} = I_{\text{RMS}}^2 \times \text{ESR}$$

- Accu-P® capacitors are specially designed to minimize

ESR and therefore RF heating. Values of ESR for Accu-P® capacitors are significantly less than those of ceramic MLC components currently available.

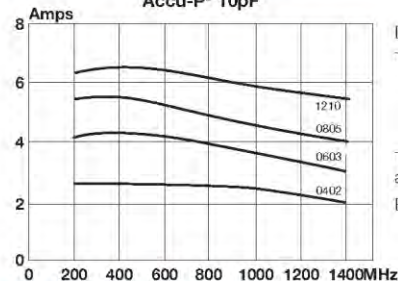
### HEAT DISSIPATION

- Heat is dissipated from a capacitor through a variety of paths, but the key factor in the removal of heat is the thermal conductivity of the capacitor material.
- The higher the thermal conductivity of the capacitor, the more rapidly heat will be dissipated.
- The table below illustrates the importance of thermal conductivity to the performance of Accu-P® in power applications.

1

| PRODUCT       | MATERIAL           | THERMAL CONDUCTIVITY W/mK |
|---------------|--------------------|---------------------------|
| Accu-P®       | Alumina            | 18.9                      |
| Microwave MLC | Magnesium Titanate | 6.0                       |

Power Handling  
Accu-P® 10pF



Data used in calculating the graph:

Thermal impedance of capacitors:

|      |         |
|------|---------|
| 0402 | 17°C/W  |
| 0603 | 12°C/W  |
| 0805 | 6.5°C/W |
| 1210 | 5°C/W   |

Thermal impedance measured using RF generator, amplifier and strip-line transformer.

ESR of capacitors measured on Boonton 34A

### THERMAL IMPEDANCE

Thermal impedance of Accu-P® chips is shown below compared with the thermal impedance of Microwave MLC's.

The thermal impedance expresses the temperature difference in °C between chip center and termination caused by a power dissipation of 1 watt in the chip. It is expressed in °C/W.

| CAPACITOR TYPE | CHIP SIZE | THERMAL IMPEDANCE (°C/W) |
|----------------|-----------|--------------------------|
| Accu-P®        | 0805      | 6.5                      |
|                | 1210      | 5                        |
| Microwave MLC  | 0505      | 12                       |
|                | 1210      | 7.5                      |

### ADVANTAGES OF ACCU-P® IN RF POWER CIRCUITS

The optimized design of Accu-P® offers the designer of RF power circuits the following advantages:

- Reduced power losses due to the inherently low ESR of Accu-P®.
- Increased power dissipation due to the high thermal conductivity of Accu-P®.

• THE ONLY TRUE TEST OF A CAPACITOR IN ANY PARTICULAR APPLICATION IS ITS PERFORMANCE UNDER OPERATING CONDITIONS IN THE ACTUAL CIRCUIT.

### PRACTICAL APPLICATION IN RF POWER CIRCUITS

- There is a wide variety of different experimental methods for measuring the power handling performance of a capacitor in RF power circuits. Each method has its own problems and few of them exactly reproduce the conditions present in "real" circuit applications.
- Similarly, there is a very wide range of different circuit applications, all with their unique characteristics and operating conditions which cannot possibly be covered by such "theoretical" testing.



# Accu-F® / Accu-P®

## Application Notes



### GENERAL

Accu-F® and Accu-P® SMD capacitors are designed for soldering to printed circuit boards or other substrates. The construction of the components is such that they will withstand the time/temperature profiles used in both wave and reflow soldering methods.

1

### CIRCUIT BOARD TYPE

The circuit board types which may be used with Accu-F® and Accu-P® are as follows:

Accu-F®: All flexible types of circuit boards  
(eg. FR-4, G-10).

Accu-P®: All flexible types of circuit boards  
(eg. FR-4, G-10) and also alumina.

For other circuit board materials, please consult factory.

### HANDLING

SMD capacitors should be handled with care to avoid damage or contamination from perspiration and skin oils. The use of plastic tipped tweezers or vacuum pick-ups is strongly recommended for individual components. Bulk handling should ensure that abrasion and mechanical shock are minimized. For automatic equipment, taped and reeled product gives the ideal medium for direct presentation to the placement machine.

### COMPONENT PAD DESIGN

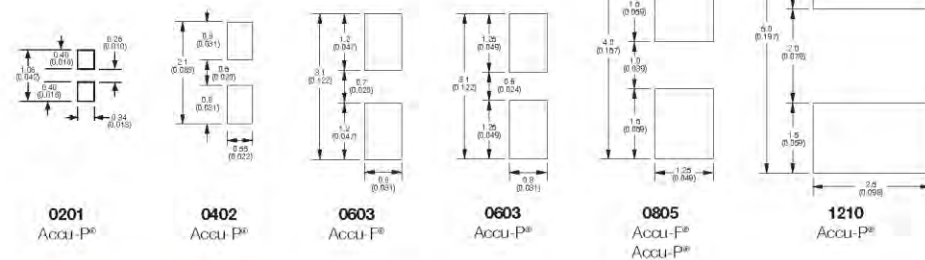
Component pads must be designed to achieve good joints and minimize component movement during reflow soldering. Pad designs are given below for both wave and reflow soldering.

The basis of these designs is:

- Pad width equal to component width. It is permissible to decrease this to as low as 85% of component width but it is not advisable to go below this.
- Pad overlap 0.5mm beneath large components. Pad overlap about 0.3mm beneath small components.
- Pad extension of 0.5mm for reflow of large components and pad extension about 0.3mm for reflow of small components. Pad extension about 1.0mm for wave soldering.

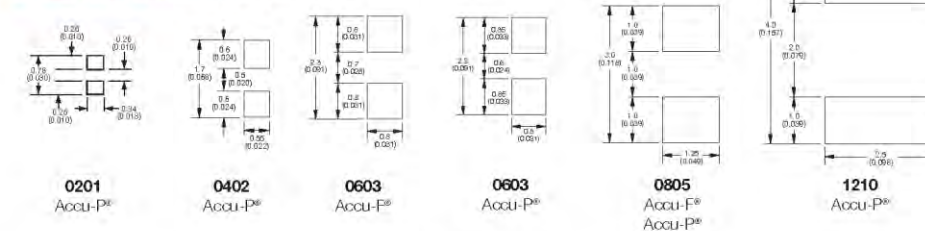
### WAVE SOLDERING

**DIMENSIONS:** millimeters (inches)



### REFLOW SOLDERING

**DIMENSIONS:** millimeters (inches)



# Accu-F® / Accu-P®

## Application Notes



### PREHEAT & SOLDERING

The rate of preheat in production should not exceed 4°C/second and a recommended maximum is about 2°C/second. Temperature differential from preheat to soldering should not exceed 100°C.

For further specific application or process advice, please consult AVX.

### COOLING

After soldering, the assembly should preferably be allowed to cool naturally. In the event of assisted cooling, similar conditions to those recommended for preheating should be used.

### HAND SOLDERING & REWORK

Hand soldering is permissible. Preheat of the PCB to 150°C is required. The most preferable technique is to use hot air soldering tools. Where a soldering iron is used, a temperature controlled model not exceeding 30 watts should be used and set to not more than 260°C.

### CLEANING RECOMMENDATIONS

Care should be taken to ensure that the devices are thoroughly cleaned of flux residues, especially the space beneath the device. Such residues may otherwise become conductive and effectively offer a lossy bypass to the device. Various recommended cleaning conditions (which must be optimized for the flux system being used) are as follows:

Cleaning liquids, . . . . . i-propanol, ethanol, acetylacetone, water and other standard PCB cleaning liquids.

Ultrasonic conditions . . . power-20w/liter max. frequency-20kHz to 45kHz.

Temperature . . . . . 80°C maximum (if not otherwise limited by chosen solvent system).

Time . . . . . 5 minutes max.

### STORAGE CONDITIONS

Recommended storage conditions for Accu-F® and Accu-P® prior to use are as follows:

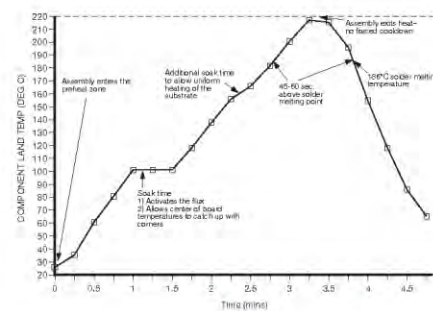
Temperature . . . . . 15°C to 35°C

Humidity . . . . . ≤65%

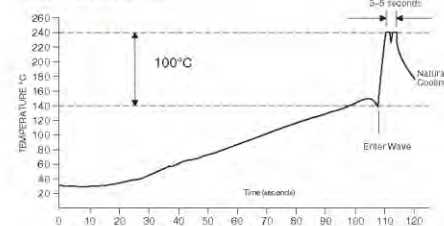
Air Pressure . . . . . 860mbar to 1060mbar

### RECOMMENDED SOLDERING PROFILE

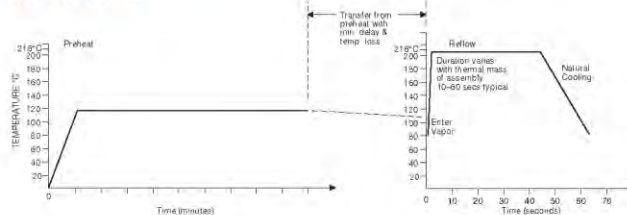
#### IR REFLOW



#### WAVE SOLDERING



#### VAPOR PHASE



AVX offers s-parameters for all of the RF/Microwave products that are offered. The s-parameter files are in standard Touchstone format and can be used with any RF software package that will allow the user to import them. They are extremely helpful when trying to model a circuit prior to prototyping and can save valuable time on the front end of your design cycle [10].



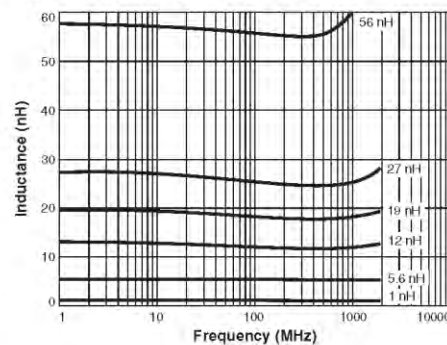


# Chip Inductors – 0402CS Series (1005)

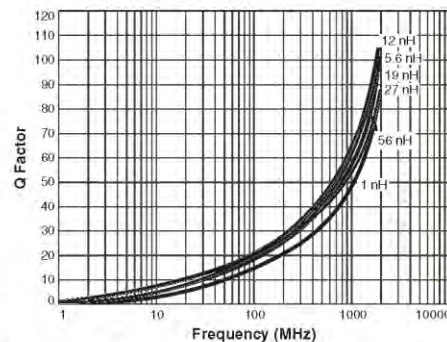
Continuing in our long tradition of innovation and leadership, Coilcraft introduced the industry's first 0402 wirewound inductor.

This series shares all of the characteristics of Coilcraft's other ceramic inductors: exceptionally high Q factors, especially at use frequencies; outstanding self-resonant frequency; tight inductance tolerance; and excellent batch-to-batch consistency.

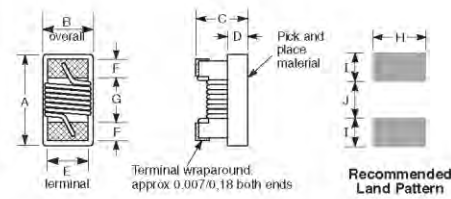
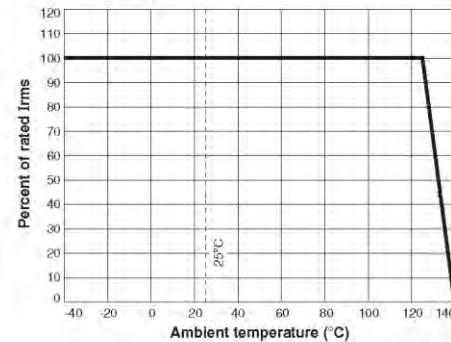
## Typical L vs Frequency



## Typical Q vs Frequency



## Irms Derating



| A     | B     | C     | D     | E     | F     | G     | H     | I     | J     |
|-------|-------|-------|-------|-------|-------|-------|-------|-------|-------|
| max   | max   | max   | ref   |       |       |       |       |       |       |
| 0.047 | 0.025 | 0.026 | 0.010 | 0.020 | 0.009 | 0.022 | 0.026 | 0.014 | 0.018 |
| 1.19  | 0.64  | 0.66  | 0.25  | 0.51  | 0.23  | 0.56  | 0.66  | 0.36  | 0.46  |
|       |       |       |       |       |       |       |       |       | mm    |

**Core material** Ceramic

**Terminations** RoHS compliant silver-palladium-platinum-glass triit. Other terminations available at additional cost.

**Weight** 0.8 – 1.0 mg

**Ambient temperature** –40°C to +125°C with I<sub>rms</sub> current, +125°C to +140°C with derated current

**Storage temperature** Component: –40°C to +140°C.

**Packaging:** –40°C to +80°C

**Resistance to soldering heat** Max three 40 second reflows at +260°C, parts cooled to room temperature between cycles

**Temperature Coefficient of Inductance (TCL)** +25 to +125 ppm/°C

**Moisture Sensitivity Level (MSL)** 1 (unlimited floor life at <30°C / 85% relative humidity)

**Failures in Time (FIT) / Mean Time Between Failures (MTBF)** One per billion hours / one billion hours, calculated per Telcordia SR-332

**Packaging** 2000 per 7" reel Paper tape: 8 mm wide, 1.68 mm thick, 2 mm pocket spacing

**PCB washing** Only pure water or alcohol recommended

**Coilcraft®**

Specifications subject to change without notice.

Please check our website for latest information.

Document 198-1 Revised 11/09/10

1102 Silver Lake Road Cary, Illinois 60013 Phone 847/639-6400 Fax 847/639-1469

E-mail [info@coilcraft.com](mailto:info@coilcraft.com) Web <http://www.coilcraft.com>

©Coilcraft, Inc. 2010





## 0402CS Series (1005)

Designer's Kits C328A and B contain 20 each of all 5% values  
 Designer's Kits C328A-2 and B-2 contain 20 each of all 2% values

| Part number <sup>1</sup> | Inductance <sup>2</sup><br>(nH) | Percent<br>tolerance <sup>3</sup> | 900 MHz |                    | 1.7 GHz |                    | SRF min <sup>5</sup><br>(GHz) | DCR max <sup>6</sup><br>(Ohms) | I <sub>rms</sub> <sup>7</sup><br>(mA) |
|--------------------------|---------------------------------|-----------------------------------|---------|--------------------|---------|--------------------|-------------------------------|--------------------------------|---------------------------------------|
|                          |                                 |                                   | L typ   | Q typ <sup>4</sup> | L typ   | Q typ <sup>4</sup> |                               |                                |                                       |
| 0402CS-1N0X_L            | 1.0                             | <b>5</b>                          | 1.02    | 77                 | 1.02    | 69                 | 12.70                         | 0.045                          | 1360                                  |
| 0402CS-1N2X_L            | 1.2                             | <b>5</b>                          | 1.17    | 28                 | 1.17    | 38                 | 12.90                         | 0.090                          | 740                                   |
| 0402CS-1N8X_L            | 1.8                             | <b>5</b>                          | 1.78    | 54                 | 1.78    | 75                 | 12.00                         | 0.070                          | 1040                                  |
| 0402CS-1N9X_L            | 1.9                             | <b>5</b>                          | 1.72    | 68                 | 1.74    | 82                 | 11.30                         | 0.070                          | 1040                                  |
| 0402CS-2N0X_L            | 2.0                             | <b>5,2</b>                        | 1.93    | 54                 | 1.93    | 75                 | 11.10                         | 0.070                          | 1040                                  |
| 0402CS-2N2X_L            | 2.2                             | <b>5,2</b>                        | 2.19    | 59                 | 2.23    | 100                | 10.80                         | 0.070                          | 960                                   |
| 0402CS-2N4X_L            | 2.4                             | <b>5,2</b>                        | 2.24    | 51                 | 2.27    | 68                 | 10.50                         | 0.068                          | 790                                   |
| 0402CS-2N7X_L            | 2.7                             | <b>5,2</b>                        | 2.58    | 42                 | 2.60    | 61                 | 10.40                         | 0.120                          | 640                                   |
| 0402CS-3N3X_L            | 3.3                             | <b>5,2</b>                        | 3.10    | 65                 | 3.12    | 87                 | 7.00                          | 0.066                          | 840                                   |
| 0402CS-3N6X_L            | 3.6                             | <b>5,2</b>                        | 3.56    | 45                 | 3.62    | 71                 | 6.80                          | 0.066                          | 840                                   |
| 0402CS-3N9X_L            | 3.9                             | <b>5,2</b>                        | 3.89    | 50                 | 4.00    | 75                 | 6.00                          | 0.066                          | 840                                   |
| 0402CS-4N3X_L            | 4.3                             | <b>5,2</b>                        | 4.19    | 47                 | 4.30    | 71                 | 6.00                          | 0.091                          | 700                                   |
| 0402CS-4N7X_L            | 4.7                             | <b>5,2</b>                        | 4.55    | 48                 | 4.68    | 68                 | 4.77                          | 0.130                          | 640                                   |
| 0402CS-5N1X_L            | 5.1                             | <b>5,2</b>                        | 5.15    | 56                 | 5.25    | 82                 | 4.80                          | 0.083                          | 800                                   |
| 0402CS-5N6X_L            | 5.6                             | <b>5,2</b>                        | 5.16    | 54                 | 5.28    | 81                 | 4.80                          | 0.083                          | 760                                   |
| 0402CS-6N2X_L            | 6.2                             | <b>5,2</b>                        | 6.16    | 52                 | 6.37    | 76                 | 4.80                          | 0.083                          | 760                                   |
| 0402CS-6N8X_L            | 6.8                             | <b>5,2</b>                        | 6.56    | 63                 | 6.93    | 78                 | 4.80                          | 0.083                          | 680                                   |
| 0402CS-7N5X_L            | 7.5                             | <b>5,2</b>                        | 7.91    | 60                 | 8.22    | 88                 | 4.80                          | 0.10                           | 680                                   |
| 0402CS-8N2X_L            | 8.2                             | <b>5,2</b>                        | 8.50    | 57                 | 8.85    | 84                 | 4.40                          | 0.10                           | 680                                   |
| 0402CS-8N7X_L            | 8.7                             | <b>5,2</b>                        | 8.78    | 54                 | 9.21    | 73                 | 4.10                          | 0.20                           | 480                                   |
| 0402CS-9N0X_L            | 9.0                             | <b>5,2</b>                        | 9.07    | 62                 | 9.53    | 78                 | 4.16                          | 0.10                           | 680                                   |
| 0402CS-9N5X_L            | 9.5                             | <b>5,2</b>                        | 9.42    | 54                 | 9.98    | 69                 | 4.00                          | 0.20                           | 480                                   |
| 0402CS-10NX_L            | 10                              | <b>5,2</b>                        | 9.8     | 50                 | 10.10   | 67                 | 3.90                          | 0.20                           | 480                                   |
| 0402CS-11NX_L            | 11                              | <b>5,2</b>                        | 10.7    | 52                 | 11.20   | 78                 | 3.68                          | 0.12                           | 640                                   |
| 0402CS-12NX_L            | 12                              | <b>5,2</b>                        | 11.9    | 53                 | 12.70   | 71                 | 3.60                          | 0.12                           | 640                                   |
| 0402CS-13NX_L            | 13                              | <b>5,2</b>                        | 13.4    | 51                 | 14.63   | 57                 | 3.45                          | 0.21                           | 440                                   |
| 0402CS-15NX_L            | 15                              | <b>5,2</b>                        | 14.6    | 55                 | 15.50   | 77                 | 3.28                          | 0.17                           | 560                                   |
| 0402CS-16NX_L            | 16                              | <b>5,2</b>                        | 16.6    | 46                 | 18.86   | 47                 | 3.10                          | 0.22                           | 560                                   |
| 0402CS-18NX_L            | 18                              | <b>5,2</b>                        | 18.3    | 57                 | 20.28   | 62                 | 3.10                          | 0.23                           | 420                                   |
| 0402CS-19NX_L            | 19                              | <b>5,2</b>                        | 19.1    | 50                 | 21.10   | 67                 | 3.04                          | 0.20                           | 480                                   |
| 0402CS-20NX_L            | 20                              | <b>5,2</b>                        | 20.7    | 52                 | 23.66   | 53                 | 3.00                          | 0.25                           | 420                                   |
| 0402CS-22NX_L            | 22                              | <b>5,2</b>                        | 23.2    | 53                 | 26.75   | 53                 | 2.80                          | 0.30                           | 400                                   |
| 0402CS-23NX_L            | 23                              | <b>5,2</b>                        | 23.8    | 49                 | 26.90   | 64                 | 2.72                          | 0.30                           | 400                                   |
| 0402CS-24NX_L            | 24                              | <b>5,2</b>                        | 25.1    | 51                 | 29.50   | 50                 | 2.70                          | 0.30                           | 400                                   |
| 0402CS-27NX_L            | 27                              | <b>5,2</b>                        | 28.7    | 49                 | 33.50   | 63                 | 2.48                          | 0.30                           | 400                                   |
| 0402CS-30NX_L            | 30                              | <b>5,2</b>                        | 31.1    | 46                 | 38.50   | 39                 | 2.35                          | 0.30                           | 400                                   |
| 0402CS-33NX_L            | 33                              | <b>5,2</b>                        | 34.9    | 31                 | 41.74   | 32                 | 2.35                          | 0.30                           | 400                                   |
| 0402CS-36NX_L            | 36                              | <b>5,2</b>                        | 39.5    | 44                 | 48.40   | 53                 | 2.32                          | 0.44                           | 320                                   |
| 0402CS-39NX_L            | 39                              | <b>5,2</b>                        | 41.7    | 47                 | 50.23   | 45                 | 2.10                          | 0.55                           | 200                                   |
| 0402CS-40NX_L            | 40                              | <b>5,2</b>                        | 39.0    | 44                 | 47.40   | 33                 | 2.24                          | 0.44                           | 320                                   |
| 0402CS-43NX_L            | 43                              | <b>5,2</b>                        | 45.8    | 46                 | 61.55   | 34                 | 2.03                          | 0.81                           | 100                                   |
| 0402CS-47NX_L            | 47                              | <b>5,2</b>                        | 50.0    | 38                 | —       | —                  | 2.10                          | 0.83                           | 150                                   |
| 0402CS-51NX_L            | 51                              | <b>5,2</b>                        | 56.6    | 40                 | —       | —                  | 1.75                          | 0.82                           | 100                                   |
| 0402CS-56NX_L            | 56                              | <b>5,2</b>                        | 62.8    | 42                 | —       | —                  | 1.76                          | 0.97                           | 100                                   |
| 0402CS-68NX_L            | 68                              | <b>5,2</b>                        | 78.2    | 36                 | —       | —                  | 1.62                          | 1.12                           | 100                                   |
| 0402CS-82NX_L            | 82                              | <b>5,2</b>                        | —       | —                  | —       | —                  | 1.26                          | 1.55                           | 50                                    |
| 0402CS-R10X_L            | 100                             | <b>5,2</b>                        | —       | —                  | —       | —                  | 1.16                          | 2.00                           | 30                                    |
| 0402CS-R12X_L            | 120                             | <b>5,2</b>                        | —       | —                  | —       | —                  | 1.90                          | 2.20                           | 50                                    |

1. When ordering, specify tolerance, termination and packaging codes:

0402CS-68NX J L W

Tolerance: G = 2% J = 5%

(Table shows stock tolerances in bold.)

Termination: L = RoHS compliant silver-palladium-platinum-glass frit.  
 Special order: T = RoHS tin-silver-copper (95.5/4.0/0.5) or  
 S = non-RoHS tin-lead (63/37).

Packaging: W = 7" machine-ready reel, EIA-481 punched paper tape  
 (2000 parts per full reel).

U = Less than full reel. In tape, but not machine ready.  
 To have a leader and trailer added (\$25 charge), use  
 code letter W instead.

2. Inductance measured at 250 MHz using a Coilcraft SMD-F test fixture  
 and Coilcraft-provided correlation pieces with an Agilent/HP 4286  
 impedance analyzer.

3. Tolerances in bold are stocked for immediate shipment.

4. Q measured using an Agilent/HP 4291A with an Agilent/HP 16193 test  
 fixture.

5. For SRF > 6 GHz, measured using an Agilent/HP 8722ES network  
 analyzer and a Coilcraft SMD-D test fixture. For SRF ≤ 6 GHz,  
 measured using an Agilent/HP 8753D network analyzer and a Coilcraft  
 SMD-D test fixture.

6. DCR measured on a micro-ohmmeter.

7. Current that causes a 15°C temperature rise from 25°C ambient.

8. Electrical specifications at 25°C.

Refer to Doc 362 "Soldering Surface Mount Components" before soldering.

**S-Parameter files**  
 ON OUR WEB SITE OR CD

**SPICE models**  
 ON OUR WEB SITE OR CD

**Coilcraft**

Specifications subject to change without notice.

Please check our website for latest information.

Document 198-2 Revised 11/09/10

1102 Silver Lake Road Cary, Illinois 60013 Phone 847/639-6400 Fax 847/639-1469  
 E-mail info@coilcraft.com Web http://www.coilcraft.com

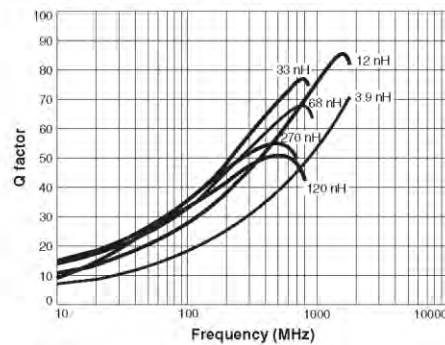
©Coilcraft, Inc. 2010



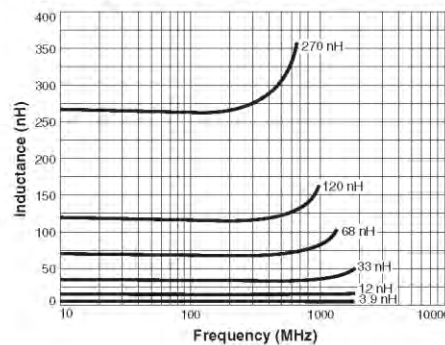
# Chip Inductors – 0603CS (1608)

Ultra-small size, exceptional Q and high SRFs make these inductors ideal for high frequency applications where size is at a premium. They also have excellent DCR and current carrying characteristics.

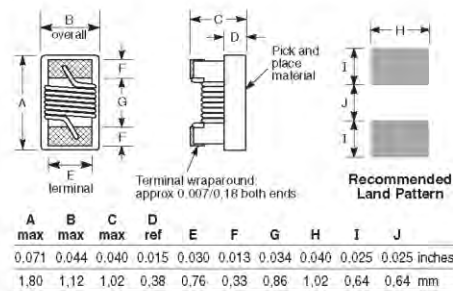
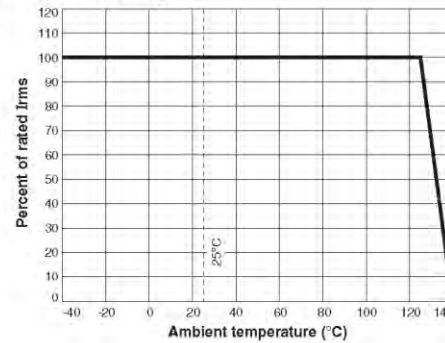
## Typical Q vs Frequency



## Typical L vs Frequency



## Irms Derating



**Core material** Ceramic

**Terminations** RoHS compliant silver-palladium-platinum-glass frit. Other terminations available at additional cost.

**Weight** 3.2 – 3.7 mg

**Ambient temperature** –40°C to +125°C with I<sub>rms</sub> current, +125°C to +140°C with derated current

**Storage temperature** Component: –40°C to +140°C, Packaging: –40°C to +80°C

**Resistance to soldering heat** Max three 40 second reflows at +260°C, parts cooled to room temperature between cycles

**Temperature Coefficient of Inductance (TCL)** +25 to +125 ppm/°C

**Moisture Sensitivity Level (MSL)** 1 (unlimited floor life at <30°C / 85% relative humidity)

**Failures in Time (FIT) / Mean Time Between Failures (MTBF)** One per billion hours / one billion hours, calculated per Telcordia SR-332

**Packaging** 2000 per 7" reel Paper tape: 8 mm wide, 1.0 mm thick, 4 mm pocket spacing

**PCB washing** Only pure water or alcohol recommended



US +1-847-639-6400 sales@coilcraft.com  
 UK +44-1236-730695 sales@coilcraft-europe.com  
 Taiwan +886-2-2264 3846 sales@coilcraft.com.tw  
 China +86-21-8218 8074 sales@coilcraft.com.cn  
 Singapore +65-6484 8412 sales@coilcraft.com.sg

Document 195-1 Revised 10/14/09

© Coilcraft Inc. 2011  
 This product may not be used in medical or high risk applications without prior Coilcraft approval. Specifications subject to change without notice. Please check our web site for latest information.



**0603CS Series (1608)**

Designer's Kits C324A and B contain 10 each of all 5% values  
Designer's Kits C324A-2 and B-2 contain 10 each of all 2% values

| Part number <sup>1</sup> | Inductance <sup>2</sup><br>(nH) | Percent<br>tolerance <sup>3</sup> | Q<br>min <sup>4</sup> | 900 MHz |       | 1.7 GHz |       | SRF<br>min <sup>5</sup><br>(GHz) | DCR<br>max <sup>6</sup><br>(Ohms) | I <sub>rms</sub> <sup>7</sup><br>(mA) | Color<br>dot |
|--------------------------|---------------------------------|-----------------------------------|-----------------------|---------|-------|---------|-------|----------------------------------|-----------------------------------|---------------------------------------|--------------|
|                          |                                 |                                   |                       | L typ   | Q typ | L typ   | Q typ |                                  |                                   |                                       |              |
| 0603CS-1N6X L            | 1.6 @ 250 MHz                   | <b>5</b>                          | 24                    | 1.67    | 49    | 1.65    | 63    | 12.5                             | 0.030                             | 700                                   | Red          |
| 0603CS-1N8X L            | 1.8 @ 250 MHz                   | <b>5</b>                          | 16                    | 1.83    | 35    | 1.86    | 50    | 12.5                             | 0.045                             | 700                                   | Black        |
| 0603CS-2N2X L            | 2.2 @ 250 MHz                   | <b>5</b>                          | 13                    | 2.22    | 31    | 2.24    | 44    | 12.5                             | 0.250                             | 100                                   | Yellow       |
| 0603CS-3N3X L            | 3.3 @ 250 MHz                   | <b>5,2</b>                        | 35                    | 3.31    | 75    | 3.38    | 88    | 5.90                             | 0.045                             | 700                                   | Blue         |
| 0603CS-3N6X L            | 3.6 @ 250 MHz                   | <b>5,2</b>                        | 22                    | 3.72    | 53    | 3.71    | 65    | 5.90                             | 0.063                             | 700                                   | Red          |
| 0603CS-3N9X L            | 3.9 @ 250 MHz                   | <b>5,2</b>                        | 22                    | 3.95    | 49    | 3.96    | 67    | 6.90                             | 0.080                             | 700                                   | Brown        |
| 0603CS-4N3X L            | 4.3 @ 250 MHz                   | <b>5,2</b>                        | 22                    | 4.32    | 50    | 4.33    | 70    | 5.90                             | 0.063                             | 700                                   | Orange       |
| 0603CS-4N7X L            | 4.7 @ 250 MHz                   | <b>5,2</b>                        | 20                    | 4.72    | 47    | 4.75    | 57    | 5.80                             | 0.116                             | 700                                   | Violet       |
| 0603CS-5N1X L            | 5.1 @ 250 MHz                   | <b>5,2</b>                        | 20                    | 4.93    | 47    | 4.95    | 56    | 5.70                             | 0.140                             | 700                                   | Green        |
| 0603CS-5N6X L            | 5.6 @ 250 MHz                   | <b>5,2</b>                        | 26                    | 5.77    | 63    | 6.05    | 80    | 4.76                             | 0.075                             | 700                                   | Black        |
| 0603CS-6N8X L            | 6.8 @ 250 MHz                   | <b>5,2</b>                        | 27                    | 6.75    | 60    | 7.10    | 81    | 5.80                             | 0.110                             | 700                                   | Red          |
| 0603CS-7N5X L            | 7.5 @ 250 MHz                   | <b>5,2</b>                        | 28                    | 7.70    | 60    | 7.82    | 65    | 4.80                             | 0.106                             | 700                                   | Brown        |
| 0603CS-8N2X L            | 8.2 @ 250 MHz                   | <b>5,2</b>                        | 30                    | 8.25    | 82    | 8.37    | 87    | 4.20                             | 0.115                             | 700                                   | Orange       |
| 0603CS-8N7X L            | 8.7 @ 250 MHz                   | <b>5,2</b>                        | 28                    | 8.86    | 62    | 9.32    | 58    | 4.60                             | 0.109                             | 700                                   | Yellow       |
| 0603CS-9N5X L            | 9.5 @ 250 MHz                   | <b>5,2</b>                        | 28                    | 9.7     | 59    | 9.92    | 61    | 5.40                             | 0.135                             | 700                                   | Blue         |
| 0603CS-10NX L            | 10 @ 250 MHz                    | <b>5,2</b>                        | 31                    | 10.0    | 66    | 10.6    | 83    | 4.80                             | 0.130                             | 700                                   | Orange       |
| 0603CS-11NX L            | 11 @ 250 MHz                    | <b>5,2</b>                        | 30                    | 11.0    | 53    | 11.5    | 56    | 4.00                             | 0.130                             | 700                                   | Gray         |
| 0603CS-12NX L            | 12 @ 250 MHz                    | <b>5,2</b>                        | 35                    | 12.3    | 72    | 13.5    | 83    | 4.00                             | 0.130                             | 700                                   | Yellow       |
| 0603CS-15NX L            | 15 @ 250 MHz                    | <b>5,2</b>                        | 35                    | 15.4    | 64    | 16.8    | 89    | 4.00                             | 0.170                             | 700                                   | Green        |
| 0603CS-16NX L            | 16 @ 250 MHz                    | <b>5,2</b>                        | 34                    | 16.2    | 55    | 17.3    | 52    | 3.30                             | 0.170                             | 700                                   | White        |
| 0603CS-18NX L            | 18 @ 250 MHz                    | <b>5,2</b>                        | 35                    | 18.7    | 70    | 21.4    | 69    | 3.10                             | 0.170                             | 700                                   | Blue         |
| 0603CS-22NX L            | 22 @ 250 MHz                    | <b>5,2</b>                        | 38                    | 22.8    | 73    | 26.1    | 71    | 3.00                             | 0.190                             | 700                                   | Violet       |
| 0603CS-23NX L            | 23 @ 250 MHz                    | <b>5,2</b>                        | 38                    | 24.1    | 71    | 28.0    | 67    | 2.85                             | 0.190                             | 700                                   | Orange       |
| 0603CS-24NX L            | 24 @ 250 MHz                    | <b>5,2</b>                        | 36                    | 24.5    | 45    | 28.7    | 39    | 2.65                             | 0.190                             | 700                                   | Black        |
| 0603CS-27NX L            | 27 @ 250 MHz                    | <b>5,2</b>                        | 40                    | 29.2    | 74    | 34.6    | 65    | 2.80                             | 0.220                             | 600                                   | Gray         |
| 0603CS-30NX L            | 30 @ 250 MHz                    | <b>5,2</b>                        | 37                    | 31.4    | 47    | 39.9    | 28    | 2.25                             | 0.220                             | 600                                   | Brown        |
| 0603CS-33NX L            | 33 @ 250 MHz                    | <b>5,2</b>                        | 40                    | 36.0    | 67    | 49.5    | 42    | 2.30                             | 0.220                             | 600                                   | White        |
| 0603CS-36NX L            | 36 @ 250 MHz                    | <b>5,2</b>                        | 37                    | 39.4    | 47    | 52.7    | 24    | 2.08                             | 0.250                             | 600                                   | Red          |
| 0603CS-39NX L            | 39 @ 250 MHz                    | <b>5,2</b>                        | 40                    | 42.7    | 60    | 60.2    | 40    | 2.20                             | 0.250                             | 600                                   | Black        |
| 0603CS-43NX L            | 43 @ 250 MHz                    | <b>5,2</b>                        | 38                    | 47.0    | 44    | 64.9    | 21    | 2.00                             | 0.280                             | 600                                   | Orange       |
| 0603CS-47NX L            | 47 @ 200 MHz                    | <b>5,2</b>                        | 38                    | 52.2    | 62    | 77.2    | 35    | 2.00                             | 0.280                             | 600                                   | Brown        |
| 0603CS-51NX L            | 51 @ 200 MHz                    | <b>5,2</b>                        | 35                    | 55.5    | 69    | 82.2    | 34    | 1.90                             | 0.270                             | 600                                   | Blue         |
| 0603CS-56NX L            | 56 @ 200 MHz                    | <b>5,2</b>                        | 38                    | 62.5    | 56    | 97.0    | 26    | 1.90                             | 0.310                             | 600                                   | Red          |
| 0603CS-68NX L            | 68 @ 200 MHz                    | <b>5,2</b>                        | 37                    | 80.5    | 54    | 168     | 21    | 1.70                             | 0.340                             | 600                                   | Orange       |
| 0603CS-72NX L            | 72 @ 150 MHz                    | <b>5,2</b>                        | 34                    | 82.0    | 53    | 135     | 20    | 1.70                             | 0.490                             | 400                                   | Yellow       |
| 0603CS-82NX L            | 82 @ 150 MHz                    | <b>5,2</b>                        | 34                    | 96.2    | 54    | 177     | 21    | 1.70                             | 0.540                             | 400                                   | Green        |
| 0603CS-R10X L            | 100 @ 150 MHz                   | <b>5,2</b>                        | 34                    | 124     | 49    | —       | —     | 1.40                             | 0.580                             | 400                                   | Blue         |
| 0603CS-R11X L            | 110 @ 150 MHz                   | <b>5,2</b>                        | 32                    | 138     | 43    | —       | —     | 1.35                             | 0.610                             | 300                                   | Violet       |
| 0603CS-R12X L            | 120 @ 150 MHz                   | <b>5,2</b>                        | 32                    | 166     | 39    | —       | —     | 1.30                             | 0.650                             | 300                                   | Gray         |
| 0603CS-R15X L            | 150 @ 150 MHz                   | <b>5,2</b>                        | 28                    | 250     | 25    | —       | —     | 0.990                            | 0.920                             | 280                                   | White        |
| 0603CS-R18X L            | 180 @ 100 MHz                   | <b>5,2</b>                        | 25                    | 305     | 22    | —       | —     | 0.990                            | 1.25                              | 240                                   | Black        |
| 0603CS-R20X L            | 200 @ 100 MHz                   | <b>5,2</b>                        | 25                    | —       | —     | —       | —     | 0.900                            | 1.98                              | 200                                   | Green        |
| 0603CS-R21X L            | 210 @ 100 MHz                   | <b>5,2</b>                        | 27                    | —       | —     | —       | —     | 0.895                            | 2.06                              | 200                                   | Gray         |
| 0603CS-R22X L            | 220 @ 100 MHz                   | <b>5,2</b>                        | 25                    | —       | —     | —       | —     | 0.900                            | 2.10                              | 200                                   | Brown        |
| 0603CS-R25X L            | 250 @ 100 MHz                   | <b>5,2</b>                        | 25                    | —       | —     | —       | —     | 0.822                            | 3.55                              | 120                                   | Violet       |
| 0603CS-R27X L            | 270 @ 100 MHz                   | <b>5,2</b>                        | 26                    | —       | —     | —       | —     | 0.830                            | 2.16                              | 170                                   | Red          |
| 0603CS-R33X L            | 330 @ 100 MHz                   | <b>5,2</b>                        | 25                    | —       | —     | —       | —     | 0.900                            | 3.89                              | 100                                   | Blue         |
| 0603CS-R39X L            | 390 @ 100 MHz                   | <b>5,2</b>                        | 25                    | —       | —     | —       | —     | 0.780                            | 4.35                              | 100                                   | Yellow       |

1. When ordering, specify tolerance, termination and packaging codes:  
0603CS-R39XJLW  
Tolerance: G = 2% J = 5% (Table shows stock tolerances in bold.)  
Termination: L = RoHS compliant silver-palladium-platinum-glass frit  
Special order: T = RoHS tin-silver-copper (95.5/4/0.5) or S = non-RoHS tin-lead (63/37).  
Packaging: W = 7" machine-ready reel, EIA-481 punched paper tape (2000 parts per full reel).  
U = Less than full reel, in tape, but not machine ready. To have a leader and trailer added (\$25 charge), use code letter W instead.

2. Inductance measured using a Coilcraft SMD-A fixture in an Agilent/HP 4286 impedance analyzer with Coilcraft-provided correlation pieces.  
3. Tolerances in bold are stocked for immediate shipment.  
4. Q measured at the same frequency as inductance using an Agilent/HP 4291A with an Agilent/HP 16193 test fixture.  
5. SRF measured using an Agilent/HP 8720D network analyzer and a Coilcraft SMD-D test fixture.  
6. DCR measured on a Cambridge Technology micro-ohmmeter and a Coilcraft CCF858 test fixture.  
7. Current that causes a 15°C temperature rise from 25°C ambient.  
8. Electrical specifications at 25°C.  
Refer to Doc 362 "Soldering Surface Mount Components" before soldering.

**S-Parameter files**  
ON OUR WEB SITE OR CD  
**SPICE models**  
ON OUR WEB SITE OR CD



US +1-847-639-6400 sales@coilcraft.com  
UK +44-1236-730695 sales@coilcraft-europe.com  
Taiwan +886-2-2264 3846 sales@coilcraft.com.tw  
China +86-21-6218 8074 sales@coilcraft.com.cn  
Singapore +65-6484 8412 sales@coilcraft.com.sg

Document 195-2 Revised 10/14/09  
© Coilcraft Inc. 2011  
This product may not be used in medical or high risk applications without prior Coilcraft approval. Specifications subject to change without notice. Please check our web site for latest information.

## Implementing Models in Microwave Office

Coilcraft provides the current and accurate versions of the models for using in modelling softwares. This information can be downloaded from the manufacturer website Fig D. 1.

## S-parameters

The S-parameters are provided in a single compressed "zipped" file. The file must be "unzipped" after downloading to obtain the separate inductor value S-parameter files. One can either link to or import the S-parameter data files.

Right click over the "Data Files" folder on the left.

Select either "Link To Data File." or "Import Data File."

Browse to the folder where the unzipped files are located and select the desired S-parameter file.

To place the data file on a schematic:

1. Select the "Elem" tab.
2. Click on the "Subcircuits" folder.
3. Click on the selected data file element.
4. Drag the element onto your schematic.

### **Lumped element (SPICE) models**

To model the chip inductors, either select the CCIND element from the Lumped Element - Inductor menu or place each individual lumped element for the model onto the schematic. An example chip inductor schematic is shown in Fig D. 1.

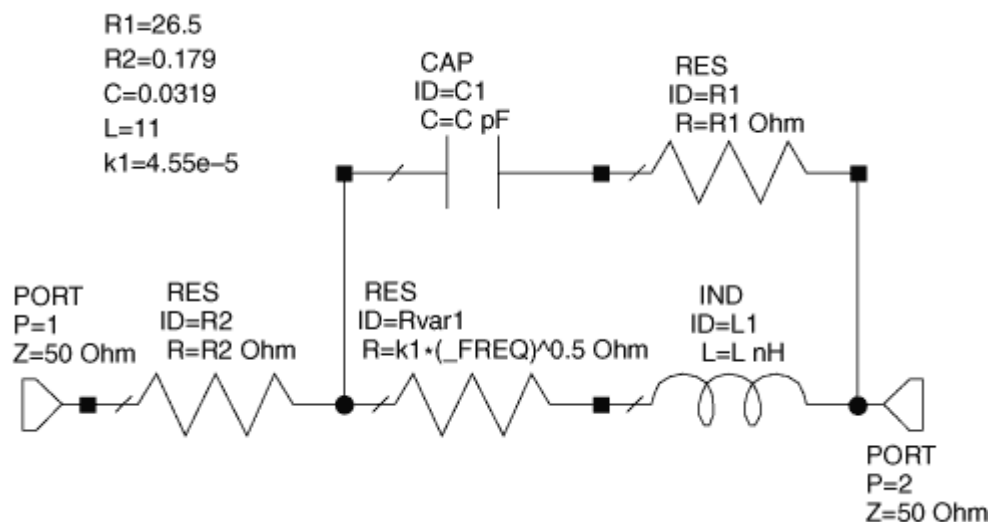


Fig D. 1 Example schematic for a Coilcraft chip inductor

### **For a frequency-dependent resistance (RVAR1, RVAR2)**

Note: This example uses RVAR1 ( $= k1 * \sqrt{\text{Frequency}}$ ).

1. Place an ideal resistor on the schematic.
2. Double click on the resistor to edit the value.
3. Rename it to identify it as a variable resistor (e.g. "Rvar1").
4. For the resistance value, enter the equation:  $k1 * (\_FREQ)^{0.5}$ .
5. Replace k1 with the value from the model table.

### **For a frequency-dependent inductance (LVAR)**

Note: This element is used in some of our power inductor models.

1. Place an ideal inductor on the schematic.
2. Double click on the inductor to edit the value.
3. Rename it to identify it as a variable inductor (e.g. "Lvar").

Note: The "log" function in the following equation is the natural logarithm, base e, not base 10.

4. For the inductance value, enter the equation:  $k3 - (k4 * \log(k5 * \_FREQ))$
5. Replace k3, k4, and k5 with the values from the model table.

### **Graphing specific model inductance and Q results**

The models represent de-embedded measurements in which fixture parasitic reactances have been removed. Fixture (or circuit board) parasitic reactances raise the effective impedance (and the effective inductance), lower the self-resonant frequency (SRF), and shift the Q curve. For the most accurate model of the inductors in a specific circuit environment, the circuit board model must be included in the simulation.

### **Inductance**

To view the effective series inductance of the model in a graph:

1. Right click on the graph name.
2. Click on "Add Measurement."

3. In the "Add Measurement" dialog box, select "Linear" as the Meas. Type. and "L\_SRL" as the Measurement.
4. Use your model schematic for the Data Source Name.
5. Check the "Sweep Proj. Freqs" box, and select the input port to your model.
6. Click "Add."

### **Quality factor (Q)**

Q values and curves in the data sheets are typically based on measurements using an impedance analyser in a 50 Ohm environment, giving a 1-port (reflection) measurement result. If Q calculations are to be compared with data sheet values and curves, they should be based on a simulation with one port of the inductor model connected to ground.

If one is interested in the Q of the inductor in a 2-port series configuration, the additional 50 Ohms impedance of the second port results in a lower simulated Q value than the 1-port configuration. This result is logical considering that the additional 50 Ohms applies to the "Re [Z]" in the denominator of the Q calculation equation.

$$Q = \text{Im} [Z] / \text{Re} [Z]$$

### **Im [Z] output equation**

1. Open the "Output Equations" window.
2. Click on the "Output Equation" icon or select it from the "Add" menu.
3. Enter a variable name, such as "x",
4. Select "Linear" as the Meas. Type and "ZIN" as the Measurement.
5. Select your model schematic for the Data Source Name.
6. Check the "Sweep Proj. Freqs" box.
7. Check "Imag" as the Complex Modifier.
8. Select the input port to your model.
9. Click "Add."

### **Re [Z] output equation**

1. Open the "Output Equations" window.
2. Click on the "Output Equation" icon, or select it from the "Add" menu.
3. Enter a different variable name than the one used in Im [Z], such as "y",
4. Select "Linear" as the Meas. Type and "ZIN" as the Measurement.
5. Use your model schematic for the Data Source Name.
6. Check the "Sweep Proj. Freqs" box.
7. Check "Real" as the Complex Modifier.
8. Select the input port to your model.
9. Click "Add."

### **Q equation**

1. Open the "Output Equations" window.
2. Click on the "Equation" icon or select it from the "Add" menu.
3. Enter a variable name, such as "Q1port",
4. Complete the equation using your Im [Z] and Re [Z] variables  
(for example:  $Q1port = x / y$ ).

### **To view the Q vs. frequency of the model in a graph**

1. Right click on the graph name, and click "Add Measurement."
2. In the "Add Measurement" dialog box, select "Output Equations" as the Meas. Type, and "Eqn" as the Measurement.
3. Use your Q equation variable name for the Data Source Name.
4. Check "Mag" as the Complex Modifier.
5. Check the "Sweep Proj. Freqs" box, and select the input port to your model.
6. Click "Add."

## Appendix D Substrate Datasheet



### TLC Low Cost RF Substrate

**TLC** laminates are engineered to provide a cost effective substrate suitable for a wide range of microwave applications. TLC laminates offer superior electrical performance compared to thermoset laminates (e.g. FR-4, PPO, BT, polyimide and cyanate ester). TLC's construction also provides exceptional mechanical stability.

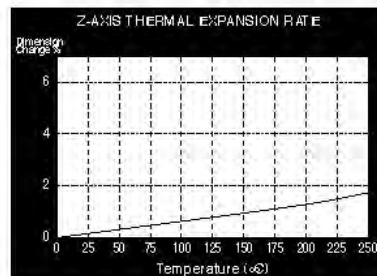
TLC laminates can be sheared, drilled, milled and plated using standard methods for PTFE/woven fiberglass materials. The laminates are dimensionally stable and exhibit virtually no moisture absorption during fabrication.

Taconic is a world leader in RF laminates and high speed digital materials, offering a wide range of high frequency laminates and prepregs. These advanced materials are used in the fabrication of antennas, multilayer RF and high speed digital boards, interconnections and devices.

#### Benefits & Applications:

- Low cost
- Tightly controlled Dk
- Low Df
- Excellent dimensional stability
- High flexural strength
- UL 94 V-0 rating

- LNBS
- Power amplifiers
- PCS/PCN large format antennas
- Passive components



#### North & South America

Taconic - Headquarters  
Petersburgh, NY 12138  
Tel: 518-658-3202 / 1-800-833-1805  
addinfo@taconic.com

#### Europe/Middle East/Australia

Taconic International Ltd.  
Republic of Ireland  
Tel: +353-44-9395600  
add@taconic.com

#### Asia

Korea Taconic Company  
Republic of Korea  
Tel: +82-31-704-1858  
sales@taconic.co.kr

#### China

Taconic Advanced Material (Suzhou) Co., Ltd.  
Suzhou City, China  
Tel: +86-512-8718-9678  
tssales@taconic.co.kr

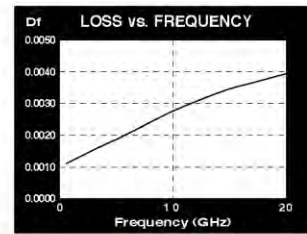
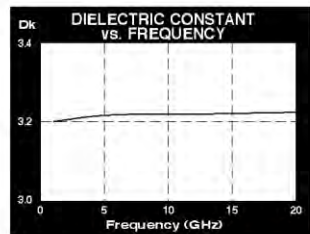
An ISO 9001:2000 Registered Company  
www.taconic-add.com



## Appendix

| TLC-32 Typical Values        |                  |                  |                 |                   |                 |
|------------------------------|------------------|------------------|-----------------|-------------------|-----------------|
| Property                     | Test Method      | Unit             | Value           | Unit              | Value           |
| Dk @ 10 GHz                  | IPC-650 2.5.5.5  |                  | 3.20            |                   | 3.20            |
| Df @ 10 GHz                  | IPC-650 2.5.5.5  |                  | 0.0030          |                   | 0.0030          |
| Moisture Absorption          | IPC-650 2.6.2.1  | %                | <0.02           | %                 | <0.02           |
| Dielectric Breakdown         | IPC-650 2.5.6    | Kv               | >60             | Kv                | >60             |
| Volume Resistivity           | IPC-650 2.5.17.1 | Mohms/cm         | 10 <sup>7</sup> | Mohms/cm          | 10 <sup>7</sup> |
| Surface Resistivity          | IPC-650 2.5.17.1 | Mohms            | 10 <sup>7</sup> | Mohms             | 10 <sup>7</sup> |
| Arc Resistance               | IPC-650 2.5.1    | seconds          | >180            | seconds           | >180            |
| Flexural Strength (MD)       | IPC-650 2.4.4    | lbs./inch        | >40,000         | N/mm <sup>2</sup> | >276            |
| Flexural Strength (CD)       | IPC-650 2.4.4    | lbs./inch        | >35,000         | N/mm <sup>2</sup> | >241            |
| Peel Strength (1 oz. copper) | IPC-650 2.4.8    | lbs./linear inch | 12.0            | N/mm              | 2.1             |
| Thermal Conductivity         | ASTM F 433       | W/m/K            | 0.24            | W/m/K             | 0.24            |
| CTE (x-y axis)               | ASTM D 3386/TMA  | ppm/°C           | 9 - 12          | ppm/°C            | 9 - 12          |
| CTE (z axis)                 | ASTM D 3386/TMA  | ppm/°C           | 70              | ppm/°C            | 70              |
| UL-94 Flammability Rating    | UL-94            |                  | V-0             |                   | V-0             |

All reported values are typical and should not be used for specification purposes. In all instances, the user shall determine suitability in any given application.



| Designation | Dk            | Dielectric Thickness<br>inches | Dielectric Thickness<br>mm |
|-------------|---------------|--------------------------------|----------------------------|
| TLC-27      | 2.75 +/-0.05  | 0.0145                         | 0.37                       |
| TLC-30      | 3.00 +/- 0.05 | 0.0200<br>0.0300 - 0.0620      | 0.50<br>0.78 - 1.5         |
| TLC-32      | 3.20 +/- 0.05 | ≥0.0300                        | ≥0.78                      |

| Available Copper Cladding |                          |                                  |                  |
|---------------------------|--------------------------|----------------------------------|------------------|
| Designation               | Weight                   | Copper Thickness<br>inches<br>μm | Description      |
| CH                        | 1/2 oz / ft <sup>2</sup> | ~0.0007<br>~18                   | Electrodeposited |
| C1                        | 1 oz / ft <sup>2</sup>   | ~0.0014<br>~35                   | Electrodeposited |
| C2                        | 2 oz / ft <sup>2</sup>   | ~0.0028<br>~70                   | Electrodeposited |

Heavy metal claddings (aluminum, brass & copper) may also be available upon request. Standard sheet size is 36" x 48" (914 mm x 1220 mm). Please contact our Customer Service Department for the availability of other sizes and claddings.

| Available Sheet Sizes |            |
|-----------------------|------------|
| Inches                | mm         |
| 12 x 18               | 304 x 457  |
| 16 x 18               | 406 x 457  |
| 18 x 24               | 457 x 610  |
| 16 x 36               | 406 x 914  |
| 24 x 36               | 610 x 914  |
| 18 x 48               | 457 x 1220 |

An example of our part number is: TLC-32-0620-CH/CH - 18" x 24" (457 mm x 610 mm)



rev. 1/09

| Standard Thickness   | Standard Panel Size   | Standard Copper Cladding   |
|--|---|--|
| <b>RO4003C:</b><br>0.008" (0.203mm), 0.012" (0.305mm), 0.016"<br>(0.406mm), 0.020" (0.508mm) 0.032" (0.813mm),<br>0.060" (1.524mm)<br><b>RO4350B:</b><br>*0.004" (0.101mm), 0.0066" (0.168mm) 0.010"<br>(0.254mm), 0.0133" (0.338mm), 0.0166" (0.422mm),<br>0.020" (0.508mm), 0.030" (0.762mm), 0.060"<br>(1.524mm)<br>Material clad with LoPro foil add .0007" (0.018mm)<br>to dielectric thickness | 12" X 18" (305 X 457 mm)<br>24" X 18" (610 X 457 mm)<br>24" X 36" (610 X 915 mm)<br>48" X 36" (1,224 m X 915 mm)<br>*0.004" material is not available in<br>panel sizes larger than 24"x18" (610<br>X 457mm). | ½ oz. (17µm), 1 oz. (35µm) and<br>2 oz. (70µm) electrodeposited<br>copper foil<br>~<br><b>LoPro Reverse Treated EDC for PIM<br/>           Sensitive Applications:</b><br>½ oz (17µm), 1 oz (35 µm)<br>Note: LoPro EDC foil adds .00035" to<br>the panel thickness per side. |

### World Class Performance

Rogers Corporation (NYSE:ROG), headquartered in Rogers, Conn., is a global technology leader in the development and manufacture of high performance, specialty material-based products for a variety of applications in diverse markets including: portable communications, communications infrastructure, computer and office equipment, consumer products, ground transportation, aerospace and defense. In an ever-changing world, where product design and manufacturing often take place on different sides of the planet, Rogers has the global reach to meet customer needs. Rogers operates facilities in the United States, Europe, and Asia. The world runs better with Rogers.®

### CONTACT INFORMATION:

|            |  |                       |                       |
|------------|--|-----------------------|-----------------------|
| USA:       | Rogers Advanced Circuit Materials, ISO 9002 certified              | Tel: 480-961-1382     | Fax: 480-961-4533     |
| Belgium:   | Rogers - BVBA Belgium  | Tel: 32-9-2353611     | Fax: 32-9-2353658     |
| Japan:     | Rogers Japan Inc.  | Tel: 81-3-5200-2700   | Fax: 81-3-5200-0571   |
| Taiwan:    | Rogers Taiwan Inc.   | Tel: 886-2-86609056   | Fax: 886-2-86609057   |
| Korea:     | Rogers Korea Inc.  | Tel: 82-31-716-6112   | Fax: 82-31-716-6208   |
| Singapore: | Rogers Technologies Singapore Inc.                                 | Tel: 65-747-3521      | Fax: 65-747-7425      |
| China:     | Rogers (Shanghai) International Trading Co., Ltd (Shanghai Office) | Tel: 86-21-62175599   | Fax: 86-21-62677913   |
| China:     | Rogers (Shanghai) International Trading Co., Ltd (Beijing Office)  | Tel: 86-10-5820-7667  | Fax: 86-10-5820-7997  |
| China:     | Rogers International Trading Co., Ltd (Shenzhen Office)            | Tel: 86-755-8236-6060 | Fax: 86-755-8236-6123 |

The information in this data sheet is intended to assist you in designing with Rogers' circuit material laminates. It is not intended to and does not create any warranties express or implied, including any warranty of merchantability or fitness for a particular purpose or that the results shown on this data sheet will be achieved by a user for a particular purpose. The user should determine the suitability of Rogers' circuit material laminates for each application.

Prolonged exposure in an oxidative environment may cause changes to the dielectric properties of hydrocarbon based materials. The rate of change increases at higher temperatures and is highly dependent on the circuit design. Although Rogers' high frequency materials have been used successfully in innumerable applications and reports of oxidation resulting in performance problems are extremely rare, Rogers recommends that the customer evaluate each material and design combination to determine fitness for use over the entire life of the end product.

These commodities, technology and software are exported from the United States in accordance with the Export Administration regulations. Diversion contrary to U.S. law prohibited.

LoPro, RO4000, RO4003, RO4350, RO4350B and RO4003C are licensed trademarks of Rogers Corporation. The world runs better with Rogers, and the Rogers' logo are licensed trademarks of Rogers Corporation.

© 1995, 1996, 1997, 1999, 2002, 2005, 2006, 2007, 2010 Rogers Corporation.

Printed in U.S.A., All rights reserved.

Revised 05/2010 0891-0110-0,5CC

Publication #92-004



Advanced Circuit Materials Division  
100 S. Roosevelt Avenue  
Chandler, AZ 85226  
Tel: 480-961-1382, Fax: 480-961-4533  
www.rogerscorp.com

Data Sheet

Advanced Circuit Materials

## RO4000® Series High Frequency Circuit Materials



| Features:   | Benefits:   |
|---|---|
| RO4000® materials are reinforced hydrocarbon/ceramic laminates  | <ul style="list-style-type: none"><li>• Designed for performance sensitive, high volume applications</li></ul>  |
| Low dielectric tolerance and low loss   | <ul style="list-style-type: none"><li>• Excellent electrical performance</li><li>• Allows applications with higher operating frequencies</li><li>• Ideal for broadband applications</li></ul> |
| Stable electrical properties vs. frequency  | <ul style="list-style-type: none"><li>• Controlled impedance transmission lines</li></ul>   |
| Lead-free process compatible  | <ul style="list-style-type: none"><li>• No blistering or delamination</li></ul>   |
| Low Z-axis expansion  | <ul style="list-style-type: none"><li>• Reliable plated through holes</li></ul>   |
| Low in-plane expansion coefficient  | <ul style="list-style-type: none"><li>• Remains stable over an entire range of circuit processing temperatures</li></ul>  |
| Volume manufacturing process  | <ul style="list-style-type: none"><li>• RO4000 laminates can be fabricated using standard glass epoxy processes</li><li>• Competitively priced</li></ul>                                      |
| Typical Applications:   |   |
| <ul style="list-style-type: none"><li>• Cellular Base Station Antennas and Power Amplifiers</li></ul> |   |
| <ul style="list-style-type: none"><li>• RF Identification Tags</li></ul>                              |   |
| <ul style="list-style-type: none"><li>• Automotive Radar and Sensors</li></ul>                        |   |
| <ul style="list-style-type: none"><li>• LNB's for Direct Broadcast Satellites</li></ul>               |   |

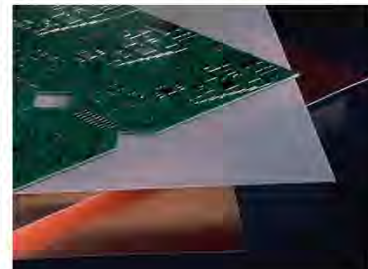
RO4000® hydrocarbon ceramic laminates are designed to offer superior high frequency performance and low cost circuit fabrication. The result is a low loss material which can be fabricated using standard epoxy/glass (FR-4) processes offered at competitive prices.

The selection of laminates typically available to designers is significantly reduced once operational frequencies increase to 500 MHz and above. RO4000 material possesses the properties needed by designers of RF microwave circuits and matching networks and controlled impedance transmission lines. Low dielectric loss allows RO4000 series material to be used in many applications where higher operating frequencies limit the use of conventional circuit board laminates. The temperature coefficient of dielectric constant is among the lowest of any circuit board material (Chart 1), and the dielectric constant is stable over a broad frequency range (Chart 2). This makes it an ideal substrate for broadband applications.

RO4000 material's thermal coefficient of expansion (CTE) provides several key benefits to the circuit designer. The expansion coefficient of RO4000 material is similar to that of copper which allows the material to exhibit excellent dimensional stability, a property needed for mixed dielectric multilayer boards constructions. The low Z-axis CTE of RO4000 laminates provides reliable plated through-hole quality, even in severe thermal shock applications. RO4000 series material has a Tg of >280°C (536°F) so its expansion characteristics remain stable over the entire range of circuit processing temperatures.

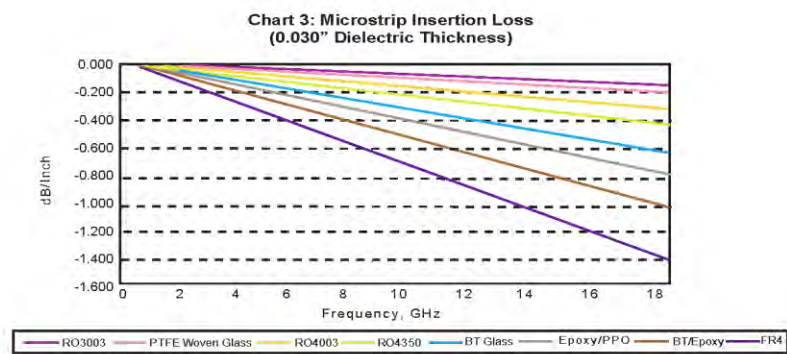
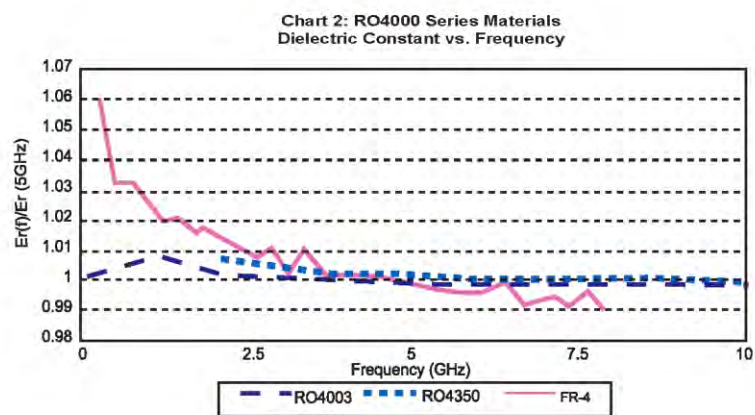
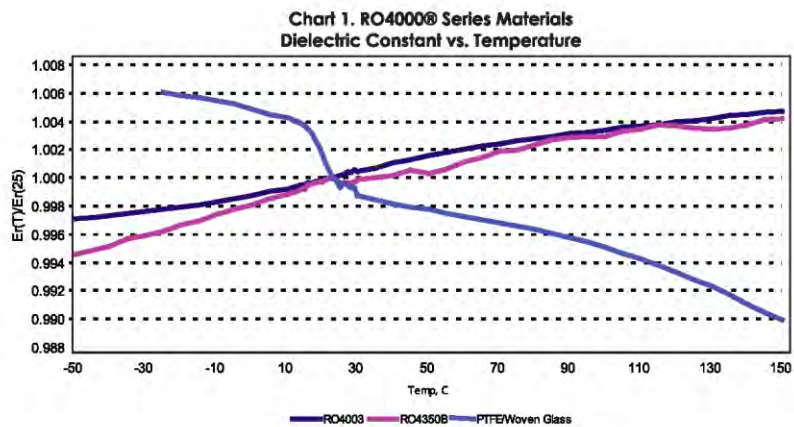
RO4000 series laminates can easily be fabricated into printed circuit boards using standard FR-4 circuit board processing techniques. Unlike PTFE based high performance materials, RO4000 series laminates do not require specialized via preparation processes such as sodium etch. This material is a rigid, thermoset laminate that is capable of being processed by automated handling systems and scrubbing equipment used for copper surface preparation.

RO4003™ laminates are currently offered in various configurations utilizing both 1080 and 1674 glass fabric styles, with all configurations meeting the same laminate electrical performance specification. Specifically designed as a drop-in replacement for the RO4003C™ material, RO4350B™ laminates utilize RoHS compliant flame-retardant technology for applications requiring UL 94V-0 certification. These materials conform to the requirements of IPC-4103, slash sheet / 10 for RO4003C and / 11 for RO4350B materials.



The world runs better with Rogers.®





## Appendix

| Property  | Typical Value          |                            | Direction   | Units               | Condition   | Test Method   |
|---|------------------------|----------------------------|-------------|---------------------|---|---|
|   | RO4003C                | RO4350B                    |             |                     |   |   |
| Dielectric Constant, $\epsilon_r$<br>(Process specification)                                | 3.38 ± 0.05            | <sup>(1)</sup> 3.48 ± 0.05 | Z           | --                  | 10 GHz/23°C   | IPC-TM-650<br>2.5.5.5<br><sup>(2)</sup> Clamped Stripline |
| <sup>(3)</sup> Dielectric Constant, $\epsilon_r$<br>(Recommended for use in circuit design) | 3.55                   | 3.66                       | Z           | --                  | FSR/23°C  | IPC-TM-650<br>2.5.5.6<br>Full Sheet Resonance             |
| Dissipation Factor tan, $\delta$  | 0.0027<br>0.0021       | 0.0037<br>0.0031           | Z           | --                  | 10 GHz/23°C<br>2.5 GHz/23°C                           | IPC-TM-650<br>2.5.5.5                                     |
| Thermal Coefficient of $\epsilon_r$   | +40                    | +50                        | Z           | ppm/°C              | -50°C to 150°C  | IPC-TM-650<br>2.5.5.5                                     |
| Volume Resistivity  | 1.7 X 10 <sup>10</sup> | 1.2 X 10 <sup>10</sup>     |             | MΩ•cm               | COND A  | IPC-TM-650<br>2.5.17.1                                    |
| Surface Resistivity   | 4.2 X 10 <sup>9</sup>  | 5.7 X 10 <sup>9</sup>      |             | MΩ                  | COND A  | IPC-TM-650<br>2.5.17.1                                    |
| Electrical Strength   | 31.2<br>(780)          | 31.2<br>(780)              | Z           | KV/mm<br>(V/mil)    | 0.51mm<br>(0.020")                                    | IPC-TM-650<br>2.5.6.2                                     |
| Tensile Modulus   | 26,889<br>(3900)       | 11,473<br>(1664)           | Y           | MPa<br>(kpsi)       | RT  | ASTM D638   |
| Tensile Strength  | 141<br>(20.4)          | 175<br>(25.4)              | Y           | MPa<br>(kpsi)       | RT  | ASTM D638   |
| Flexural Strength   | 276<br>(40)            | 255<br>(37)                |             | MPa<br>(kpsi)       |   | IPC-TM-650<br>2.4.4                                       |
| Dimensional Stability   | <0.3                   | <0.5                       | X,Y         | mm/m<br>(mils/inch) | after etch<br>+E2/150°C                               | IPC-TM-650<br>2.4.39A                                     |
| Coefficient of Thermal Expansion  | 11<br>14<br>46         | 14<br>16<br>35             | X<br>Y<br>Z | ppm/°C              | -55 to 288°C  | IPC-TM-650<br>2.1.41                                      |
| Tg  | >280                   | >280                       |             | °C DSC              | A   | IPC-TM-650<br>2.4.24                                      |
| Td  | 425                    | 390                        |             | °C TGA              |   | ASTM D3850  |
| Thermal Conductivity  | 0.71                   | 0.69                       |             | W/m²K               | 80°C  | ASTM C518   |
| Moisture Absorption   | 0.06                   | 0.06                       |             | %                   | 48 hrs immersion<br>0.060" sample<br>Temperature 50°C | ASTM D570   |
| Density   | 1.79                   | 1.86                       |             | gm/cm³              | 23°C  | ASTM D792   |
| Copper Peel Strength  | 1.05<br>(6.0)          | 0.88<br>(5.0)              |             | N/mm<br>(pli)       | after solder float<br>1 oz. EDC Foil                  | IPC-TM-650<br>2.4.8                                       |
| Flammability  | N/A                    | <sup>(4)</sup> V-0         |             |                     |   | UL 94   |
| Lead-Free Process Compatible  | Yes                    | Yes                        |             |                     |   |   |

(1) Dielectric constant typical value does not apply to 0.004" (0.101mm) laminates. Dielectric constant specification value for 0.004" RO4350B material is 3.33 ± 0.05.

(2) The IPC clamped stripline method can potentially lower the actual dielectric constant due to presence of airgaps between the laminates under test and the resonator card. Dielectric constant in practice may be higher than the values listed.

(3) The design Dk is an average number from several different tested lots of material and on the most common thickness/s. If more detailed information is required please contact Rogers Corporation. Refer to Rogers' technical paper "Dielectric Properties of High Frequency Materials" available at <http://www.rogerscorp.com/acm>.

(4) \*\* Note on 94V-0 \*\* RO4350B LoPro™ laminates do not share the same UL designation as standard RO4350B laminates. A separate UL qualification may be necessary.

Typical values are a representation of an average value for the population of the property. For specification values contact Rogers Corporation.

RO4000 LoPro laminates uses a modified version of RO4000 resin system to bond reverse treated foil. Values shown above are RO4000 laminates with out the addition of the LoPro resin. For double-sided board, the LoPro foil results in a thickness increase of approximately 0.0007" (0.018mm) and the Dk is approximately 2.4. Therefore, effective Dk is highly dependent on core thickness.

Prolonged exposure in an oxidative environment may cause changes to the dielectric properties of hydrocarbon based materials. The rate of change increases at higher temperatures and is highly dependent on the circuit design. Although Rogers' high frequency materials have been used successfully in innumerable applications and reports of oxidation resulting in performance problems are extremely rare, Rogers recommends that the customer evaluate each material and design combination to determine fitness for use over the entire life of the end product.

## References

- [1] “CST Microwave Studio Tutorials,” *Computer Simulation Technology*, [www.cst.de](http://www.cst.de), vol. Version 4, July 2002.
- [2] T. Weiland, “A discretization method for the solution of Maxwell’s equations for six-component fields,” *Electronics and Communications AEÜ*, vol. 31, pp. 116-120, 1977.
- [3] M. Clemens and T. Weiland, “Discrete electromagnetism with the finite integration technique,” *Progress in Electromagnetics Research*, vol. 32, pp. 65-87, 2001.
- [4] “Advanced topics,” *CST Microwave Studio menu*, Version 5, 2004.
- [5] “EMPIRE XCcel Reference Manual,” <http://www.empire.de/>.
- [6] K. S. Yee, “Numerical solution of initial boundary value problems involving Maxwell’s equations in isotropic media,” *IEEE Trans. Antennas Propagat.*, vol. AP-14, pp. 302–307, 1966.
- [7] C. A. Balanis, *Antenna Theory Analysis and Design*, by John Wiley & Sons, INC, 2005.
- [8] Z. N. Chen, *Antennas for Portable Devices*, John Wiley & Sons Ltd, ISBN 978-0-470-03073-8, West Sussex, England, 2007.
- [9] B.S. Collins and S.A. Saario, “The use of baluns for measurements on antennas mounted on small ground planes,” *IEEE International Workshop on Antenna Technology, IWAT 05*, Singapore, Jun 2005, pp 266–269.
- [10] <http://www.avx.com/SpiApps/default.asp#rfmicrowave>